

Geochemistry and Petrography of the Ultramafic Metavolcanic Rocks in the Eastern Portion of the Shebandowan Greenstone Belt, Northwestern Ontario

Sheree Laina Kirsten Hinz

Thesis submitted in partial fulfillment of the requirements for the degree of

Masters of Science in Geology



Supervisors: Dr. Peter Hollings, Dr. Robert Lodge

Lakehead University

Geology Department

Thunder Bay, Ontario

September 2018

Abstract

The 2.7 Ga Shebandowan greenstone belt in the Wawa-Abitibi terrane contains unusual ultramafic rocks. The two main assemblages present within the study area are the Greenwater and Shebandowan assemblages. The 2719.7 ± 1.0 Ma Greenwater assemblage is characterized by tholeiitic magmatism whereas the 2690-2680 Ma Shebandowan assemblage is characterized by calc-alkalic magmatism. Mapping of a 16 km² area and 7 trenches has identified the following lithologies in the field area: orthocumulate ultramafic rocks, komatiites, pyroxenite, vesicular komatiites, serpentinite, ultramafic breccia, variolitic ultramafic rocks, mafic intrusive rocks, intermediate intrusive and extrusive rocks, felsic volcanoclastic rocks, monzonite, conglomerate, banded iron formation, argillite and chert.

The ultramafic rocks are dark black in colour, but light green on surface as a product of serpentine alteration of olivine. They are highly magnetic, with magnetic susceptibility readings from 20 to 150 x10⁻³ SI. In some areas they occur as fine-grained, massive rocks with no distinct textures, and they also occur as medium-grained dark black rocks with a cumulate texture. The komatiites occur as fine-grained, light grey, highly silicified rocks. Several types of spinifex texture were observed throughout the field area, including: thin chaotic spinifex, thick chaotic spinifex, oriented spinifex, and pyroxene spinifex. Mafic intrusive rocks are massive, medium-grained, equigranular grey-blue gabbro with weakly disseminated pyrite. The intermediate intrusive rocks consist of a fine-grained, green-grey matrix with hornblende phenocrysts and red-pink autoliths. The intermediate extrusive rocks are fine-grained, light grey-blue metavolcanic rocks with medium-grained plagioclase phenocrysts. Felsic rocks in the field area are very fine-grained, light grey, siliceous rocks. They are massive with no flow textures observed in any of the outcrops and the weathered surfaces range in colour from beige to blue-grey. A monzonite dyke occurs alongside an interpreted fault through the field area. The distinctly magnetic rock consists of a fine-grained, green-grey matrix with hornblende phenocrysts and red-pink autoliths. The conglomerate is a heterolithic pebble to boulder conglomerate consisting of a fine-grained matrix with clasts of

basalt, monzonite, and jasper ranging in size from ~2 cm to 40 cm. The argillite is a very fine-grained dark black mudstone. It typically showed no bedding and locally contains graphite and abundant radial pyrite concretions up to 5cm in diameter. It is seen in the trenches intercalated with the hypabyssal komatiitic intrusions.

The komatiitic rocks have SiO₂ values of 47-67 wt. % and MgO values of 2-17 wt. %. Despite being outside the accepted values for komatiites, these rocks were identified as komatiites based on spinifex texture and spatial association with other ultramafic units. The abnormally high silica content in the ultramafic rocks was determined to be caused by silica alteration, and was not a primary feature of the rocks when they were emplaced. The rocks in the field area have undergone silica and carbonate alteration as well as greenschist facies metamorphism. The Al₂O₃/TiO₂ ratios of the ultramafic rocks are 17-29, and the CaO/Al₂O₃ ratios of the ultramafic rocks are 2-2.5. These ratios, combined with a flat pattern on a primitive mantle normalized multi-element diagram, identify the rocks as aluminium-undepleted komatiites. A distinct negative Nb anomaly is present in all samples, which could be caused by either the melt being derived from a heterogeneous deep-mantle source, where perovskite fractionation depleted the Nb, or crustal contamination. Sm-Nd isotope analysis was completed on six ultramafic samples from the field area. The ε_{Nd} of all samples ranged from +2.34 to +2.83, which is not consistent with contamination by older continental crust. Consequently, melting of a heterogeneous deep mantle source is the favoured model for petrogenesis of the ultramafic rocks.

Based on the close spatial association of tholeiitic and calc-alkalic rocks as well as the presence of thick sequences of deep-ocean argillites, the geological environment was determined to be an oceanic-rifted arc through which a plume of heterogeneous deep-mantle melts ascended, that subsequently closed and then collided with the Superior Province.

Acknowledgments

"I am a series of small victories and large defeats, and I am as amazed as any other that I have gotten from there to here."

-Charles Bukowski

I would like to thank all of the people who have helped me get from there to here. First and foremost, Pete Hollings for his support and unique brand of motivation that has gotten me through the past three years. Rob Lodge was an integral part of this project and his knowledge of the field area as well as the Shebandowan greenstone belt has been invaluable to me. His assistance in the field, along with Maile Olson and Samuel Helmuth in the summer of 2016 was insightful and entertaining. I thank the Ontario Geological Survey for funding the geochemical analysis of my samples and the Northern Lake Superior Research Grant, which provided funding for this project. I am truly grateful to have been given this scholarship. Anne Hammond and Kristi Tavener's detailed and meticulous thin-section work have benefited so many Lakehead geology students, myself included- thank you so much.

This thesis would not be complete without the invaluable assistance and support of the Resident Geologist Program. Field visits, maps, and reports from Dorothy Campbell and Mark Puumala greatly helped with technical and logistical aspects of the project. Dorothy's fearless bush driving skills brought the canoe to and from Thunder Lake, and will never be forgotten. Genevieve Dorland provided the air photos, which became the basis of my fieldwork planning. I avoided many swamps and cliffs because of this, and I am so grateful. Rohan Millar and the rest of the Thunder Bay RGP staff provided much-needed encouragement and support

during the past year while I was working and completing my thesis. This project would not be complete without my co-workers asking about my writing progress constantly and cheering me to the finish line. Leah Schmidt, in particular, ensured that I was celebrating every milestone (however small), reminding me that we achieve big goals one step at a time.

A million thanks to all my golden girls, my Geosisters for their love and friendship through tough times: Sarah Pemberton, Vicki Stinson, Chanelle Boucher, Emily Gorner, Kira Arnold, and Maddie Hodder. To my parents, who were often on the receiving end of my stressful moods: thank you for your unwavering support, encouragement, and love. To my mother, this would not have been possible without you. Thank you for showing up to support me at every presentation even when you had no idea what was happening. To my father, thank you for sharing your passion for geology with me. I look forward to many more years of rock-talk and learning from each other (and of course, IN YOUR FACE). To my four closest friends, thank you for keeping me sane and reminding me who I am when I'm not buried under buckets of rocks or lost within a loop of geochemistry. Claudia Ochnicki, Bianca Cava, Sarah McFarlane, and Connor-Lynn Phillips, you mean the world to me.

Table of Contents

Abstract	ii
Acknowledgments	iv
Table of Contents	vi
List of Figures	viii
List of Tables	x
Chapter 1: Introduction	1
1.1 Objective	1
1.2 Location	1
1.3 Komatiites	2
1.4 Siliceous High-Magnesium Basalt	5
1.5 Boninites	8
1.6 Structure of the Thesis	9
Chapter 2: Regional Geology and Mineralization	10
2.1 The Superior Province	10
2.2 The Wawa-Abitibi Terrane	12
2.3 The Shebandowan Greenstone Belt	14
2.4 Previous Work	16
Chapter 3: Methodology	18
3.1 Regional and Trench Mapping	18
3.2 Petrography	19
3.3 Geochemistry	19
3.4 Sm-Nd Isotopes	20
Chapter 4: Results	22
4.1 Lithology Descriptions	22
4.1.1 Orthocumulate Ultramafic Rocks	23
4.1.2 Komatiites	25
4.1.3 Other Ultramafic Lithologies	28
4.1.4 Pyroxenite	30
4.1.5 Mafic Rocks	32
4.1.5 Intermediate Rocks	34
4.1.7 Felsic Rocks	37
4.1.8 Sedimentary Rocks	39
4.2 Trench Mapping	40
4.2.1 Series 1 Trenches	40
4.2.2 Series 4 Trenches	43
Chapter 5: Geochemistry	47
5.1 Alteration	47
5.2 Orthocumulate Ultramafic Rocks	51
5.3 Komatiites	52
5.4 Massive Ultramafic Rocks	54
5.5 Basaltic Komatiites	54
5.6 Pyroxenite	55

5.7 Mafic Rocks	56
5.8 Intermediate Metavolcanic Rocks	57
5.9 Felsic Rocks	58
5.10 Monzonite	59
5.11 Sm-Nd Isotopic Geochemistry	60
Chapter 6: Discussion	61
6.1 Stratigraphic Relationships	61
6.2 Shebandowan Assemblage	61
6.3 Greenwater Assemblage	65
6.4 Petrogenesis	70
6.5 Comparisons with the Southern Abitibi Greenstone Belt.....	80
Conclusions	84
References.....	88
Appendix I: Thin Section Descriptions	99
Appendix II: Samarium-Neodymium Isotope Geochemistry	115
Appendix II: Sample Locations.....	117
Summer 2015 Sample Locations	118
Summer 2016 Sample Locations	120
Appendix III: Geochemical Data.....	125

List of Figures

1.1	Regional geology map showing the location of Conmee Township	2
1.2	Location of the four sampled trench sites	3
1.3	Idealized section of a komatiite flow	6
2.1	Map of the Superior Province	11
2.2	Regional geology map of the Shebandowan greenstone belt	14
3.1	Detailed geology map of the thesis area	18
4.1	Geology map of the study area	22
4.2	Photographs of field samples and outcrops	24
4.3	Photomicrograph of sample TL-16-SH-057	24
4.4	Photomicrograph of sample TL-16-SH-071	25
4.5	Photographs of field samples and outcrops	26
4.6	Photomicrograph of sample TL-16-SH-051	27
4.7	Photomicrograph of sample TL-16-SH-070	27
4.8	Photomicrograph of sample TL-16-SH-074	28
4.9	Photographs of field samples and outcrops	30
4.10	Photographs of field samples and outcrops	31
4.11	Photomicrograph of sample TL-16-SH-116A	32
4.12	Photomicrograph of sample TL-16-SH-116B	32
4.13	Photographs of field samples and outcrops	33
4.14	Photomicrograph of sample TL-16-SH-025	34
4.15	Photomicrograph of sample TL-16-SH-026	34
4.16	Photographs of field samples and outcrops	35
4.17	Photomicrograph of sample TL-16-SH-020	36
4.18	Photomicrograph of sample TL-16-SH-078	36
4.19	Photograph of felsic metavolcanic rock	37
4.20	Photomicrograph of sample TL-16-SH-090)	38
4.21	Photographs of sedimentary units	39
4.22	Geology map of the study area, highlighting trench locations	40
4.23	Trench map of Series 1 trenches, including trench 1A, 1B, 1C, 1D, 1E, and 1F	41
4.24	Various textures seen in trench set 1	43
4.25	Map of trench 4A from Series 4 trenches displaying lithologies and the transitions between them	45
4.26	Silicification of komatiite in trench 4A	46
5.1	Variation plots of MgO versus major element oxides	49
5.2	Variation diagrams of trace elements versus Al ₂ O ₃	50
5.3	Primitive mantle normalized multi-element diagram of orthocumulate ultramafic rocks	52
5.4	Variation diagram of Al ₂ O ₃ versus TiO ₂	53
5.5	Primitive mantle normalized multi-element diagram of komatiites	53

5.6	Primitive mantle normalized multi-element diagram of massive ultramafic rocks	54
5.7	Primitive mantle normalized multi-element diagram of basaltic komatiites	55
5.8	Primitive mantle normalized multi-element diagram of pyroxenites	56
5.9	Primitive mantle normalized multi-element diagram of mafic rocks	57
5.10	Primitive mantle normalized multi-element diagram of intermediate rocks	58
5.11	Primitive mantle normalized multi-element diagram of felsic volcanoclastic rocks	58
5.12	Primitive mantle normalized multi-element diagram of monzonite rocks	59
6.1	Geological map of the study area based on data collected in the summer of 2016	63
6.2	Primitive mantle normalized multi-element diagram of Tower mountain syenite rocks and monzonite rocks from the field area	64
6.3	Primitive mantle normalized multi-element diagram of Shebandowan assemblage rocks	65
6.4	Map of trench 4A from Series 4 trenches	69
6.5	Primitive mantle normalized multi-element diagram of Greenwater assemblage rocks	70
6.6	Primitive mantle normalized multi-element spider diagrams of typical AUK and ADK from the Lumby Lake greenstone belt	72
6.7	Variation diagram showing $\text{CaO}/\text{Al}_2\text{O}_3$ vs. $\text{Al}_2\text{O}_3/\text{TiO}_2$ of ultramafic lithologies	73
6.8	Variation diagrams of SiO_2 vs. La/Sm and Nb/Nb^*	77

List of Tables

5.1	Representative MgO, SiO ₂ , Ni, and Cr contents of the ultramafic lithologies	51
5.2	MgO, SiO ₂ , Ni, and Cr contents of the mafic and intermediate lithologies	57
5.3	Summary table of Sm/Nd isotopic values	60

Chapter 1: Introduction

1.1 Objective

The purpose of this project was to study the ultramafic volcanic rocks of the southeastern portion of the Shebandowan greenstone belt in order to determine their petrogenesis and tectonic setting. This study utilized whole-rock and trace element geochemistry, to investigate fractionation trends, mixing, and/or crustal contamination signatures to understand the petrogenesis and tectonic setting of the komatiites. Detailed mapping was completed in order to delineate different geologic units and correlate them over a broader area. Petrography was used, in addition to bedrock mapping, to develop more detailed descriptions of the igneous textures and assist in examining the volcanology of the area. The ultramafic metavolcanic rocks in the Greenwater assemblage of the Shebandowan greenstone belt in the study area have many of the characteristics of komatiites and siliceous high-magnesium basalt (SHMB). This thesis investigated the geochemistry and rock associations to determine the petrogenesis and tectonic setting of the ultramafic rocks.

1.2 Location

The Shebandowan greenstone belt is located in northwestern Ontario, beginning west of Lake Superior and extending southwest to Minnesota (Fig. 1.1). The study area is located in the southeastern portion of the Shebandowan greenstone belt, in Conmee Township and Dawson Road Lots, approximately 38 km outside of Thunder Bay on Highway 11/17 (Fig. 1.1). The main study area was accessed down West Mokomon road and then by ATV to travel down Tienharra

road. Two other study locations were accessed further down Highway 11/17, 60 km west of Thunder Bay with access directly alongside the highway (Fig. 1.2).

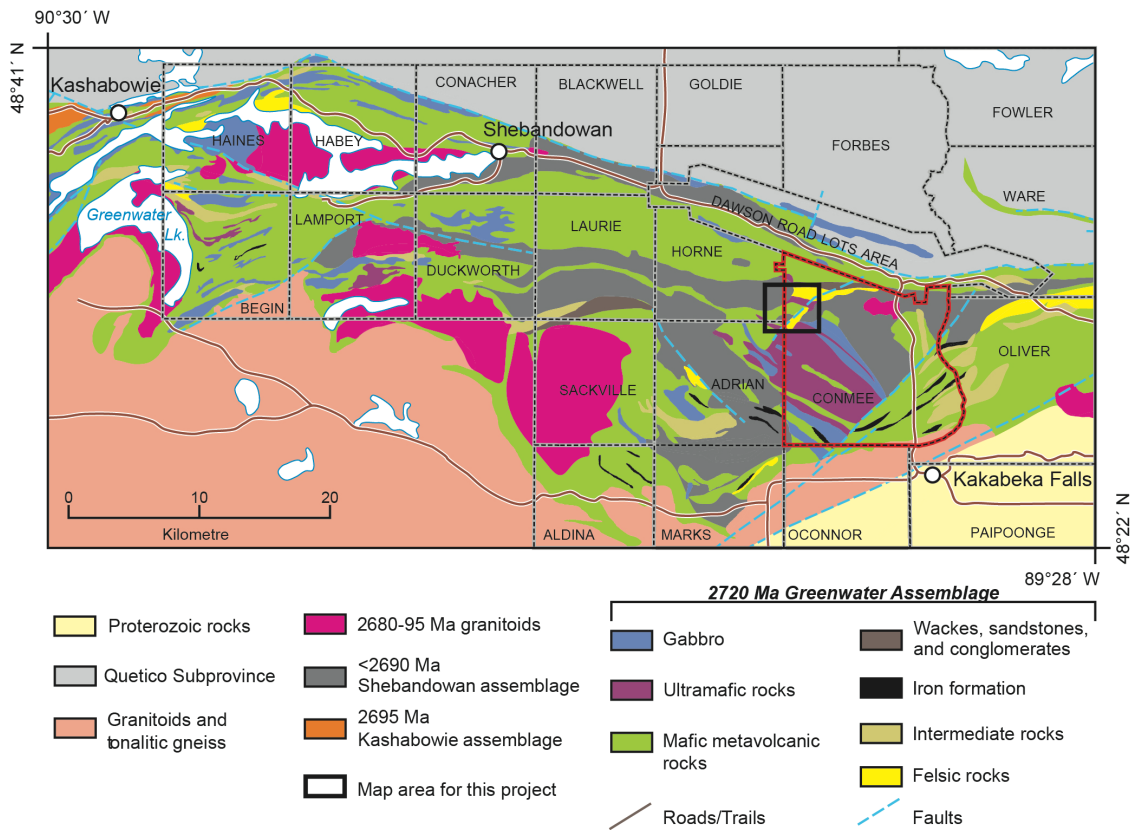


Figure 1.1 Regional geology map showing the location of Conmee Township (outlined in red) in relation to the Shebandowan greenstone belt, with field area outlined in black. Bedrock geology modified from Santaguida (2001a, 2001b) and Lodge et al. (2015).

1.3 Komatiites

Komatiites are extrusive ultramafic rocks that were erupted at temperatures of about 1600° (Dostal, 2008; Arndt et al., 2008). They are found mainly in the Archean (with a few notable exceptions such as a Cretaceous occurrence on Gorgona Island; Kerr et al., 1996; Arndt et al., 2008), when the Earth’s mantle temperature was significantly hotter than present day. Komatiites are defined by both geochemistry and textures in order to distinguish them from other ultramafic rocks.

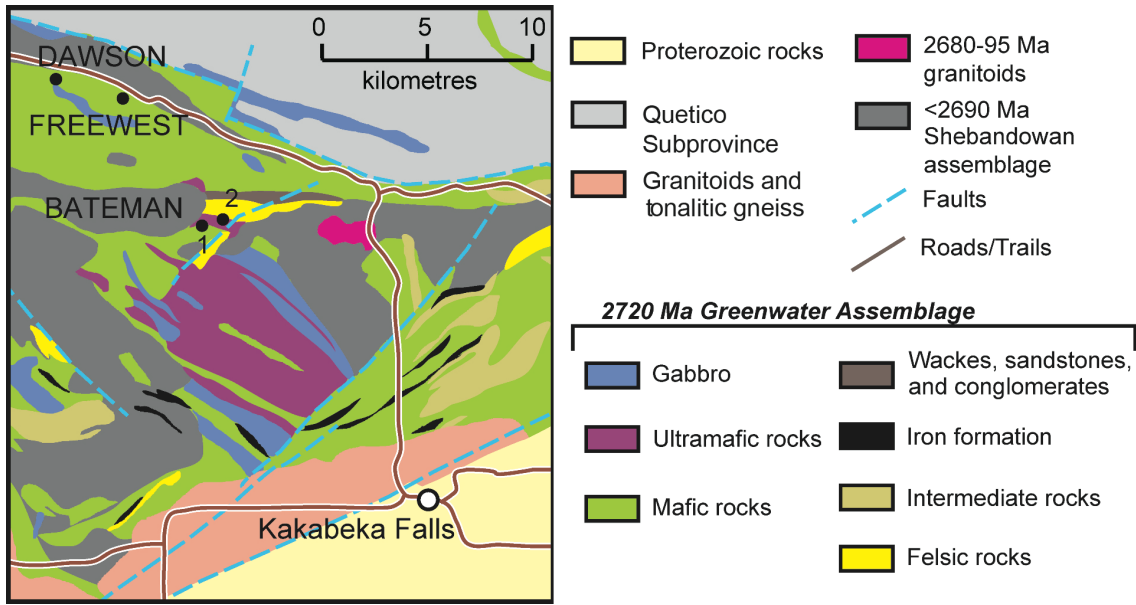


Figure 1.2 Location of the four sampled trench sites (geology modified from Santaguida, 2001a,b)

Komatiites can be chemically distinguished from other rock types by MgO contents greater than 18 wt. %, and 40-45% wt. % SiO₂. The distinct textural requirement for a rock to be a komatiite is the presence of spinifex texture (Arndt et al., 2008).

Spinifex is a texture that has been long believed to be present only in komatiitic rocks, but recently there have been other rock types identified with a spinifex-like texture such as basaltic komatiites and SHMB (O'Driscoll et al., 2006). Spinifex is formed through undercooling of hot, magnesium-rich lava. Komatiites erupt at temperatures greater than 1600° C, with a thermal gradient (difference between the liquidus and the solidus of the melt) of 500° C. This thermal gradient causes undercooling of the magma, resulting in crystallization below the liquidus; this produces a delay in nucleation of olivine grains and results in the melt being in disequilibrium (Dostal, 2008).

There are two main types of komatiites are Al-depleted komatiites (ADK) and Al-undepleted komatiites (AUK). Aluminum-depleted komatiites have a low

$\text{Al}_2\text{O}_3/\text{TiO}_2$ ratio (<12), a $\text{CaO}/\text{Al}_2\text{O}_3$ ratio of 2-2.5 and fractionated heavy rare earth element patterns on a multi-element spider diagram; they are interpreted by Herzberg (1995) to have formed at depths of around 300-450 km and approximately 30% partial melting. Aluminum-undepleted komatiites have a higher $\text{Al}_2\text{O}_3/\text{TiO}_2$ ratio (~ 20), a $\text{CaO}/\text{Al}_2\text{O}_3$ ratio of 1 and flat heavy rare earth element patterns on a multi-element spider diagram; they are interpreted by Herzberg (1995) to have formed at depths of around 150-200 km and approximately 50% partial melting.

Arndt et al. (1977) and Pyke et al. (1973) have compiled idealized stratigraphic columns of komatiite flows, showing relative thicknesses and positioning of various textural changes within the flow. These stratigraphic columns depict the changes in textures based on the undercooling of the flow. It is not possible to create a universal stratigraphic column, as every flow will differ in some ways, but one example from Pyke et al. (1973) shows the textural differences listed in groups A_1 to B_4 (Fig. 1.3). The top of the flow is section A_1 , which comprises ~ 1 -10 cm thick chilled margins and flow tops followed by fractures and polyhedral jointing caused by the contraction of the lava as it cools and solidifies (Pyke et al., 1973); these polyhedral joints are analogous to columnar jointing in basalt. The section below this is A_2 where the spinifex texture is generally present. At the top of this section the spinifex is seen as chaotic, short, and thin, but moving downwards and approaching the B layer, it becomes oriented vectoring to the bottom of the flow; the spinifex here is parallel, long, and thicker (Pyke et al., 1973). B_1 is a thin layer (2-5cm) that consists of elongate olivine grains with an orientation that is parallel to

the layers in the flow. Moving downwards, the preferred orientation becomes less obvious in sections B₂ – B₄ (Pyke et al., 1973). Sections B₂ – B₄ consist of olivine cumulate layers that comprise a peridotite of varying grain sizes (fine- to medium-grained) as well as what Pyke et al. (1973) described as a “knobby peridotite” section (B₃ of the flow) where “knobs” of pyroxene glass accumulate and resist weathering.

1.4 Siliceous High-Magnesium Basalt

Siliceous high-magnesium basalts (SHMB) are a distinct class of volcanic rocks that occur most commonly at the Archean-Proterozoic boundary; even in Archean greenstone belts, they are considered rare (Sensarma et al. 2002; Srivastava, 2006, 2008; Srivastava et al. 2010; Peng et al. 2013). Redman and Keays (1985) first described these rocks from Western Australia in their classification of different basalt types based on magnesium content (low magnesian series basalt, high magnesian series basalt and siliceous high magnesian series basalt). The geochemistry of SHMB is distinct as they have SiO₂ contents of 51-55 wt%, and MgO contents within or above the range for average basalts (>8 wt%), this is accompanied by low HFSE contents and low TiO₂ (<0.5%; Redman and Keays, 1985; Sun et al., 1989; Smithies, 2002; Gao and Zhou, 2013; Sensarma et al., 2002; Peng et al., 2013).

The origin of SHMB has been a controversial and hotly debated topic since their discovery; their similarities to boninites, close spatial association to komatiites, and lack of modern-day analogues further complicate their origin (Sun et al., 1989; Sensarma et al., 2002; Peng et al., 2013; Zhao and Zhou, 2013).

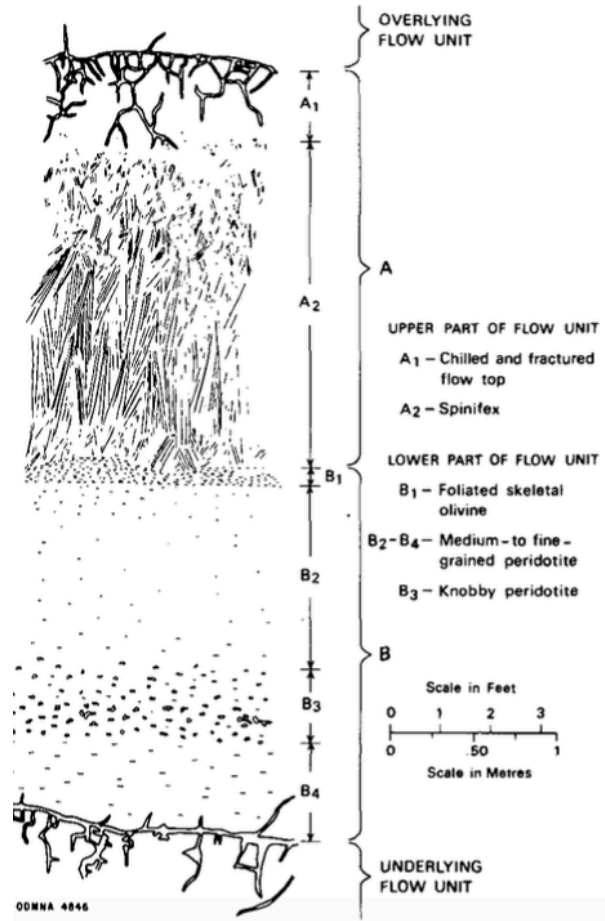


Figure 1.3 Idealized section of a komatiite flow displaying textural changes (from Pyke et al., 1973)

There are two main theories for their petrogenesis: 1) SHMB are derived from komatiite magmas through crustal assimilation and fractional crystallization (AFC) processes or 2) they are Archean equivalents of Phanerozoic boninites that are derived from subduction-modified refractory continental lithospheric mantle (Peng et al., 2013).

The AFC model has been described in detail by Sun et al. (1989) and accounts for many of the distinct characteristics of SHMB. Assuming a komatiitic source for SHMB, the magma would have a sufficient amount of heat to undergo substantial crustal contamination upon ascent and differentiation in a magma chamber

(Campbell, 1985; Huppert and Sparks, 1985; Crawford et al., 1989; Sensarma et al., 2002). Sensarma et al. (2002) proposed that in order for the SHMB to have anomalously high silica contents, the wall rock being assimilated would have to be at least 75 wt% SiO₂. Sensarma et al. (2002) also state that the unique characteristics of SHMB cannot be generated solely from a primary mantle-derived magma; this implies that additional processes need to be involved in the genesis of SHMB.

The subduction model explains SHMB in the context of boninite petrogenesis with adjustments to account for the changes in geochemistry that make these rock types distinct. Peng et al. (2013) state that the LILE and LREE enrichment in SHMB combined with the HFSE depletion and siliceous nature are a result of the melting of the metasomatically enriched lithospheric mantle. They are separated from Phanerozoic boninites partially based on a lack of relative Zr enrichment and U-shaped REE patterns (Sun et al., 1989; Peng et al., 2013). SHMB are distinct from boninites in their geochemical signatures as well as differing implications for petrogenesis. In order to account for the differences between boninites and SHMB (SHMB have enriched Th and La, higher Th/La, Th/Nb, and Th/Yb ratios, absence of U-shaped REE patterns and large positive Zr anomalies), there needs to be a specific circumstance that alters the subduction process enough to cause these differences (Elliot et al., 1997; Sensarma et al., 2002; Peng et al., 2013). Peng et al. (2013) proposed that slab rollback during subduction allows for a depleted and refractory mantle, metasomatized by adakitic melts/fluids, which causes the SHMB to form instead of adakitic or boninitic rocks.

1.5 Boninites

Boninites are high-magnesian, high silica rocks that are products of high temperature (1000-1300° C), low pressure (<10 kbar) second stage partial melting of a hydrous, depleted refractory mantle source above subducted oceanic lithosphere at convergent plate boundaries (Crawford et al., 1989; Pearce et al., 1992; Polat and Kerrich, 2004). Melting of the mantle wedge by dehydration of a subducting slab is accelerated by solidus depression owing to the presence of subduction-derived fluids as well as steep geothermal gradients (Crawford et al., 1989; Polat and Kerrich, 2004).

Boninites are characterized by MgO of 7-18 wt %, SiO₂ of >53 wt %, low TiO₂ (<0.5 wt %) and Zr, high Al₂O₃/TiO₂ ratios and distinctive U-shaped patterns on a chondrite-normalized REE spider diagram (Crawford et al., 1989; Polat and Kerrich, 2004). They form in a variety of tectonic settings including: forearc regions of intra-oceanic island arcs (Pearce et al., 1992), Phanerozoic and Proterozoic supra-subduction zone ophiolites (Wyman, 1999), and continental margin arc-backarc magmatic systems (Piercy et al., 2001). They are also found in Archean greenstone belts (Kerrich et al., 1998). Boninites are an important rock type for delineating the emergence of subduction zones as they typically form in the proto-arc stages of subduction (Crawford et al., 1989). Crawford et al. (1989) have argued that boninites are derived from a refractory mantle source as opposed to a fertile mantle source typical for tholeiites.

1.6 Structure of the Thesis

This thesis consists of a summary of the regional geology surrounding the study area and the methods used to investigate the petrogenesis of these rocks. The detailed mapping completed in the summers of 2015 and 2016 is discussed and explained including lithology descriptions, trench map summaries and regional map summaries to investigate the relationships between the broad area and specific locations of assimilation. Geochemistry was used to investigate the nature and petrogenesis of these rocks including whole rock geochemical data and Sm-Nd isotopes. The discussion investigates whether the ultramafic rocks are komatiites, SHMB, or another rock type and uses that information to propose a model for the tectonic evolution of this portion of the Superior Province.

Chapter 2: Regional Geology and Mineralization

2.1 The Superior Province

One of the Earth's largest exposed Archean cratons, the Superior Province is located in the central part of North America (Fig. 2.1). It is bounded to the north and west by the Trans-Hudson orogen, to the east by the New Quebec orogen, to the south by the Penokean orogen and to the southeast by the Grenville orogen (Card, 1990).

Card and Ciesielski (1986) subdivided the Superior Province into volcano-plutonic, metasedimentary, plutonic, and high-grade gneiss subprovinces using the criteria of lithology, metamorphism, structure, geophysics and metallogenetic characteristics, as well as ages of rock units and tectonic events. The high-grade gneissic subprovinces are generally characterized by upper amphibolite to granulite gneisses of supracrustal and plutonic origins (Card, 1990), whereas the volcano-plutonic subprovinces comprise low-grade greenstone belt sequences consisting of metavolcanic and metasedimentary rocks commonly surrounded and intruded by granitic batholiths (Card, 1990). The metasedimentary subprovinces consist mainly of supracrustal sedimentary rocks that have undergone low-grade greenschist to lower amphibolite metamorphism (Card and Ciesielski, 1986). The plutonic subprovinces are characterized by a distinct lack of supracrustal packages and intrusive and extrusive volcanic rocks (Card and Ciesielski, 1986).

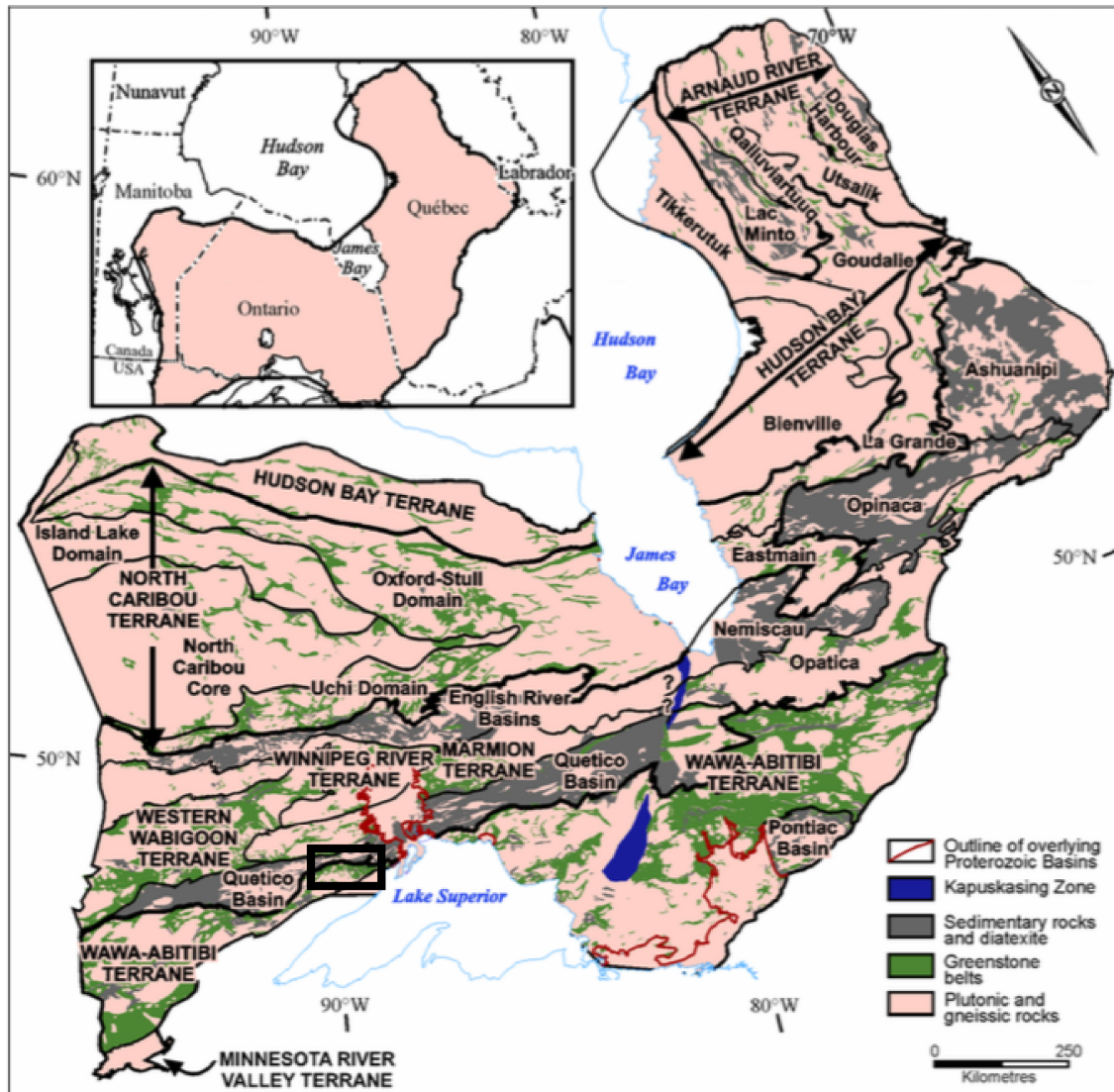


Figure 2.1 Map of the Superior Province, showing the updated terranes and domains (from Stott et al., 2010). Black box approximately indicates location of study area.

The subdivision boundaries are generally defined using structural and metamorphic transitions such as metamorphic facies, fault zones or changes in structural trend and style (Card, 1990). Stott et al. (2010) have revised the subdivisions proposed by Card and Ciesielski (1986). The new classification scheme proposed four different categories: 1) superterrane - an amalgamation of two or more terranes before the Neoproterozoic assembly of the Superior Province; 2) terrane

- a tectonically bounded region with internal characteristics distinct from those in adjacent regions prior to the Neoproterozoic assembly of the Superior Province; 3) domain - a typically younger, lithologically distinct part of a terrane, but with either juvenile crust or sharing a common basement; 4) tectonic or tectonostratigraphic assemblage - distinct in time, lithology and tectonic setting and composed of one or more stratigraphic groups or formations (Fig. 2.1; Stott et al., 2010).

Rocks of the Superior Province have been determined to range from about 3.1 Ga to 2.6 Ga, with evidence for major magmatic periods at approximately 3.0 Ga and 2.7 Ga (Card, 1990; Corfu and Stott, 1998; Stott et al., 2010; Percival, 2007; Percival et al., 2006; Percival et al., 2012). During these periods of magmatism tholeiitic, calc-alkalic, komatiitic and alkalic volcanic rocks, as well as volcanogenic clastic rocks were deposited (Card, 1990).

2.2 The Wawa-Abitibi Terrane

The Wawa-Abitibi terrane of the Superior Province contains both the Wawa and Abitibi subprovinces that are separated by the Kapuskasing structural zone (Fig. 2.1; Percival, 2007). It consists of Archean greenstone belts and Tonalite-Trondhjemite-Granodiorite. The terrane is bounded to the north by a tectonic contact with the structurally overlying Quetico terrane, which consists of Archean metasedimentary rocks (Williams et al., 1991). The Wawa-Abitibi terrane is bounded to the south by rocks of the Animikie basin (Williams et al., 1991).

There are two main clusters of greenstone belts in the Wawa-Abitibi terrane - one occurring in the Gamitagama-Mishibishu-Michipicoten region and the second at the northern boundary with the Quetico terrane. Greenstone belts in the first region

include: Gamitagama, Mishibishu, Michipicoten, Dayohessarah-Kabinakagami, Manitouwadge-Hornpayne, Schreiber-Hemlo, with the Shebandowan and Saganagons greenstone belts in the second region (Williams et al., 1991). The major granitic bodies that separate the two clusters are the Pukaskwa and Black-Pic batholiths in the eastern portion of the terrane (Williams et al., 1991). The age of the Wawa-Abitibi terrane is constrained to 2.89-2.68 Ga; based on ages from the earliest known assemblage (Hawk assemblage), and the youngest assemblage (Lake Vermillion formation; Percival, 2007; Lodge et al., 2013). The greenstone belts in the Wawa-Abitibi terrane generally consist of komatiite, basalt, dacite, and rhyolite as well as metasedimentary rocks, that all have undergone at least greenschist facies metamorphism (Williams et al., 1991). The metasedimentary rocks within the greenstone belts consist mainly of turbiditic wacke and to a lesser extent conglomerate and iron formation (Williams et al., 1991).

Williams et al. (1991) found that the grade of metamorphism is not homogeneous throughout the terrane, and that the changes correlate to the ratio of supracrustal and plutonic rocks; smaller greenstone belts with more granitoid intrusions associated with them have a higher grade of metamorphism than large greenstone belts with fewer associated granitoid intrusions. The highest grade of metamorphism found within the Wawa-Abitibi terrane is granulite facies and is found within the Manitouwadge-Hornpayne greenstone belt directly south of the Quetico terrane boundary; the lowest grade of metamorphism (within a greenstone belt) is lower greenschist facies and is found with the Michipicoten greenstone belt (Williams et al., 1991).

2.3 The Shebandowan Greenstone Belt

The two main greenstone belts in the western portion of the Wawa terrane are the Shebandowan and the Saganagons greenstone belts, which have been interpreted by Corfu and Stott (1998) to be a single succession of supracrustal rocks. The Shebandowan greenstone belt extends from Lake Superior in a southwest direction, where it transitions into the Saganagons greenstone belt.

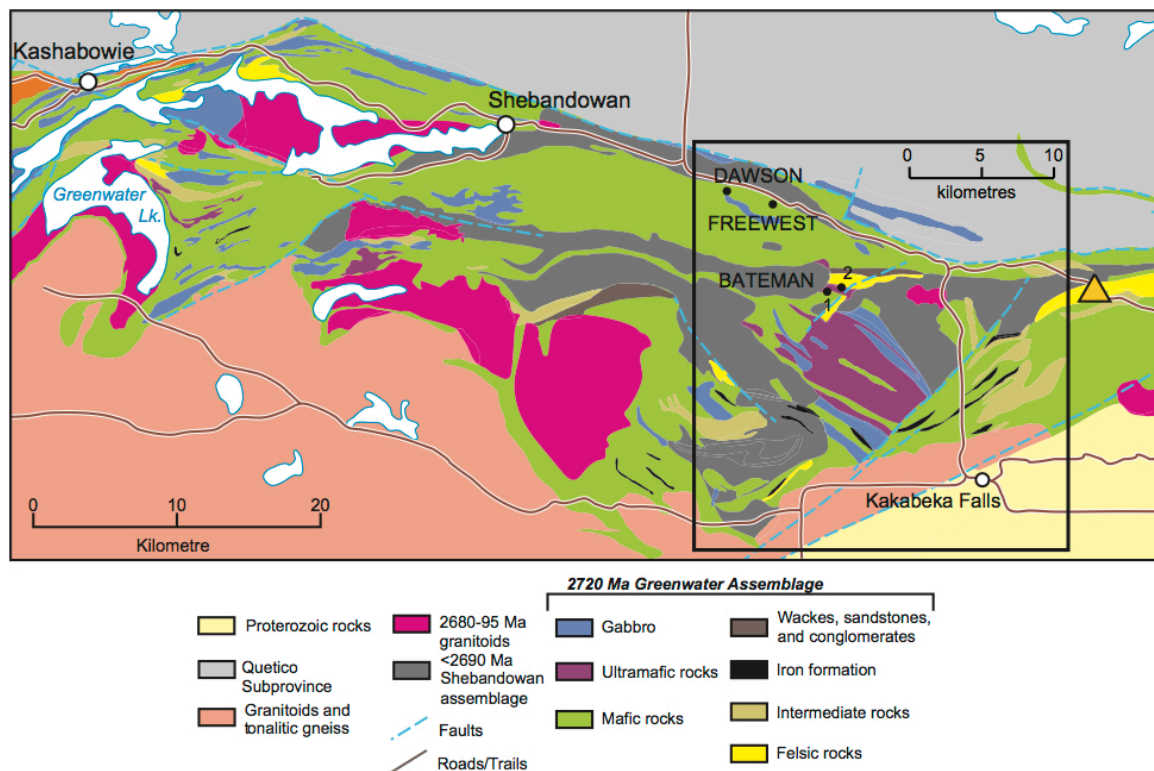


Figure 2.2 Regional geology map of the Shebandowan greenstone belt. Study area outlined in black. Bedrock geology modified from Santaguida (2001a, 2001b) and Lodge et al. (2015).

Within the Lake Superior region, Proterozoic rocks overlay the area southeast of the Shebandowan greenstone belt, including rocks of the Animikie Basin and Keweenawan volcanic and gabbroic complexes associated with the Midcontinent Rift (Williams et al., 1991).

The Shebandowan greenstone belt has been divided into three main volcanic assemblages based on geochronological studies by Corfu and Stott (1998) and Lodge (2012); namely, the Greenwater assemblage (circa 2719.7 ± 1.0 Ma; based on $^{207}\text{Pb}/^{206}\text{Pb}$ dating of four zircons in a massive felsic flow), the Kashabowie assemblage (circa 2693.87 ± 0.87 Ma; based on $^{207}\text{Pb}/^{206}\text{Pb}$ dating of four zircons in a bedded felsic tuff and crystal tuff) and the Shebandowan assemblage (circa 2690 to 2680 Ma; based on detrital zircons analyzed from various sedimentary units). The Greenwater assemblage consists of tholeiitic basalts, basaltic komatiites, komatiite flows, intermediate and felsic extrusive volcanic rocks and pyroclastic flows, as well as banded iron formation, wackes, sandstones and conglomerates (Williams et al., 1991; Corfu and Stott, 1998; Lodge, 2012). The Kashabowie assemblage consists of calc-alkalic diorite sills, intermediate volcanic rocks, heterolithic volcanoclastic debris flows, and feldspar porphyry dikes (Corfu and Stott, 1998; Lodge et al., 2013). Finally, the Shebandowan assemblage consists of calc-alkalic to alkalic mafic to felsic volcanic rocks and clastic sedimentary rocks including argillite, wacke, turbiditic wacke, iron formation, sandstone, conglomerate, and volcanic breccia (Williams et al., 1991; Corfu and Stott, 1998; Lodge, 2013). These three assemblages are interpreted by Williams et al. (1991) to be the product of subaqueous to locally subaerial arc volcanism and subsequent sedimentation.

2.4 Previous Work

The first mapping in the region was carried out by Bell in 1872 for the Geological Survey of Canada (Bell, 1873). Following this, Tanton completed a full township-wide mapping program in 1924, focusing on the eastern portion of the Matawin Iron Range (Tanton, 1924). In 1980, Parker mapped the Finmark sedimentary rocks as part of an honours thesis, focusing on structure and stratigraphy (Parker, 1980). Brown further expanded upon this work in 1985 in a Master's thesis, which entailed further mapping and structural studies (Brown, 1985). Carter (1990) completed mapping of the Conmee and Forbes townships in 1986. More recently, the Ontario Geological Survey began a multi-year bedrock geology mapping project to remap the eastern part of the Shebandowan greenstone belt and to provide an updated interpretation of the regional geology (Lodge, 2012; Lodge et al., 2013, 2014; Ratcliffe, 2015). Sackville, Aldina, Adrian, and Conmee townships have been partially to completely remapped since 2013 (Lodge, 2013; Lodge et al., 2014; Ratcliffe, 2015).

There has been increasing interest in both gold and nickel-copper mineral potential in Conmee Township (MacLean and Rees, 2008; Clark, 2011a and b). Gold was described in the brecciated metavolcanic unit and syenite intrusion of the Tower Mountain property formerly held by ValGold Resources Ltd. (Jobin-Bevans et al., 2006; Lodge et al., 2014). The Bateman property was passed from Kwiatkowski Prospecting to Linear Metals in 2008 and then to Denalii Resources in 2011. It has been examined for nickel-copper-gold mineralization in the ultramafic flows and associated conglomerates. Linear Metals completed a trenching and sampling

program in 2008 with follow-up sampling by Denalii Resources in 2011 (MacLean and Rees, 2008; Clark, 2011a). The past-producing Shebandowan mine is located approximately 35 km west of the study area. The Shebandowan mine was active from 1972 until 1998 producing Ni, Cu and PGE's. Inco Shebandowan Mine produced 8.64 million tons grading 1.92% Ni, 0.98% Cu and 2.62 g/t PGE (Schnieders et al., 2000). The ore body sits at the contact of an ultramafic intrusion with a Mg-rich basalt unit (Morton, 1979).

Chapter 3: Methodology

3.1 Regional and Trench Mapping

The majority of trench mapping took place in the summer of 2015 with follow up work in 2016 by a research team led by the author. Linear Metals dug the trenches in 2008 during exploration for Ni-Cu-PGE mineralization, focusing on areas of assimilation between the ultramafic units and sedimentary strata. There are two main trench sets, named by Linear Metals as Series 1 and Series 4, which are approximately 1 km apart (Fig. 3.1).

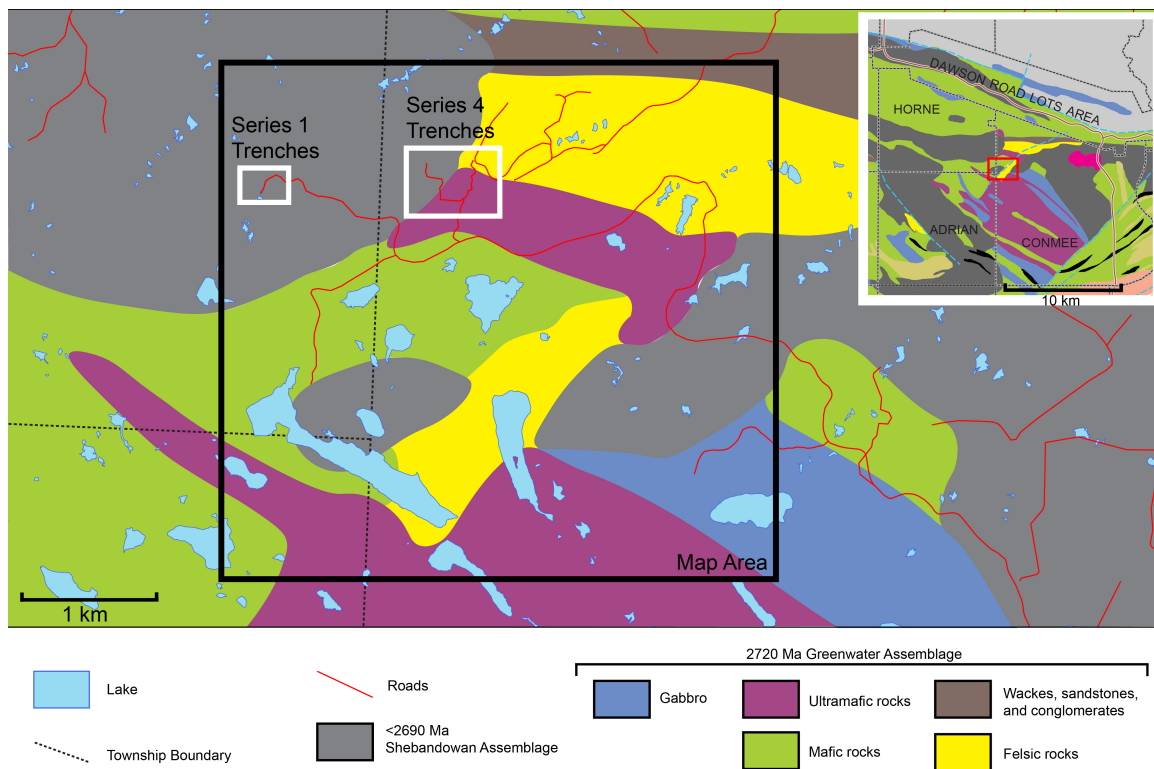


Figure 3.1 Detailed geology map of the thesis area. Area mapped during this project outlined in black. Series one and series four trenches outlined in white. Inset map is the surrounding area showing the townships surrounding the map area. Bedrock geology modified from Santaguida (2001a, 2001b) and Lodge et al. (2015).

During the summer of 2016, mapping of a 16 km² area was completed, in order to give context to the assimilation textures seen in the trenches, determine the

petrogenesis of the ultramafic rocks and to link this to the tectonic evolution of the region. During the mapping project 35 traverses were completed, 163 stations were noted, and 124 samples were taken from the 16 km² area. Magnetic susceptibility was measured using a magnetic susceptibility meter. Approximately 10 measurements were taken per outcrop and then averaged. This data was collected in SI units.

3.2 Petrography

Forty samples were selected for petrography and polished thin-sections were prepared at Lakehead University. Twenty samples were selected from the 2015 trench mapping project and 20 samples from the 2016 regional mapping. Once the polished thin-sections were completed, detailed petrography was undertaken using transmitted light microscopy to define the mineralogy, textures, alteration, constrain the rock names, and to complement the corresponding geochemistry.

3.3 Geochemistry

One hundred and thirty five samples were sent to Ontario Geoscience Laboratories in Sudbury, Ontario where they underwent a full suite of geochemical analysis. Before the samples underwent analysis they were prepared by ball mill sample preparation using Al-Oxide bowls; the samples were pulverized in a 99.8% pure aluminum oxide (Al₂O₃) planetary ball mill. Loss on ignition was determined by heating samples to 105 °C under nitrogen atmosphere and then further at 1000 °C under oxygen atmosphere while weight loss was measured. The calcined samples were then fused with a borate flux to produce a glass bead for analysis. Major and chosen trace elements were analyzed using wavelength dispersive X-ray

Fluorescence spectrometry with an XRF-PANalytical instrument. Major elements were analyzed as borate fused glass discs and trace elements were analyzed as pressed powder pellets. Detection limits for major elements were 0.1 weight % and relative standard deviations of duplicate analyses were within 2%. Samples for trace and rare earth elements underwent a closed vessel multi-acid digestion by a solution of HCl, HF, and HNO₃, and were then analyzed on a PerkinElmer Elan 9000 Inductively Coupled Plasma-Mass Spectrometer. Regular procedures of Ontario Geoscience Laboratories were followed during these analyses, including the use of standards, blanks, and duplicates of samples.

After the geochemical data was obtained, the data was normalized to anhydrous values and trace element geochemistry was normalized to primitive mantle values for use on primitive mantle normalized trace element plots. After this was completed, plots were generated with ioGAS software.

3.4 Sm-Nd Isotopes

Six samples were sent to Memorial University of Newfoundland in St. John's for Sm-Nd isotope analyses. The samples were analyzed using a Finnigan MAT 262V TI-mass spectrometer within a class 100 clean lab complex. Whole rock powders were dissolved in Savilex Teflon capsules using an 8 ml (4:1) mixture of 29 M HF–15 M HNO₃. Prior to acid digestion, a mixed ¹⁵⁰Nd/¹⁴⁹Sm spike was added to each sample. After five days of acid digestion on a hotplate, the solution was then evaporated to dryness, and rehydrated in 6M HCl for 4-5 days. The samples were dried and then re-dissolved in 2.5M HCL. Samples were then loaded into a column

containing cation exchange resin AG-50W-X8, H⁺ form, 200-400 mesh. This bulk solution was then dried and taken up in 0.18 M HCl and loaded on a second column containing Eichrom© Ln resin (50-100 mesh) to separate Sm and Nd from the other REEs. Analyses of the USGS standard BCR-2 yielded Nd = 27.58 ppm, Sm = 6.31 ppm, and $^{146}\text{Nd}/^{144}\text{Nd} = 0.512637 \pm 5$ (n= 19). The international La Jolla standard produced: $^{143}\text{Nd}/^{144}\text{Nd} = 0.512096 \pm 9$ (n=20) (Feb–Oct 2017) and an internal lab standard = 0.512100 ± 8 (n=214) (Oct 2010-present).

Chapter 4: Results

4.1 Lithology Descriptions

A northeast trending fault was the only major structure observed in the field area; this fault corresponds to a linear magnetic anomaly on the airborne magnetic geophysical map of the area (Ontario Geological Survey, 2003; Fig. 4.1). Evidence for the fault was seen in a conglomerate outcrop in only one location, where the increased strain was observed within cobbles. This fault is interpreted to extend through the field area based on the geophysical data (Ontario Geological Survey, 2003).

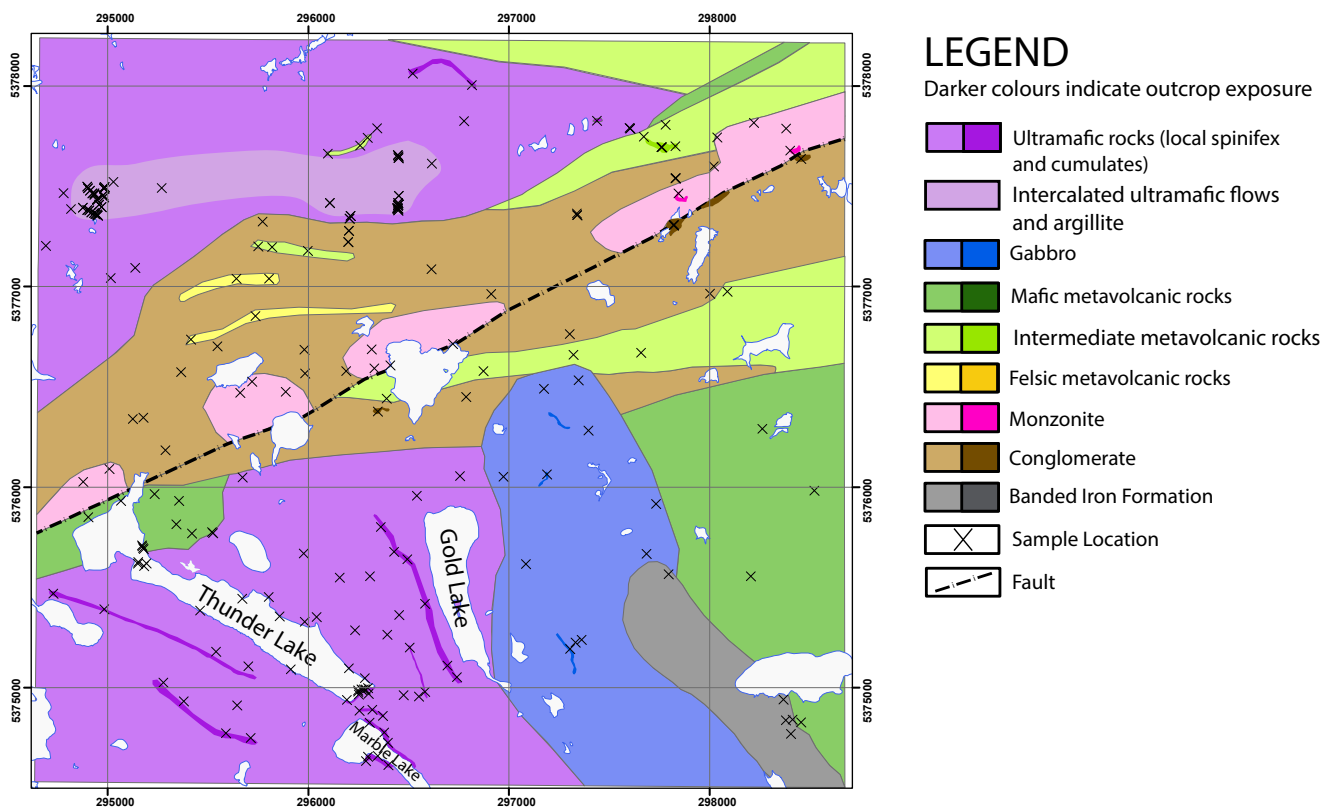


Figure 4.1 Geology map of the study area based on data collected summer 2016.

4.1.1 Orthocumulate Ultramafic Rocks

These ultramafic rocks occur throughout the northern and southern portion of the map area as dark black rocks, usually light green on a fresh surface, as a product of serpentine alteration of olivine (Fig. 4.1). These rocks are highly magnetic, with magnetic susceptibility readings from 20 to 150 $\times 10^{-3}$ SI. In some areas they occur as fine-grained, massive rocks with no distinct textures (Fig. 4.2 A). They also occur as medium-grained dark black rocks with a cumulate texture (Fig. 4.2 B) of euhedral minerals that now consists entirely of serpentine, magnetite, and talc; this mineralogy accounts for the strongly magnetic nature of the rocks, as well as the softness, as they scratch readily. These rocks occur along ridges near Gold and Thunder lakes (Fig. 4.1); the ultramafic rocks also occur in the northern portion of the map area, where they are seen intercalated with sedimentary units including argillite and chert layers (Fig. 4.2 C), or as thick ridges with no observed contacts with adjacent lithologies. As no contact relationships were observed, these rocks might be peridotites or the olivine cumulate layer of a thick komatiitic flow. The orthocumulate ultramafic rocks consist of medium-grained relict olivine crystals displaying a cumulate texture, which have been entirely replaced by serpentine (Fig. 4.3 A, B). In several of these samples, there is a network of thin calcite veins separating the serpentine crystals (Fig. 4.4 A, B). Magnetite occurs in all samples as fine-grained, subhedral crystals, which results in the high magnetic susceptibility readings. The thin section TL-16-SH-057 consists of 85% serpentine, 5% magnetite, 5% pyroxene, and 5% chlorite; this sample is characteristic of the orthocumulate ultramafic lithology.

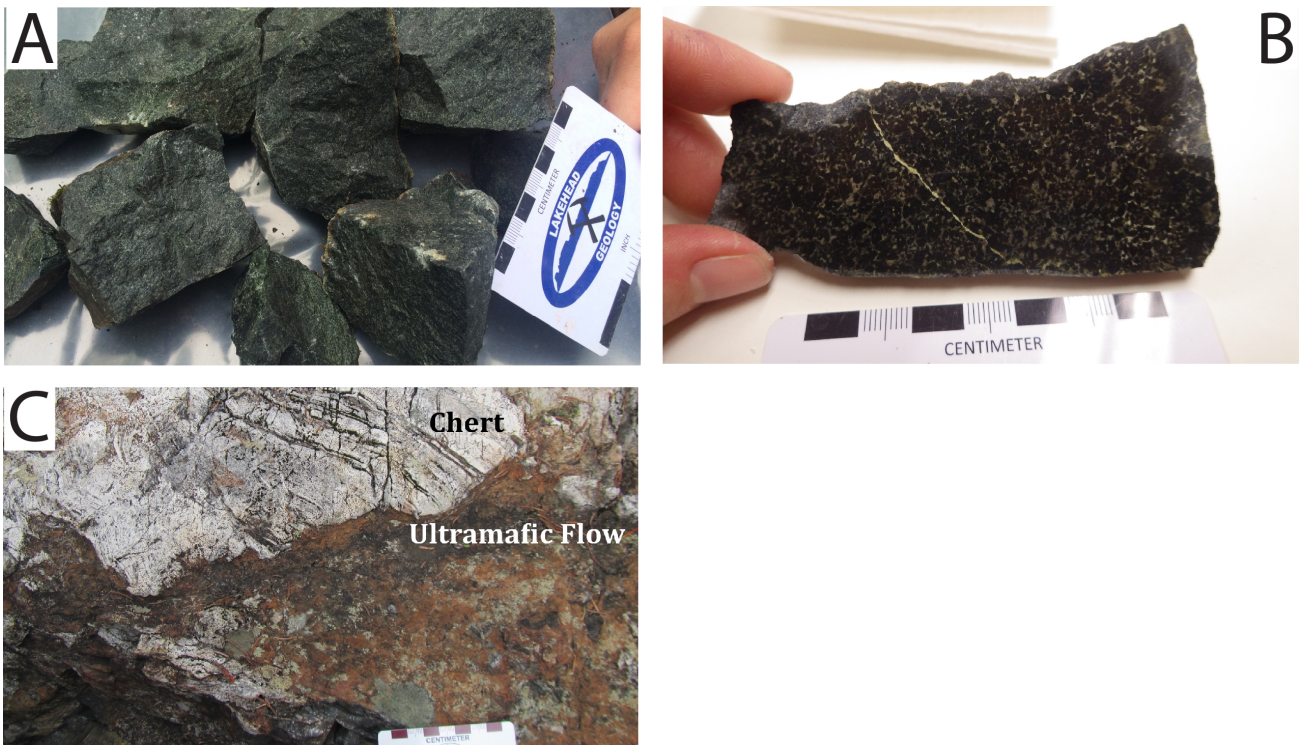


Figure 4.2 Photographs of field samples and outcrops. A) Massive peridotite (TL-16-SH-034); B) Cumulate texture in peridotite (TL-16-SH-057); C) Ultramafic flow intercalated with chert (Trench 4A).

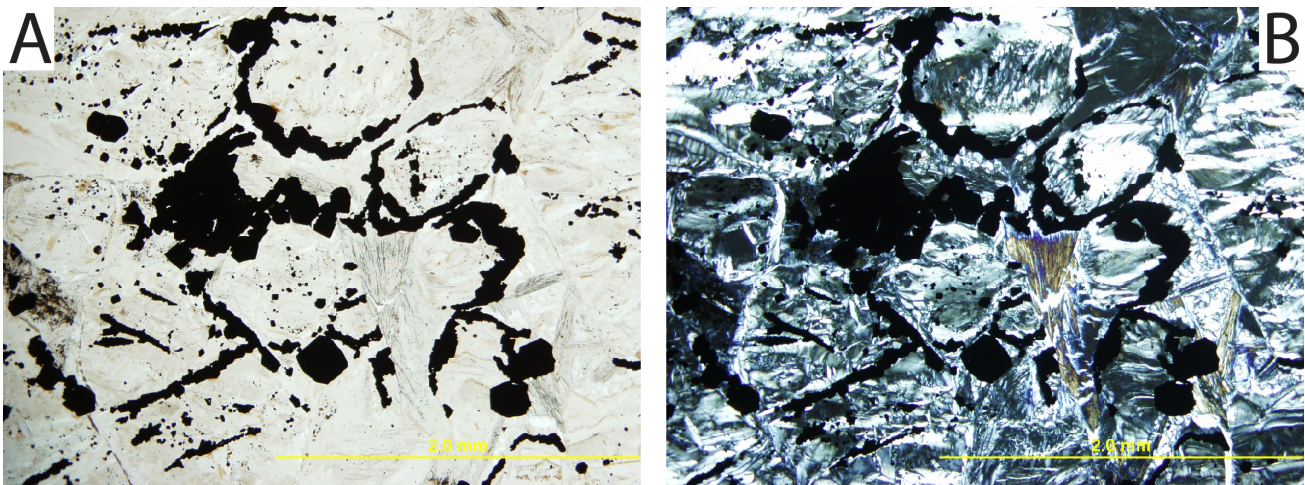


Figure 4.3 A) Photomicrograph of relict olivine cumulate texture and magnetite within orthocumulate ultramafic rock in PPL B) Photomicrograph of relict cumulate texture completely serpentinized in XPL (sample TL-16-SH-057).

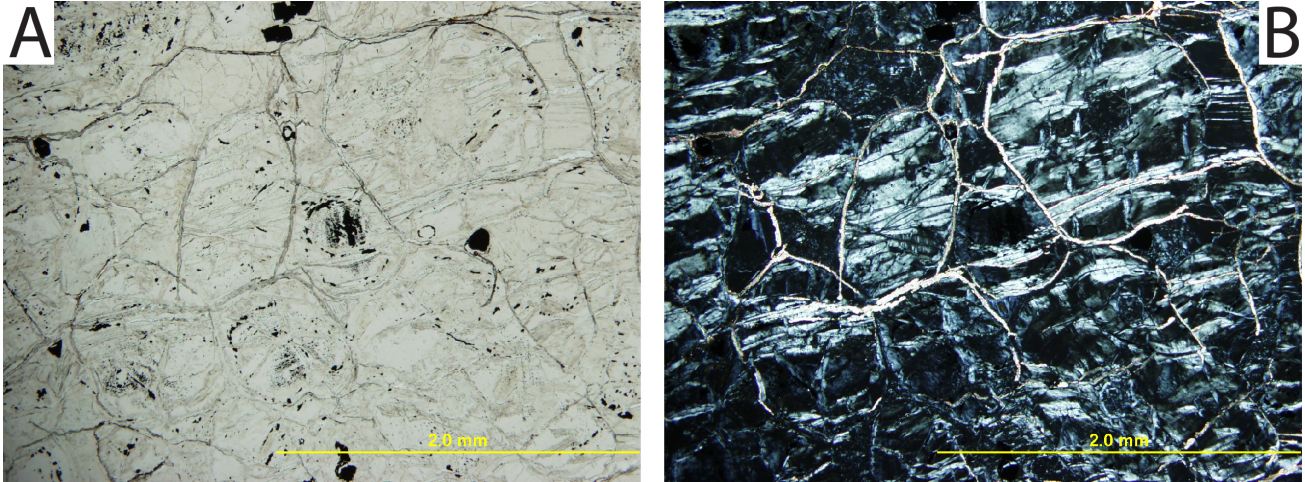


Figure 4.4 A) Photomicrograph of relict olivine cumulate texture with calcite interstitially between crystals in PPL B) Photomicrograph of relict olivine cumulate texture completely serpentinized with calcite interstitially between crystals in XPL (sample TL-16-SH-071).

4.1.2 Komatiites

Spinifex textured komatiites were seen throughout the study area in both the northern and southern portions (Fig. 4.1). Overburden has obscured the majority of lithological contacts; consequently the outcrops are difficult to correlate.

Komatiites occur as fine-grained, light grey, highly silicified rocks (Fig. 4.5 A). Several types of spinifex texture were observed throughout the field area. The first being chaotic spinifex with thin (0.05-1 mm thick and ~1-3 cm long) randomly oriented crystals (Fig. 4.5 B). The needles are darker grey than the groundmass, and sometimes difficult to distinguish on a fresh surface; weathered surfaces show spinifex texture more distinctly as the needles have preferentially weathered away. The second type of spinifex was chaotic spinifex with thick crystals, which was only seen at one location at the south end of Thunder Lake (Fig. 4.5 C). It consists of 1 cm thick spinifex crystals with lengths up to 20 cm. The final type of spinifex encountered during mapping was oriented spinifex (Fig. 4.5 D). It was seen at the north end of Thunder Lake, as well as along the northern edge of Marble Lake (Fig.

4.1). In outcrop there is very little interstitial matrix and the spinifex needles comprise the majority of the rock (Fig. 4.5 E). Magnetic susceptibility varied from 0.32 to 68×10^{-3} SI.

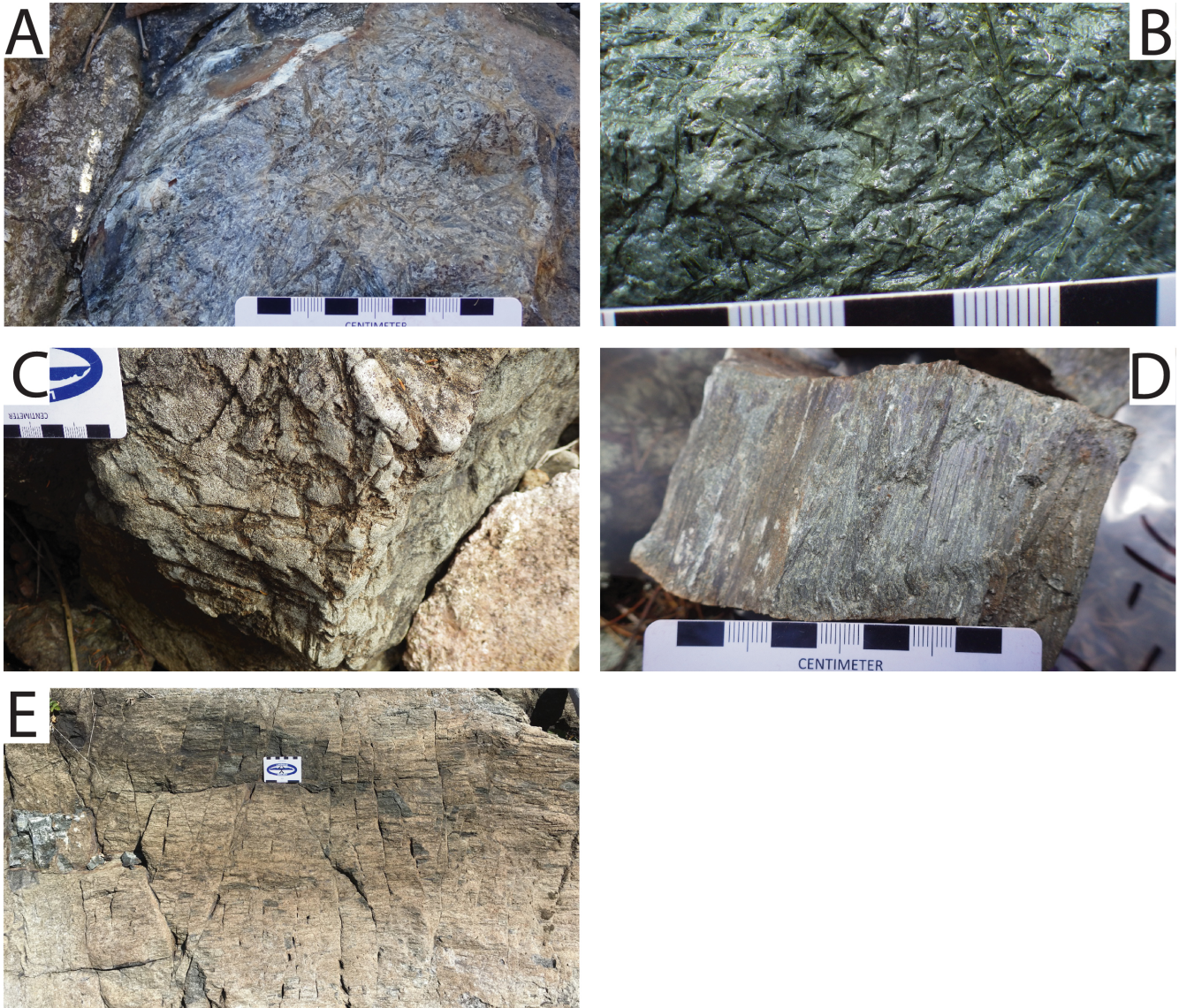


Figure 4.5 Photographs of field samples and outcrops taken during mapping. A) Siliceous komatiite (Trench 1E); B) Chaotic spinifex texture in komatiite (TL-16-SH-070); C) Thick chaotic spinifex texture in komatiite (TL-16-SH-117); D) Oriented spinifex (TL-16-SH-073); E) Oriented spinifex in outcrop (TL-16-SH-119).

Petrographic analysis shows that the komatiites displayed varying degrees of carbonitization, as well as lesser serpentinization. In some samples, spinifex needles

have been altered to calcite (Fig. 4.6), while in others they are altered to talc and chlorite rimmed with iddingsite (Fig. 4.7). In one sample from the north end of Thunder Lake and in one trench in the northern portion of the field area, pyroxene spinifex was found (Fig. 4.7). Sample TL-16-SH-070 is a characteristic example of chaotic spinifex in a komatiite; the thin section consists of 60% serpentine, 15% chlorite, 15% iddingsite and 10% talc. The groundmass surrounding the spinifex needles is finer skeletal serpentine crystals as seen in Figure 4.6.

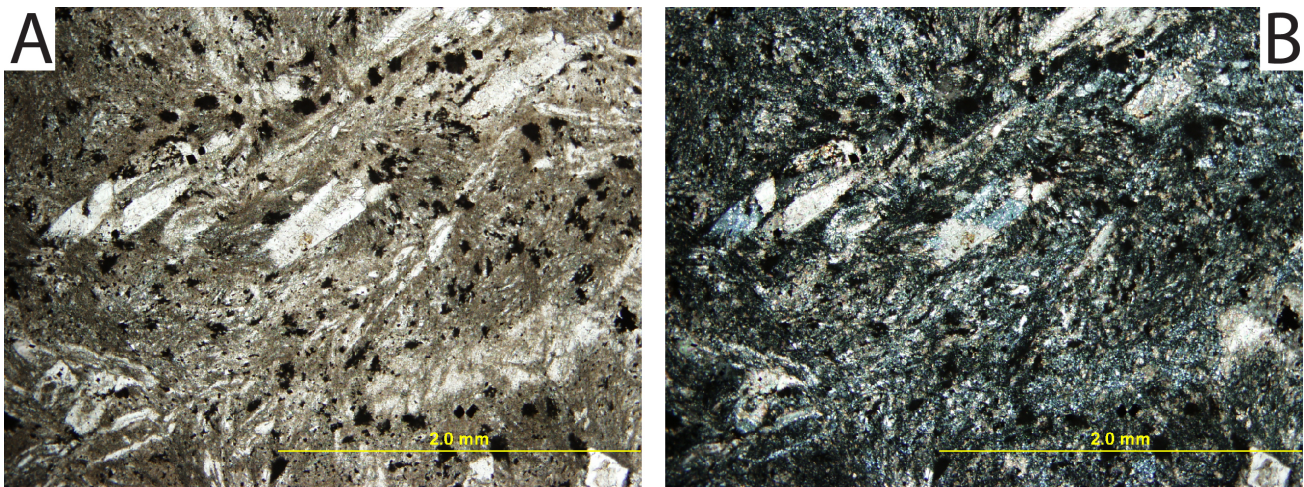


Figure 4.6 A) Photomicrograph of spinifex needles that have been replaced by calcite in PPL B) Photomicrograph of spinifex needles that have been replaced by carbonate in XPL (sample TL-16-SH-051).

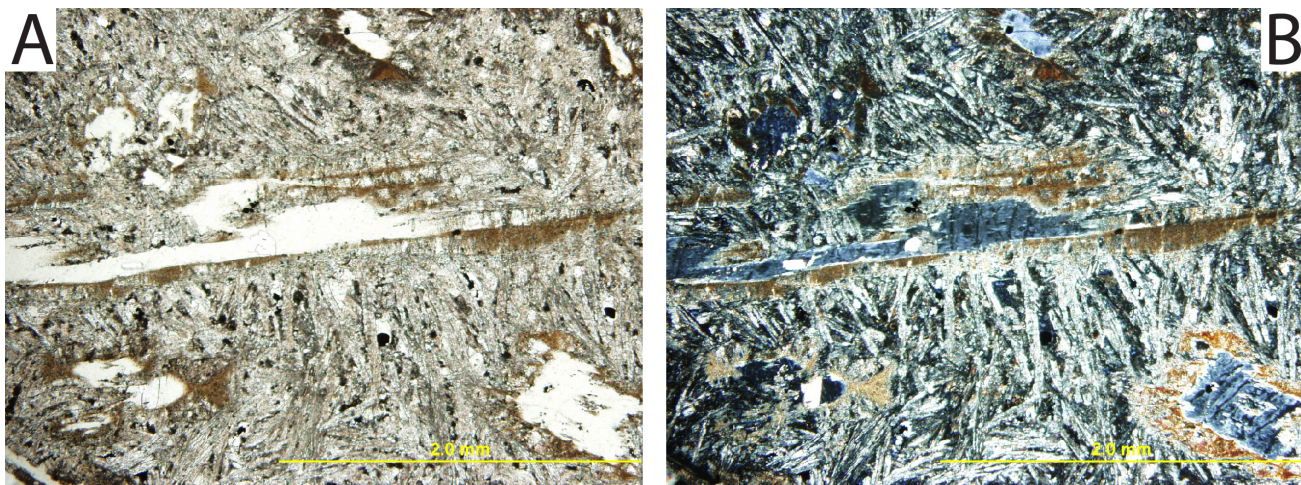


Figure 4.7 A) Photomicrograph of spinifex needles that have been altered to chlorite and iddingsite in PPL B) Photomicrograph of spinifex needles that have been altered to chlorite and iddingsite in XPL (sample TL-16-SH-070).

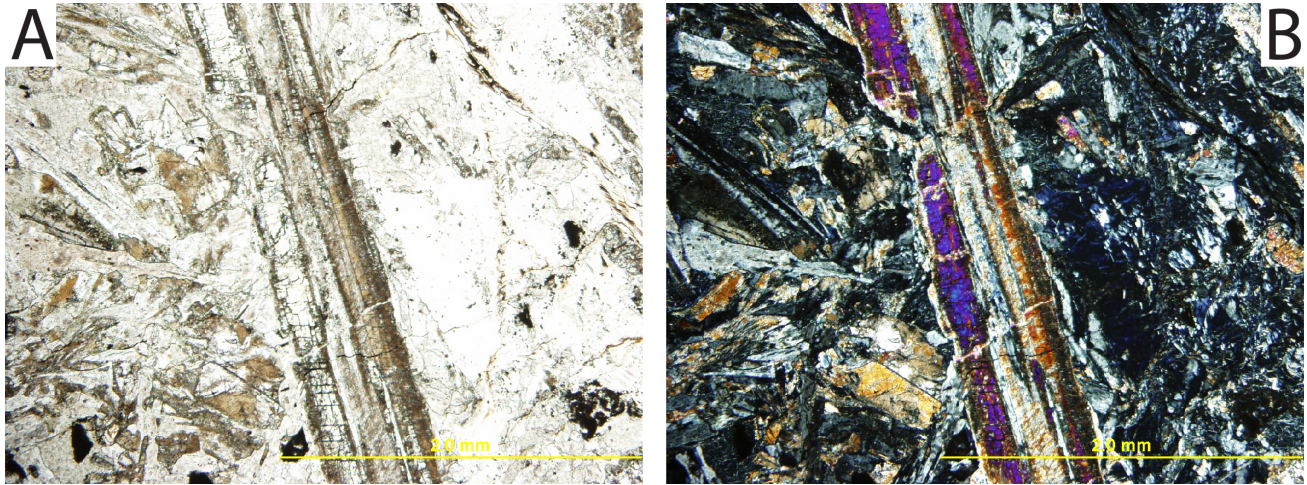


Figure 4.8 A) Photomicrograph of pyroxene spinifex in a komatiite in PPL B) Photomicrograph of pyroxene spinifex in a komatiite in XPL (sample TL-16-SH-074).

4.1.3 Other Ultramafic Lithologies

All of the ultramafic rocks present in the field area contain some degree of serpentine alteration but one outcrop at the south end of Thunder Lake consists entirely of serpentine. This rock is fine-grained, black with layers of pistachio green serpentine present as a glassy veneer on the weathered surface. The magnetic susceptibility of this rock is 1×10^{-3} SI.

Only one example of vesicular komatiite was found at the south end of Thunder Lake. It is a fine-grained rusted brown rock with large, elongate vesicles (~3-4 cm in diameter) weathered out on surface. On a fresh surface the rock is very fine-grained, light grey with vesicles filled with calcite. The mineralogy of this rock consists of 70% calcite, 10% pyroxene, 10% iddingsite and 10% serpentine. The magnetic susceptibility of this rock is 0.5×10^{-3} SI.

In several outcrops of the field area there are examples of ultramafic breccia with spinifex-textured clasts. The clasts are sub-angular and anywhere from 0.5 cm-

20 cm in diameter. The clasts are light grey with thin chaotic spinifex texture. The groundmass is very fine-grained dark grey interstitial material. The magnetic susceptibility of this lithology is $0.13-0.5 \times 10^{-3}$ SI. No contacts were observed between the ultramafic breccia outcrops and other lithologies.

In several locations within the Linear Metals trenches, a variolitic ultramafic rock was present. One variety found in trench 1D consists of pistachio green varioles 1-2 cm in diameter. It is very fine-grained with mineralogy of 75% quartz, 15% calcite, and 10% serpentine (Fig. 4.9 A). The magnetic susceptibility of this rock is 0.022×10^{-3} SI. The second variety was found in trench 4A and consists of white varioles from 2-10 cm in diameter in a very fine-grained black matrix.

Another distinct facies was found within the Linear Metals trenches at the contact between the sedimentary facies and komatiites, which consisted of a heterolithic contact breccia. These contact breccias show both globular and blocky morphologies in different trenches and within each trench. In trench 1E, blocks of chert have been ripped up by the komatiitic flow (Fig. 4.9 B), in trench 4A fragments of ultramafic lava have been incorporated into the chert (Fig. 4.9 C), the chert horizons have been cut by an ultramafic flow (Fig. 4.9 D), and pod-like, siliceous lobes are present (Fig. 4.9 E). These contacts occur at several locations parallel to one another other within trench 4A, which indicates several periods of sedimentation and subsequent ultramafic volcanic activity. These rocks are interpreted to be peperites.

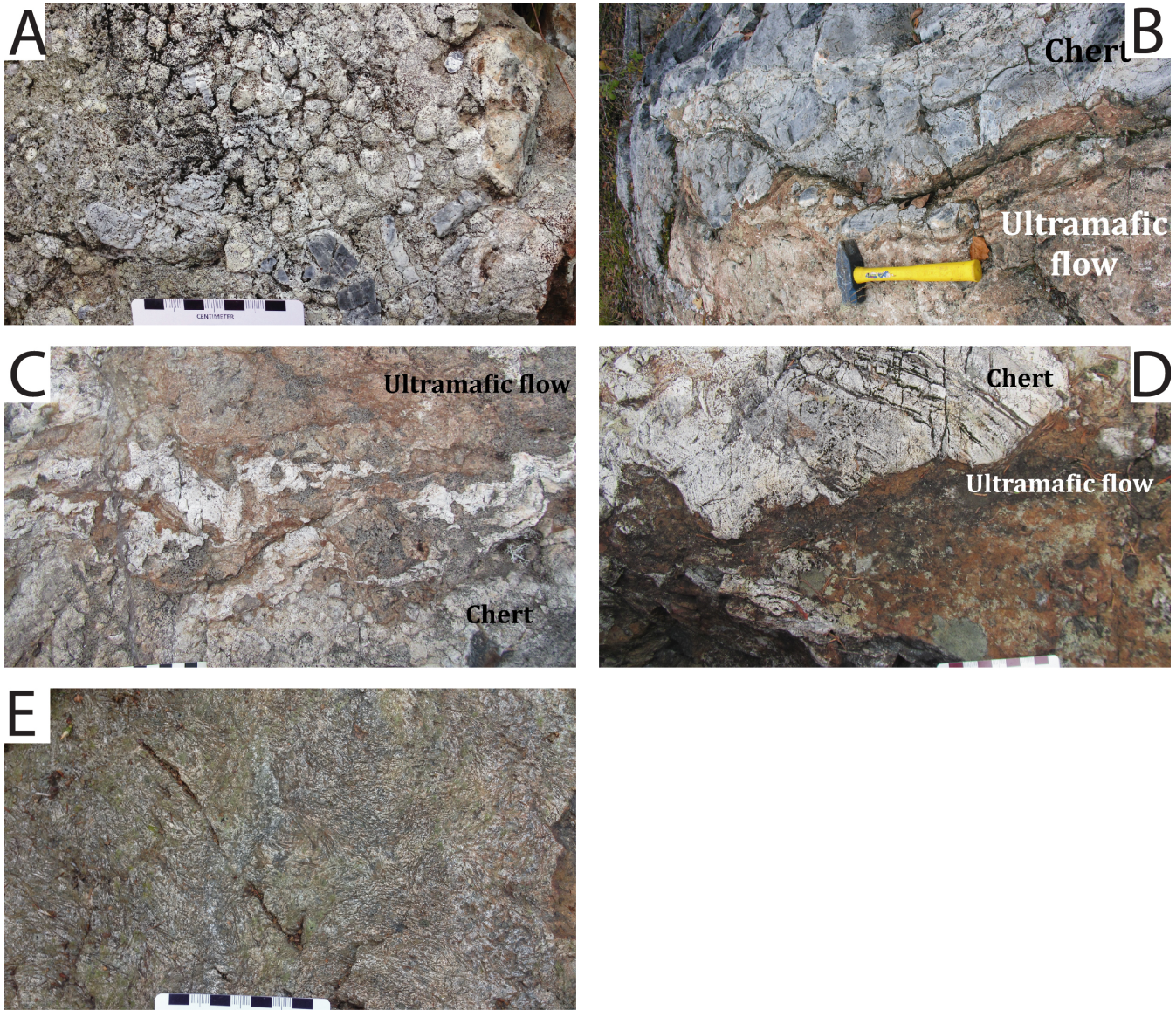


Figure 4.9 Photographs of field samples and outcrops taken during mapping. A) Variole texture (trench 1D); B) Contact between chert and ultramafic units showing rip-up clasts of chert within the ultramafic groundmass (trench 1E); C) Peperite contact with angular fragments of ultramafic rock and chert; D) Chert unit being cut off by ultramafic flow; E) Spinifex texture.

4.1.4 Pyroxenite

The pyroxenite was seen at two locations in the field area, along a ridge south of Thunder Lake, and on the shore at the south end of Thunder Lake (Fig. 4.1). These two pyroxenites are very similar in composition but have varying grain size and shapes. In the pyroxenite ridge south of Thunder Lake, the rock consists of medium-

grained twinned tabular pyroxenes (Fig. 4.10 A). At the southern shore of Thunder Lake, there are two different textures that occur in the pyroxenite. These textures are present in a northwest trending dyke that extends from the shore into the lake. The easternmost side of the dyke consists of a medium-grained pyroxenite with rounded, subhedral pyroxenes (Fig. 4.10 B), as opposed to the tabular crystals found on the ridge. The westernmost side of the dyke consists of a fine-grained pyroxenite with an unusual texture that shows green and grey pyroxenes being segregated in aggregates (Fig. 4.10 C).

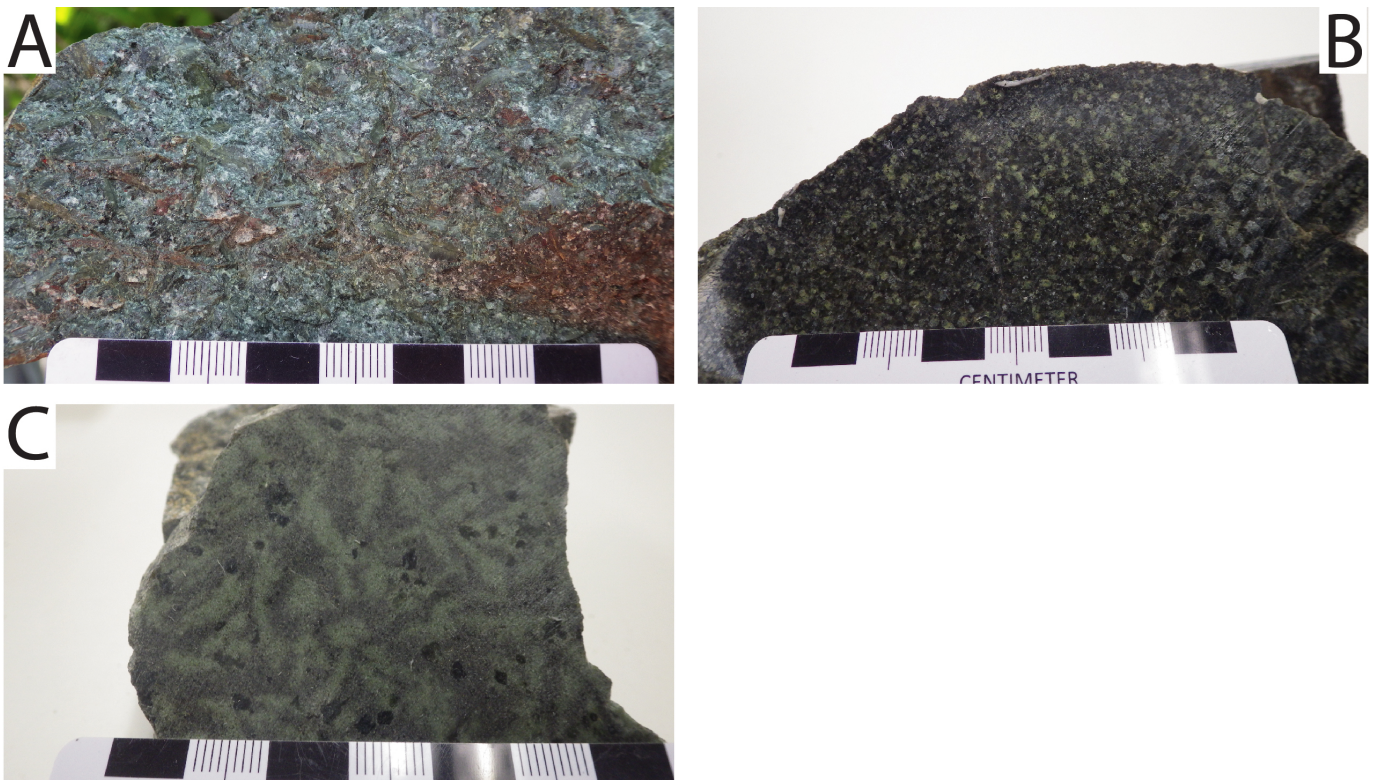


Figure 4.10 Photographs of field samples and outcrops taken during mapping. A) Pyroxenite with tabular pyroxenes (TL-16-SH-076); B) Pyroxenite with rounded pyroxenes (TL-16-SH-116 A); C) Pyroxenite with fine-grained pyroxenes (TL-16-SH-116 B).

Petrographic analysis showed that the two differently textured pyroxenites have a similar mineralogy. The first sample is medium-grained, with rounded crystals of orthopyroxene, clinopyroxene, and serpentine altered from olivine (Fig.

4.11); whereas the second consists of fine-grained, rounded grains of orthopyroxene, clinopyroxene, and chlorite (Fig. 4.12). There is no obvious petrographical explanation for the colour varying from grey to green within the sample.

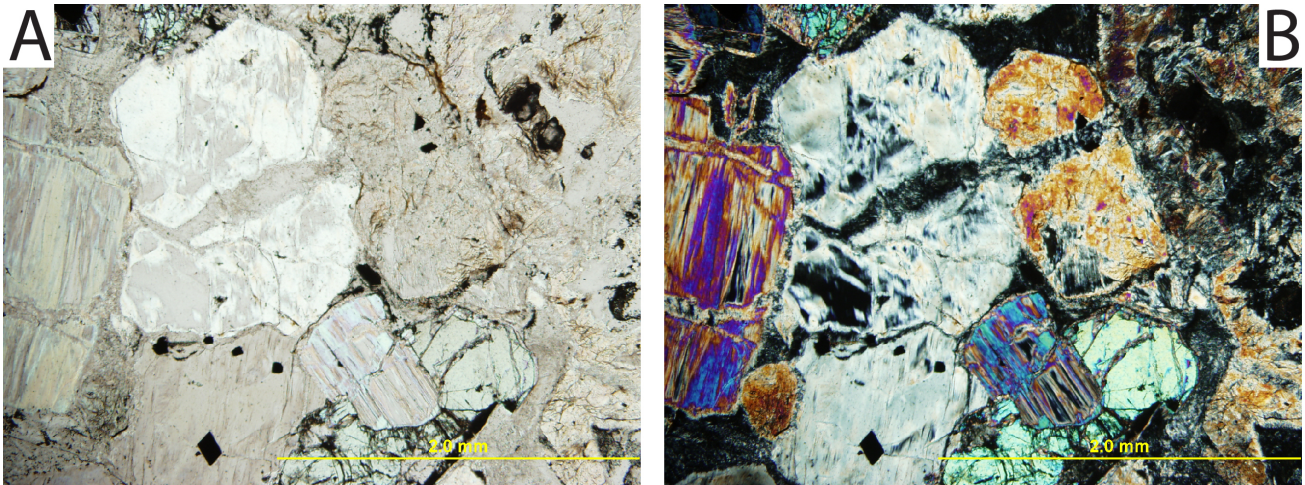


Figure 4.11 A) Photomicrograph of medium-grained serpentine and pyroxene crystals in PPLB) Photomicrograph of medium-grained serpentine and pyroxene crystals in XPL (sample TL-16-SH-116A).

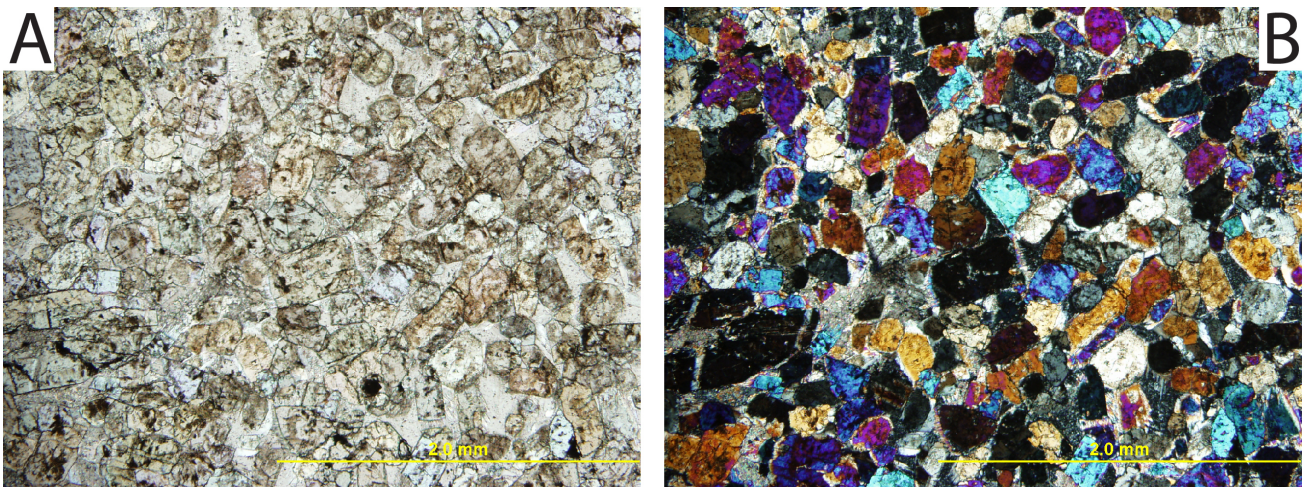


Figure 4.12 A) Photomicrograph of pyroxenite with fine-grained pyroxene crystals in PPL B) Photomicrograph of pyroxenite with fine-grained pyroxene crystals in XPL (sample TL-16-SH-116B).

4.1.5 Mafic Rocks

The mafic intrusive rocks seen in the field area occur as a single gabbroic body, which is approximately 700 m wide with a northwest trend (Fig. 4.1). As there

was a lot of overburden in the field area, no contact relationships were observed, and as such the boundaries of this gabbro are inferred. The gabbros are massive, medium-grained, equigranular, grey-blue with weakly disseminated pyrite (Fig. 4.13 A).

The majority of mafic metavolcanic rocks predominantly occur south of the fault, with only one discontinuous lens north of the fault (Fig. 4.1). These metavolcanic rocks are fine-grained, dark grey-blue, with local carbonate veins and rare pyrite (Fig. 4.13 B). No pillows or flow textures were seen in the field area.



Figure 4.13 Photographs of field samples and outcrops taken during mapping A) Gabbro (TL-16-SH-014); B) Mafic metavolcanic rock (TL-16-SH-077).

Petrographic analysis shows all the mafic rocks to be carbonatized. Sample TL-16-SH-025 is characteristic of the mafic volcanic rocks in the field area and consists of 60% plagioclase, 30% calcite and 10% chlorite. Plagioclase grains are medium-grained, subhedral with deformed twins and sericitization and chlorite is present as fine-grained crystals (Fig. 4.14). Sample TL-16-SH-026 is a characteristic sample of gabbro in the field area and displays medium-grained plagioclase, with fine-to medium-grained tremolite being the most abundant mineral (Fig. 4.15). The

mineralogy of this sample is 50% tremolite, 30% plagioclase, 10% calcite, 5% quartz, and 5% chlorite.

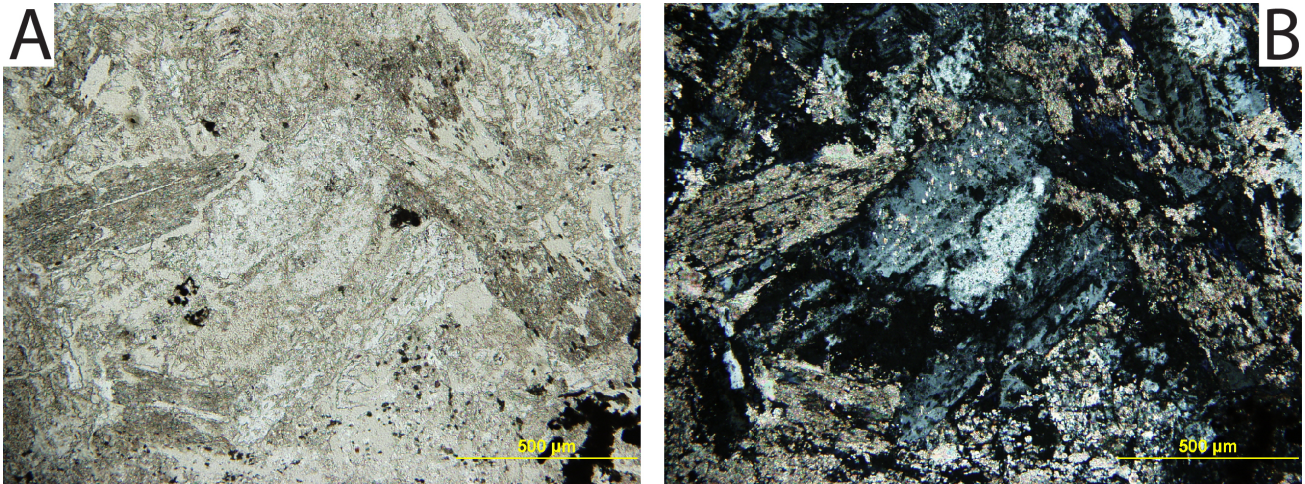


Figure 4.14 A) Photomicrograph of deformation twins within plagioclase in PPL B) Photomicrograph of deformation twins within plagioclase in XPL (sample TL-16-SH-025).

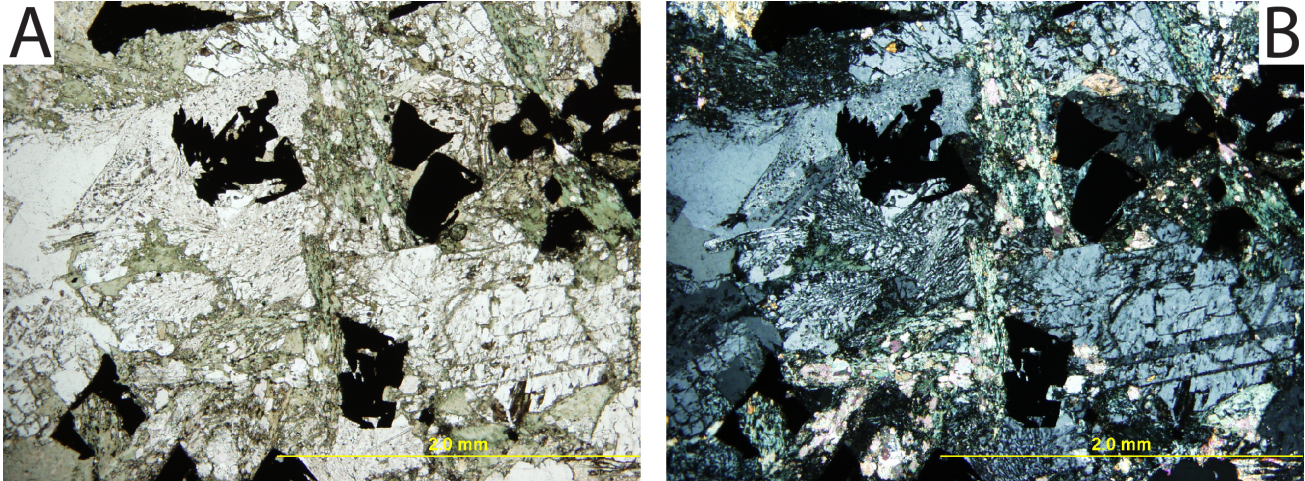


Figure 4.15 A) Photomicrograph of tremolite and plagioclase in PPL B) Photomicrograph of tremolite and plagioclase in XPL (sample TL-16-SH-026).

4.1.5 Intermediate Rocks

The intermediate intrusive rocks in the field area comprise a monzonite dike that intrudes along the northeast trending fault. It is distinctly magnetic and aligns

with the northeastern linear magnetic anomaly on the airborne magnetic geophysical map of the area (Ontario Geological Survey, 2003). The intermediate rocks consist of a fine-grained, green-grey matrix with hornblende phenocrysts and red-pink autoliths (Fig. 4.16 A). The autoliths are angular and 2-4 cm in length; they show the same grain size and mineralogy and are distinguished by a slightly darker shade of red.

The intermediate metavolcanic rocks in the field area are fine-grained, light grey-blue metavolcanic rocks with medium-grained plagioclase phenocrysts (Fig. 4.16 B). They are seen in the middle of the field area as a discontinuous lens that is cut off by the northeast trending fault, as well as two thin lenses interlayered with the conglomerate and ultramafic units (Fig. 4.1).

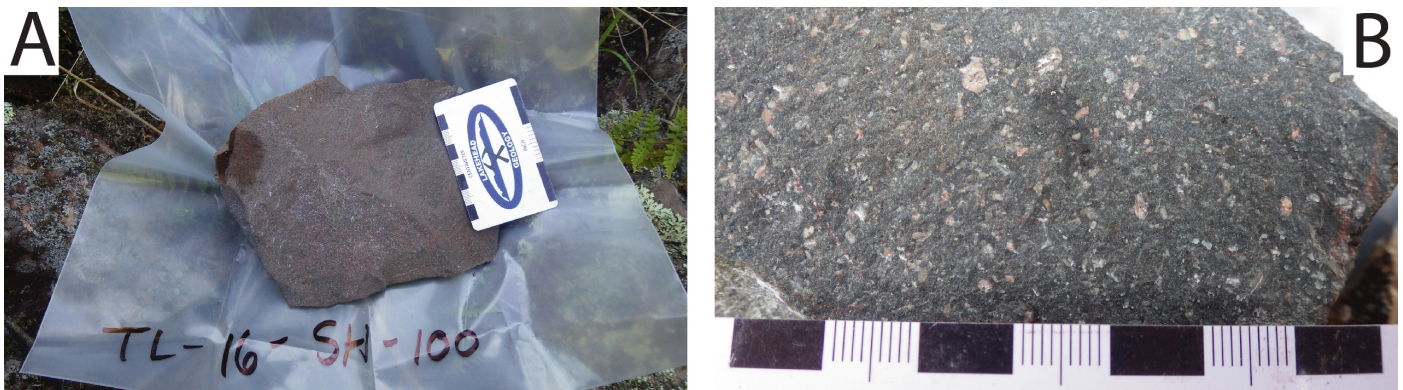


Figure 4.16 Photographs of field samples and outcrops taken during mapping. F) Monzonite (TL-16-SH-100); G) Intermediate metavolcanic (TL-16-SH-079).

Intermediate rocks are rare within the field area. Petrographic analysis shows the intermediate volcanic rocks have undergone carbonatization and ankerite alteration. Sample TL-16-SH-020 is characteristic of this lithology and consists of 50% plagioclase, 15% calcite, 15% sericite, 10% quartz, 5% chlorite and 5% epidote (Fig. 4.17). The groundmass is very fine-grained with medium-grained

plagioclase phenocrysts being altered to sericite. Veins of calcite cut through the groundmass. The magnetic susceptibility of these rocks is $0.22-0.5 \times 10^{-3}$ SI. The intermediate intrusive rocks are monzonites comprised of alkali feldspar and lesser plagioclase and quartz. The alkali feldspar gives the rocks their reddish/pink colour (Fig. 4.18).

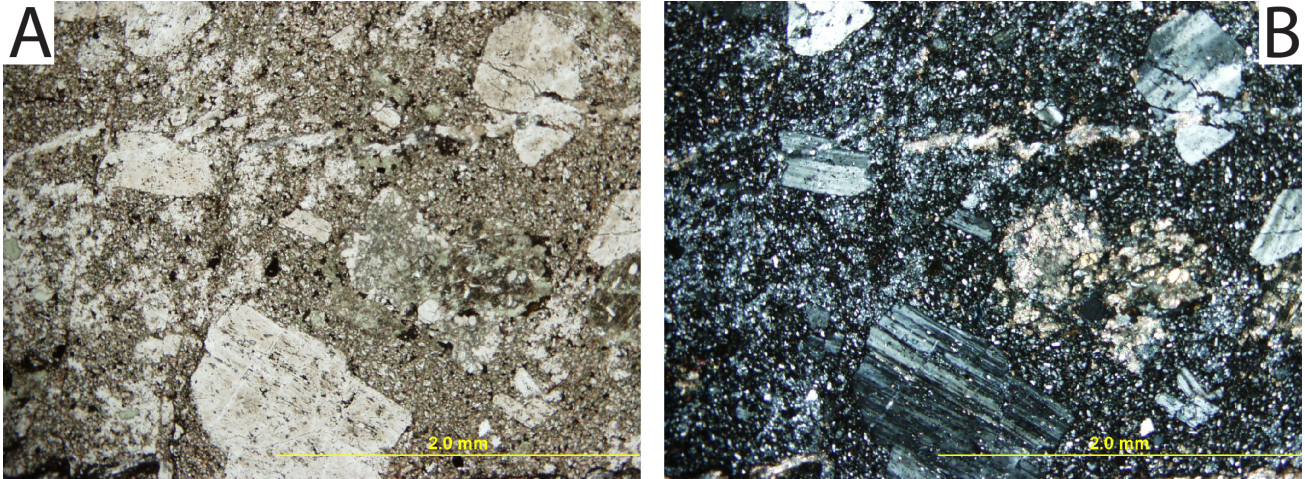


Figure 4.17 Photomicrograph of carbonate and ankerite alteration within an intermediate volcanic rock in PPL (A) and XPL (B; sample TL-16-SH-020).

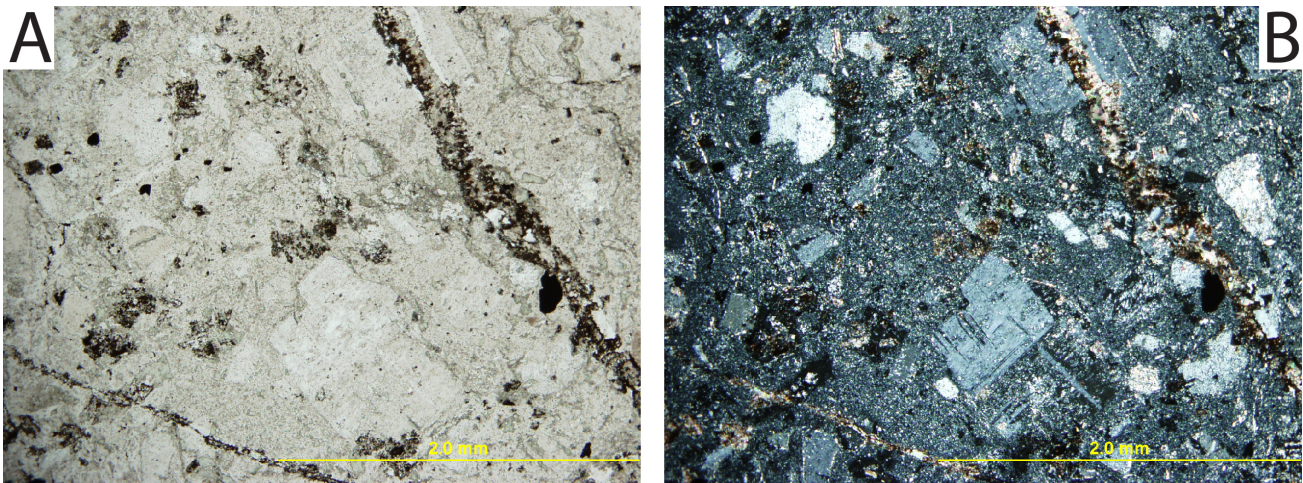


Figure 4.18 A) Photomicrograph of alkali feldspar and calcite present in monzonite in PPL B) Photomicrograph of alkali feldspar and calcite present in monzonite as well as deformation twins in plagioclase in XPL (sample TL-16-SH-078).

Sample TL-16-SH-78 is characteristic of the intrusive rocks and consists of 30% potassium feldspar, 20% plagioclase, 20% quartz, 15% calcite and 15%

chlorite. The sample has a very fine-grained groundmass with medium-grained plagioclase phenocrysts that display deformation twinning. Calcite veins are seen throughout the sample and calcite also comprises the majority of the groundmass alongside quartz. The magnetic susceptibility of these rocks is $10\text{-}41 \times 10^{-3}$ SI.

4.1.7 Felsic Rocks

There was only one felsic lithology observed in the central portion of the field area occurring as thin lenses of metavolcanic rocks within the conglomerate unit (Fig. 4.1). Though only observed in four locations, these rocks were distinct as very fine-grained, light grey, siliceous rocks. In some places they occur with calcite phenocrysts. They are massive with no flow textures observed in any of the outcrops and the weathered surfaces range in colour from beige to blue-grey (Fig. 4.19).



Figure 4.19 Photograph of field sample: felsic metavolcanic rock (TL-16-SH-088).

Sample TL-16-SH-090 is characteristic of this lithology with mineralogy of 55% quartz, 20% calcite, 15% chlorite and 10% actinolite (Fig. 4.20). The sample groundmass is very fine-grained, with medium-grained calcite crystals and veins of

chlorite separating the groundmass. The magnetic susceptibility of these rocks is $0.35-0.55 \times 10^{-3}$ SI.

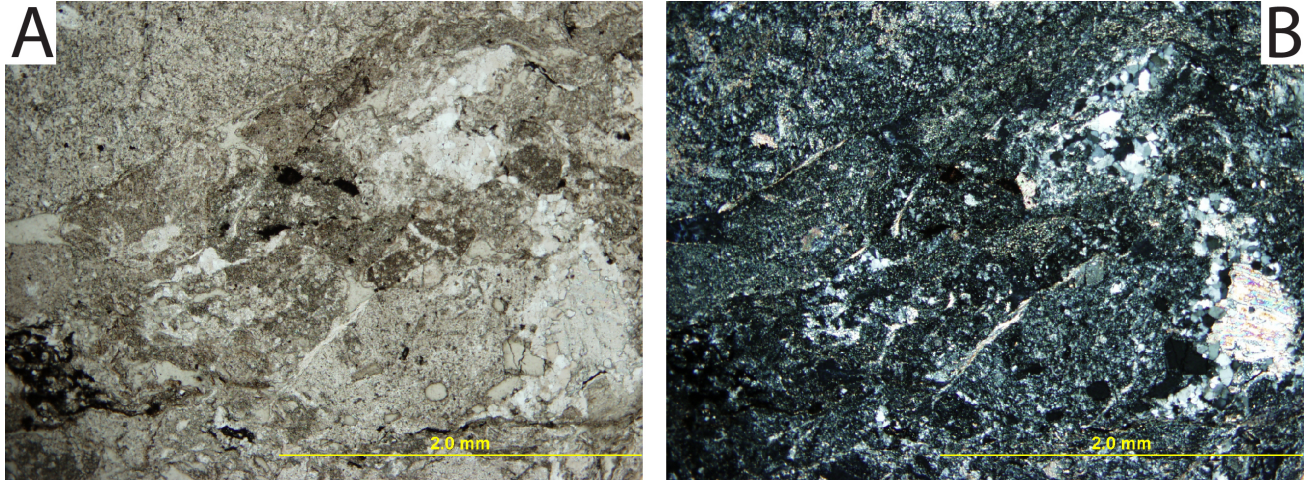


Figure 4.20 A) Photomicrograph of felsic volcanic rock in PPL B) Photomicrograph of felsic volcanic rock in XPL (sample TL-16-SH-090).

4.1.8 Sedimentary Rocks

The conglomerate unit is the second most abundant lithology in the field area (Fig. 4.1). The conglomerate is a heterolithic pebble to boulder conglomerate consisting of a fine-grained matrix with clasts of basalt, monzonite, and jasper ranging in size from ~2 cm to 40 cm (Fig. 4.21 A). It is intruded by the monzonite dyke and has clasts of felsic and intermediate metavolcanic rocks within it.

The other major sedimentary lithology in the field area is argillite. The argillite is seen intercalated with ultramafic flows in the trenches north of the fault. It is a very fine-grained dark black mudstone. The argillite typically shows no bedding and locally contains graphite and abundant radial pyrite concretions up to 5 cm in diameter (Fig. 4.21 B). Radial pyrite growths in the argillite show multiple generations of growth based on the layers of pyrite seen in cross-sectional view, and are locally weathered resulting in a vuggy texture.

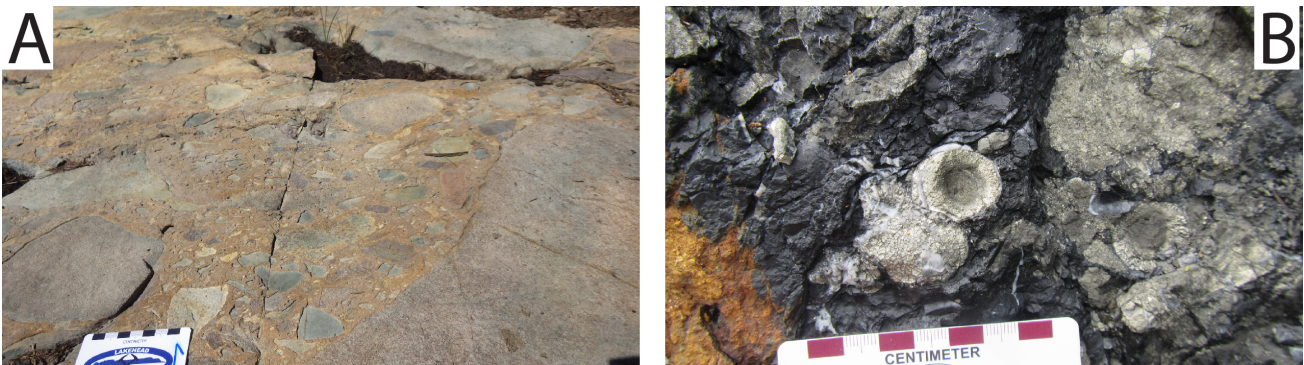


Figure 4.21 Photographs of sedimentary units A) Conglomerate (Hinze 98); B) Radial pyrite in argillite (Trench 3A).

4.2 Trench Mapping

4.2.1 Series 1 Trenches

The series 1 trenches are located in the northwestern portion of the map area (Fig. 4.22). The series consists of six trenches ranging in length from 10-60 m, with an average width of 4-5 m. They were remapped for this study during the summers of 2015 and 2016 in order to get a more detailed view of contacts between lithologies that were not observed during field mapping (Fig. 4.23). Linear Metals labeled the trenches as follows: 1A, 1B, 1C, 1D, 1E, and 1F (Fig. 4.23). All trenches are dominantly comprised of ultramafic lithologies. The southernmost end of trench 1A consists of massive bedded argillite with radial pyrite concretions up to 5 cm in diameter, as well as graphite present in the very fine-grained black rock (Fig. 4.23).

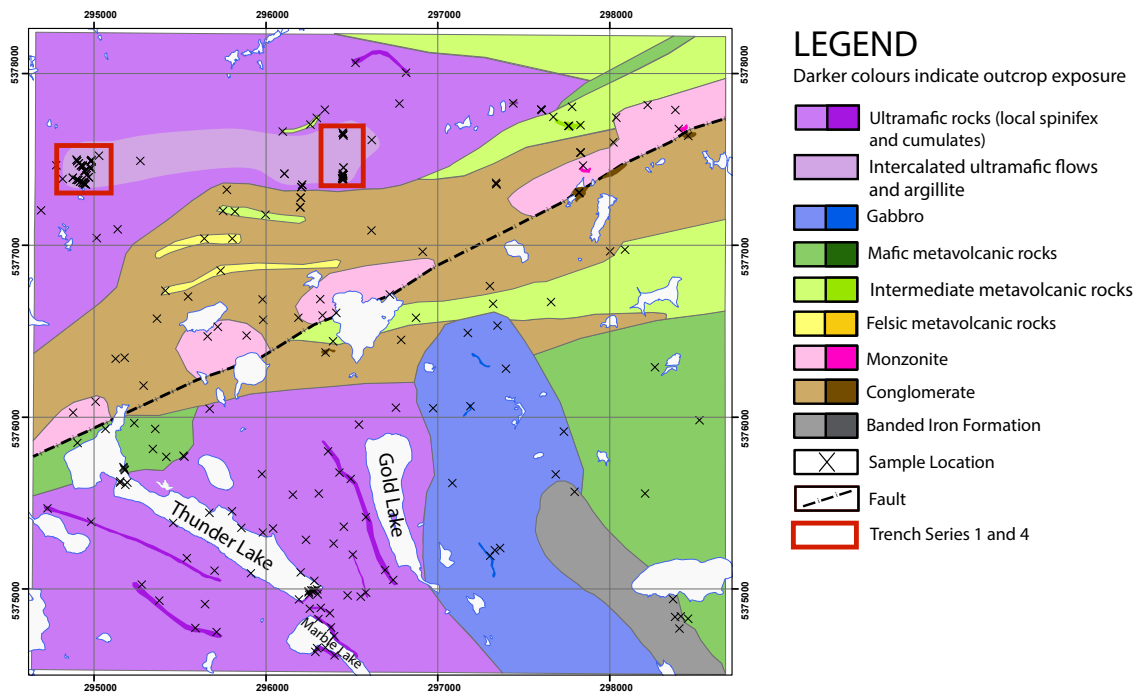


Figure 4.22 Geology map of the study area, data collected summer 2016 by the lead author. Red boxes indicate location of trenches. Trench series 1 is further to the west; trench series 4 is to the east.

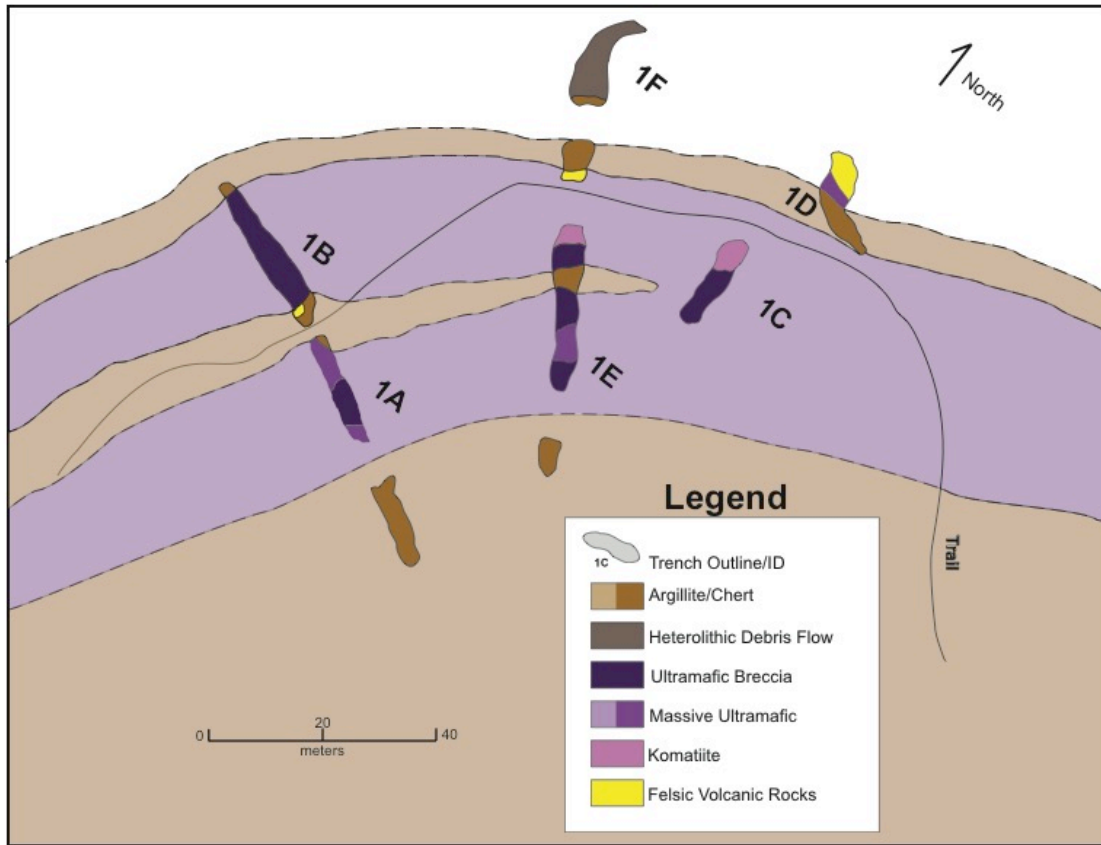


Figure 4.23 Trench map of Series 1 trenches, including trenches 1A, 1B, 1C, 1D, 1E, and 1F. Located in the northwest of the field area (modified from Hinz et al., 2016).

This was the largest showing of argillite found in the field area. There is no visible contact between the argillite and ultramafic unit in this trench as the rock has weathered away preferentially along the inferred contact. Moving north within trench 1A, there is a massive ultramafic unit that is interrupted by an ultramafic breccia unit approximately 4 m long. At the northernmost point of trench 1A, there is a 0.5 m section of argillite that continues on the other side of the trail into trench 1B.

Trench 1B is the northern extension of 1A. The southernmost point is an argillite unit that is interpreted to be the continuation of the unit in trench 1A, it contains a 0.7 m section of felsic volcanic rocks. The remainder of the trench

consists of ultramafic breccia capped at the northern end with another 1 m exposure of argillite.

Trench 1C is approximately 20 m long and consists mainly of ultramafic breccia. The northernmost part of this trench is polysutured komatiite. Each polyhedral joint is surrounded by a thin rim (1-2 cm thick) of serpentine. In the interstitial space between joints, the rock is chaotic and jagged (Fig. 4.24 A).

Trench 1D contains a chaotic contact between a chert/argillite unit and a massive ultramafic unit (Fig. 4.9 B). This ultramafic rock shows a variolitic texture only seen elsewhere in trench 4A. The varioles are pistachio green and approximately 1-2 cm in diameter, congregated together in a 1 m by 1 m area (Fig. 4.9 A). The varioles are comprised of quartz, calcite, and serpentine, giving the varioles the pistachio green colour. This unit is separated from felsic volcanic rocks by a 0.5 m gap in the trench, where overburden obscures the bedrock. The felsic volcanic rocks are very fine-grained, light grey, siliceous rocks that extend to the end of the trench.

Trench 1E contains the most varied lithologies, beginning in the southernmost part of the trench with an argillite unit, cut off by a pit where the contact between the argillite and ultramafic breccia has been preferentially weathered away. The ultramafic breccia gradually grades into polysutured komatiite, with the same polyhedral jointing texture as trench 1C (Fig. 4.24 B), then gradually grades back into ultramafic breccia. The ultramafic breccia has a sharp contact with a light grey chert unit approximately 2 m wide. The laminations in this unit indicate a northward younging direction (Fig. 4.24 C). The upper contact of the

chert with the overlying unit shows rip-up clasts of chert within the ultramafic breccia (Fig. 4.9 B), consistent with the northward younging direction indicated by the lamination. The ultramafic breccia transitions into komatiite with the presence of chaotic spinifex texture at the northernmost portion of this trench (Fig. 4.5 A).

Trench 1F consists of a small amount of massive ultramafic rocks at the southernmost point of the trench grading into argillite, with much of the trench covered by overburden.



Figure 4.24 Various textures seen in trench set 1: A) Polyhedral jointing (trench 1C); B) Polyhedral jointing (trench 1E); C) Lamination in chert unit, white arrow indicates a northward younging direction (trench 1E).

4.2.2 Series 4 Trenches

The series 4 trenches are located in the northwestern portion of the map area approximately 1km east of the series 1 trenches (Fig. 4.1). This series consists of six trenches ranging in length from 10-90 m, with an average width of 4-5 m. Linear Metals labeled the trenches as follows: 4A, 4B, 4C, 4D, 4E, and 4F. Not all

trenches contain ultramafic lithologies, and only the most relevant trench, trench 4A, containing lithology contacts is discussed here (Fig. 4.25).

Trench 4A is the longest trench in the field area, approximately 90 m long and 4-5 m in width and contains many contacts between ultramafic and sedimentary units (Fig. 4.25). This section describes the trench from the south to north. At the southern end of the trench there is a brecciated komatiite flow that becomes a peperite at the contact with a chert-to-chert breccia unit.

A peperite is a rock texture caused by the mixing of extrusive igneous rocks with wet sediments, which causes a chaotic and brecciated contact between the two units (Skilling et al., 2002). The peperite contact consists of sub-rounded brecciated fragments of chert with the ultramafic rock (Fig. 4.9 C). Both ultramafic and sedimentary units show an increase in alteration towards the peperitic contact, which also corresponds to an increase in talc, serpentine, quartz, and calcite. The peperites consist of angular ultramafic clasts that are separated by jagged and randomly oriented sedimentary rocks that have wispy contacts reaching into the ultramafic unit (Fig. 4.9 C). Areas of the contact show chert units being cut by the ultramafic flow (Fig. 4.9 D). After the peperite there is a 15 m long competent chert or chert breccia unit followed by a variolitic ultramafic unit. This variolitic unit is very similar to the one seen in trench 1D with 2 cm varioles that are white in colour on a fresh surface (Fig. 4.22 D). This is followed by another thin peperite and then ultramafic breccia. The rest of the trench has komatiite with spinifex texture present with the size of spinifex needles decreasing moving north (Fig. 4.9 E). The final peperite is marked with an anomalous texture of silicification in komatiite with a

variolite-like texture (Fig. 4.22 D), which appears as white siliceous blobs in a dark black ultramafic groundmass.

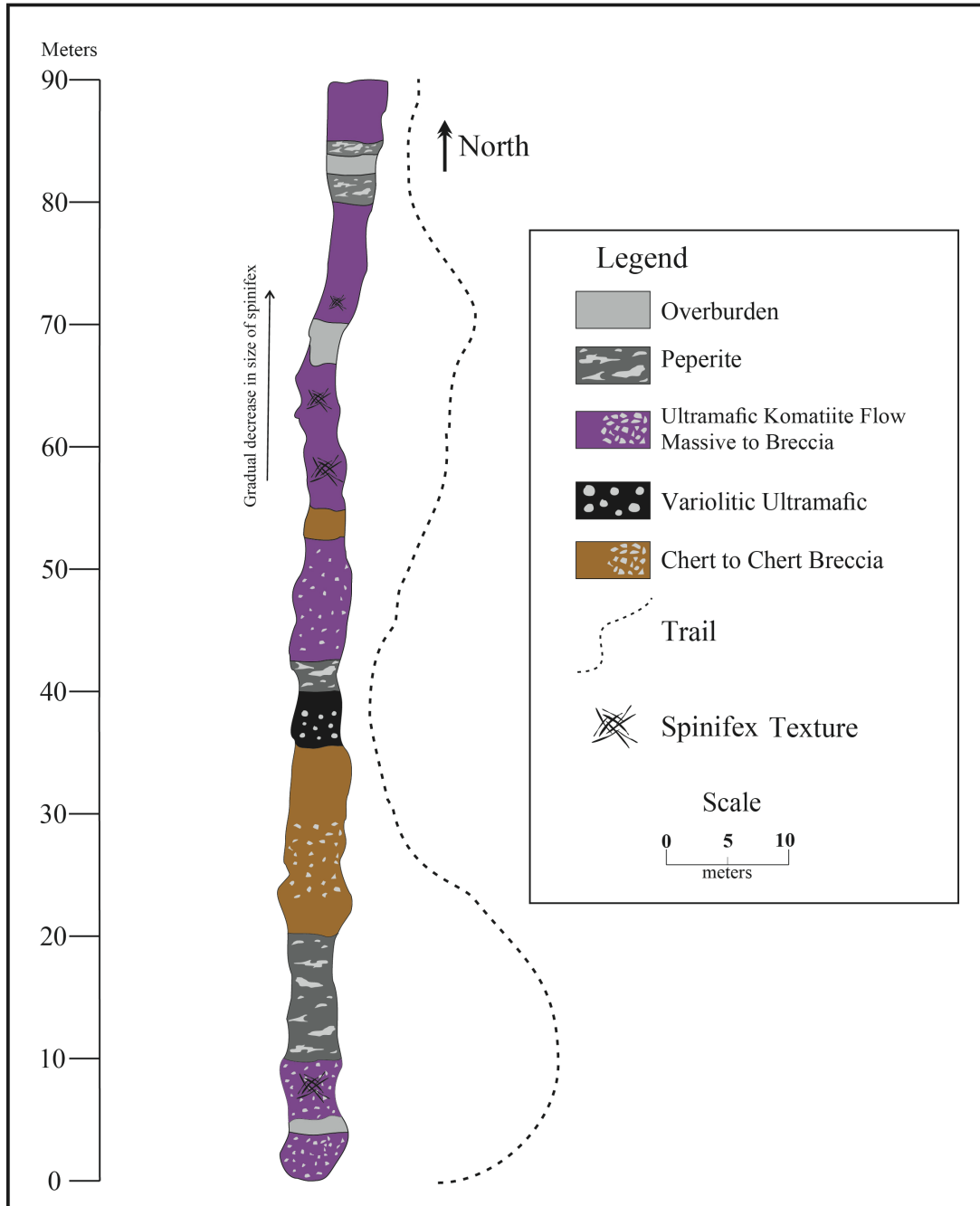


Figure 4.25 Map of trench 4A from Series 4 trenches displaying lithologies and the transitions between them (modified from Hinz et al., 2016).



Figure 4.26 Silicification of komatiite with a variolite-like texture in trench 4A.

Chapter 5: Geochemistry

The ultramafic lithologies have been divided into three groups based on texture: rocks that display an orthocumulate texture (orthocumulate ultramafic), rocks that display spinifex texture (komatiite), and rocks that have no distinct texture (ultramafic). The remaining lithologies identified within the study area are felsic volcanic, intermediate volcanic, mafic volcanic, pyroxenite, monzonite, and basaltic komatiite.

5.1 Alteration

The degree of alteration needs to be taken into account when analyzing geochemical data from Archean rocks, as both major and trace element mobility caused by post-depositional alteration and metamorphism can affect the reliability of geochemical data. Rollinson (1993) characterized element mobility as chemical changes which take place in a rock after its formation, usually caused by hydrothermal alteration or metamorphism. The commonly mobile major elements in komatiites are Si, Ca, Na and K (Arndt, 1983). Overall the major element geochemistry of the samples in this study display substantial scatter on variation diagrams (Fig. 5.1) and must therefore be interpreted with caution. The loss on ignition values (LOI) are fairly high (1.5-17 wt. %), which is likely caused by hydrothermal alteration and subsequent mobilization of major elements (Fig. 5.1). When plotted against MgO, both Al₂O₃ and TiO₂ show slightly less scatter than K₂O, SiO₂, CaO, and Na₂O₃, which are interpreted to be more mobile (Fig. 5.1). The likely mobility of the major elements makes it difficult to classify samples using typical discrimination diagrams. Consequently, in this study lithologies have been classified

by petrography rather than chemistry. There is a poor agreement between the geochemically determined rock name and the one based on petrography. For example, sample TL-16-SH-106 was classified as a komatiite based on hand sample and petrography descriptions, but fell within the high-Mg tholeiitic basalt field on the Jensen cation plot (Jensen, 1976).

Arndt et al. (2008) noted that carbonate alteration is common in ultramafic rocks, and it is present in many samples in the field area. This is seen more noticeably in the petrography, which shows calcite spread throughout many of the ultramafic samples. A typical unaltered komatiite has low CaO, with CaO and Na₂O combined typically less than 2 wt. % (Arndt et al., 2008). The ultramafic rocks in this study have CaO values between 5-23 wt. % (Fig. 5.1). This suggests that a carbonate-rich fluid has modified the geochemistry of the rocks in the field area.

Given the evidence for hydrothermal alteration, it is important to ensure that trace element data has not been affected. In order to demonstrate that geochemistry of the typically immobile elements has not been affected; variation diagrams were plotted displaying the immobile elements versus major elements. Arndt et al. (2008) showed that the high field strength elements (HFSE) generally remain immobile in ultramafic rocks during alteration. When plotted on variation diagrams versus Al₂O₃ (Fig. 5.2), the HFSE display a positive trend with little scatter suggesting that they have remained immobile during alteration and metamorphism. Within the variation diagrams, there is more scatter within the plots of U, Th, and Ta as Al₂O₃ increases.

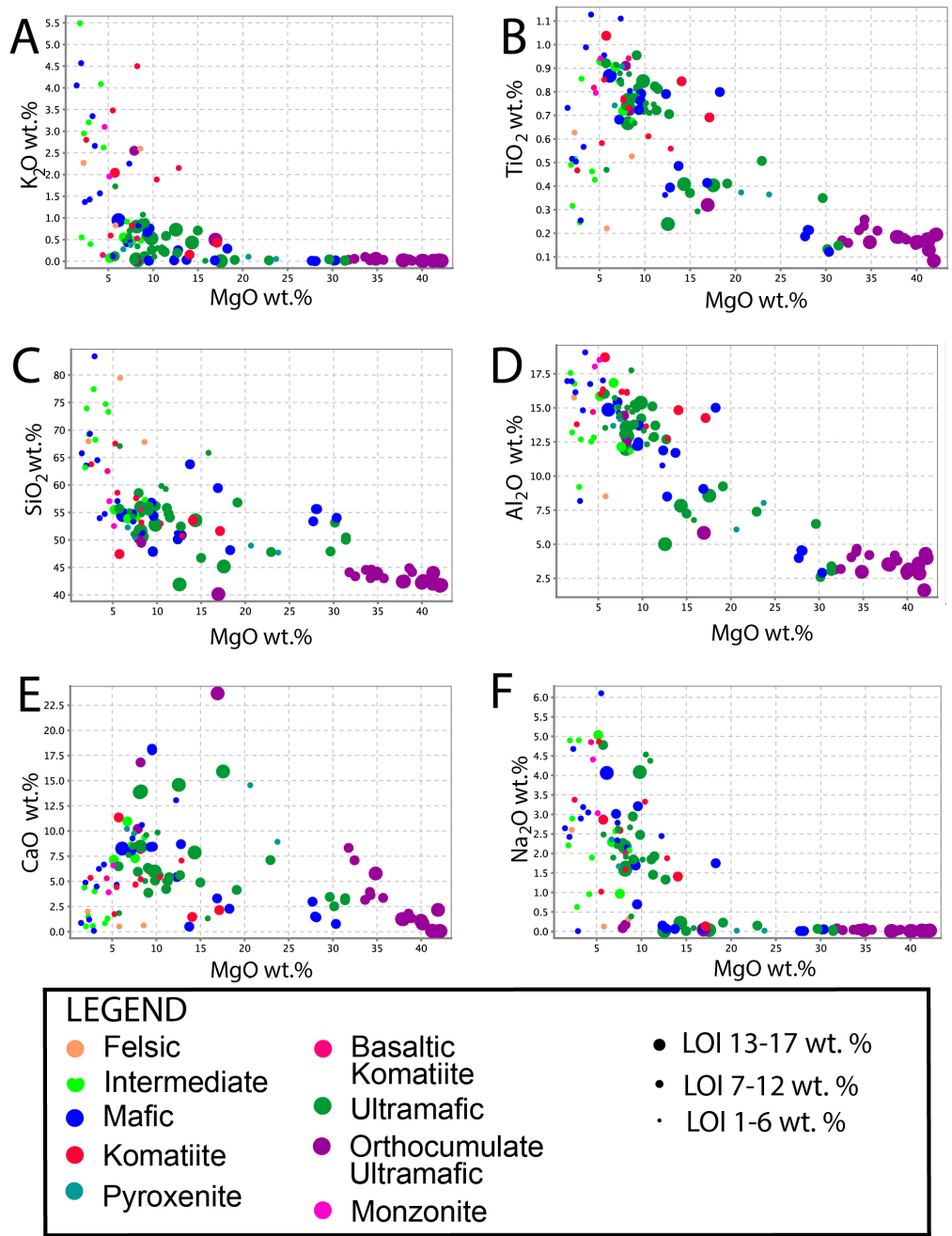


Figure 5.1 Variation plots of MgO versus major element oxides (K₂O, TiO₂, SiO₂, Al₂O₃, CaO, Na₂O), with LOI as a variable on all plots.

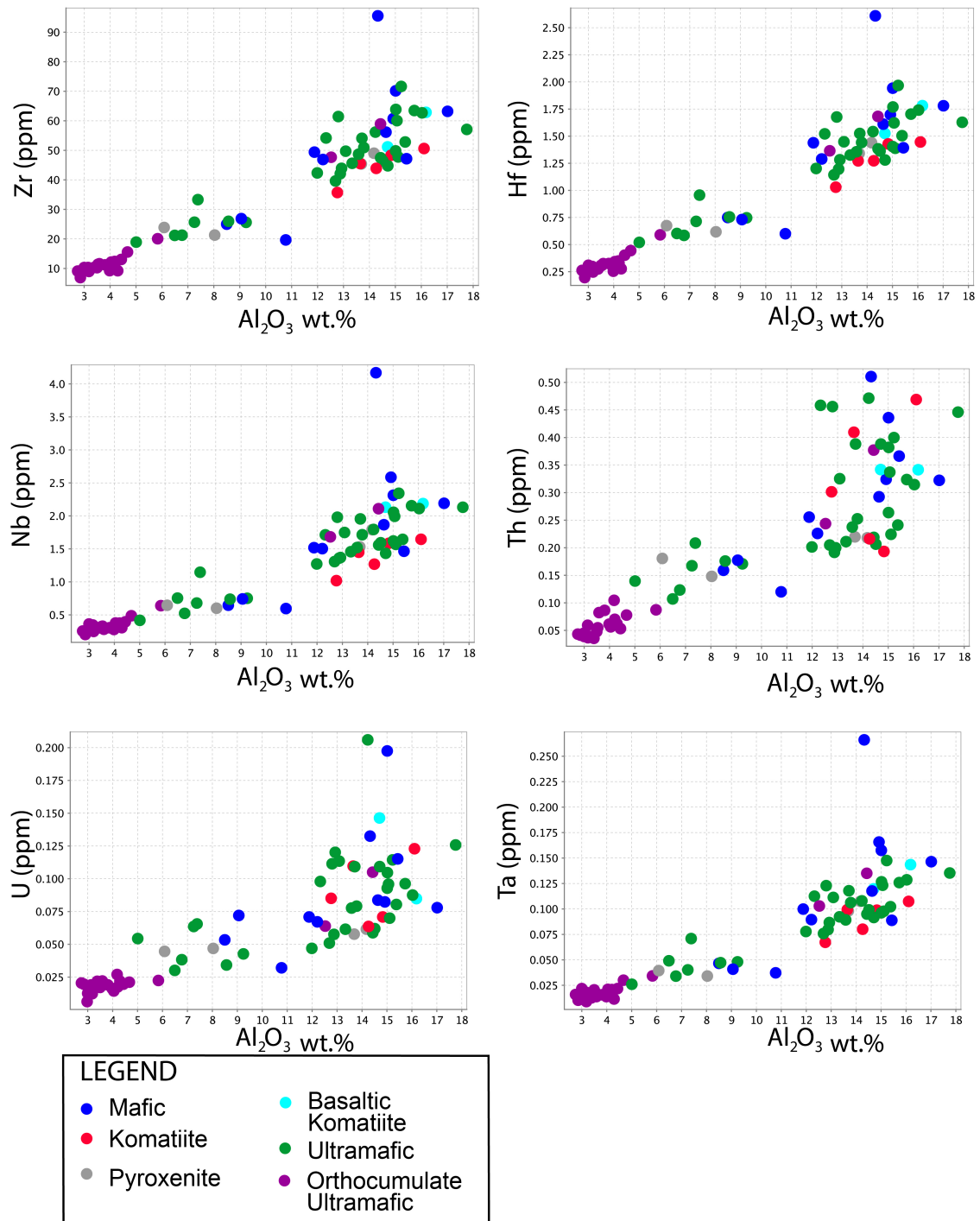


Figure 5.2 Variation diagrams of trace elements versus Al_2O_3 .

5.2 Orthocumulate Ultramafic Rocks

The orthocumulate ultramafic rocks in the study area are characterized by high MgO (16-42 wt. %) and low SiO₂ (41-44 wt. %) with elevated Ni and Cr (Ni =1175-2817 ppm; Cr= 2438-5202 ppm; Table 5.1). The samples are weakly enriched to weakly depleted in light rare earth elements (LREE; La/Sm_n= 0.79-1.66) with flat heavy rare earth elements (HREE; Gd/Yb_n= 0.99-1.42; Fig. 5.3). The orthocumulate samples display negative Nb anomalies (Th/Nb_n= 0.10-0.31). The orthocumulate ultramafic rocks have a high Al₂O₃/TiO₂ ratios (~20), which along with flat to depleted HREE patterns are characteristic of Al-undepleted komatiites (AUK; Fig. 5.4).

Table 5.1 Representative MgO, SiO₂, Ni, and Cr contents of the ultramafic lithologies

Rock Type	Sample #	MgO (wt. %)	SiO₂ (wt. %)	Ni (ppm)	Cr (ppm)	Nb/Nb*
Orthocumulate Ultramafic	TL-107	35	43	1552	4930	0.61
	TL-112	41	42	2176	5175	0.25
Massive Ultramafic	LM-047	17	45	1733	3220	0.31
	BT-056	7	54	88	94	0.54
Komatiite	16SH26	14	53	540	1410	0.48
	TL-010	17	51	295	867	0.64
Basaltic Komatiite	16SH21	4	62	310	890	0.48
	16SH22	8	55	103	652	0.55
Pyroxenite	TL-066	6	52	60	18	0.67
	TL-116A	23	47	178	3117	0.47

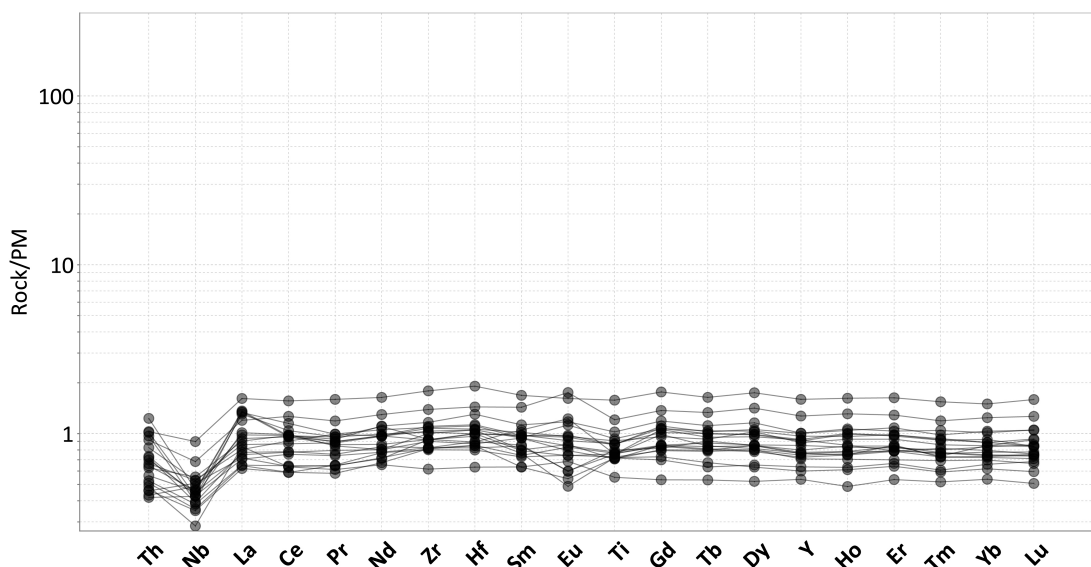


Figure 5.3 Primitive mantle normalized multi-element diagram of orthocumulate ultramafic rocks (normalizing values from Sun and McDonough, 1989)

5.3 Komatiites

The komatiitic rocks in the field area were classified based on the presence of spinifex texture, but are lacking some geochemical signatures typical of komatiites. According to Arndt et al. (1997; 2004), the accepted composition of a komatiitic rock is MgO >18 wt. %, SiO₂ of 40-45 wt. %, Ni >400 ppm and Cr >800 ppm. The komatiites in this study are characterized by MgO contents that are lower than the accepted values for komatiites (2-17 wt. %) and variable SiO₂ (47-67 wt. %; Table 5.1). The Ni and Cr are variable with most samples within the accepted range for komatiitic rocks (Ni= 47-540 ppm; Cr= 188-1410 ppm; Table 5.1). The komatiite samples show two distinct patterns. One is characterized by enriched LREE (La/Sm_n= 1.02-3.22) with slightly fractionated HREE (Gd/Yb_n= 1.4-2.13). The second pattern is characterized by relatively depleted LREE (La/Sm_n= 1.02-1.63) and flat HREE (Gd/Yb_n= 1.01-2.13; Fig. 5.5). Both groups show a negative Nb anomaly and have Al₂O₃/TiO₂ indicative of AUK (Al₂O₃/TiO₂= 17-29; Fig. 5.4). Figure

5.4 shows the Al_2O_3 vs. TiO_2 trend lines of AUK and ADK komatiites. The majority of samples plot along the AUK trend line, with some plotting closer to ADK on Figure 5.4.

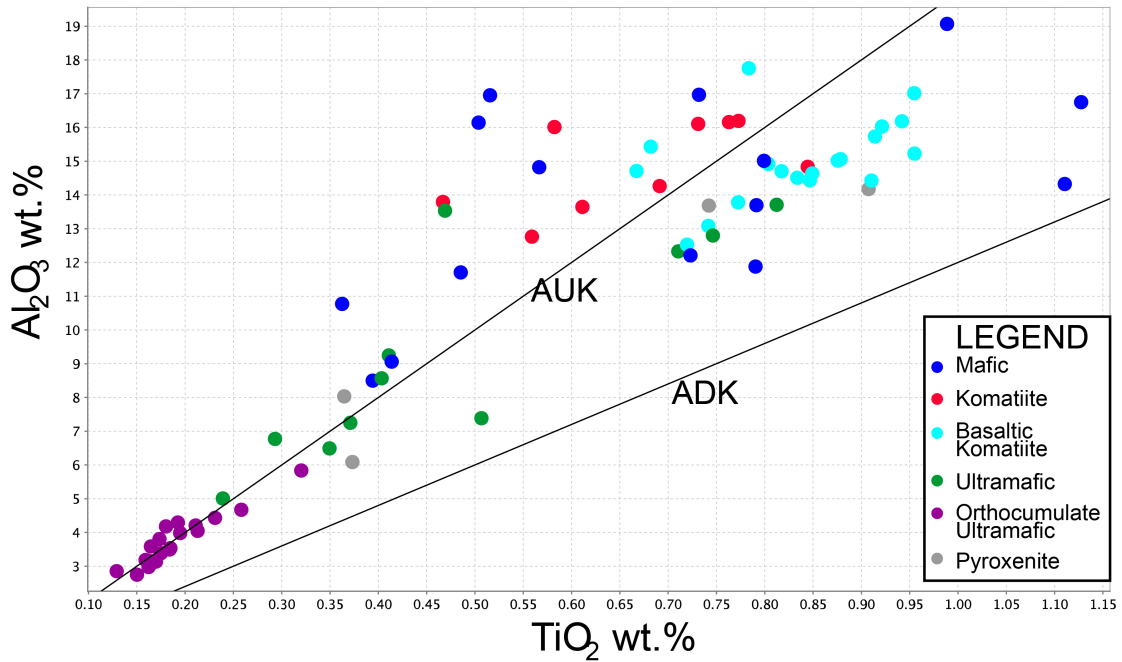


Figure 5.4 Variation diagram of Al_2O_3 versus TiO_2 . The black lines represent typical AUK and ADK (values from Nesbitt et al., 1979 and Arndt et al., 1997).

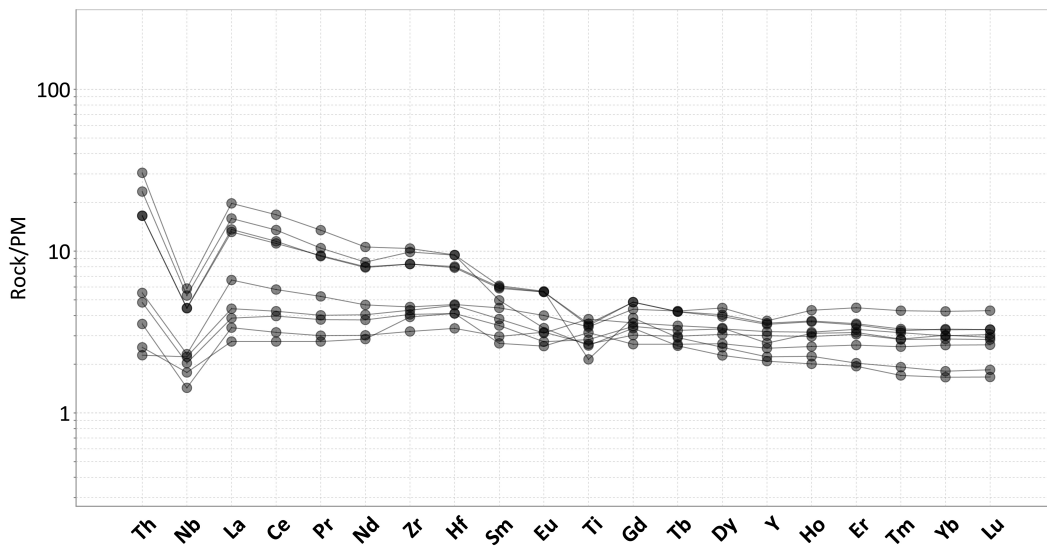


Figure 5.5 Primitive mantle normalized multi-element diagram of komatiites (normalizing values from Sun and McDonough, 1989).

5.4 Massive Ultramafic Rocks

These samples show MgO values that are both higher and lower than is typical for an ultramafic rock (5-29 wt.%) with anomalously high SiO₂ (41-65 wt.%; Table 5.1). There is a large range of Ni and Cr contents, which vary from depleted to enriched relative to a typical ultramafic rock (Ni= 349-3237 ppm; Cr= 449-5423 ppm; Table 5.1). With one exception, the samples have depleted LREE (La/Sm_n= 0.86-2.42) and flat HREE (Gd/Yb_n= 0.83-1.45) similar to the komatiites (Fig. 5.6). The outlying sample shows elevated LREE (La/Sm_n= 3.49) and fractionated HREE (Gd/Yb_n= 1.45; Fig. 5.6). All samples have a negative Nb anomaly and Al₂O₃/TiO₂ indicative of AUK (Al₂O₃/TiO₂= 16-28; Fig. 5.4). These samples plot with a linear correlation just below the AUK trend line (Fig. 5.4).

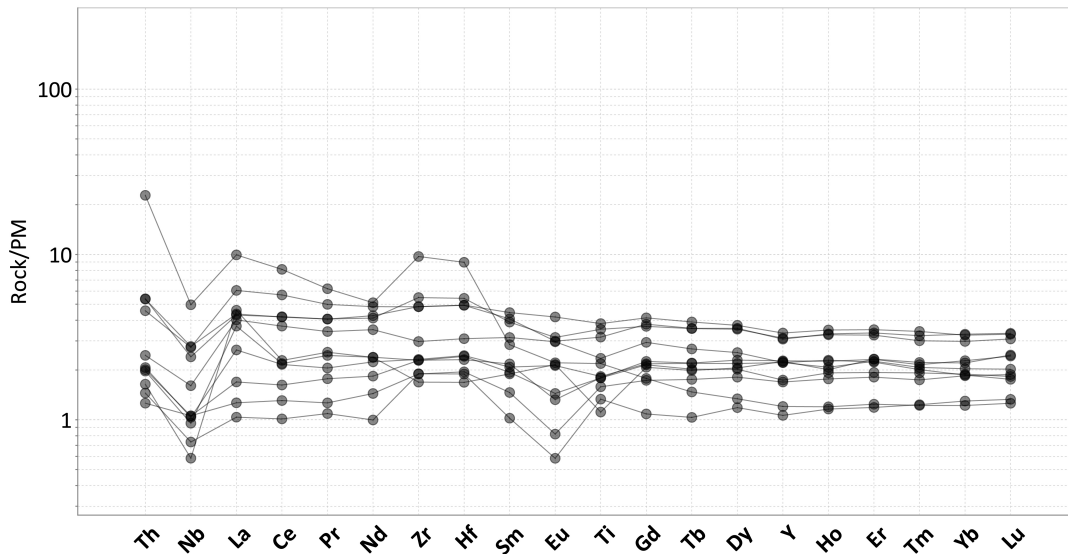


Figure 5.6 Primitive mantle normalized multi-element diagram of massive ultramafic rocks (normalizing values from Sun and McDonough, 1989).

5.5 Basaltic Komatiites

There are 19 basaltic komatiite samples in the sample set. They display low MgO for an ultramafic rock (4-9 wt.%), high SiO₂ (49-62 wt.%), and a range of Ni

and Cr (Ni= 75-1324 ppm; Cr= 60-3526 ppm; Table 5.1). The basaltic komatiites have depleted LREE ($La/Sm_n = 0.84-1.32$) and flat HREE ($Gd/Yb_n = 1.08-1.42$; Fig. 5.7). Samples show a slight negative Nb anomaly and Al_2O_3/TiO_2 consistent with AUK ($Al_2O_3/TiO_2 = 17$; Fig. 5.4). These samples plot below the AUK trend line on Figure 5.4.

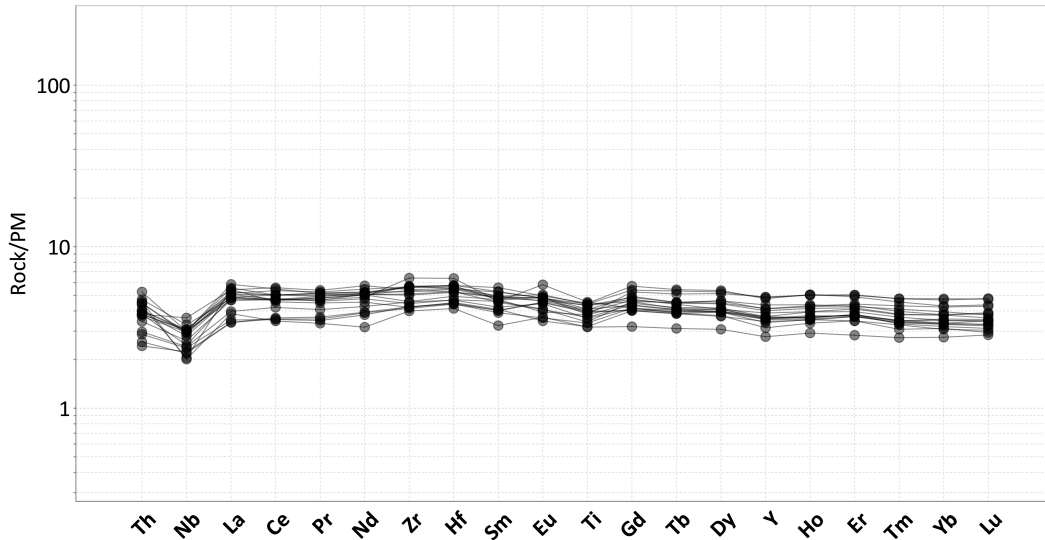


Figure 5.7 Primitive mantle normalized multi-element diagram of basaltic komatiites (normalizing values from Sun and McDonough, 1989).

5.6 Pyroxenite

Four pyroxenite samples were recognized within the field area. They are characterized by variable MgO (6-23 wt. %) and SiO_2 (47-52 wt. %) with low Ni and variable Cr (Ni= 60-277 ppm; Cr= 18-3849 ppm; Table 1). The primitive mantle normalized trace element diagrams show depleted LREE ($La/Sm_n = 0.75-1.23$) and flat HREE ($Gd/Yb_n = 0.9-1.23$; Fig. 5.8).

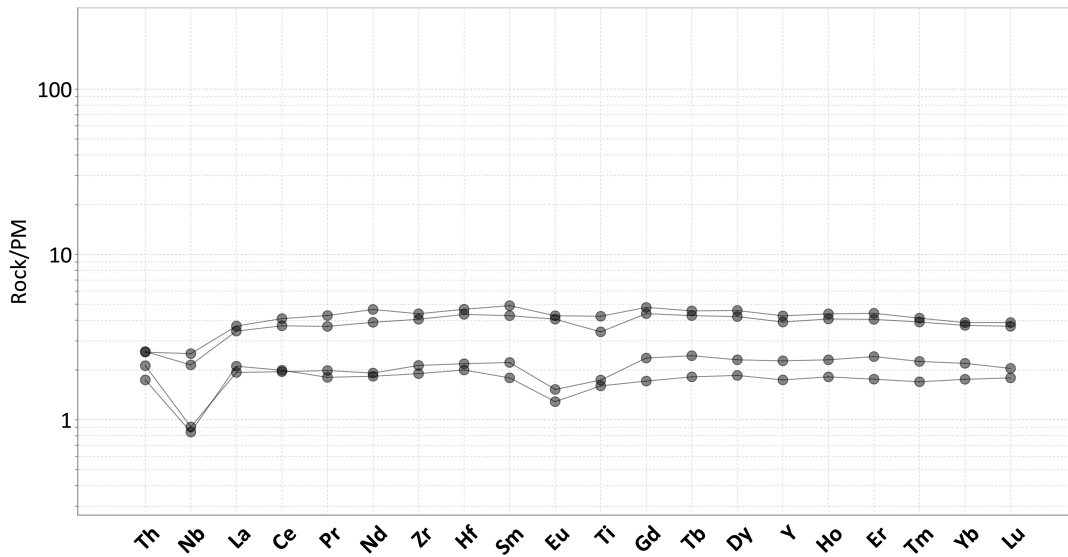


Figure 5.8 Primitive mantle normalized multi-element diagram of pyroxenites (normalizing values from Sun and McDonough, 1989).

5.7 Mafic Rocks

The mafic rocks comprise 15 samples in the sample set, and the chemistry within this lithology is variable. The samples show variable MgO (1-18 wt. %), SiO₂ (48-63 wt. %), Ni and Cr (Ni= 28-2304 ppm; Cr= 47-4836 ppm; Table 5.2). Samples can be divided into two groups based on their rare earth elements. The first is characterized by slight depletion to enrichment in LREE (La/Sm_n= 0.67-1.9) and a flat to weakly fractionated HREE (Gd/Yb_n= 0.94-1.33). The second pattern shows enriched LREE (La/Sm_n 2.26-3.8) and fractionated HREE (Gd/Yb_n= 2.05-5.03; Fig. 5.9). Both patterns are characterized by negative Nb anomalies.

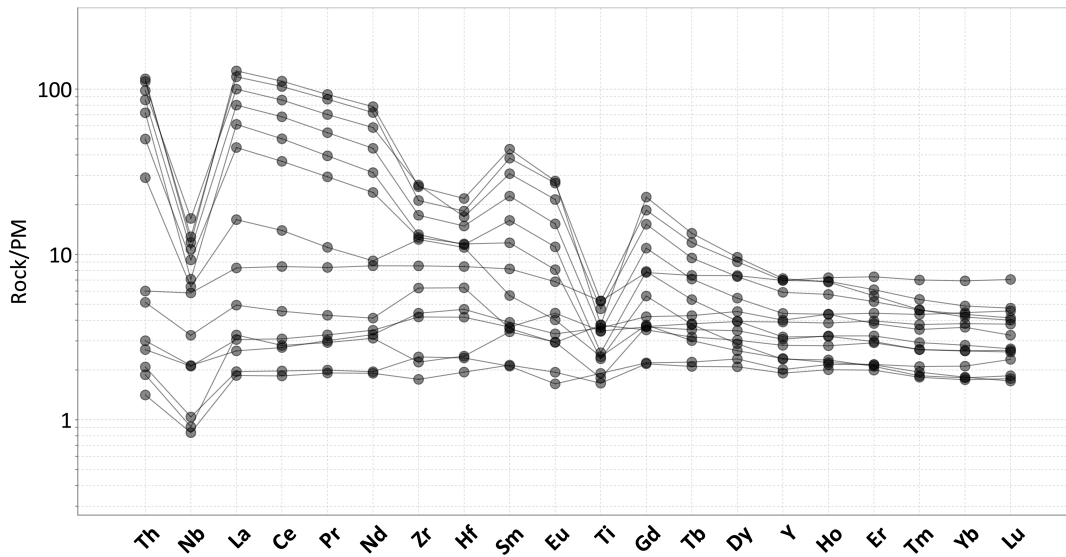


Figure 5.9 Primitive mantle normalized multi-element diagram of mafic rocks (normalizing values from Sun and McDonough, 1989).

Table 5.2 MgO, SiO₂, Ni, and Cr contents of the mafic, intermediate, and felsic lithologies

Rock Type	Sample #	MgO (wt. %)	SiO ₂ (wt. %)	Ni (ppm)	Cr (ppm)	Nb/Nb*
Mafic	TL-062	7	51	66	221	0.71
	LM-037	16	59	2304	4836	0.53
Intermediate	TL-022	1	63	11	26	0.13
	TL-093	8	57	212	740	0.67
Felsic	LM-028	2	83	24	22	0.23
	16SH01	8	67	201	504	0.22
Monzonite	TL-078	5	52	45	89	0.10
	TL-079	4	57	75	182	0.14

5.8 Intermediate Metavolcanic Rocks

The intermediate metavolcanic rocks contain variable MgO (1.8-8.6 wt.%) and SiO₂ (53-77 wt.%) with low Ni and Cr contents (Ni= 11-277 ppm; Cr= 26-885 ppm; Table 5.2). The samples show two distinct patterns. The first has slightly depleted LREE (La/Sm_n= 0.87-1.06) with flat HREE (Gd/Yb_n= 1.10-1.40), whereas the second pattern has enriched LREE (La/Sm_n= 3.52-5.22) with fractionated HREE (Gd/Yb_n= 1.75-2.78; Fig. 5.10). All samples display negative Nb anomalies.

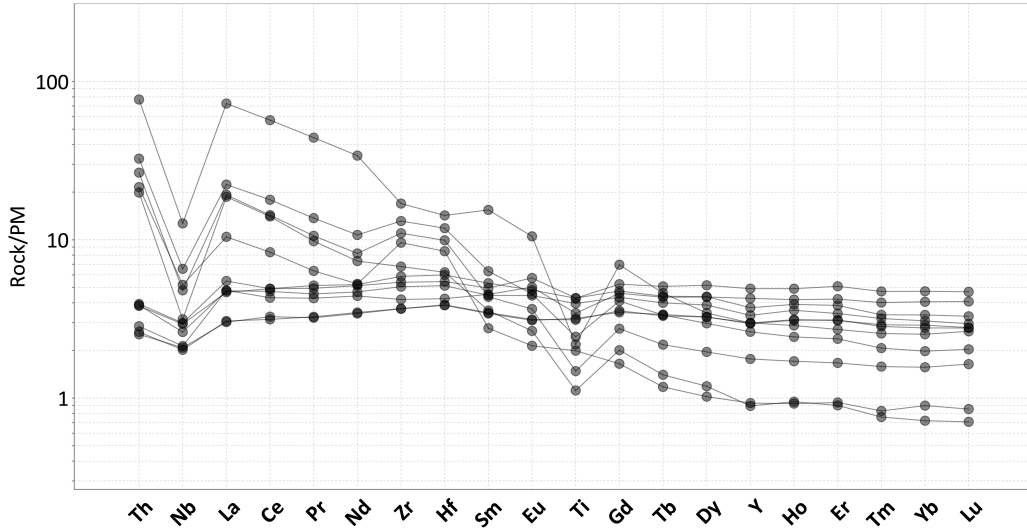


Figure 5.10 Primitive mantle normalized multi-element diagram of intermediate rocks (normalizing values from Sun and McDonough, 1989).

5.9 Felsic Rocks

The felsic rocks (four samples) have low MgO (2-8 wt.%) and high SiO₂ (67-83 wt.%), along with low Ni and Cr (Ni= 24-201 ppm; Cr= 34-201 ppm; Table 5.2). The samples show uniform patterns with enriched LREE (La/Sm_n= 3.02-3.77) and slightly fractionated HREE (Gd/Yb_n= 1.83-2.33; Fig. 5.11). All samples display negative Nb anomalies.

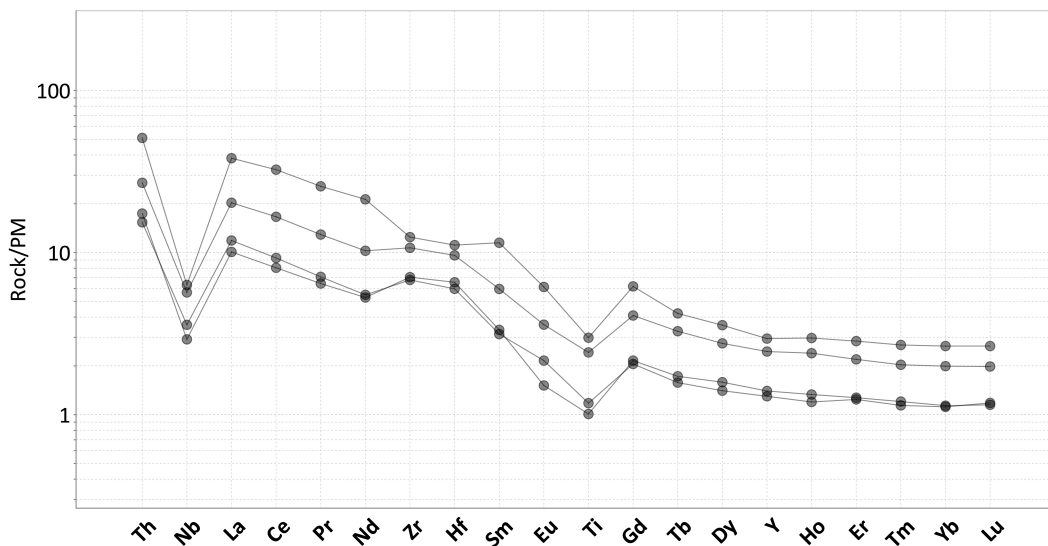


Figure 5.11 Primitive mantle normalized multi-element diagram of volcanoclastic rocks (normalizing values from Sun and McDonough, 1989).

5.10 Monzonite

The monzonites comprise a small portion of the sample set (two samples). They contain low MgO (4-5 wt.%) and high SiO₂ (52-57 wt.%), along with low Ni and Cr (Ni= 45-75 ppm; Cr= 89-182 ppm; Table 5.2). The samples show enriched LREE (La/Sm_n= 3.33-4.16) and slightly fractionated HREE (Gd/Yb_n= 3.21-4.09; Fig. 5.12). All samples display negative Nb anomalies.

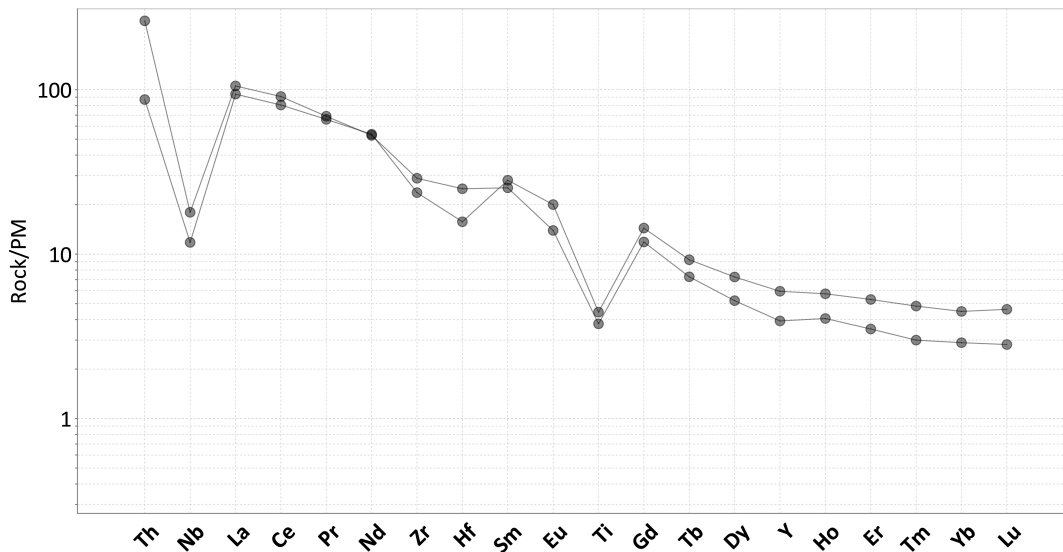


Figure 5.12 Primitive mantle normalized multi-element diagram of monzonite rocks (normalizing values from Sun and McDonough, 1989).

5.11 Sm-Nd Isotopic Geochemistry

The samples display a small range of ϵ_{Nd} values from +2.34 to +2.83. The samples show initial $^{143}Nd/^{144}Nd$ ratios from 0.50936 to 0.50948 and current $^{143}Nd/^{144}Nd$ ratios range from 0.51128 to 0.51276 (Table 5.3).

Table 5.3 Summary table of Sm/Nd isotopic values.

Sample	$^{143}Nd/^{144}Nd$ current	$\epsilon_{Nd}(2719)$ Ma)	$^{143}Nd/^{144}Nd$ initial	Model Age (Ma)
TL-16-SH-074	0.51276	2.76	0.50948	2353
TL-16-SH-075	0.51266	2.74	0.50948	2540
TL-16-SH-098	0.51209	2.40	0.50942	2687
TL-16-SH-106	0.51247	2.67	0.50946	2587
16-SH-21	0.51258	2.83	0.50947	2486
16-SH-29	0.51128	2.34	0.50936	2726

Chapter 6: Discussion

6.1 Stratigraphic Relationships

The two assemblages of the Shebandowan greenstone belt present within the study area are the Shebandowan and Greenwater assemblages. The Shebandowan assemblage consists of calc-alkalic to alkalic mafic to felsic volcanic rocks and volcanic breccia, as well as clastic sedimentary rocks including conglomerate, with minor argillite, wacke, and iron formation (Williams et al., 1991; Corfu and Stott, 1998; Lodge, 2013). The Greenwater assemblage consists of tholeiitic basalts, basaltic komatiites, komatiite flows, intermediate and felsic extrusive volcanic rocks and pyroclastic flows, as well as banded iron formation, wackes, and argillite (Williams et al., 1991; Corfu and Stott, 1998; Lodge, 2012).

6.2 Shebandowan Assemblage

The Shebandowan assemblage contains the youngest rocks within the field area, with an age of 2690 Ma to 2680 Ma. The 2690 Ma age was based on $^{206}\text{Pb}/^{207}\text{Pb}$ dating of zircons from intermediate volcanics and Tower Stock done by Corfu and Stott (1998), while the 2680 Ma age was based on $^{206}\text{Pb}/^{207}\text{Pb}$ dating of detrital zircons analyzed from several sedimentary lithologies (Lodge et al., 2013). The lithologies in the field area interpreted to be a part of the Shebandowan assemblage include mafic metavolcanic rocks (located in the western portion of the field area), intermediate metavolcanic rocks, volcanoclastic rocks, a monzonite dyke, and conglomerate. Shegelski (1980) interpreted the Shebandowan assemblage to have been deposited in shallow water to subaerial environment. In the study area, these lithologies are seen adjacent to the NE trending fault (Fig. 6.1).

The conglomerate, which comprises the largest portion of the Shebandowan assemblage in the study area, is a heterolithic pebble conglomerate with plutonic, volcanic, and sedimentary clasts, rock types which are found in the surrounding area (Lodge, 2013; Lodge et al., 2014). The conglomerate was deposited in a shallow-water to sub-aerial environment, likely before and after the main period of volcanism (Shegelski, 1980; Corfu and Stott, 1998). It contains clasts of the older Greenwater assemblage lithologies and is interlayered with laterally discontinuous units of Shebandowan assemblage intermediate volcanoclastic rocks, implying that the deposition of the conglomerate would have been after the formation of the Greenwater assemblage and co-depositional with the emplacement of these Shebandowan assemblage felsic and intermediate volcanoclastic rocks.

Based on cross-cutting relationships, the monzonite dyke appears to be the youngest lithology in the assemblage, however the monzonite clasts in the conglomerate imply that the monzonite predates the conglomerate, and the appearance of the cross-cutting dyke is interpreted to be the result of paleotopography. The monzonite is a fine- to medium-grained, highly magnetic, pink rock. It contains plagioclase, potassium feldspar, and magnetite, with lesser amounts of quartz and hornblende. It is physically, petrographically, and geochemically similar to the Tower Mountain Intrusive Complex approximately 5 km to the northeast which varies in composition from syenite and monzonite to diorite (Fig. 6.2; Lodge et al., 2013; Gelinis et al., 2016). It is likely that this monzonite dyke is petrogenetically related to the Tower Mountain Intrusive Complex, which is known to host gold mineralization (Jobin-Bevans et al., 2006).

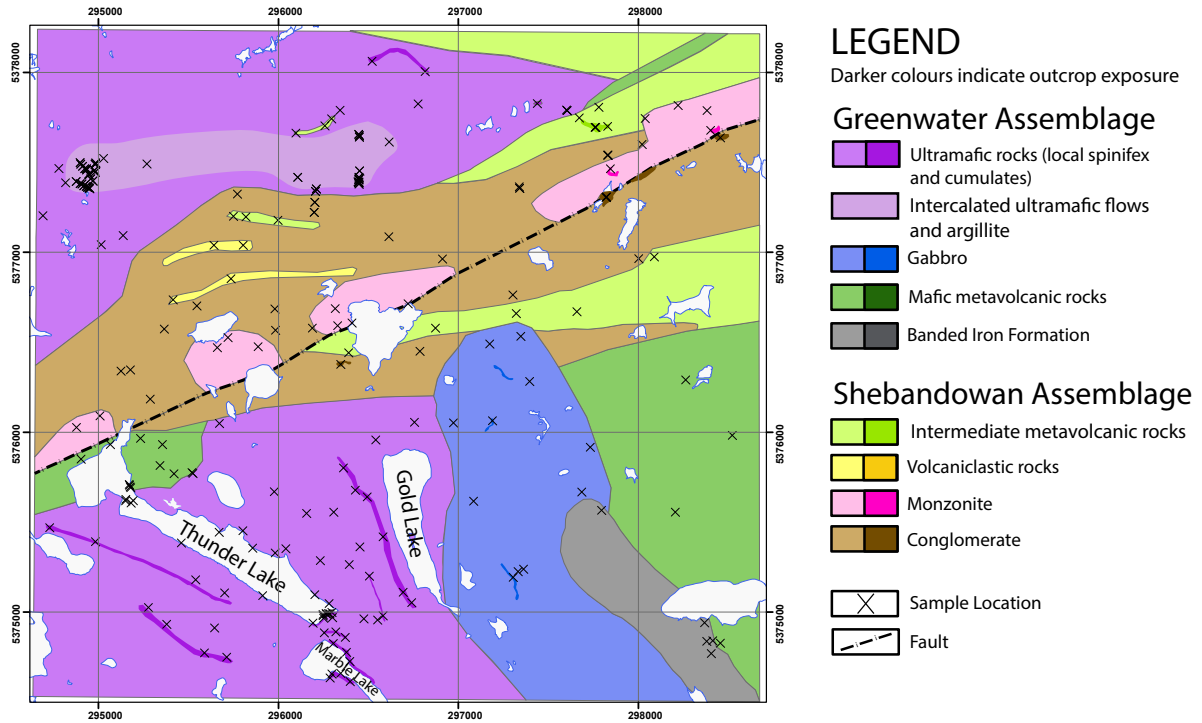


Figure 6.1 Geological map of the study area based on data collected in the summer of 2016. The younger Shebandowan assemblage is located in the central map area along the fault, between two packages of the Greenwater assemblage rocks.

Lenses of the felsic and intermediate volcaniclastic rocks are found within the conglomerate, implying that they were co-depositional with the conglomerate (Fig. 6.1). The felsic and intermediate volcaniclastic rocks contain no flow textures, tuffaceous bedding, or any other indicators of how they were emplaced. It is likely that these subtle indicators and textures have been overprinted and destroyed as the very fine-grained nature of these rocks makes them susceptible to physical changes during greenschist facies metamorphism and subsequent hydrothermal alteration that occurred in the study area.

The felsic and intermediate volcaniclastic rocks display LREE enrichment with negative Nb and Ti anomalies, variable Zr/Hf anomalies, as well as fractionated HREE ($Gd/Yb_{cn} = 1-5$), which suggests that the melt was sourced from within the

garnet stability field (Irving and Frey, 1978; Fig. 6.3); these geochemical features are characteristic of the calc-alkalic Shebandowan assemblage and distinguish it from the Greenwater assemblage (Williams et al., 1991; Corfu and Stott, 1998). The mafic rocks in the Shebandowan assemblage are similar to Greenwater assemblage mafic rocks in the field, and were distinguished through geochemistry (Fig. 6.3).

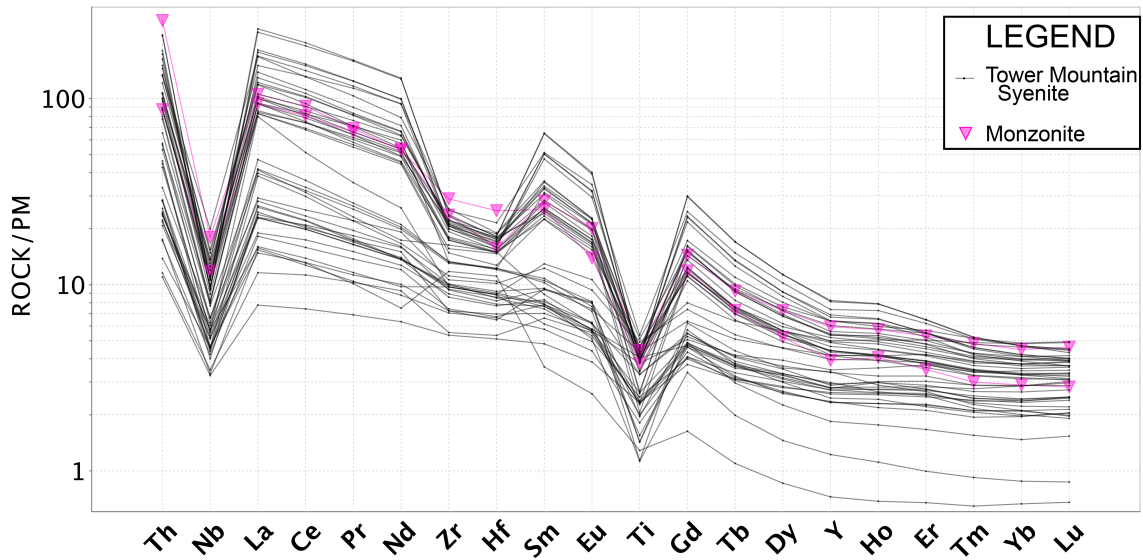


Figure 6.2 Primitive mantle normalized multi-element diagram of A) Tower mountain syenite rocks and B) monzonite rocks from the field area (Gélinas et al., 2016; normalizing values from Sun and McDonough, 1989).

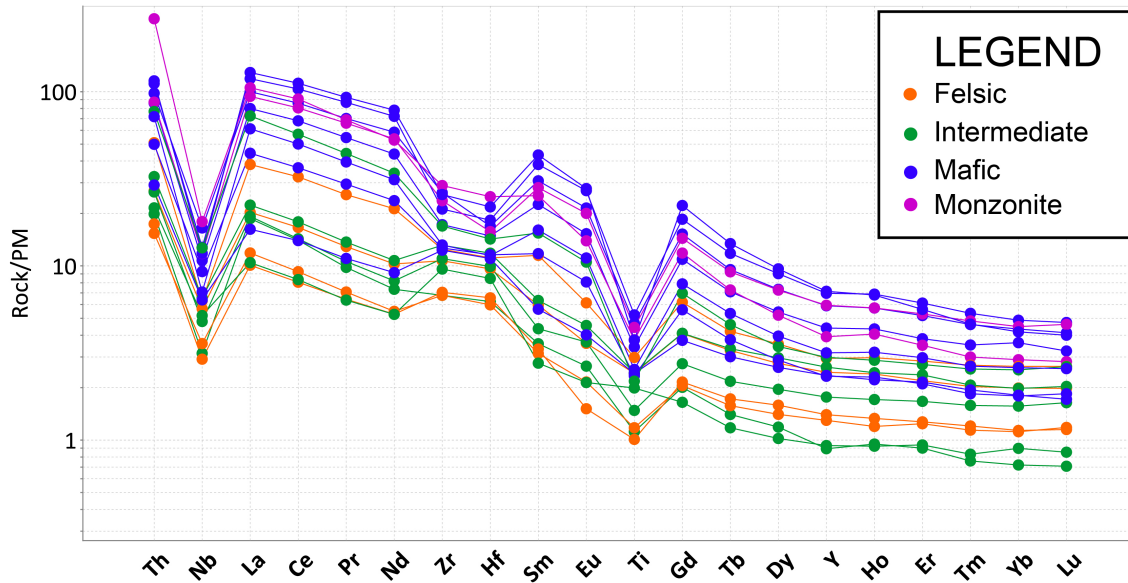


Figure 6.3 Primitive mantle normalized multi-element diagram of Shebandowan assemblage rocks (normalizing values from Sun and McDonough, 1989).

6.3 Greenwater Assemblage

The Greenwater assemblage in the eastern portion of the Shebandowan greenstone belt has been dated between 2718 ± 2 Ma and 2722 ± 2 Ma (based on $^{207}\text{Pb}/^{206}\text{Pb}$ dating of four zircons from felsic units in different parts of the assemblage, including: Kabaigon Lake, Gold Creek, Marks Lake, and Mud Lake), making them the oldest rocks in the study area (Corfu and Stott, 1998). The Greenwater assemblage is distinguished from the Shebandowan assemblage by the presence of tholeiitic volcanism and argillite-dominated sedimentary sequences (Williams et al., 1991; Corfu and Stott, 1998). There are thick argillite and chert beds present within the trenches and elsewhere in the field area. These rocks are sulfide-rich and contain radial pyrite concretions up to 5 cm in diameter. In order for the argillite beds to form at thicknesses of up to 15 m (as seen in trench 1A), an undisturbed deep-water environment (below wave base) is necessary (Price, 1964).

All of the contacts in the field area are inferred, except in the trenches where contacts were observed. The stratigraphy and timing of the ultramafic rocks are difficult to determine as overburden covered any contacts. The best exposure was found in trench 4A. The 90 m long trench contained a repetitive sequence of massive to brecciated komatiite flows, peperite zones, brecciated to massive chert, peperite zone, and then back to komatiite (Fig. 6.4). This repetitive sequence could be the result of hypabyssal ultramafic intrusions, or komatiites being emplaced at the sediment-surface interface (Skilling et al., 2002). Due to the density contrast between unconsolidated sediment and ultramafic magma, the most likely cause of these repetitive sequences would be hypabyssal intrusions, as the magma would not be buoyant enough to reach the sediment-surface interface. A segment of the trench (at the 50-60 m mark) where a chert horizon has no peperitic contacts above or below it could be caused by thermal erosion of the peperitic contact, or the peperite not being universally developed (Fig. 6.4). Polyhedral jointing in the komatiitic rocks of trench 1E could have been formed within a hypabyssal intrusion, much like columnar basaltic dykes seen in Iceland and Italy (Vinciguerra et al., 2005).

The hypabyssal intrusions within the trench exposure are 5-10 m thick and may be laterally extensive, however; they were not traced out in the field so the true lateral extent is not known. Some intrusions in the field area are thicker than the hypabyssal intrusions and contain different textures than those seen in the trenches. There is still uncertainty surrounding the possible lateral extent of komatiite flows and hypabyssal intrusions as they cannot be observed in modern day settings (Arndt et al., 2008). Arndt et al. (1979) have described examples at every scale from

small dykes and sills less than a meter thick up to large dunitic intrusions several hundreds of meters thick. In the southern portion of the field area there are several ridges approximately 1 km in length that correspond to linear magnetic anomalies on the regional aeromagnetic maps (Ontario Geological Survey, 2003). These linear ridges are composed of orthocumulate ultramafic rocks with medium-grained serpentinized olivine crystals. They are interpreted to be large intrusive units, which would take longer to cool, resulting in the observed medium-grained cumulate textured olivine that was observed.

Basaltic komatiites are abundant in the trench exposures of the northern portion of the map area, but were not identified in the southern portion of the field area. These rocks were difficult to distinguish in outcrop, and were mainly identified through geochemistry. The basaltic komatiites in the study area have MgO contents ranging from 4-9 wt. % with SiO₂ ranging from 49-62 wt. %. Arndt et al. (2008) stated that basaltic komatiites can be distinguished from other basalts and associated with nearby komatiites through spatial relationships, textural features, and chemical characteristics. The basaltic komatiites of the Greenwater assemblage are found in close spatial association with the komatiitic rocks, and are geochemically similar to the associated komatiites and orthocumulate ultramafic rocks (Fig. 6.5). Basaltic komatiites can form either by contamination or fractionation of komatiitic magma (Puchtel and Humayun, 2001; Malviya et al., 2006). The basaltic komatiites in the field area are interpreted to have formed through fractionation of komatiitic magma, as there is insufficient evidence to support a crustal contamination petrogenesis for the field area (see section 6.4).

There are several pyroxenites seen in the south, one being a northwest trending ridge, but none were found in the north (Fig. 6.1). Pyroxenites can form through fractionation of an ultramafic magma (Sobolev et al., 2007). Based on geochemical similarities (flat LREE and HREE on primitive mantle normalized rare earth element diagram) and the proximity between them, this pyroxenite ridge is likely related to the orthocumulate ultramafic rocks in the area.

The tholeiitic rocks of the Greenwater assemblage display flat HREE on a primitive mantle normalized multi-element diagram (Fig. 6.5). The coexistence of Greenwater tholeiitic and Shebandowan calc-alkalic magmatism, coupled with a close association of sulfide-rich, deep-water argillites with komatiitic flows (as seen in the trenches) is consistent with a rifted active arc to back-arc system (Johnson et al., 1994; Polat et al., 1999).

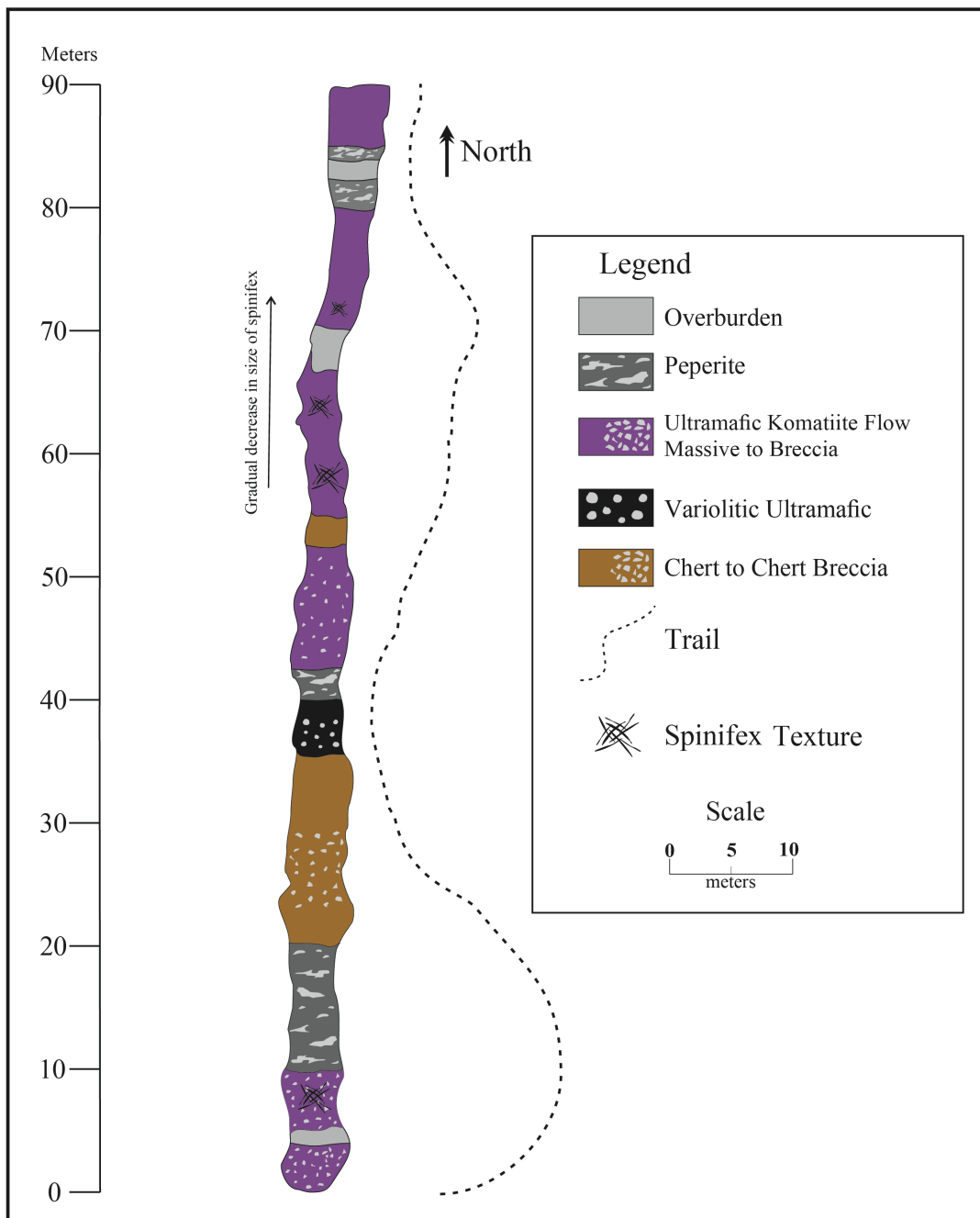


Figure 6.4 Map of trench 4A from Series 4 trenches displaying lithologies and the transitions between them (modified from Hinz et al., 2016).

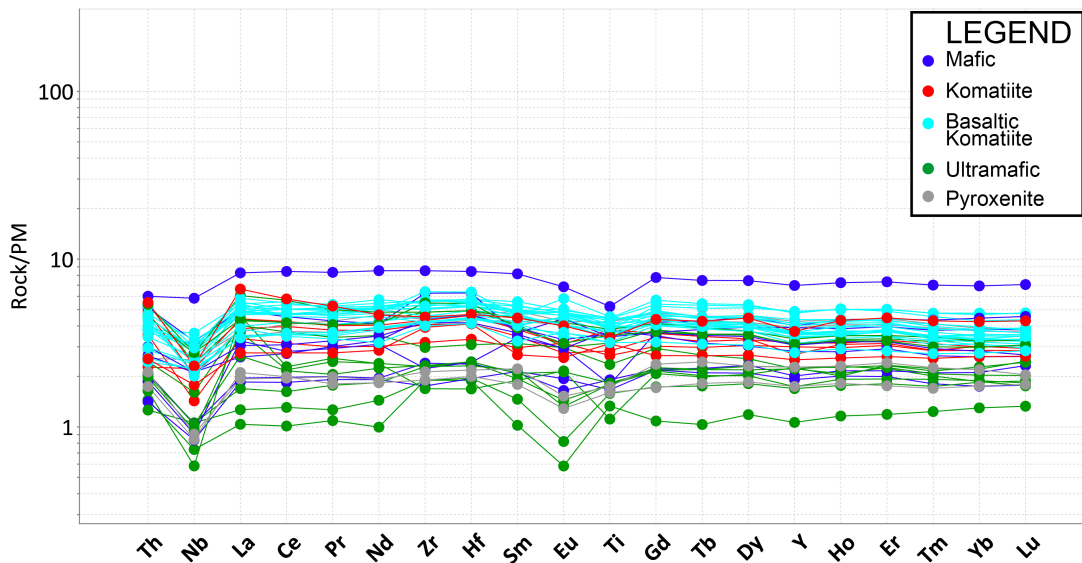


Figure 6.5 Primitive mantle normalized multi-element diagram of Greenwater assemblage rocks (normalizing values from Sun and McDonough, 1989).

6.4 Petrogenesis

The majority of komatiitic rocks formed in the Archean with only a few examples found in the Phanerozoic, such as a Cretaceous occurrence on Gorgona Island (Kerr et al., 1996; Arndt et al., 2008; Dostal, 2008). In the Archean, the geothermal gradient was much higher than the present day, and as such, it was easier to generate the large percentage of partial melting of the mantle necessary for komatiite formation (Nesbitt et al., 1979; Arndt et al., 2008). Most researchers believe that the mantle has cooled significantly since the Archean, this being the main reason for the absence of komatiites in recent geologic history (Nisbet et al., 1993; Vlaar et al., 1994; Herzberg, 1995; Herzberg and O'Hara, 1998; Arndt et al., 2004; Arndt et al., 2008; Herzberg et al., 2010). It is generally accepted that komatiitic rocks have a mantle plume origin (Nesbitt et al., 1979; Campbell et al., 1989; Arndt et al., 2008). This requires partial melting of the mantle and a subsequent upwelling of this magma into the lithosphere (Campbell et al., 1989). In

the Archean mantle, temperatures up to 1600-1900 °C would be required to produce a komatiitic composition, as higher MgO contents results from higher melting temperatures and higher degrees of melting (Green et al., 1975; Campbell et al., 1989; Dostal, 2008).

Aluminum-undepleted komatiites (Munro-type) have high MgO contents and low abundance of incompatible trace elements, which indicates that the melt was generated by a high-degree of partial melting when Mg-rich olivine and orthopyroxene were the dominant phases entering the melt (Herzberg, 1995; Dostal, 2008). Aluminum undepleted komatiites have a high $\text{Al}_2\text{O}_3/\text{TiO}_2$ ratio (~ 20), a $\text{CaO}/\text{Al}_2\text{O}_3$ ratio of 1 and flat heavy rare earth element patterns on a multi-element spider diagram (Fig. 6.6) and are interpreted by Herzberg (1995) to have formed at depths of 150-200 km and approximately 50% partial melting.

Aluminum-depleted komatiites (Barberton-type) have slightly lower MgO contents than AUK and relatively higher abundances of incompatible trace elements, which suggests that the melt was generated by a lower-degree of partial melting ($\sim 30\%$), aluminum depleted komatiites have a low $\text{Al}_2\text{O}_3/\text{TiO}_2$ ratio (<12), a $\text{CaO}/\text{Al}_2\text{O}_3$ ratio of 2-2.5 and fractionated heavy rare earth element patterns on a multi-element spider diagram (Fig. 6.6); they are interpreted by Herzberg (1995) to have formed at depths of 300-450 km and approximately 30% partial melting when garnet was the dominant phase entering the melt (Herzberg, 1995; Dostal, 2008).

The komatiites in the study area have an average $\text{Al}_2\text{O}_3/\text{TiO}_2$ ratio of 19.85, an average $\text{CaO}/\text{Al}_2\text{O}_3$ ratio of 0.76, and they display a flat HREE pattern on a multi-element spider diagram (Figs. 6.5; 6.6). Based on major and trace element

geochemistry, the komatiites in the study area are interpreted to be AUK-type (Figs. 6.5, 6.6). Archean plumes are thought to be comprised of depleted mantle material, which is consistent with the low abundance of incompatible trace elements in AUK (Campbell et al., 1989; Leshner and Arndt, 1995; Dostal, 2008). A mantle plume can account for the high temperatures required for komatiite formation, however, others suggest this can also be achieved by adding water to the melt, decreasing the melting temperature; possibly in the mantle wedge above subduction zones (Parman et al., 1997; 2001; 2004; Grove and Parman, 2004; Dostal, 2008).

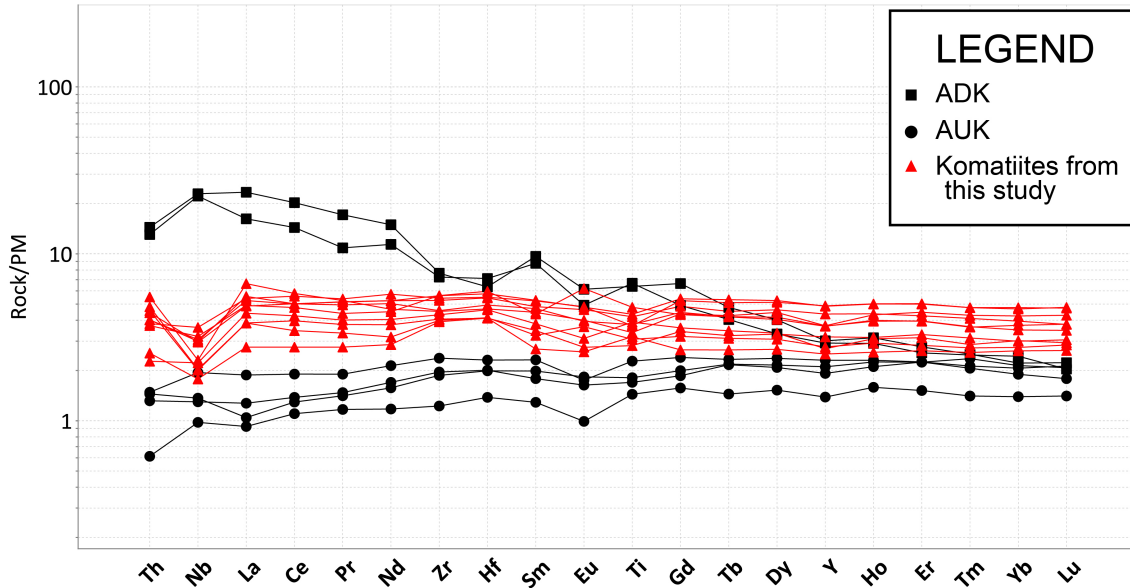


Fig. 6.6 Primitive mantle normalized multi-element spider diagrams of typical AUK and ADK from the Lumby Lake greenstone belt and komatiites from this study (Hollings and Wyman, 1999; normalizing values from Sun and McDonough, 1989).

Several inconsistencies complicate the classification of the ultramafic rocks within the study area. Many of the samples were described as ultramafic rocks in the field based on spinifex texture and colour index as the rocks were very fine-grained and most minerals could not be distinguished in the field (except spinifex texture).

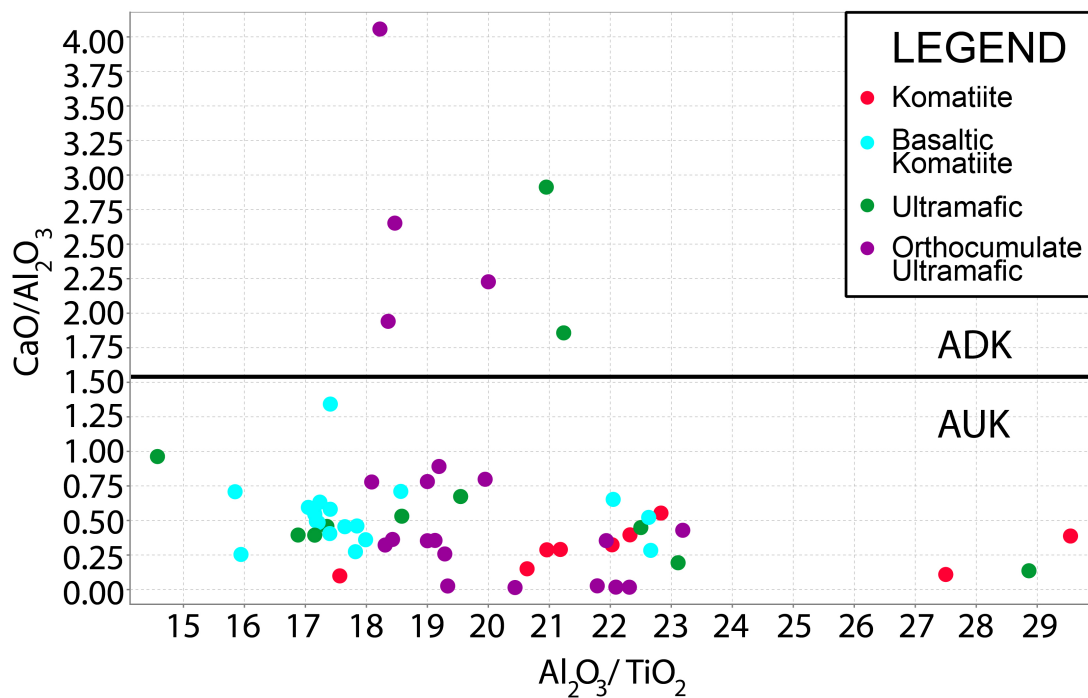


Figure 6.7 Variation diagram showing CaO/Al_2O_3 vs. Al_2O_3/TiO_2 of ultramafic lithologies, showing that the majority of samples fit within the AUK field. Dividing line is from Dostal (2008).

These ultramafic samples contain MgO of greater than 18 wt. % and fit the AUK trend of flat to LREE depleted primitive mantle normalized multi-element patterns (Fig. 6.5), but contain SiO_2 between 45 and 66 wt. %. The typical SiO_2 for AUK would be between 40-45 wt. % (Arndt et al., 2008). The high SiO_2 in the samples could be caused by: 1) the rocks being contaminated by crustal material during emplacement, 2) the rocks having been silicified during alteration and metamorphism, 3) the rocks not being komatiites.

The ultramafic rocks in the field area all have higher CaO than is normal for these rock types, which combined with the anomalously high SiO_2 suggests hydrothermal alteration. The rocks of the study area do not fit the many geochemical characteristics of siliceous high-magnesium basalt, and therefore are interpreted to be altered komatiites. Therefore, it is likely that the high SiO_2 in these

rocks was added after emplacement through alteration and metamorphism; this was the case in the Barberton greenstone belt, South Africa (Hanor and Duchač, 1990; Hofmann and Harris, 2008)

One unusual characteristic of the rocks in the study area is a distinct negative Nb anomaly (Fig. 6.5). Typical AUK and ADK komatiites do not usually show this feature (Jochum et al., 1991; Fig. 6.6). Niobium is an incompatible element that is stable in the melt and unstable in the crust. Negative Nb anomalies can be caused by the melt interacting with crustal material derived through subduction processes, by being formed above a subduction zone, by the melt being crustally contaminated, or by the melt evolving from a heterogeneous deep mantle source, where depleted Nb is the result of fractionation of perovskite (Jochum et al., 1991; Pearce and Peate, 1995; Dostal, 2008; Pearce, 2008). Determining which of these processes caused the negative Nb anomaly in the rocks of the field area will help define the petrogenesis of the area.

Isotope and trace element geochemistry can be used to examine the petrogenesis of ultramafic rocks. The ϵ_{Nd} for the komatiites was calculated for all samples using an age of 2719 Ma, the accepted age for the Greenwater assemblage (Corfu and Stott, 1998). The ϵ_{Nd} of all six samples of ultramafic rock ranged between 2.34 and 2.83. Several researchers proposed that the Archean mantle had a more primitive ϵ_{Nd} signature of about +4 at 3.5 Ga, based on rocks from Archean greenstone belts and felsic gneiss complexes (Chase and Patchett, 1988; Bennett et al., 1993). Henry et al. (1998) averaged the ϵ_{Nd} of mafic rocks of the Shebandowan greenstone belt as +2.6, which is similar to the data from the field area. If the rocks

were contaminated by thick, old, continental crust, the ϵ_{Nd} would tend to be more negative as Nd is more incompatible in the crust; it is abundant in the melt and mostly absent from continental crust. For Nd to be present within the lithology it would need to obtain the negative Nd signature from contamination of crustal rocks. (Henry et al., 1998; 2000; Tomlinson et al., 2004). The radiogenic isotope data displays characteristics of magmas unaffected by interaction with older crustal material.

If contamination occurred, it can be further evaluated using plots of SiO_2 vs. Nb/Nb^* and SiO_2 vs. La/Sm , as well as examining the Nb/Th ratio (Fig. 6.8; Jochum et al., 1991). Other elements that would partition into the melt during crustal contamination are La, Sm, Nb and Th. As the magma ascends, it may assimilate the crust, causing contamination by SiO_2 and the incompatible elements, creating positive linear trends on variation diagrams (Jochum et al., 1991). There are no positive correlations between SiO_2 , Nb/Nb^* , and La/Sm for the ultramafic lithologies in the field area (Fig. 6.7).

Jochum et al. (1991) showed that the Nb/Th ratios of AUK komatiitic and basaltic rocks are relatively close to the estimated primitive mantle values, and are noticeably lower than those of modern ocean island basalt with similar Nb contents. Jochum et al. (1991) suggested that if the ratio is much higher than the primitive mantle value, crustal contamination occurred. The primitive mantle value of Nb/Th is ~ 9 , and the ultramafic rocks in the study area have Nb/Th values between 1.5 and 9.5, implying there was no contamination by continental crust. This suggests that crustal contamination was not the cause of the negative Nb anomaly. The crust in

the Shebandowan area at 2.7 Ga consisted mainly of oceanic and not continental crust (Corfu and Stott, 1998). There is a 2750 Ma tonalitic phase in the Northern Light Gneissic complex, approximately 100 km to the southwest of the study area (Corfu and Stott, 1998). This complex accounts for the majority of continental crust in the belt; however, it is not seen within the study area (Corfu and Stott, 1998). The nature and association of the assemblages in the field area infers an oceanic formation (tholeiitic ultramafic rocks, thick argillite sequences). Therefore if the melt assimilated oceanic crust during its ascent, the geochemical contamination effect on the melt would be minimal. Oceanic crust is composed of mafic material, and would have a similar composition and ϵ_{Nd} content as the melt (Hofmann and White, 1982). Therefore, crustal contamination had little to no effect on the petrogenesis of the rocks in the field area.

The generally accepted model for komatiite formation involves mantle plumes. However, there are other theories that may account for the negative Nb anomaly present in the geochemistry. The other proposed models for komatiite petrogenesis are emplacement in a suprasubduction zone setting (Pearce and Peate, 1995; Pearce, 2008) or the melt being sourced from a heterogeneous deep mantle (Jochum et al., 1991).

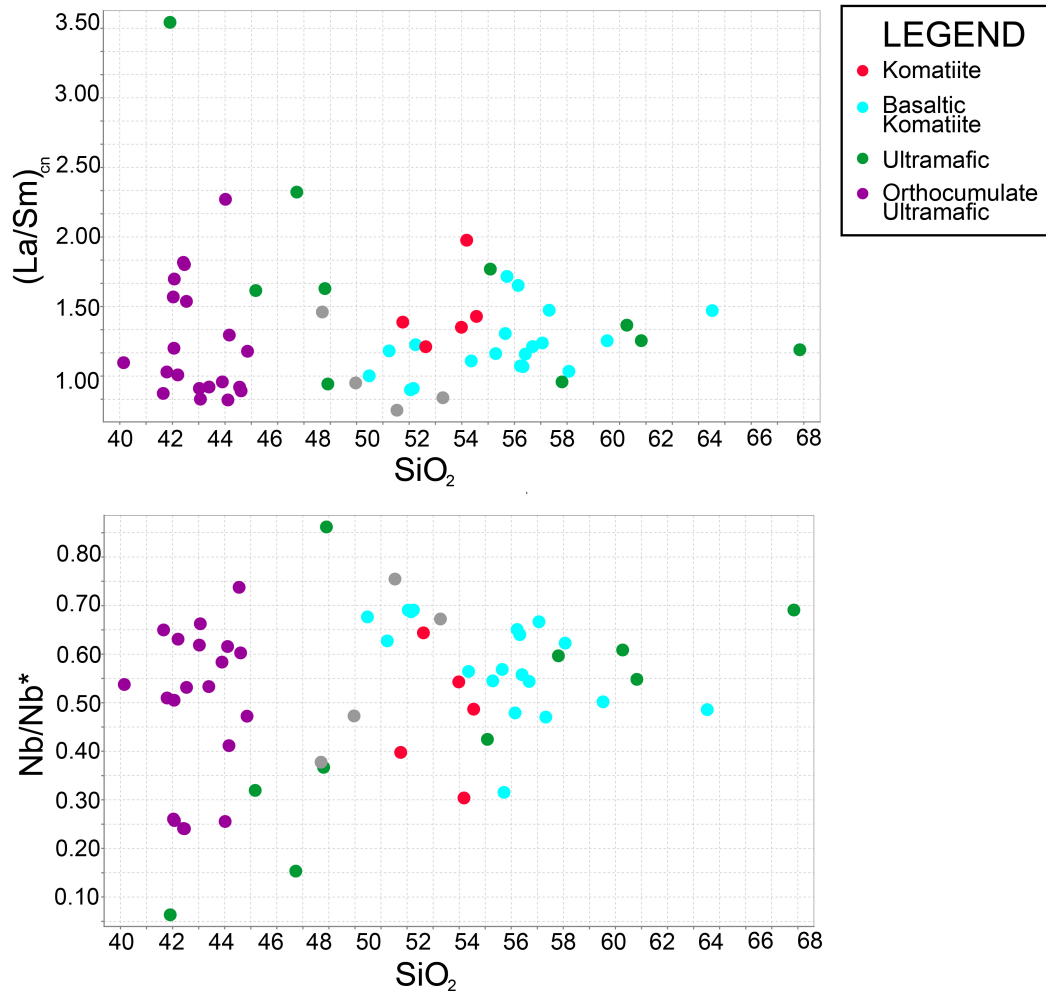


Figure 6.8 Variation diagrams of SiO_2 vs. La/Sm and Nb/Nb^* which show no positive linear trends, implying that crustal contamination did not occur.

Some researchers have proposed that Archean komatiites form in subduction zone settings by hydrous mantle melting (Parman et al., 1997; 2001; 2004). Parman et al. (1997) argued that the preserved igneous minerals, specifically olivine and clinopyroxene spinifex, in komatiite samples from the Komati formation in South Africa could have only been produced from komatiitic magmas that contained >3 wt. % H_2O , which is higher than any modern mantle magma (which average around 0.01 wt. % H_2O ; Bercovici and Karato, 2003). Parman et al. (1997) further suggested that the many similarities between boninites and komatiites is evidence that both

rock types form within subduction zones. Both rock types are characterized by high MgO, low SiO₂, low Ti/Zr, and Zr/Hf enrichments relative to REE. Barr et al. (2009) used experimental mineral chemistry studies to support the hydrous nature of a primary komatiitic magma from Comondale, South Africa. Barr et al. (2009) argued that the presence of Mg-rich pyroxene spinifex indicate magmatic H₂O was a significant part of the melt (~2-5 wt. %) as the Mg# of the initial pyroxenes remained more Mg-rich than the most primitive natural pyroxene. The composition of pyroxene spinifex, specifically the high Cr₂O₃ and Al₂O₃ wt. %, was explained by Barr et al. (2009) to be caused by water in the melt suppressing the pyroxene crystallization. There is pyroxene spinifex present within the field area, however mineral chemistry was not measured due to alteration of the pyroxene crystals, therefore the field area rocks could not be corroborated with the research done by Barr et al. (2009) to determine if the thesis area rocks were formed in a subduction zone.

The third hypothesis for komatiite formation that would produce a negative Nb anomaly is a heterogeneous deep mantle source. Jochum et al. (1991) stated that a heterogeneous mantle could explain the depletion of Th and Nb in some komatiites and basalts. This deep, depleted source in a heterogeneous mantle was likely caused by fractionation of a perovskite phase, as the high field strength elements Th, Nb, Zr, Hf, and Ti are all compatible with Mg-perovskite. Negative HFSE anomalies can be explained by early segregation of this mineral (Kato et al., 1988; 1996; Taura et al., 2001; Corgne et al., 2005; Jochum et al., 1991; Xie et al., 1993; Robin-Popieul et al., 2012).

The komatiites in the study area do not show evidence of crustal contamination. Although crustal contamination theory could account for the negative Nb anomaly visible in all primitive mantle normalized multi-element spider diagrams, it is not supported by linear trends in other variation diagrams such as La/Sm vs. SiO₂, Nb/Nb* vs. SiO₂ (Fig. 6.8). The ε_{Nd} data from the six samples also does not support crustal contamination. The subduction zone theory for the study area komatiites is consistent with the negative Nb anomaly visible in all primitive mantle normalized multi-element spider diagram. A heterogeneous, depleted, deep mantle source for the komatiites in the field area is also consistent with the negative Nb anomalies. It would produce this anomaly without crustal contamination. Therefore, it is plausible that the komatiites in the field area were formed in either a rifted arc setting or from a heterogeneous, depleted, deep mantle source.

The time interval between the deposition of the Greenwater assemblage and the Shebandowan assemblage is approximately 30 million years (2719 Ma and 2690 Ma respectively; Corfu and Stott, 1998). This amount of time allows for large-scale changes in the geodynamic setting and emplacement of the two assemblages. The Greenwater assemblage was likely formed during rifting of oceanic crust where the thinning of the lithosphere caused decompression melting of the mantle, upwelling and emplacement of the ultramafic lithologies in the deep ocean (Begg et al., 2010). This is supported by the association of deep-water lithologies in the Greenwater assemblage such as thick argillite sequences intercalated with hypabyssal ultramafic rocks. The Shebandowan assemblage was likely formed as an oceanic arc colliding

with the continent. The associated erosion created the large packages of clastic sedimentary rocks seen throughout the assemblage.

6.5 Comparisons with the Southern Abitibi Greenstone Belt

In order to understand how greenstone belts form in different locations and link this to Archean plate tectonic processes, it is important to compare assemblages with similar ages and lithologies. This helps determine whether or not similar aged assemblages were formed in the same geological environment. This is especially important in the Archean as the global tectonic style is still poorly understood (Wyman et al., 1999; Wyman, 2013; Bedard et al., 2003; Bedard, 2006, 2013). The Southern Abitibi greenstone belt (SAGB) and the Shebandowan greenstone belt (SGB) are similar in many ways; both form part of the Wawa-Abitibi terrane, they are approximately the same age (~2750-2675 Ma), have undergone greenschist (up to amphibolite) facies metamorphism, contain both tholeiitic and calc-alkaline magmatism, and sedimentary sequences ranging from heterolithic pebble conglomerate to graphitic argillite (Jackson et al., 1994; Corfu and Stott, 1998; Ayer et al., 2002). Ayer et al. (2002) divided the SAGB into nine assemblages based on lithology, geochemistry, facies associations, geophysical signatures, structural style, isotopic data and age. Many of these assemblages are similar to the Greenwater and Shebandowan assemblages in the SGB, with several being roughly the same age. In the SAGB, the Stoughton-Roquemaure assemblage is 2723-2720 Ma and the Kidd-Munro assemblage is 2719-2711 Ma (Ayer et al., 2002). These are similar to the 2722-2718 Ma Greenwater assemblage in the SGB (Corfu and Stott, 1998). In the SAGB, the Porcupine assemblage is 2696-2690 Ma, similar to the 2690-2680 Ma

Shebandowan assemblage in the SGB. This provides the opportunity to investigate the tectonic setting along the length of the southern margin of the Superior Province.

In the Southern Abitibi greenstone belt, the intercalation of tholeiitic, komatiitic, and calc-alkaline rocks indicates that it was formed in a complex geodynamic settings with different mantle sources possibly in a rifted-arc setting (Jackson et al., 1994; Dostal and Mueller, 1997; Corfu and Stott, 1998; Wyman, 1999; Ayer et al., 2002). As the Shebandowan greenstone belt also contains intercalations of tholeiitic, komatiitic, and calc-alkaline rocks, it is possible that it formed in a similar complex geodynamic setting. Jackson et al. (1994) proposed that large-scale accretion of fragments onto the Superior Province would explain the presence of the metavolcanic-plutonic Wabigoon and Wawa-Abitibi terranes as well as the accretionary wedges represented by the English River, Quetico, and Pontiac terranes. The Wawa-Abitibi terrane hosts the Southern Abitibi and Shebandowan greenstone belts, both of which display evidence of relatively rapid accretion of fragments onto the Superior Province in the late Archean. The SGB and SAGB preserve ~40 m.y. (2720-2675 Ma) and ~50 million years (2750-2697 Ma) of island arc formation respectively, and were subsequently accreted onto the Superior Province at approximately the same time period (2690-2675 Ma; Corfu and Stott, 1998; Ayer et al., 2002).

Ayer et al. (2002) attributed the large volumes of komatiites and tholeiitic rocks of the Southern Abitibi greenstone belt to extension early in its evolution. However, this model does not fit with the intercalated komatiitic and tholeiitic

rocks, which suggest subduction processes and compression (Ayer et al., 2002). Ayer et al. (2002) account for these contrasting views by suggesting the autochthonous repetition of different geodynamic environments over the 50 million year history of the Abitibi greenstone belt results in complex, large-scale and long-lived interaction between mantle plumes and subduction zone magmas. Jackson et al. (1994) suggested that a “simplified” tectonic setting, such as a single subduction zone, does not account for all the variations in the SAGB, and instead proposed a more complicated setting for the 50 million year history of the area. Jackson et al. (1994) proposed the existence of numerous small “microplates” to explain the complex tectonic setting for the SAGB, as this would allow for the coexistence of several coeval subduction zones and spreading centers to generate the complex lithological associations. Dostal and Mueller (1997) proposed a mantle plume rising through an arc to account for the intercalation of komatiites, tholeiites, and calc-alkalic magmatism. The former model proposed by Ayer et al. (2002) would seem to be the most favourable for the southern margin of the Superior Province at ~2.7 Ga given the evidence from this study.

Ayer et al. (2002) and Dostal and Mueller (1997) found that the tholeiitic and komatiitic rocks of the SAGB were not contaminated by older crustal material, based on Th/Nb, La/Nb, Th/La ratios as well as ϵ_{Nd} isotope data. This lack of contamination by older crustal material is similar to the rocks of the SGB, however, the SAGB rocks do not contain the distinct negative Nb anomaly. As the negative Nb anomaly was proposed to have formed from a heterogeneous deep-mantle source where Nb was partitioned into perovskite, this would suggest that the SGB and SAGB magmas

originated from different mantle sources. This is reasonable based on the approximate 800km distance between the greenstone belts.

The Southern Abitibi and Shebandowan greenstone belts have similar lithology associations and are interpreted broadly to have formed during accretion of fragments onto the Superior Province (Ayer et al., 2002; Corfu and Stott 1998). Despite their similarities, no two greenstone belts will be entirely equivalent as there are a multitude of variables to take into account during accretion including: different fragment compositions, angle of subduction, rate of subduction, among others. Therefore the SAGB and SGB are comparable because of their relationship in space and time, but the details of formation and the models proposed for the SAGB will not fit the SGB exactly.

In order to produce the intercalation of tholeiitic-komatiitic and calc-alkaline rocks in the Greenwater and Shebandowan assemblages of the Shebandowan greenstone belt, as well as the pervasive negative Nb anomaly in the study area rocks, it is proposed a mantle plume of heterogeneous, depleted, deep mantle source erupting through a rifted oceanic-arc, which later collided onto the continent. The emplacement through an oceanic rift with subsequent accretion onto the Superior Province is consistent with the model proposed by Stott et al. (1987) and Corfu and Stott (1998), and Percival et al. (2012), which describes the growth of the Superior Province through progressive southward accretion of terranes.

Conclusions

The 2.7 Ga Shebandowan greenstone belt in the Wawa-Abitibi terrane of the Superior Craton contains various assemblages and lithologies indicative of a complex geodynamic setting. The older Greenwater assemblage is dated at 2719.7 ± 1.0 Ma and consists of tholeiitic basalts, basaltic komatiites, komatiite flows, intermediate and felsic extrusive volcanic rocks and pyroclastic flows, as well as banded iron formation, wackes, and argillites. The younger 2690-2680 Ma Shebandowan assemblage consists of calc-alkalic to alkalic mafic to felsic volcanic rocks and clastic sedimentary rocks including conglomerate with minor argillite, wacke, iron formation, and volcanic breccia. The ultramafic rocks of the Greenwater assemblage are unusual in both their physical appearance and geochemistry.

The lithologies identified through geological mapping in the field area were: orthocumulate ultramafic rocks, komatiites, pyroxenite, vesicular komatiites, serpentinite, ultramafic breccia, variolitic ultramafic rocks, mafic intrusive rocks, intermediate intrusive and extrusive rocks, volcaniclastic rocks, monzonite, conglomerate, banded iron formation, argillite and chert. The ultramafic rocks are dark black, light green on surface as a product of alteration of olivine. In some areas they occur as fine-grained, massive rocks with no distinct textures, and also occur as medium-grained dark black rocks with a cumulate texture. The cumulate olivine has been completely altered to serpentine. The komatiites occur as fine-grained, light grey, highly siliceous rocks. Several types of spinifex texture were observed throughout the field area including: thin chaotic spinifex, thick chaotic spinifex, oriented spinifex, and pyroxene spinifex. In thin section, the spinifex has been

altered from olivine to serpentine and calcite, often rimmed with iddingsite. In one mapped trench, there are sequences of chert, peperite, komatiite, peperite, chert, which imply that they formed as hypabyssal intrusions. Mafic intrusive rocks are massive, medium-grained, equigranular grey-blue gabbro with weakly disseminated pyrite. In thin section the gabbros have been heavily carbonate-altered. The intermediate intrusive rocks consist of a fine-grained, green-grey matrix with hornblende phenocrysts and red-pink autoliths. The intermediate extrusive rocks are fine-grained, light grey-blue metavolcanic rocks with medium-grained plagioclase phenocrysts. Felsic rocks in the field area are very fine-grained, light grey, siliceous rocks. They are massive with no flow textures observed in any of the outcrops and the weathered surfaces range in colour from beige to blue-grey. A monzonite dyke occurs alongside an interpreted fault through the field area. The distinctly magnetic rock consists of a fine-grained, green-grey matrix with hornblende phenocrysts and red-pink autoliths. The conglomerate is a heterolithic pebble to boulder conglomerate consisting of a fine-grained matrix with clasts of basalt, monzonite, and jasper ranging in size from ~2 cm to 40 cm. The argillite is a very fine-grained dark black mudstone. It typically showed no bedding and locally contained graphite and abundant radial pyrite concretions up to 5 cm in diameter. The trench exposures show several chaotic contacts outlining hypabyssal ultramafic intrusions where hot, low-viscosity ultramafic magma has mingled with the argillite when it was unconsolidated sediment creating chaotic contacts. These chaotic contacts between argillite and ultramafic intrusions have been interpreted as

peperites and suggest that the Greenwater assemblage was deposited in a deep-water environment.

There were few structural features seen during mapping, as the field area was interpreted to have been uplifted early during the collision of the Wawa subprovince and therefore did not undergo intense deformation and metamorphism. The Shebandowan greenstone belt has undergone up to upper greenschist facies metamorphism. There was one major structural feature seen in the center of the map area, with a northeast strike; it is a lithospheric scale fault and has been traced through the field area using magnetic airborne geophysics. The monzonite dyke occurs alongside the fault.

The field area consists of both tholeiitic and calc-alkalic rocks (which correspond to the Greenwater and Shebandowan assemblages, respectively). Through the geochemical analysis, the majority of ultramafic rocks were found to have average $\text{Al}_2\text{O}_3/\text{TiO}_2$ and $\text{CaO}/\text{Al}_2\text{O}_3$ characteristic of aluminum-undepleted komatiites. Rocks of the study area are characterized by negative Nb anomalies. These anomalies were not caused by crustal contamination, nor subduction-related melts, but likely by a heterogeneous deep-mantle source where perovskite fractionation of Nb depleted the Nb content of the melt.

The komatiitic rocks in the field area are not typical komatiites which are characterized by 40-45 wt. % SiO_2 and greater than 18 wt. % MgO; the komatiitic rocks in the field area have 45-66 wt. % SiO_2 and 2-17 wt. % MgO. They were classified as komatiites based on spinifex texture and other geochemical

characteristic such as $\text{Al}_2\text{O}_3/\text{TiO}_2$ and $\text{CaO}/\text{Al}_2\text{O}_3$ ratios and primitive mantle normalized multi-element diagram patterns.

Sm-Nd isotope analysis was completed on six ultramafic samples from the Greenwater assemblage rocks of the field area in order to better constrain the petrogenesis of the greenstone belt. The ϵ_{Nd} of these samples ranged between +2.34 and +2.83, which indicates that crustal contamination by older crust was not a major feature in the genesis of the ultramafic rocks in the field area at 2.7 Ga. Consequently, the elevated silica was determined to be caused by hydrothermal alteration, as there was no basis for crustal contamination or the rocks being siliceous high-Mg basalt.

Based on the close spatial association of tholeiitic and calc-alkalic rocks, as well as the presence of thick sequences of deep-ocean argillites, the geological environment was determined to be a deep-water rifted arc through which a mantle plume of the heterogeneous deep-mantle melts ascended. This ocean floor was later uplifted onto the Superior Province during the collision of the Wawa subprovince. Subsequent erosion of the orogeny caused the clastic sedimentary of the Shebandowan assemblage.

References

- Arndt, N. T., Naldrett, A. J., and Pyke, D. R., 1977. Komatiitic and iron-rich tholeiitic lavas of Munro Township, northeast Ontario. *Journal of Petrology* v.18, pp.319-369.
- Arndt, N.T., Francis, D. and Hynes, A.J., 1979. The field characteristics and petrology of Archean and Proterozoic komatiites. *Canadian Mineralogist* v.17, pp. 147-163.
- Arndt, N. T., 1983. Element mobility during komatite alteration. *EOS: Earth & Space Science News* v.64 (18), pp. 331-331.
- Arndt, N.T., Albarede, F., and Nisbet, E.G., 1997, Mafic and ultramafic magmatism, in de Wit, M.J. and Ashwal, L. D., eds., *Greenstone Belts*: Oxford University Press, Oxford, pp. 233-254.
- Arndt, N.T., Leshner, C.M., Houle, M.G., Lewin, E., and Lacaze, Y., 2004, Intrusion and crystallization of a spinifex- textured komatiite sill in Dundonald Township, Ontario: *Journal of Petrology*, v.45, pp. 2555-2571.
- Arndt, N. T., C. M. Leshner, and S. J. Barnes. 2008. *Komatiite*. Cambridge: Cambridge University Press. 489p.
- Ayer, J., Amelin, Y., Corfu, F., Kamo, S., Ketchum, J., Kwok, K. and Trowell, N., 2002. Evolution of the southern Abitibi greenstone belt based on U-Pb geochronology: autochthonous volcanic construction followed by plutonism, regional deformation and sedimentation. *Precambrian Research*, v. 115 (1), pp. 63-95.
- Barr, J.A., Grove, T.L. and Wilson, A.H., 2009. Hydrous komatiites from Comondale, South Africa: an experimental study. *Earth and Planetary Science Letters*, v. 284 (1-2), pp. 199-207.
- Bédard, J.H., Brouillette, P., Madore, L. and Berclaz, A., 2003. Archaean cratonization and deformation in the northern Superior Province, Canada: an evaluation of plate tectonic versus vertical tectonic models. *Precambrian Research*, v.127(1-3), pp. 61-87.
- Bédard, J.H., 2006. A catalytic delamination-driven model for coupled genesis of Archaean crust and sub-continental lithospheric mantle. *Geochimica et Cosmochimica Acta*, v.70(5), pp. 1188-1214.
- Bédard, J.H., 2013. How many arcs can dance on the head of a plume?: A 'Comment' on: A critical assessment of Neoproterozoic 'plume only' geodynamics: Evidence from the Superior province, by Derek Wyman, *Precambrian Research*, 2012. *Precambrian Research*, v.229, pp.189-197.

Begg, G.C., Hronsky, J.A., Arndt, N.T., Griffin, W.L., O'Reilly, S.Y. and Hayward, N., 2010. Lithospheric, cratonic, and geodynamic setting of Ni-Cu-PGE sulfide deposits. *Economic geology*, v. 105(6), pp.1057-1070.

Bell, R. 1873. Report on the country between Lake Superior and Lake Winnipeg; in, Report of progress for 1872-73; Selwyn, A R C. Geological Survey of Canada, Report of Progress 1872-73, 1873; pp. 87-111.

Bennett, V.C., Nutman, A.P. and McCulloch, M.T., 1993. Nd isotopic evidence for transient, highly depleted mantle reservoirs in the early history of the Earth. *Earth and Planetary Science Letters*, 119(3), pp.299-317.

Bercovici, D. and Karato, S.I., 2003. Whole-mantle convection and the transition-zone water filter. *Nature*, 425 (6953), pp.39.

Brown, G.H. 1985: A Structural and Stratigraphic Study of the Keewatin-type and Shebandowan-type Rocks west of Thunder Bay, Ontario. Unpublished M.Sc. Thesis, Lakehead University, Thunder Bay, Ontario.

Campbell, I.H., Griffiths, R.W., and Hill, R.I., 1989, Melting in an Archean mantle plume: Heads it is basalts and tails it is komatiites: *Nature*, v. 339, pp. 697-699.

Campbell, I.H., 1985. The difference between oceanic and continental tholeiites: a fluid dynamic explanation. *Contributions to Mineralogy and Petrology*, 91(1), pp.37-43.

Card, K.D. 1990. A review of the Superior Province of the Canadian Shield, a product of Archean accretion. *Precambrian Research*. v. 48, pp. 99-156.

Card, K.D., and Ciesielski, A. 1986. DNAG No. 1. Subdivisions of the Superior Province of the Canadian Shield. *Geoscience Canada*. v. 13, pp.5-13

Carter, M.W. 1990. Geology of Forbes and Conmee townships/ Ontario Geological Survey, Open File Report 5726, 188p.

Chase, C.G. and Patchett, P.J., 1988. Stored mafic/ultramafic crust and early Archean mantle depletion. *Earth and Planetary Science Letters*, 91(1-2), pp.66-72.

Corfu, F. and Stott, G.M. 1998. Shebandowan greenstone belt, western Superior Province: U/Pb ages, tectonic implications, and correlations; *Geological Society of America Bulletin*, v.110, pp.1467-1484.

Corgne, A., Liebske, C., Wood, B. J., Rubie, D. C., Frost, D. J., 2005. Silicate perovskite-melt partitioning of trace elements and geo-chemical signature of a deep perovskitic reservoir. *Geochimica et Cosmochimica Acta* 69, pp.485-496.

Clark, G. 2011a. Report of Sampling of Bateman Lake Property, District of Thunder Bay, northwest Ontario, NTS 52 A/5, prepared for Denarii Resources Inc; Thunder Bay Resident Geologist's office, assessment file AFRO# 2.49588, AFRI# 20000006863, 18p.

Clark, G. 2011b. Report of Rock and Lake Bottom Sampling of Bateman Lake Property, District of Thunder Bay, northwestern Ontario, NTS 52 A/5, prepared for Double Crown Resources. 19p.

Crawford, A.J., Falloon, T.J., and Green, D.H. 1989, Classification, petrogenesis, and tectonic setting of boninites, in Crawford, A.J., ed., *Boninites and related rocks*: London, Unwin-Hyman, pp. 1-49.

Dostal, J. 2008. Igneous rock associations 10; komatiites. *Geoscience Canada* 35 (1), 21-31, 15p.

Dostal, J. and Mueller, W.U., 1997. Komatiite flooding of a rifted Archean rhyolitic arc complex: geochemical signature and tectonic significance of the Stoughton-Roquemaure Group, Abitibi greenstone belt, Canada. *The Journal of Geology*, 105(5), pp. 545-564.

Elliott, T., Plank, T., Zindler, A., White, W., Bourdon, B. 1997. Element transport from slab to volcanic front at the Mariana Arc. *Journal of Geophysical Research* 102, pp. 14991-15019.

Gao, J.F., and Zhou, M.F. 2013. Generation and evolution of siliceous high magnesium basaltic magmas in the formation of the Permian Huangshandong intrusion (Xinjiang, NW China). *Lithos*, v. 162-163, pp.128-139.

Gélinas, B.R., Lodge, R.W.D. and Gibson, H.L. 2016. Characterization of the mineralization and alteration at Tower Mountain, Conmee Township, Shebandowan greenstone belt; Ontario Geological Survey, Miscellaneous Release—Data 330.

Green, D.H., Nicholls, I.A., Viljoen, M., and Viljoen R., 1975, Experimental demonstration of the existence of peridotitic liquids in earliest Archean magmatism: *Geology*, v. 3, pp. 11-14.

Grove, T.L. and Parman, S.W., 2004. Thermal evolution of the Earth as recorded by komatiites. *Earth and Planetary Science Letters*, 219(3-4), pp.173-187.

Hanor, J.S. and Duchač, K.C., 1990. Isovolumetric silicification of early Archean komatiites: geochemical mass balances and constraints on origin. *The Journal of Geology*, 98(6), pp.863-877.

Henry, P., Stevenson, R.K., Gariépy, C., 1998. Late Archean mantle composition and crustal growth in the Western Superior Province of Canada: neodymium and lead isotopic evidence from the Wawa, Quetico and Wabigoon subprovinces. *Geochim. Cosmochim. Acta* 62, pp. 143–157.

Henry, P., Stevenson, R.K., Larbi, Y. and Gariépy, C., 2000. Nd isotopic evidence for Early to Late Archean (3.4–2.7 Ga) crustal growth in the western Superior Province (Ontario, Canada). *Tectonophysics*, 322(1-2), pp.135-151.

Herzberg, C. 1995. Generation of plume magmas through time: an experimental perspective. *Chemical Geology*, 126, pp. 1–17.

Herzberg, C., Condie, K. and Korenaga, J., 2010. Thermal history of the Earth and its petrological expression. *Earth and Planetary Science Letters*, 292(1-2), pp. 79-88.

Herzberg, C. and O Hara, M.J., 1998. Phase equilibrium constraints on the origin of basalts, picrites, and komatiites. *Earth-Science Reviews*, 44(1-2), pp. 39-79.

Hinz, S., Hollings, P., Lodge, R.W.D., Olson, M.J., and Helmuth, S.L., 2016. Preliminary Geology and Macroscopic Textures of the Ultramafic Rocks from Conmee Township, Eastern Shebandowan Greenstone Belt in Summary of Field Work and Other Activities, 2016; Ontario Geological Survey, Open File Report 6323, pp. 13-1 to 13-9

Hofmann, A.W. and Harris, C., 2008. Silica alteration zones in the Barberton greenstone belt: a window into seafloor processes 3.5–3.3 Ga ago. *Chemical Geology*, 257(3), pp. 221-239.

Hofmann, A.W. and White, W.M., 1982. Mantle plumes from ancient oceanic crust. *Earth and Planetary Science Letters*, 57(2), pp. 421-436.

Hollings, P. and Wyman, D., 1999. Trace element and Sm–Nd systematics of volcanic and intrusive rocks from the 3 Ga Lumby Lake Greenstone belt, Superior Province: evidence for Archean plume–arc interaction. *Lithos*, 46(2), pp. 189-213.

Huppert, H.E., Stephen, R. and Sparks, J., 1985. Cooling and contamination of mafic and ultramafic magmas during ascent through continental crust. *Earth and Planetary Science Letters*, 74(4), pp. 371-386.

Irving A.J., and Frey F.A., 1978. Distribution of trace elements between garnet megacrysts and host volcanic liquids of kimberlitic to rhyolitic composition. *Geochimica et Cosmochimica Acta*, v.42. pp. 771-787.

Jackson, S.L., Fyon, J.A. and Corfu, F., 1994. Review of Archean supracrustal assemblages of the southern Abitibi greenstone belt in Ontario, Canada: products of microplate interaction within a large-scale plate-tectonic setting. *Precambrian Research*, 65(1-4), pp. 183-205.

Jensen, L.S., 1976. A new cation plot for classifying subalkalic volcanic rocks (Vol. 66). Ministry of Natural Resources.

Jobin-Bevans, S., Kelso, I., Cullen, D., 2006. NI 43-101 Technical Report on the Tower Mountain Gold Deposit, Conmee Township, Northwestern Ontario. ValGold Resources Ltd, Canada, 95p.

Jochum, K.P., Arndt, N.T. and Hofmann, A.W., 1991. Nb-Th-La in komatiites and basalts: constraints on komatiite petrogenesis and mantle evolution. *Earth and Planetary Science Letters*, 107(2), pp. 272-289.

Kato, T., Ohtani, E., Ito, Y., and Onuma, K., 1996. Element partitioning between silicate perovskites and calcic ultrabasic melt. *Physics of the Earth and Planetary Interiors* 96, pp. 201-207.

Kato, T., Ringwood, A. E., and Irifune, T., 1988. Experimental determination of element partitioning between silicate perovskites, garnets and liquids: constraints on early differentiation of the mantle. *Earth and Planetary Science Letters* 89, pp. 123-145.

Kerr, A C., Marriner, G.F., Arndt, N.T., Tarney, J., Nivia, A., Saunders, A.D., and Duncan, R.A. 1996. The petrogenesis of Gorgona komatiites, picrites and basalts: new field, petrographic and geochemical constraints; in *Lithos* 37.2, pp. 245-260.

Kerrick, R., Wyman, D., Fan, J., and Bleeker, W. 1998. Boninite–low Ti–tholeiite associations from the 2.7 Ga Abitibi greenstone belt: *Earth and Planetary Science Letters*, v. 164, pp. 303–316.

Leshner, C.M., and Arndt, N.T., 1995. REE and Nd isotope geochemistry, petrogenesis and volcanic evolution of contaminated komatiites at Kambalda, Western Australia: *Lithos*, v. 34, p. 127-157.

Lodge, R.W.D. 2012. Preliminary results of uranium–lead geochronology from the Shebandowan greenstone belt, Wawa Subprovince; in *Summary of Field Work and Other Activities 2012*, Open File Report 6280, pp.10-1 to 10-10.

Lodge, R.W.D., 2013. Geology and Mineral Potential of Aldina Township, Wawa Subprovince; in *Summary of Field Work and Other Activities 2013*, Ontario Geological Survey, Open File Report 6290, pp. 6-1 to 6-13.

Lodge, R.W.D., Gibson, H.L., Stott, G.M., Hudak, G.J. and Jirsa, M. 2013. New U/Pb geochronology from Timiskaming-type assemblages in the Shebandowan and Vermilion greenstone belts, Wawa Subprovince, Superior Craton: Implications for the Neoproterozoic development of the southwestern Superior Province; *Precambrian Research*, v.235, pp. 264-277.

Lodge, R.W.D., Ratcliffe, L.M., and Walker, J.A., 2014. Geology and Mineral Potential of Sackville and Conmee Townships, Wawa Subprovince; in Summary of Field Work and Other Activities 2014, Ontario Geological Survey, Open File Report 6300, pp. 9-1 to 9-17.

Lodge, R.W.D., Gibson, H.L., Stott, G.M., Franklin, J.M. and Hudak, G.J., 2015. Geodynamic setting, crustal architecture, and VMS metallogeny of ca. 2720 Ma greenstone belt assemblages of the northern Wawa subprovince, Superior Province. *Canadian Journal of Earth Sciences*, 52(3), pp. 196-214.

MacLean, D. and Rees, M. 2008. Report on soil geochemistry, prospecting and trenching on the Bateman Lake property, Horne and Conmee townships, District of Thunder Bay, northwest Ontario, NTS 52 A/12 and 52 A/5, prepared for Linear Metals Corporation; Thunder Bay Resident Geologist's office, assessment file AFRO# 2.39695, AFRI# 20000003608, 100p.

Malviya, V.P., Arima, M., Pati, J.K. and Kaneko, Y. 2006. Petrology and geochemistry of metamorphosed basaltic pillow lava and basaltic komatiite in the Mauranipur area: subduction related volcanism in the Archean Bundelkhand craton, Central India. *Journal of Mineralogical and Petrological Sciences*, 101(4), pp. 199-217.

Morton, P., 1979. Volcanic stratigraphy in the Shebandowan Ni-Cu mine area, Ontario; in Current Research Part B. Geological Survey of Canada. v.79, pp. 39-43.

Nesbitt, R.W., Sun, S.S. and Purvis, A.C., 1979. Komatiites; geochemistry and genesis. *The Canadian Mineralogist*, 17(2), pp. 165-186.

Nisbet, E.G., Cheadle, M.J., Arndt, N.T. and Bickle, M.J., 1993. Constraining the potential temperature of the Archean mantle: a review of the evidence from komatiites. *Lithos*, 30(3-4), pp. 291-307.

O'Driscoll, B., Donaldson, C.H., Troll, V.R., Jerram, D.A., and Emeleus, C.H. 2006. An origin for harrisitic and granular olivine in the Rum Layered Suite, NW Scotland: a crystal size distribution study. *Journal of Petrology*: v.48, n.2., pp. 253-270.

Ontario Geological Survey 2003. Ontario airborne geophysical surveys, Magnetic and Electromagnetic Data, Shebandowan Area (ASCII and Geosoft® formats), magnetic supergrids; Ontario Geological Survey, Geophysical Data Set 1021—Revised.

Parker, J.R. 1980: The Structure and Environment of Deposition of the Finmark metasediments, Thunder Bay, Ontario. Unpublished Hon. B.Sc. Thesis, Lakehead University, Thunder Bay, Ontario, 90 p.

Parman, S.W., Dann, J.C., Grove, T.L., and de Wit, M.J. 1997. Emplacement conditions of komatiite magmas from the 3.49 Ga Komati Formation, Barberton Greenstone Belt, South Africa. *Earth and Planetary Science Letters*, v. 150, pp. 303-323.

Parman, S.W., Grove, T.L. and Dann, J.C., 2001. The production of Barberton komatiites in an Archean subduction zone. *Geophysical Research Letters*, 28(13), pp. 2513-2516.

Parman, S.W., Grove, T.L., Dann, J.C. and De Wit, M.J., 2004. A subduction origin for komatiites and cratonic lithospheric mantle. *South African Journal of Geology*, 107(1-2), pp.107-118.

Pearce, J.A., van der Laan, S.R., Arculus, R.J., Murton, B.J., Ishii, T., Peate, D.W., and Parkinson, I.J. 1992, Boninite and harzburgite from Leg 125 (Bonin- Mariana forearc): A case study of magma genesis during the initial stages of subduction, in Fryer, P., et al., *Proceedings of the Ocean Drilling Program, scientific results, Sites 778–786, Bonin/Mariana Region: College Station, Texas, Ocean Drilling Program*, pp. 623–659.

Pearce, J.A. and Peate, D.W., 1995. Tectonic implications of the composition of volcanic arc magmas. *Annual Review of Earth and Planetary Sciences*, 23(1), pp. 251-285.

Pearce, J.A., 2008. Geochemical fingerprinting of oceanic basalts with applications to ophiolite classification and the search for Archean oceanic crust. *Lithos*, 100(1-4), pp. 14-48.

Peng, T., Wilde, S.A., Fan, W., and Peng, B., 2013. Neoproterozoic siliceous high-Mg basalt (SHMB) from the Taishan granite–greenstone terrane, Eastern North China Craton: Petrogenesis and tectonic implications. *Precambrian Research*, 228, pp. 233-249.

Percival, J.A., 2007. Geology and metallogeny of the Superior Province, Canada, in Goodfellow, W.D., ed., *Mineral Deposits of Canada: A Synthesis of Major Deposit-Types, District Metallogeny, the Evolution of Geological Provinces, and Exploration Methods: Geological Association of Canada, Mineral Deposits Division, Special Publication No. 5*.

Percival, J.A., Sanborn-Barrie, M., Skulski, T., Stott, G.M., Helmstaedt, H. and White, D.J., 2006. Tectonic evolution of the western Superior Province from NATMAP and Lithoprobe studies. *Canadian Journal of Earth Sciences*, 43(7), pp. 1085-1117.

Percival, J.A., Skulski, T., Sanborn-Barrie, M., Stott, G.M., Leclair, A.D., Corkery, M.T., and Boily, M., 2012. Geology and tectonic evolution of the Superior Province, Canada. In *Tectonic Styles in Canada: The Lithoprobe Perspective. Geological Association of Canada Special Paper 49*, pp. 321-378

- Piercey, S.J., Murphy, D.C., Mortensen, J.K., and Paradis, S., 2001. Bonanitic magmatism in a continental margin setting, Yukon-Tanana terrane, southeastern Yukon, Canada; in *Geology*. v. 29, no. 8, pp. 731–734
- Polat, A., and Kerrich, R., 2004. Precambrian arc associations; boninites, adakites, magnesian andesites, and Nb-enriched basalts; in *Precambrian ophiolites and related rocks*. pp. 567-597.
- Polat, A., Kerrich, R. and Wyman, D.A., 1999. Geochemical diversity in oceanic komatiites and basalts from the late Archean Wawa greenstone belts, Superior Province, Canada: trace element and Nd isotope evidence for a heterogeneous mantle. *Precambrian Research*, 94(3), pp. 139-173.
- Price, R.A., 1964. The Precambrian Purcell System in the Rocky Mountains of southern Alberta and British Columbia. *Bulletin of Canadian Petroleum Geology*, 12(2), pp. 399-426.
- Puchtel, I.S. and Humayun, M. 2001. Platinum group element fractionation in a komatiitic basalt lava lake. *Geochimica et Cosmochimica Acta*, 65(17), pp. 2979-2993.
- Pyke, D. R., Naldrett, A. J., and Eckstrand, O. R., 1973. Archean ultramafic flows in Munro Township, Ontario. *Bulletin of the Geological Society of America*, 84, pp. 955–978.
- Ratcliffe, L.M., 2015. Geology and Mineral Potential of Adrian Township, Shebandowan Greenstone Belt, Wawa–Abitibi Terrane; in *Summary of Field Work and Other Activities 2015*, Ontario Geological Survey, Open File Report 6313, pp. 11-1 to 11-14.
- Redman, B.A., and Keays, R.R., 1985. Archaean basic volcanism in the Eastern Goldfields Province, Yilgarn Block, Western Australia. *Precambrian Research* 30, pp. 113–152.
- Robin-Popieul, C.C., Arndt, N.T., Chauvel, C., Byerly, G.R., Sobolev, A.V. and Wilson, A., 2012. A new model for Barberton komatiites: deep critical melting with high melt retention. *Journal of Petrology*, 53(11), pp. 2191-2229.
- Rollinson, H.R. 1993. *Using geochemical data: evaluation, presentation, interpretation*. Routledge. 384p.
- Santaguida, F., 2001a. Precambrian geology compilation series—Quetico sheet; Ontario Geological Survey, Map 2663, scale 1:250 000.

Santaguida, F., 2001b. Precambrian geology compilation series—Thunder Bay sheet; Ontario Geological Survey, Map 2664, scale 1:250 000.

Schnieders, B.R., Scott, J.F., Smyk, M.C. and O'Brien, M.S. 2000. Report of Activities 1999, Resident Geologist Program, Thunder Bay South Regional Resident Geologist Report: Thunder Bay South District; Ontario Geological Survey, Open File Report 6005, 50p.

Sensarma, S., Palme, H. and Mukhopadhyay, D., 2002. Crust–mantle interaction in the genesis of siliceous high magnesian basalts: evidence from the Early Proterozoic Dongargarh Supergroup, India. *Chemical Geology*, 187(1-2), pp. 21-37.

Shegelski, R.J., 1980. Archean cratonization, emergence and red bed development, Lake Shebandowan area, Canada. *Precambrian Research*, 12(1-4), pp. 331-347.

Skilling, I.P., White, J.D.L., and McPhie, J., 2002. Peperite: a review of magma–sediment mingling. *Journal of Volcanology and Geothermal Research*, 114(1), pp. 1-17.

Smithies, R.H. 2002. Archean boninite-like rocks in an intracratonic setting. *Earth and Planetary Science Letters* 197, pp. 19–34.

Sobolev, A.V., Hofmann, A.W., Kuzmin, D.V., Yaxley, G.M., Arndt, N.T., Chung, S.L., Danyushevsky, L.V., Elliott, T., Frey, F.A., Garcia, M.O. and Gurenko, A.A., 2007. The amount of recycled crust in sources of mantle-derived melts. *Science*, 316(5823), pp. 412-417.

Srivastava, R.K., 2006. Geochemistry and petrogenesis of neoarchean high-Mg low-Ti mafic igneous rocks in an intracratonic setting, Central India Craton: evidence for boninite magmatism. *Geochemical Journal* 40, pp. 15–31.

Srivastava, R.K., 2008. Global intracratonic boninite–norite magmatism during the Neoarchean–Paleoproterozoic: evidence from the central Indian Bastar Craton. *International Geology Review* 50, pp. 61–74.

Srivastava, R.K., Mondal, S.K., Balaram, V., and Gautam, G.C., 2010. PGE geochemistry of low-Ti high-Mg siliceous mafic rocks within the Archean Central Indian Bastar Craton: implications for magma fractionation. *Mineralogy and Petrology* 98, pp. 329–345.

Stott, G.M., Sanborn-Barrie, M. and Corfu, F., 1987. Major transpression events recorded across Archean subprovince boundaries in northwestern Ontario. *Geol Assoc Can Meet, Yellowknife 87 Abstracts*, pp. 4.

Stott, G.M., Corkery, M.T., Percival, J.A., Simard, M, and Goutier, J., 2010. A revised terrane subdivision of the Superior Province; in Summary of Field Work and Other Activities 2010, Ontario Geological Survey, Open File Report 6260, pp. 20-1 to 20-10.

Sun, S.S. and McDonough, W.S., 1989. Chemical and isotopic systematics of oceanic basalts: implications for mantle composition and processes. Geological Society, London, Special Publications, 42(1), pp. 313-345.

Sun, S.S., Nesbitt, R.W., and McCulloch, M.T., 1989. Geochemistry and petrogenesis of Archean and early Proterozoic siliceous high-magnesian basalts. In: Crawford, A.J. (Ed.), Boninites and Related Rocks. Unwin Hyman, London, pp. 148–173.

Tanton, T.L., 1924. Eastern part of Matawin Iron Range, Thunder Bay District, Ontario; in Geol. Surv. Canada, Summ. Rept. for 1924, part c, p. 1c-27c (published 1926). Accompanied by Map 2069, at a scale of 1 inch to 1 mile.

Taura, H., Yurimoto, H., Kato, T., and Sueno, S., 2001. Trace element partitioning between silicate perovskites and ultracalcic melt. Physics of the Earth and Planetary Interiors 124, pp. 25-32.

Tomlinson, K.Y., Stott, G.M., Percival, J.A. and Stone, D., 2004. Basement terrane correlations and crustal recycling in the western Superior Province: Nd isotopic character of granitoid and felsic volcanic rocks in the Wabigoon subprovince, N. Ontario, Canada. Precambrian Research, 132(3), pp. 245-274.

Vinciguerra, S., Trovato, C., Meredith, P.G. and Benson, P.M., 2005. Relating seismic velocities, thermal cracking and permeability in Mt. Etna and Iceland basalts. International Journal of Rock Mechanics and Mining Sciences, 42(7-8), pp. 900-910.

Vlaar, N.J., Van Keken, P.E. and Van den Berg, A.P., 1994. Cooling of the Earth in the Archaean: consequences of pressure-release melting in a hotter mantle. Earth and Planetary Science Letters, 121(1-2), pp. 1-18.

Williams, H.R., Stott, G.M., Heather K.B., Muir T.L., and Sage, R.P., 1991. Wawa Subprovince. In: Thurston, P.C., Williams, H.R., Sutcliffe, R.H., Stott, G.M. (Eds.), Geology of Ontario; Ontario Geological Survey Special Vol. 4.

Wyman, D.A., 1999. Paleoproterozoic boninites in an ophiolite-like setting, Trans-Hudson orogen, Canada: Geology, v. 27, pp. 455–458.

Wyman, D.A., Bleeker, W. and Kerrich, R., 1999. A 2.7 Ga komatiite, low Ti tholeiite, arc tholeiite transition, and inferred proto-arc geodynamic setting of the Kidd Creek deposit: Evidence from precise trace element data. Economic Geology Monograph, 10, pp. 511-528.

Wyman, D.A., 2013. A critical assessment of Neoproterozoic “plume only” geodynamics: evidence from the Superior Province. *Precambrian Research*, 229, pp. 3-19.

Xie, Q., Kerrich, R., and Fan, J., 1993. HFSE/REE fractionations recorded in three komatiite-basalt sequences, Archean Abitibi greenstone belt: Implications for multiple plume sources and depths. *Geochimica et Cosmochimica Acta* 57, pp. 4111-4118.

Zhao, J.H. and Zhou, M.F., 2013. Neoproterozoic high-Mg basalts formed by melting of ambient mantle in South China. *Precambrian Research*, 233, pp. 193-205.

Appendix I: Thin Section Descriptions

Sample ID	FW-15-SH-001
Field Name	Ultramafic
Field Description	Weathered brown/green with visible spinifex on surface, fine-grained, light grey/green, pyrite cubes sparsely within, thin fracture in-filled with pyrite & white mineral
Mineralogy	Sericite: 65%, Quartz: 20%, Calcite: 15%, Opaques: >1%, Actinolite: >1%
Alteration	Significantly sericite altered, no primary grains
Mineralization	Some opaques (pyrite) fine-grained, black spots throughout sample with irregular grain boundaries.
Mineral Description	Significantly altered, no primary minerals or textures observed. Sample is fine-grained with several veins of altered quartz running through sample (width of vein about 1mm). Irregular grain boundaries observed in many minerals.
Thin Section Description	Sericite: majority of sample, very fine-grained, seen as oblong blebs with no set boundaries. Quartz: fine-grained throughout groundmass as well as in medium-grained recrystallized blebs and in vein sets running through sample. Most grains have undulose extinction. Some grains exhibit sub-grain boundaries. Calcite: fine-grained blebs throughout sample. Fairly high relief and sharp boundaries with other minerals. Opaques: fine-grained, black spots throughout sample with irregular grain boundaries. Actinolite: fine-grained, seen sparsely in sample as fibrous bundles with sharp boundaries with other minerals.

Sample ID	FW-15-SH-002
Field Name	Gabbro
Field Description	Weathered surface brown/red, no sulfide staining, some ankerite, fine-grained dark grey, pyrite visible sparsely, olivine clusters
Mineralogy	Calcite: 30%, Sericite: 20%, Quartz: 10%, Serpentine: 5%, Opaques: >1%
Alteration	Sericite, calcite and serpentine
Mineralization	Fine- to medium-grained sparsely within sample. Some grains with irregular grain boundaries and others seen as pseudo-cubic.
Mineral Description	Significantly altered, no primary minerals or textures observed. Sample is fine-grained with several veins of altered quartz running through sample (width of vein about 0.5 mm). Irregular grain boundaries observed in many minerals.
Thin Section Description	Calcite: fine-grained throughout sample with sharp grain boundaries with other minerals. Sericite: very fine-grained in groundmass throughout sample. Quartz: fine-grained in groundmass throughout sample as well as in thin veins (about 0.5mm width). Some grains exhibit undulose extinction and sub-grain boundaries. Serpentine: fine-grained sparsely within sample. Seen in fibrous bundles with sharp grain boundaries with other minerals. Opaques (pyrite): fine- to medium-grained sparsely within sample. Some grains with irregular grain boundaries and others seen as pseudo-cubic.

Sample ID	FW-15-SH-003
Field Name	Ultramafic
Field Description	Weathered surface light brown/red, spinifex visible (needles 2-4cm in length), fine-grained, light grey, sulfides visible disseminated throughout, and in thin fractures
Mineralogy	Calcite: 45%, Serpentine: 25%, Opaques: 10%, Sericite: 10%, Actinolite: 5%, Quartz 5%
Alteration	Calcite, sericite and serpentine
Mineralization	Fine grained euhedral opaques- likely pyrite
Mineral Description	Significantly altered, no primary minerals or textures observed. Sample is fine-grained with several veins of quartz and calcite running through (width of vein about 0.3mm). Grain boundaries all irregular, except opaques many of which are euhedral (square) with a thin rim of actinolite around them.
Thin Section Description	Calcite: very fine-grained to fine-grained. All high relief with birdseye extinction. Several thin veins running through. Blebs of alteration calcite seen throughout Quartz: Seen as fine-grained within groundmass. No veins present Sericite: very fine-grained alteration throughout Actinolite: seen as fine-grained blebs throughout sample, also as rims around several opaques Opaques: seen as fine-grained with irregular grain boundaries and also as euhedral cubes throughout. Possibly pyrite. Serpentine: Seen as several thin veins (~0.5mm) throughout. Also as a fine-grained anastomosing groundmass that separates calcite blebs within majority of sample

Sample ID	FW-15-SH-006-A
Field Name	Ultramafic Volcanic Breccia
Field Description	Weathered brown, fine-grained light grey with angular clasts of black chert, blebs of sulfide, quartz veins <0.5mm
Mineralogy	Calcite: 45%, Quartz: 20%, Serpentine: 20%, Opaques: 10%, Actinolite: 5%
Alteration	Calcite
Mineralization	Medium-grained euhedral cubic opaques- likely pyrite
Mineral Description	Significantly altered, no primary minerals or textures observed. Sample is very fine to fine-grained and clasts seen in hand sample are not easily observed in thin section (irregular, gradational grain boundaries). All grain boundaries are irregular. Serpentine occurs as anastomosing groundmass in between blebs of calcite. Larger calcite grains, actinolite and undulose quartz occur as rims on opaques
Thin Section Description	Calcite: very fine to fine-grained occurs as blebs as well as discrete grains Quartz: very fine- to fine-grained. Occurs in groundmass as well as rims on opaques Serpentine: very fine-grained, occurs as groundmass in anastomosing pattern and also as discrete grains Opaques: medium-grained cubic euhedral likely pyrite Actinolite: Fine-grained, occurs as blebs within groundmass as well as rims on opaques.

Sample ID	FW-15-SH-006-B
Field Name	Ultramafic Volcanic Breccia
Field Description	Weathered brown, fine-grained light grey with angular clasts of black chert, blebs of sulfide, quartz veins <0.5mm
Mineralogy	Calcite: 40%, Serpentine: 35%, Quartz: 10%, Opaques: 10%, Actinolite: 5%
Alteration	Calcite, quartz and serpentine
Mineralization	Fine- to medium-grained euhedral- likely pyrite
Mineral Description	Significantly altered, irregular (no sharp) boundaries between fragments and groundmass. Groundmass is mainly fibrous serpentine. Medium-grained euhedral opaques (likely pyrite) seen in aggregates in several parts of the sample
Thin Section Description	Calcite: Occurs as very fine- to fine-grained blebs throughout sample, also as fine-grained veins in several portions of sample Serpentine: Occurs as main constituent of groundmass as anastomosing veins surrounding calcite blebs Quartz: occurs as very fine- to fine-grained throughout groundmass and also as veins Opaques: fine to medium-grained euhedral cubes- likely pyrite Actinolite: occurs as fine-grained blebs in groundmass and also as thin rims around several opaque grains

Sample ID	FW-15-SH-011
Field Name	Ultramafic Volcanic Breccia
Field Description	Weathered red/brown, fine-grained grey with bright green spinifex needles within (1.5-2cm in length), pyrite visible throughout
Mineralogy	Calcite: 40%, Quartz: 15%, Serpentine: 30%, Opaques: 10%, actinolite: 5%
Alteration	Calcite, quartz
Mineralization	Fine- to medium-grained euhedral- likely pyrite
Mineral Description	Significantly altered, irregular grain boundaries, quartz veins. Groundmass is mainly blebs of calcite with very fine-grained actinolite blades and serpentine. Thin (several mm) spinifex-like texture visible in the hand sample and RPL but difficult to see in XPL (no specific mineral composition of blades- altered)
Thin Section Description	Calcite: occurs as very fine to fine-grained blebs and discrete grains within groundmass Quartz: Occurs as fine-grained within groundmass and medium-grained in veins. Undulose extinction and subgrain boundaries Serpentine: Occurs as fine- to very fine-grained within groundmass. Sometimes in an anastomosing pattern around calcite blebs but not as dominant as in other samples Opaques: Fine- to medium-grained. Fine-grained grains have irregular grain boundaries and medium grains are cubic euhedral Actinolite: Very fine-grained blades in groundmass and as rims on some euhedral opaques

Sample ID	FW-15-SH-013
Field Name	Ultramafic
Field Description	Weathered red/brown, fine-grained grey/green with 1-2cm long spinifex
Mineralogy	Calcite: 45%, Quartz: 25%, Serpentine: 20%, Opaques: 10%, Muscovite: 5%
Alteration	Calcite, serpentine
Mineralization	Coarse-grained euhedral pyrite
Mineral Description	Significantly altered, irregular grain boundaries. Groundmass is mainly blebs of calcite with anastomosing serpentine. Several coarse grains of pyrite within.
Thin Section Description	Calcite: occurs as very fine- to fine-grained blebs throughout groundmass Quartz: Fine-grained within groundmass, sub-grain boundaries and undulose extinction visible Serpentine: Occurs as very fine-grained within groundmass as well as anastomosing around blebs of calcite Opaques: Coarse grains of euhedral pyrite Muscovite: very fine-grained blades within groundmass and associated with opaques

Sample ID	FW-15-SH-021
Field Name	Ultramafic
Field Description	Weathered red/brown, fine-grained grey/green with spinifex (blades up to 4cm), pyrite veins
Mineralogy	Calcite: 40%, Quartz: 25%, Serpentine: 20%, Opaques: 10%, Muscovite: 5%
Alteration	Calcite, serpentine
Mineralization	Fine- to medium-grained euhedral- likely pyrite
Mineral Description	Altered, irregular grain boundaries. Groundmass is blebs of calcite with interstitial serpentine and quartz. Medium euhedral grains of opaques (likely pyrite)
Thin Section Description	Calcite: occurs as very fine- to fine-grained blebs throughout groundmass as well as discrete grains Quartz: Fine-grained within groundmass, subgrain boundaries and undulose extinction visible Serpentine: occurs within groundmass as fibrous wisps and in veins (~0.3mm) Opaques: occurs as fine to medium-grained in groundmass, cubic euhedral likely pyrite Muscovite: occurs as fine-grained along edges of opaques, as rims (high birefringence, low relief, birdseye extinction)

Sample ID	LM-15-SH-023
Field Name	Intermediate
Field Description	Weathered white/grey, fine-grained light grey
Mineralogy	Quartz: 70%, Calcite: 15%, Serpentine: 10%, Opaques: 5%,
Alteration	Serpentine, calcite
Mineralization	Very fine-grained, anhedral
Mineral Description	Significantly altered, irregular grain boundaries. Mostly qtz (72% in geochem)
Thin Section Description	Quartz: very fine- to fine-grained, composes majority of groundmass as well as discrete grains Calcite: occurs as fine-grained within groundmass. Irregular grain boundaries of all grains Serpentine: occurs as anastomosing thin (0.2mm) veinlets within groundmass Opaques: very fine-grained, follows anastomosing serpentine

Sample ID	LM-15-SH-028
Field Name	Mafic
Field Description	Very fine-grained dark grey/black, massive (UM)
Mineralogy	Quartz: 85%, serpentine: 10%, opaques: 5%
Alteration	Silicification
Mineralization	Very fine-grained, anhedral
Mineral Description	Mostly quartz (82%) irregular grain boundaries
Thin Section Description	Quartz: very fine- to fine-grained, majority of sample. Occurs as entire groundmass as well as in short discontinuous veins Serpentine: Occurs as thin wisps throughout groundmass Opaques: occurs as very fine-grained anhedral grains sparsely throughout groundmass

Sample ID	LM-15-SH-032
Field Name	Intermediate
Field Description	Weathered red/brown, fine-grained dark grey with spherical green blebs throughout. Blebs weathered white on surface
Mineralogy	Quartz: 75%, Calcite: 10%, Serpentine: 10%, Opaques: 5%
Alteration	Silicification and serpentinization
Mineralization	N/A
Mineral Description	Fragments all composed of very fine-grained calcite, quartz and serpentine. Quartz veins interstitial to these fragments. Anastomosing serpentine veinlets running throughout interstitial material
Thin Section Description	Quartz: majority of sample. Occurs as very fine-grained in groundmass as well as fine-grained discrete grains and within veins. Displays undulose extinction as well as subgrain boundaries Calcite: occurs as discrete grains within groundmass. Very fine- to fine-grained Serpentine: occurs very-fine grained in veins with an anastomosing pattern

Sample ID	LM-15-SH-039
Field Name	Mafic
Field Description	Weathered beige, Fine-grained dark black/green
Mineralogy	Talc: 70%, serpentine: 10%, biotite: 10%, calcite: 5%, opaques: 5%
Alteration	Talc and serpentine
Mineralization	Fine-grained euhedral
Mineral Description	Relict olivine grains composed entirely of talc (olivine-> serpentine-> talc) with interstitial biotite and serpentine
Thin Section Description	Talc: majority of sample, fine-grained and infill relict olivine grains (olivine>serpentine>talc) Calcite: occur as fine-grained discrete grains inside relict olivine boundaries Serpentine: occurs as fine-grained wavy veinlets that are broken and displaced (green to brown pleochroism) also occurs as very fine-grained aggregates within and outside of relict grain boundaries Biotite: occurs as fine-grained books within groundmass Opaques: occurs as fine-grained euhedral sparsely throughout groundmass

Sample ID	LM-15-SH-044
Field Name	Intermediate
Field Description	Weathered white/grey, fine-grained light grey. Looks brecciated
Mineralogy	Quartz: 75%, chlorite: 10%, opaques: 10%, calcite: 5%
Alteration	Chlorite and calcite
Mineralization	Fine-grained euhedral likely pyrite
Mineral Description	Majority of sample is quartz with groundmass being fine-grained quartz with sparse calcite, chlorite and opaques. Veins of medium-grained quartz in veins (~1mm) give fragmental look.
Thin Section Description	Quartz: occurs as fine-grained in groundmass as well as medium-grained in veinlets that exhibit undulose extinction and subgrain boundaries Calcite: occurs as fine-grained within groundmass sparsely as well as thin veinlets Chlorite: occurs as fine-grained aggregates with medium-relief, dark brown/black in XPL Opaques: fine-grained euhedral likely pyrite

Sample ID	BT-15-SH-052
Field Name	Mafic
Field Description	Weathered beige/brown, fine-grained dark grey/green, carbonate stringers throughout
Mineralogy	Serpentine: 60%, calcite: 20%, chlorite: 10%, opaques: 10%
Alteration	Serpentine, calcite, chlorite
Mineralization	Fine-grained anhedral
Mineral Description	Fragments are actually assimilated sections that appear to be apart. Gradational changed between everything. Most of sample consists of various varieties of serpentine groundmass with aggregates of calcite within.
Thin Section Description	Serpentine: makes up majority of groundmass as well as veins within sample. Occurs as a deep blue birefringence with wavy form in veins Calcite: occurs as aggregates within sample as well as veinlets. Aggregates are fragmented and roughly 1-2mm in size- difficult to confirm as they are partially assimilated into groundmass Opaques: fine-grained anhedral Chlorite: occurs as small brown blebs throughout groundmass as well as in aggregates

Sample ID	BT-15-SH-055
Field Name	Mafic
Field Description	Weathered beige/brown, fine-grained grey/green, some carbonate veins visible within
Mineralogy	Calcite: 55%, plagioclase: 30%, serpentine: 15%, talc: 5%
Alteration	Calcite, serpentine
Mineralization	Very fine-grained anhedral
Mineral Description	Fine- to medium-grained, everything very irregular grain boundaries- chewed up. Majority of sample calcite and plagioclase laths with interstitial serpentine, talc and opaques.
Thin Section Description	Calcite: majority of groundmass, occurs as partially assimilated blebs and aggregates throughout Plagioclase: medium-grained, partially assimilated plagioclase laths compose large portion of sample Serpentine: fine-grained fibrous serpentine occurs interstitial to calcite and plagioclase Talc: very fine- to fine-grained, occurs sparsely in sample interstitial to calcite and serpentine

Sample ID	BT-15-SH-063
Field Name	Ultramafic
Field Description	Weathered beige/grey, very fine-grained grey with thin black veins throughout also quartz veins
Mineralogy	Serpentine: 60%, calcite: 20%, chlorite: 10%, opaques: 10%
Alteration	Serpentine, Calcite, Chlorite
Mineralization	N/A
Mineral Description	Very fine to fine-grained, everything irregular grain boundaries. Feathery texture within all of sample
Thin Section Description	Serpentine: fine-grained, makes up majority of sample and accounts for feathery texture in majority of sample. Calcite: fine-grained, occurs in veins as well as grains sparse throughout sample. Edges jagged and irregular when in contact with serpentine. Chlorite: Fine-grained, occurs in veins as discrete grains that are eating into other minerals. Opaques: very fine-grained. Seen throughout samples, as well as in thin veinlets

Sample ID	BT-15-SH-066
Field Name	Ultramafic Volcanic Breccia
Field Description	Weathered beige/grey, fine-grained dark grey/green, grey angular clasts in dark grey matrix
Mineralogy	Serpentine: 40%, Calcite: 40%, Opaques: 20%
Alteration	Serpentine, calcite
Mineralization	N/A
Mineral Description	Very fine- to fine-grained, everything w/ irregular grain boundaries. Boundaries of fragments not sharp, Large aggregates of calcite grains in several interstitial spaces between fragments
Thin Section Description	Serpentine: Fine-grained laths, some in a feathery texture, most just straight laths. Needle-like, and pervasive throughout sample. Calcite: fine- to coarse-grained, seen as irregular shaped grains throughout sample, and also as large (2mm) aggregates within matrix between fragments. Opaques: fine-grained, subrounded grains with irregular grain boundaries

Sample ID	BT-15-SH-067
Field Name	Ultramafic
Field Description	Weathered beige/grey, fine-grained grey/green
Mineralogy	Plagioclase: 35%, Clinopyroxene: 20%, Calcite: 20%, Serpentine: 10%, Opaques: 10%, Talc: 5%,
Alteration	Calcite, serpentine
Mineralization	N/A
Mineral Description	Very fine- to medium-grained. Everything with irregular grain boundaries. Clinopyroxenes still euhedral and distinguishable but clearly altered- Pyroxene spinifex
Thin Section Description	Plagioclase: fine-grained laths that have been altered, w/ irregular grain boundaries. Clinopyroxene: medium-grained laths that are euhedral, though altered at both rims and cores. Pyroxene spinifex. Calcite: found in fine-grained sparsely throughout sample as well as in thin veinlets. Serpentine: found as very fine-grained aggregates within sample. Opaques: fine-grained circular grains within sample. Talc: fine-grained mineral found sparsely throughout sample.

Sample ID	TL-16-SH-020
Field Name	Intermediate Volcanic
Field Description	Fine-grained light grey/blue with medium-grained phenocrysts of feldspar (plag and kspar). Intermediate
Mineralogy	Plagioclase: 50%, Quartz: 10%, Calcite: 15%, Chlorite: 5%, Sericite 15%, Epidote: >1% Opaques: 2%
Alteration	Greenschist (chlorite, epidote)
Mineralization	N/A
Mineral Description	Very fine- to fine-grained, most of sample is altered to various alteration minerals, difficult to distinguish different minerals within the groundmass. Plagioclase crystals display deformation twins as well as sericitization
Thin Section Description	Plagioclase: Appears as medium-grained euhedral crystals that have been severely altered to sericite as well as deformation twins present (pinched twins, discontinuous twins). Quartz: Appears in veins along with calcite and displays subgrain boundaries and undulose extinction. Calcite: Appears in veins along with quartz and as blebs within groundmass associated with ankerite. Chlorite: Seen within groundmass as well as associated with altered plagioclase. Sericite: Seen altering plagioclase. Very fine- to fine-grained crystals within euhedral plagioclase crystals. Epidote: fine-grained euhedral red crystals seen within plagioclase crystals. Ankerite: Seen in "clumps" spread throughout thin section, as well as in veins of calcite/quartz. Rusty red/brown in XPL and PPL

Sample ID	TL-16-SH-025
Field Name	Mafic Volcanic
Field Description	Fine-grained grey/blue, veinlets running through (fracture fill), from 0.5cm-1cm in thickness. White/yellow/green in colour.
Mineralogy	Plagioclase: 60%, Calcite: 30%, Chlorite: 10%
Alteration	Greenschist (chlorite, sericite)
Mineralization	N/A
Mineral Description	Medium-grained, most of the sample is plagioclase that has been altered to sericite. Difficult to distinguish between plagioclase crystals as they are so altered
Thin Section Description	Plagioclase: Appears as euhedral and anhedral medium-grained crystals with some deformation twins visible. Grains have undergone sericitization. Calcite: Calcite is seen throughout the sample as mottled and anhedral. Masses of fine-grained calcite clumped together. Chlorite: Seen as medium-grained elongate minerals throughout thin section. Associated with both plagioclase and calcite. Likely altered from pyroxene.

Sample ID	TL-16-SH-026
Field Name	Gabbro
Field Description	Medium-grained dark black mafic rock, some sulfides, plagioclase, pyroxene,
Mineralogy	Tremolite: 50%, Plagioclase: 20%, Quartz: 10%, Calcite: 5%, Chlorite: 5%, Opaques: 5%
Alteration	Greenschist (actinolite, chlorite)
Mineralization	Pyrite
Mineral Description	Medium- to fine-grained, most of the sample is made up of bright green pleochroic tremolite with large quartz and plagioclase phenocrysts that have been altered. Myrmekitic texture is also common. Opaques are likely pyrite
Thin Section Description	Tremolite: fine- to medium-grained crystals seen as fibrous, elongate, platy and Generally anhedral. Composes majority of sample. Occurring with calcite. Plagioclase: Seen mainly as myrmekitic texture within quartz crystals, some subhedral crystals with deformation twins also visible within thin section. Quartz: Seen as mainly myrmekitic texture with many grains undeformed, no subgrain boundaries or undulose extinction present. Calcite: Seen as fine-grained aggregates around opaques and actinolite (twins visible within fine-grained crystals)

Sample ID	TL-16-SH-034
Field Name	Komatiite
Field Description	Very fine-grained to fine-grained dark black/green rock. No distinct phenocrysts visible. Talcose powdering when hit. Distinct elongate black minerals in a pistachio green groundmass within several pseudo-layers (~2cm thick). Green groundmass likely serpentine.
Mineralogy	Serpentine: 70%, Magnetite: 15%, Pyroxene: 10%, Amphibole: 5%
Alteration	Greenschist (magnetite, serpentine)
Mineralization	N/A
Mineral Description	Fine-grained, most of sample is altered to serpentine with interstitial magnetite throughout in a capillary-like network. Some pyroxene present, though most are fractured and altered. Serpentine and magnetite have significantly altered every remnant olivine grain present (anhedral w/ altered edges).
Thin Section Description	Serpentine: Fine- to medium-grained, makes up majority of sample. Seen as blebby and continuous throughout. Magnetite: Occurs concentrated in elongate masses, where it appears to have nearly entirely altered certain crystals, as well as spread sparsely throughout. Pyroxene: medium-grained, anhedral, fractured and altered significantly Amphibole: fine-grained, fibrous, forms in fans in small blebs throughout sample. In disequilibrium with serpentine

Sample ID	TL-16-SH-041
Field Name	Conglomerate
Field Description	Fine-grained groundmass grey/blue with visible black minerals within. Fragments rounded to sub-rounded with different compositions- some jasper clasts visible within (>1cm in diameter)
Mineralogy	Quartz: 60%, Chlorite: 20%, Jasper: 5%, Pyroxene: 5%, Plagioclase: 5%, Calcite 5%, Sericite: 5%
Alteration	Greenschist (chlorite, sericite)
Mineralization	N/A
Mineral Description	Fine- to medium-grained, sample is altered to greenschist facies shown by significant chloritization throughout. Groundmass is made of chlorite, quartz and plagioclase. Fragments of altered pyroxenes as well as jasper clasts are seen within thin section.
Thin Section Description	Quartz: Seen throughout groundmass as well as in blebs. When in blebs, undulose extinction and subgrain boundaries present. Chlorite: Chlorite seen altering pyroxene crystals, makes up a large portion of the groundmass Jasper: medium- to coarse-grained dark red in PPL and black in XPL. Have clearly been effected by alteration around edges Pyroxene: Pyroxene crystals are seen in this sample as medium- to coarse-grained, being altered to chlorite. Distinct crystals have grain boundaries and pieces of unaltered pyroxene still present though crystals are now mostly chlorite. Plagioclase: Seen altered to sericite, with vague twins still present. Calcite: Seen alongside chlorite, as fine-grained grains. Sericite: Seen altering plagioclase crystals very fine- to fine-grained.

Sample ID	TL-16-SH-051
Field Name	Komatiite
Field Description	Fine-grained light grey/blue with thin (>1mm) black elongate minerals throughout (spinifex). No orientation of spinifex, short lengths (>0.5cm). Chaotic emplacement. Not black like peridotite. Light grey like trench komatiites
Mineralogy	Calcite: 70%, Talc: 5%, Quartz: 15%, Opaques: 5%, Hematite: 5%
Alteration	Greenschist plus significant carbonitization
Mineralization	N/A
Mineral Description	Very fine- to fine-grained, most of sample is calcite seen both as vfgr groundmass as well as in elongate aggregates which in hand sample make up spinifex texture
Thin Section Description	Calcite: very fine- to fine-grained, composes majority of sample in both elongate aggregates as well as groundmass. Spinifex needles seen in hand sample are entirely altered to calcite. Talc: fine-grained, seen as small blebs in sample alongside calcite aggregates. Quartz: very fine-grained within groundmass Opaque: very fine-grained blebs in aggregates sparsely throughout sample Hematite: fine-grained, euhedral, sparsely throughout sample.

Sample ID	TL-16-SH-053
Field Name	Pyroxenite
Field Description	Medium-grained dark grey/green with elongate/tabular minerals within (not spinifex). Tabular minerals are elongate (>1cm), green with some cleavage.
Mineralogy	Orthopyroxene: 40%, Clinopyroxene: 30%, Tremolite: 15%, Chlorite: 15%
Alteration	Chlorite
Mineralization	N/A
Mineral Description	Medium- to coarse-grained, mostly pyroxenes. Minor alteration. Chlorite appears interstitial to pyroxene crystals.
Thin Section Description	Orthopyroxene: medium- to coarse-grained, subhedral, minor alteration, crystals are fresh. Clinopyroxene: medium- to coarse-grained, subhedral, minor alteration, crystals are fresh Tremolite: medium- to coarse-grained, elongate euhedral crystals Chlorite: fine-grained, occurs as aggregates interstitial to coarse-grained orthopyroxene, clinopyroxene, and tremolite

Sample ID	TL-16-SH-070
Field Name	Komatiite
Field Description	Very fine-grained grey/green with thin (1-2mm) elongate black spinifex needles. Chaotic orientation from 0.5cm-2cm in length
Mineralogy	Serpentine: 60%, Chlorite: 15%, Iddingsite: 15%, Talc: 10%
Alteration	Serpentine, chlorite, iddingsite
Mineralization	N/A
Mineral Description	Medium- to coarse-grained spinifex needles consisting of a core of chlorite/talc, rimmed by iddingsite. The groundmass consists of thin serpentine needles in a dendritic habit
Thin Section Description	Serpentine: fine- to medium-grained elongate needles present as majority of groundmass. Seen in both a straight and dendritic habit. Chlorite: Seen as fine- to medium-grained cores of larger spinifex needles Iddingsite: rimming the chlorite and talc in spinifex needles Talc: seen within larger spinifex needles alongside chlorite

Sample ID	TL-16-SH-071
Field Name	Peridotite
Field Description	Medium-grained black/green pseudo-cumulate texture within. Black phenocrysts with pistachio green interstitial material
Mineralogy	Serpentine: 90%, Magnetite: 5%, Calcite: 5%, Talc: >1%
Alteration	Serpentine, calcite
Mineralization	N/A
Mineral Description	Fine- to medium-grained, entire sample is altered to serpentine with minor magnetite, talc and calcite.
Thin Section Description	Serpentine: medium-grained rounded aggregates, appear to be in a pseudo-cumulate texture altered from olivine. Magnetite: very fine- to fine-grained, anhedral. Spread sparsely throughout pseudo-cumulates. Calcite: fine-grained, seen as thin veins separating serpentine cumulates (corona)

Sample ID	TL-16-SH-074
Field Name	Komatiite
Field Description	Northern-most part of outcrop fine-grained grey/green phenocrysts of fine-grained dark black sub-rounded (euhedral) grains within. Southern-most part of outcrop fine-grained darker grey/green no euhedral phenocrysts but spinifex present. Blades up to 3-4mm thick & 2-3cm long. Spinifex black in colour and oriented in a N trend (345N).
Mineralogy	Pyroxene: 30%, Chlorite: 30%, Calcite: 10%, Quartz: 10%, Plagioclase: 10%, Talc: 5%, Opaques: 5%
Alteration	Calcite, chlorite
Mineralization	N/A
Mineral Description	Fine- to coarse-grained, whole sample is sub to anhedral crystals. Significant alteration has occurred throughout sample. Pyroxene spinifex appears relatively fresh
Thin Section Description	Pyroxene: medium- to coarse-grained seen as anhedral as well as elongate crystals within thin section (pyroxene spinifex), Some alteration, though not pervasive or extensive. Chlorite: fine- to medium-grained, seen in veins and blebs of groundmass as well as in thin veins. Calcite: fine-grained within groundmass, some aggregates sparsely throughout. Quartz: fine-grained sparsely throughout thin section as well as within groundmass. Undulose extinction present. Plagioclase: fine- to medium-grained elongate crystals with some deformed twins present within. Talc: fine-grained sparsely throughout thin section. Opaque: fine-grained anhedral.

Sample ID	TL-16-SH-078
Field Name	Monzonite
Field Description	Fragmental fine-grained green/ grey matrix with hornblende phenocrysts. Sub-rounded autoliths. Red/pink in colour with hornblende phenocrysts throughout everything. Magnetic.
Mineralogy	Potassium feldspar: 40%, Quartz: 30%, Calcite: 15%, Chlorite: 15%
Alteration	Chlorite, calcite
Mineralization	N/A
Mineral Description	Very fine-grained groundmass with plagioclase phenocrysts throughout as well as several veins of calcite. Groundmass consists of quartz and potassium feldspar (giving the sample a reddish-pink colour)
Thin Section Description	Potassium Feldspar: Seen as coarse-grained phenocrysts as well as very fine-grained within groundmass. Deformation twins present. Quartz: very fine- to fine-grained within groundmass, composes majority of groundmass. Calcite: fine- to medium-grained, seen as vein running through sample, as well as sparsely throughout. Chlorite: very fine- to fine-grained within groundmass

Sample ID	TL-16-SH-090
Field Name	Felsic Volcaniclastic
Field Description	Fragmental light grey very fine-grained Fragments between 0.3cm to 3cm in diameter. Mostly angular, sub angular very siliceous.
Mineralogy	Quartz: 50%, Calcite: 20%, Chlorite: 15%, Actinolite: 10%, Opaques: 5%
Alteration	Chlorite, calcite, actinolite
Mineralization	N/A
Mineral Description	Fragmental, very altered, very fine- to fine-grained, few medium-grained minerals (calcite, quartz), Calcite veins seen throughout.
Thin Section Description	Quartz: fine- to medium-grained, undulose extinction, subgrain boundaries, seen in veins with calcite as well as throughout groundmass. Calcite: Seen within groundmass as well as in veins and blebs, quartz associated with calcite. Chlorite: fine-grained, seen as thin veins throughout sample. Actinolite: Seen as thin veins separating quartz crystals.

Sample ID	TL-16-SH-100
Field Name	Monzonite
Field Description	Fine- to medium-grained pink rock (magnetic). Phenocrysts of hornblende and magnetite, within pink groundmass.
Mineralogy	Calcite: 30%, Plagioclase: 20%, Potassium Feldspar: 15%, Chlorite: 15%, Magnetite: 10%, Epidote: 10%
Alteration	Chlorite, epidote, calcite
Mineralization	N/A
Mineral Description	Very fine-grained, fragmental, altered to greenschist facies. Fragments have been altered until they are similar grain size and composition of groundmass
Thin Section Description	Calcite: fine-grained seen in veins and aggregates within fragments, as well as throughout groundmass. Plagioclase: Seen throughout groundmass as fine-grained elongate crystals. Potassium Feldspar: very fine-grained throughout groundmass giving the sample its red/pink colour. Chlorite: fine-grained within groundmass Magnetite: fine-grained, anhedral, broken up crystals. Epidote: very fine- to fine-grained, subhedral, throughout groundmass.

Sample ID	TL-16-SH-057
Field Name	Peridotite
Field Description	Fine-grained black/green ultramafic rock with thin pistachio green veinlets running through (very fine-grained light green, serpentine)
Mineralogy	Serpentine: 85%, Magnetite: 5%, Pyroxene 5%, Chlorite: 5%
Alteration	Serpentine, chlorite
Mineralization	N/A
Mineral Description	Fine- to medium-grained, Entire sample is altered to serpentine with minor magnetite, pyroxene. Pseudo-cumulate texture present
Thin Section Description	Serpentine: medium-grained rounded aggregates, appear to be in a pseudo-cumulate texture altered from olivine. Magnetite: fine-grained, anhedral to subhedral, in aggregates and spread sparsely throughout thin section. Pyroxene: fine- to medium-grained, fractured and altered to serpentine, few fractures of fresh pyroxene remain. Chlorite: fine-grained, seen interstitial to serpentine within groundmass

Sample ID	TL-16-SH-116A
Field Name	Pyroxenite Dike
Field Description	Medium grained pyroxenite with tabular grains of pyroxene throughout. There are cobble of pyroxenite with hornblende phenocrysts within.
Mineralogy	Clinopyroxene: 40%, Orthopyroxene: 30%, Serpentine 15%, Chlorite 10%, Opaques: 5%
Alteration	Serpentine, chlorite
Mineralization	N/A
Mineral Description	Medium- to coarse-grained, composed of relatively fresh pyroxene group minerals and serpentine taken over from olivine grains.
Thin Section Description	Clinopyroxene: medium-grained, euhedral to subhedral, slightly altered and fractured but mostly fresh. Orthopyroxene: medium-grained, subhedral, slightly altered to serpentine, abundant throughout thin section Serpentine: medium-grained, appears as relict olivine crystals. Chlorite: fine-grained, seen as alteration sparsely throughout. Opaques: fine-grained, anhedral.

Sample ID	TL-16-SH-116B
Field Name	Pyroxenite Dike
Field Description	Medium-grained pyroxenite with tabular grains of pyroxene throughout. There are cobble of pyroxenite with hornblende phenocrysts within.
Mineralogy	Orthopyroxene: 40%, Clinopyroxene: 40%, Calcite: 10%, Chlorite: 10%
Alteration	Chlorite, calcite
Mineralization	N/A
Mineral Description	Fine grained, with several medium-grained orthopyroxene phenocrysts. The majority of the sample consists of euhedral pyroxenes with interstitial calcite and chlorite
Thin Section Description	Orthopyroxene: fine- to medium-grained, appears as fine-grained euhedral grains throughout sample as well as several medium-grained phenocrysts, composes majority of sample. Clinopyroxene: fine-grained, euhedral crystals throughout sample- generally unaltered. Calcite: fine-grained, appears as interstitial material to the pyroxenes within groundmass. Chlorite: fine-grained, appears as interstitial material within groundmass

Sample ID	TL-16-SH-117
Field Name	Ultramafic Volcanic Breccia
Field Description	Flow top breccia unit. One sample is more cobble-like, other is more fragmental
Mineralogy	Orthopyroxene: 40%, Clinopyroxene: 40%, Chlorite: 15%, Opaques: 5%
Alteration	Chlorite
Mineralization	N/A
Mineral Description	Very fine- to fine-grained, mostly pyroxenes, completely
Thin Section Description	Pyroxene: very fine- to fine-grained altered and taken over by other minerals. Some aggregates are more heavily altered than others. Chlorite: fine-grained, seen sparsely throughout thin section. Opaques: very fine- to fine-grained, subhedral, spread sparsely throughout

Sample ID	TL-VK
Field Name	Vesicular Komatiite
Field Description	Very fine-grained black/green on surface with many vesicles. Fgr white sediment infilling vesicles.
Mineralogy	Calcite: 70%, Pyroxene: 10%, Iddingsite: 10%, Serpentine: 10%
Alteration	Calcite, serpentine, iddingsite
Mineralization	N/A
Mineral Description	Very fine- to fine-grained, majority of sample is calcite (interstitial to everything also filling voids within vesicles). Iddingsite is alteration mineral present most commonly. Pyroxenes mark non-vesicle portion of sample.
Thin Section Description	Calcite: fine-grained, majority of sample as well as the mineral filling vesicles within sample. Pyroxene: Contributes to non-vesicle portion of rock, fine-grained, very altered. Iddingsite: Alteration composes non-vesicle portion of sample. Serpentine: fine-grained, alteration, seen within non-vesicle portion of sample

**Appendix II: Samarium-Neodymium Isotope
Geochemistry**

Sample	Nd (ppm)	Sm (ppm)	$^{147}\text{Sm}/^{144}\text{Nd}$	$^{143}\text{Nd}/^{144}\text{Nd}$	2s	Epsilon
TL-16-SH-074	4.82	1.56	0.1953	0.512761	8	2.4
TL-16-SH-075	6.51	2.05	0.1907	0.512665	7	0.5
TL-16-SH-098	8.59	2.27	0.1595	0.512098	6	-10.5
TL-16-SH-106	6.99	2.08	0.1797	0.512473	7	-3.2
16-SH-21	6.23	1.93	0.1872	0.512602	7	-0.7
16-SH-29	10.72	2.03	0.1145	0.511282	7	-26.5

Sample	T De Paolo	T _{DM2}
TL-16-SH-074	2353	3216
TL-16-SH-075	2540	3205
TL-16-SH-098	2687	2945
TL-16-SH-106	2587	3024
16-SH-21	2581	3141
16-SH-29	2726	2855

Appendix II: Sample Locations

Summer 2015 Sample Locations

Sample ID	Trench Location	Datum	Zone	Easting	Northing
LM-15-SH-023	Linear Metals	NAD 83	UTM 16	294985	5377494
LM-15-SH-024	Linear Metals	NAD 83	UTM 16	294981	5377494
LM-15-SH-025	Linear Metals	NAD 83	UTM 16	294986	5377484
LM-15-SH-026	Linear Metals	NAD 83	UTM 16	294989	5377483
LM-15-SH-027	Linear Metals	NAD 83	UTM 16	294986	5377490
LM-15-SH-028	Linear Metals	NAD 83	UTM 16	294985	5377489
LM-15-SH-029	Linear Metals	NAD 83	UTM 16	294990	5377485
LM-15-SH-030	Linear Metals	NAD 83	UTM 16	294985	5377491
LM-15-SH-031	Linear Metals	NAD 83	UTM 16	294979	5377491
LM-15-SH-032	Linear Metals	NAD 83	UTM 16	294982	5377491
LM-15-SH-033	Linear Metals	NAD 83	UTM 16	294983	5377445
LM-15-SH-034	Linear Metals	NAD 83	UTM 16	294985	5377447
LM-15-SH-035	Linear Metals	NAD 83	UTM 16	294939	5377439
LM-15-SH-036	Linear Metals	NAD 83	UTM 16	294943	5377433
LM-15-SH-037	Linear Metals	NAD 83	UTM 16	294947	5377429
LM-15-SH-038	Linear Metals	NAD 83	UTM 16	294955	5377411
LM-15-SH-039	Linear Metals	NAD 83	UTM 16	294954	5377419
LM-15-SH-040	Linear Metals	NAD 83	UTM 16	294950	5377425
LM-15-SH-041	Linear Metals	NAD 83	UTM 16	294905	5377376
LM-15-SH-042	Linear Metals	NAD 83	UTM 16	294911	5377376
LM-15-SH-043	Linear Metals	NAD 83	UTM 16	294923	5377369
LM-15-SH-044	Linear Metals	NAD 83	UTM 16	294878	5377396
LM-15-SH-045	Linear Metals	NAD 83	UTM 16	294882	5377393
LM-15-SH-046	Linear Metals	NAD 83	UTM 16	294890	5377386
LM-15-SH-047	Linear Metals	NAD 83	UTM 16	294892	5377382
LM-15-SH-048	Linear Metals	NAD 83	UTM 16	294894	5377385
BT-15-SH-049	Bateman	NAD 83	UTM 16	296453	5377536
BT-15-SH-050	Bateman	NAD 83	UTM 16	296451	5377537
BT-15-SH-051	Bateman	NAD 83	UTM 16	296451	5377542
BT-15-SH-052	Bateman	NAD 83	UTM 16	296453	5377549
BT-15-SH-053	Bateman	NAD 83	UTM 16	296449	5377565
BT-15-SH-054	Bateman	NAD 83	UTM 16	296446	5377573
BT-15-SH-055	Bateman	NAD 83	UTM 16	296450	5377586
BT-15-SH-056	Bateman	NAD 83	UTM 16	296453	5377619
BT-15-SH-057	Bateman	NAD 83	UTM 16	296456	5377624
BT-15-SH-058	Bateman	NAD 83	UTM 16	296450	5377630
BT-15-SH-059	Bateman	NAD 83	UTM 16	296450	5377635
BT-15-SH-060	Bateman	NAD 83	UTM 16	296450	5377646

Sample ID	Trench Location	Datum	Zone	Easting	Northing
BT-15-SH-061	Bateman	NAD 83	UTM 16	296446	5377655
BT-15-SH-062	Bateman	NAD 83	UTM 16	296443	5377662
BT-15-SH-063	Bateman	NAD 83	UTM 16	296531	5377696
BT-15-SH-064	Bateman	NAD 83	UTM 16	296528	5377693
BT-15-SH-065	Bateman	NAD 83	UTM 16	296523	5377680
BT-15-SH-066	Bateman	NAD 83	UTM 16	296517	5377666
BT-15-SH-067	Bateman	NAD 83	UTM 16	296516	5377642
BT-15-SH-068	Bateman	NAD 83	UTM 16	296446	5377462
BT-15-SH-069	Bateman	NAD 83	UTM 16	296447	5377451
BT-15-SH-070	Bateman	NAD 83	UTM 16	296444	5377437
BT-15-SH-071	Bateman	NAD 83	UTM 16	296445	5377423
BT-15-SH-072	Bateman	NAD 83	UTM 16	296447	5377389
BT-15-SH-073	Bateman	NAD 83	UTM 16	296444	5377376
BT-15-SH-074	Bateman	NAD 83	UTM 16	296199	5377296
BT-15-SH-075	Bateman	NAD 83	UTM 16	296213	5377350
BT-15-SH-076	Bateman	NAD 83	UTM 16	296205	5377328
BT-15-SH-077	Bateman	NAD 83	UTM 16	296633	5378103
BT-15-SH-078	Bateman	NAD 83	UTM 16	296558	5377798
BT-15-SH-079	Bateman	NAD 83	UTM 16	296532	5377756
LM-15-SH-080	Linear Metals	NAD 83	UTM 16	294939	5377441

Summer 2016 Sample Locations

Station #	Traverse Code	Sample ID	Datum	Zone	Easting	Northing
Hinz-1	T-1	TL-16-SH-001	NAD83	UTM 16	298974	5374447
Hinz -2	T-1		NAD83	UTM 16	298984	5374269
Hinz 3-A	T-1	TL-16-SH-002	NAD83	UTM 16	299002	5374493
Hinz 3-B	T-1		NAD83	UTM 16	299014	5374489
Hinz 4	T-1	TL-16-SH-003	NAD83	UTM 16	299273	5374490
Hinz 5	T-1	TL-16-SH-004	NAD83	UTM 16	299142	5374657
Hinz 6	T-2		NAD83	UTM 16	298381	5375062
Hinz 7	T-2	Rep Sample	NAD83	UTM 16	298368	5374942
Hinz 8	T-2	TL-16-SH-005	NAD83	UTM 16	298455	5374828
Hinz 9	T-2		NAD83	UTM 16	298413	5374841
Hinz 10	T-2		NAD83	UTM 16	298404	5374771
Hinz 11	Q-15	TL-16-SH-006	NAD83	UTM 16	295342	5375815
Hinz 12	Q-15	TL-16-SH-007	NAD83	UTM 16	295420	5375771
Hinz 13	Q-15	TL-16-SH-008	NAD83	UTM 16	295520	5375776
	Q-15	TL-16-SH-009	NAD83	UTM 16	295524	5375772
Hinz 14	Q-15	TL-16-SH-010	NAD83	UTM 16	295671	5376049
Hinz 15	Q-15	TL-16-SH-011	NAD83	UTM 16	295355	5375932
Hinz 16	Q-5	TL-16-SH-012	NAD83	UTM 16	298206	5375557
Hinz 17	Q-5		NAD83	UTM 16	297795	5375567
Hinz 18	Q-5	TL-16-SH-013	NAD83	UTM 16	297684	5375668
Hinz 19	Q-5	TL-16-SH-014	NAD83	UTM 16	297732	5375918
Hinz 20	Q-13	TL-16-SH-015	NAD83	UTM 16	296314	5376687
Hinz 21	Q-13	TL-16-Sh-016	NAD83	UTM 16	296329	5376593
Hinz 22	Q-13	TL-16-SH-017	NAD83	UTM 16	296409	5376608
Hinz 23	Q-13	TL-16-SH-018	NAD83	UTM 16	296390	5376441
Hinz 24	Q-13	TL-16-SH-019	NAD83	UTM 16	296346	5376377
Hinz 25	Q-13		NAD83	UTM 16	296189	5376579
Hinz 26	Q-8	TL-16-SH-020	NAD83	UTM 16	298088	5376975
Hinz 27	Q-8	TL-16-SH-021	NAD83	UTM 16	298002	5376966
Hinz 28	Q-8	TL-16-SH-022	NAD83	UTM 16	297658	5376671
Hinz 29	Q-10	TL-16-SH-023	NAD83	UTM 16	297303	5376765
Hinz 30	Q-10	TL-16-SH-024	NAD83	UTM 16	297321	5376660
Hinz 31	Q-10	TL-16-SH-025	NAD83	UTM 16	297347	5376534
Hinz 32	Q-10	TL-16-SH-026	NAD83	UTM 16	297173	5376491
Hinz 33	Q-10	TL-16-SH-027	NAD83	UTM 16	296873	5376579
Hinz 34	Q-14	TL-16-SH-028A	NAD83	UTM 16	295979	5376686
Hinz 34	Q-14	TL-16-SH-028B	NAD83	UTM 16	295979	5376686
Hinz 35	Q-14	TL-16-SH-029	NAD83	UTM 16	295983	5376567

Station #	Traverse Code	Sample ID	Datum	Zone	Easting	Northing
Hinz 36	Q-14	TL-16-SH-030	NAD83	UTM 16	295887	5376476
Hinz 37	Q-14	TL-16-SH-031	NAD83	UTM 16	295661	5376470
Hinz 38	Q-14	TL-16-SH-032	NAD83	UTM 16	295719	5376521
Hinz 39	Q-2	TL-26-SH-033	NAD83	UTM 16	296786	5376450
Hinz 40	Q-2	TL-16-SH-034	NAD83	UTM 16	296756	5376056
Hinz 41	Q-2	TL-16-SH-035	NAD83	UTM 16	296972	5376053
Hinz 42	Q-2	TL-16-SH-036	NAD83	UTM 16	297188	5376065
Hinz 43	Q-2	TL-16-SH-037	NAD83	UTM 16	297395	5376283
Hinz 44	Q-16	TL-16-SH-038A	NAD83	UTM 16	295176	5376347
Hinz 44	Q-16	TL-16-SH-038B	NAD83	UTM 16	295176	5376347
Hinz 45	Q-16		NAD83	UTM 16	295126	5376341
Hinz 46	Q-16	TL-16-SH-039	NAD83	UTM 16	294878	5376026
Hinz 47	Q-16	TL-16-SH-040	NAD83	UTM 16	295007	5376092
Hinz 48	Q-12	TL-16-SH-041	NAD83	UTM 16	296911	5376964
Hinz 49	Q-12	TL-16-SH-042	NAD83	UTM 16	296613	5377087
Hinz 50	Q-12	TL-16-SH-043	NAD83	UTM 16	296719	5376715
Hinz 51	C-1	TL-16-SH-044	NAD83	UTM 16	295801	5375453
Hinz 52	C-1	TL-16-SH-045	NAD83	UTM 16	296427	5375678
Hinz 53	C-1	TL-16-SH-046	NAD83	UTM 16	296361	5375803
Hinz 54	C-1	TL-16-SH-047	NAD83	UTM 16	295976	5375671
Hinz 55	C-6	TL-16-SH-048	NAD83	UTM 16	295912	5375093
Hinz 56	C-6	TL-16-SH-049	NAD83	UTM 16	295701	5375107
Hinz 57	C-6	NO SAMPLE	NAD83	UTM 16	295540	5375180
Hinz 58	C-6	TL-16-SH-050	NAD83	UTM 16	295460	5375385
Hinz 59	C-2	TL-16-SH-051	NAD83	UTM 16	295856	5375357
Hinz 60	C-2	TL-16-SH-052	NAD83	UTM 16	296040	5375353
Hinz 61	C-2	TL-16-SH-053	NAD83	UTM 16	296233	5375287
Hinz 62	C-2	Hinz 62	NAD83	UTM 16	296396	5375265
Hinz 63	C-2	TL-16-SH-054	NAD83	UTM 16	296452	5375364
Hinz 64	C-2	Hinz 64	NAD83	UTM 16	296307	5375556
Hinz 65	C-2	TL-16-SH-055	NAD83	UTM 16	296155	5375549
Hinz 66	C-3	TL-16-SH-056	NAD83	UTM 16	296201	5375097
Hinz 67	C-3	TL-16-SH-057	NAD83	UTM 16	296282	5375048
Hinz 68	C-3	TL-16-SH-058	NAD83	UTM 16	296475	5374963
Hinz 69	C-3	TL-16-SH-059	NAD83	UTM 16	296550	5374957
Hinz 70	C-3	TL-16-SH-060	NAD83	UTM 16	296582	5374980
Hinz 71	C-3	Hinz 71	NAD83	UTM 16	296506	5375200
Hinz 72	Q-3	TL-16-SH-061	NAD83	UTM 16	297085	5375617
Hinz 73	Q-3	TL-16-SH-062	NAD83	UTM 16	297305	5375194
Hinz 74	Q-3	HINZ 74	NAD83	UTM 16	297331	5375226

Station #	Traverse Code	Sample ID	Datum	Zone	Easting	Northing
Hinz 75	Q-3	TL-16-SH-063	NAD83	UTM 16	297362	5375240
Hinz 76	C-5	TL-16-SH-064	NAD83	UTM 16	295713	5374750
Hinz 77	C-5	TL-16-SH-065	NAD83	UTM 16	295588	5374774
Hinz 78	C-5	TL-16-SH-066	NAD83	UTM 16	295379	5374933
Hinz 79	C-5	TL-16-SH-067	NAD83	UTM 16	295277	5375027
Hinz 80	C-5	TL-16-SH-068	NAD83	UTM 16	295645	5374913
Hinz 81	C-4	TL-16-SH-069	NAD83	UTM 16	296248	5374988
Hinz 82	C-4	TL-16-SH-070	NAD83	UTM 16	296253	5374886
Hinz 83	C-4	TL-16-SH-071	NAD83	UTM 16	296305	5374825
Hinz 84	C-4	TL-16-SH-072	NAD83	UTM 16	296378	5374777
Hinz 85	C-4	TL-16-SH-073	NAD83	UTM 16	296397	5374726
Hinz 86	C-7	TL-16-SH-074	NAD83	UTM 16	295150	5375619
Hinz 87	C-7	TL-16-SH-075	NAD83	UTM 16	294984	5375391
Hinz 88	C-7	TL-16-SH-076	NAD83	UTM 16	294728	5375469
Hinz 89	C-7	HINZ 89	NAD83	UTM 16	295066	5375933
Hinz 90	C-7	TL-16-SH-077	NAD83	UTM 16	294903	5375850
Hinz 91	Q-11	TL-16-SH-078	NAD83	UTM 16	297845	5377465
Hinz 92	Q-11	NO SAMPLE	NAD83	UTM 16	297829	5377539
Hinz 93	Q-11	TL-16-SH-079	NAD83	UTM 16	297764	5377696
Hinz 94	Q-11	Rep Sample	NAD83	UTM 16	297672	5377748
Hinz 95	Q-11	TL-16-SH-080	NAD83	UTM 16	297601	5377791
Hinz 96	Q-11	TL-16-SH-081	NAD83	UTM 16	297437	5377828
Hinz 97	Q-11	NO SAMPLE	NAD83	UTM 16	297338	5377365
Hinz 98	Q-11	NO SAMPLE	NAD83	UTM 16	297822	5377309
Hinz 99	Q-23	TL-16-SH-082	NAD83	UTM 16	294816	5377387
Hinz 100	Q-23	TL-16-SH-083	NAD83	UTM 16	294691	5377204
Hinz 101	Q-23	NO SAMPLE	NAD83	UTM 16	294779	5377467
Hinz 102	Q-23	TL-16-SH-084	NAD83	UTM 16	295029	5377523
Hinz 103	Q-21&22	TL-16-SH-085	NAD83	UTM 16	295136	5377095
Hinz 104	Q-21&22	TL-16-SH-086	NAD83	UTM 16	295015	5377044
Hinz 105	Q-21&22	TL-16-SH-087	NAD83	UTM 16	295269	5377492
Hinz 106	Q-18	TL-16-SH-088	NAD83	UTM 16	295803	5377040
Hinz 107	Q-18	TL-16-SH-089	NAD83	UTM 16	295641	5377040
Hinz 108	Q-18	TL-16-SH-090	NAD83	UTM 16	295414	5376436
Hinz 109	Q-18	Rep Sample	NAD83	UTM 16	2957335	5376853
Hinz 110	Q-20&19	TL-16-SH-091	NAD83	UTM 16	296295	5377743
Hinz 111	Q-20&19	TL-16-SH-092	NAD83	UTM 16	296257	5377703
Hinz 112	Q-20&19	Rep Sample	NAD83	UTM 16	296097	5377663
Hinz 113	Q-20&19	NO SAMPLE	NAD83	UTM 16	295771	5377325
Hinz 114	Q-20&19	TL-16-SH-093	NAD83	UTM 16	295749	5377201

Station #	Traverse Code	Sample ID	Datum	Zone	Easting	Northing
Hinz 115	Q-20&19	NO SAMPLE	NAD83	UTM 16	295819	5377197
Hinz 116	Q-20&19	Rep Sample	NAD83	UTM 16	295997	5377179
Hinz 117	Q-28	TL-16-SH-094	NAD83	UTM 16	296519	5378063
Hinz 118	Q-28	TL-16-SH-095	NAD83	UTM 16	296815	5378005
Hinz 119	Q-28	TL-16-SH-096	NAD83	UTM 16	297779	5377807
Hinz 120	Q-28	TL-16-SH-097	NAD83	UTM 16	297829	5377701
Hinz 121	Q-24	TL-16-SH-098	NAD83	UTM 16	296776	5377825
Hinz 122	Q-24	Rep Sample	NAD83	UTM 16	296615	5377614
Hinz 123	Q-24	TL-16-SH-099	NAD83	UTM 16	296342	5377789
Hinz 124	Q-26	TL-16-SH-100	NAD83	UTM 16	298401	5377678
Hinz 125	Q-26	NO SAMPLE	NAD83	UTM 16	298456	5377637
Hinz 126	Q-26	TL-16-SH-101	NAD83	UTM 16	298381	5377788
Hinz 127	Q-26		NAD83	UTM 16	298221	5377817
Hinz 128	Q-26		NAD83	UTM 16	298037	5377745
Hinz 129	Q-26		NAD83	UTM 16	298020	5377600
Hinz 130	Q-4	Rep Sample	NAD83	UTM 16	298522	5375983
Hinz 131	Q-4	Rep Sample	NAD83	UTM 16	298262	5376292
Hinz 132	Marble Lake	TL-16-SH-102	NAD83	UTM 16	296297	5374657
Hinz 133	Marble Lake	TL-16-SH-103	NAD83	UTM 16	296346	5374660
Hinz 134	Marble Lake	TL-16-SH-104	NAD83	UTM 16	296398	5374615
Hinz 135	Marble Lake		NAD83	UTM 16	296287	5374635
Hinz 136	Marble Lake	TL-16-SH-105	NAD83	UTM 16	296371	5374861
Hinz 137	Marble Lake		NAD83	UTM 16	296319	5374891
Hinz 138	Marble Lake	TL-16-SH-106	NAD83	UTM 16	296299	5374970
Hinz 139	Gold Lake	TL-16-SH-107	NAD83	UTM 16	296740	5375054
Hinz 140	Gold Lake	TL-16-SH-108	NAD83	UTM 16	296693	5375112
Hinz 141	Gold Lake	TL-16-SH-109	NAD83	UTM 16	296580	5375420
Hinz 142	Gold Lake	TL-16-SH-110	NAD83	UTM 16	296493	5375640
Hinz 143	Gold Lake	TL-16-SH-111A&B	NAD83	UTM 16	296541	5375957
Hinz 144	Thunder Lake South		NAD83	UTM 16	295982	5375330
Hinz 145	Thunder Lake South	TL-16-SH-112	NAD83	UTM 16	296296	5374999
Hinz 146	Thunder Lake South	TL-16-SH-113	NAD83	UTM 16	296285	5374992
Hinz 147	Thunder Lake South	TL-16-SH-114	NAD83	UTM 16	296276	5374993
Hinz 148	Thunder Lake South	TL-16-SH-115	NAD83	UTM 16	296266	5374991
Hinz 149	Thunder Lake South	TL-16-SH-116A&B	NAD83	UTM 16	296264	5374992

Station #	Traverse Code	Sample ID	Datum	Zone	Easting	Northing
Hinz 150	Thunder Lake South	TL-16-SH-117	NAD83	UTM 16	296247	5374980
Hinz 151	Thunder Lake South	TL-16-SH-118	NAD83	UTM 16	296191	5374939
Hinz 152	Thunder Lake South		NAD83	UTM 16	295669	5375444
Hinz 153	Thunder Lake North	TL-16-SH-119	NAD83	UTM 16	295151	5375628
Hinz 154	Thunder Lake North	TL-16-SH-120	NAD83	UTM 16	295181	5375607
Hinz 155	Thunder Lake North	TL-16-SH-121	NAD83	UTM 16	295192	5375620
Hinz 156	Thunder Lake North	TL-16-SH-122	NAD83	UTM 16	295178	5375692
Hinz 157	Thunder Lake North	TL-16-SH-123	NAD83	UTM 16	295175	5375696
Hinz 158	Thunder Lake North		NAD83	UTM 16	295173	5375705
Hinz 159	Thunder Lake North	TL-16-SH-124	NAD83	UTM 16	295171	5375710
Hinz 160	Thunder Lake Road		NAD83	UTM 16	295232	5375966
Hinz 161	Thunder Lake Road		NAD83	UTM 16	295288	5376184
Hinz 162	Thunder Lake Road		NAD83	UTM 16	295366	5376573
Hinz 163	Thunder Lake Road		NAD83	UTM 16	295546	5376703

Appendix III: Geochemical Data

	16SH01	16SH02	16SH04	16SH05	16SH06	16SH07	16SH08	16SH09	16SH10	16SH11	16SH13	16SH15
Al ₂ O ₃ (wt.%)	13.81	12.7	3.96	3.83	2.03	3.21	10.39	7.67	8.1	3.9	2	2.66
BaO	0.04	0.05	0.01	0.01	0.01	0.004	0.01	0.03	0.03	0.004	0.01	0.004
CaO	0.58	1.727	0.047	0.013	0.025	25.246	0.246	0.066	0.49	0.072	0.028	2.731
Cr ₂ O ₃	0.06	0.06	0.01	0.002	0.01	0.31	0.01	0.002	0.002	0.01	0.01	0.63
Fe ₂ O ₃	4.24	6.47	1.12	0.27	2.55	5.55	19.75	8.93	4.18	0.82	0.22	10.54
K ₂ O	2.42	1.62	0.38	0.26	0.36	0.01	0.12	1.57	0.79	0.05	0.27	0.02
LOI	5.63	5.35	12.38	3.5	3.99	22.78	8.16	6.93	3.73	1.52	2.66	10.85
MgO	7.99	5.42	0.15	0.1	0.12	10.16	4.43	1.09	5.53	0.9	0.11	27.46
MnO	0.039	0.088	0.002	0.003	0.002	0.334	0.264	0.035	0.071	0.008	0.002	0.123
Na ₂ O	0.3	2.33	0.41	0.17	0.07	0.04	1.27	0.6	0.12	1.24	0.34	0.04
P ₂ O ₅	0.102	0.093	0.019	0.009	0.003	0.02	0.08	0.046	0.048	0.019	0.007	0.012
SiO ₂	63.2	62.93	81.33	91.7	90.54	31.47	53.27	72.17	75.61	90.97	94.02	43.78
TiO ₂	0.49	0.44	0.08	0.05	0.04	0.16	0.35	0.2	0.21	0.07	0.05	0.13
Total	98.92	99.3	99.9	99.91	99.75	99.29	98.35	99.34	98.92	99.58	99.72	98.98
Al (ppm)	74753	43781	20389	19998	10472	17110	55048	39817	43312	19690	10325	13965
Ba	375	264	60	61	69	9	37	247	224	18	52	7
Be	1	1	1	1	1	1	1	1	1	1	1	1
Ca	4250	11524	374	129	264	100000	1764	510	3536	534	239	19156
Cd	1	1	1	1	1	1	1	1	1	1	1	1
Co	15	24	7	1	7	79	204	35	9	3	1	110
Cr	445	379	40	30	56	1300	65	39	36	70	34	1300
Cu	7	7	57	14	32	23	1704	66	6	6	16	18
Fe	30313	41179	7572	1786	17510	37970	95000	61205	28806	5524	1559	70019
K	20804	12959	3033	1915	2909	70	897	12624	6635	363	2187	70
Li	84	34	4	2	4	15	45	18	56	20	3	7
Mg	48267	21121	690	407	547	59419	25991	6161	32855	5080	439	150468
Mn	303	628	3	22	5	2553	2004	270	553	64	8	923
Mo	1	1	5	2	3	1	1	3	1	4	2	1
Na	1944	15550	2685	923	500	500	8492	3912	587	8308	2106	500
Ni	177	142	24	2	30	1429	3488	119	27	21	3	2317
P	467	397	82	33	30	86	342	196	208	81	30	53
Pb	15	15	54	74	16	15	15	36	15	15	135	15
S	130	130	5389	544	16000	520	16000	16000	130	130	474	1065
Sc	12	3	6	3	2	12	4	4	3	1	4	11
Sr	26	76	15	8	3	155	24	12	7	33	14	33
Ti	2916	2555	485	275	201	1000	2062	1165	1221	374	305	772
V	86	76	21	13	10	68	44	27	25	9	17	61
W	6	6	6	6	6	6	6	6	6	6	6	6
Y	11	4	9	5	2	4	6	5	6	3	6	3
Zn	18	25	218	19	64	41	302	42	52	6	12	62
Ba	391.5	330.3	64.2	66.9	70.4	6.4	37.3	254.3	231.7	19.1	53.4	3.4
Be	0.79	0.39	0.14	0.19	0.11	0.13	0.25	0.44	0.41	0.14	0.16	0.21
Bi	0.47	0.47	0.77	0.96	0.47	0.47	1.99	0.58	0.47	0.47	0.47	0.47

	16SH01	16SH02	16SH04	16SH05	16SH06	16SH07	16SH08	16SH09	16SH10	16SH11	16SH13	16SH15
Cd	0.028	0.027	0.402	0.074	0.097	0.015	0.505	0.079	0.036	0.014	0.03	0.019
Ce	27.83	13.64	8.51	7.48	1.63	1.44	14.85	24.05	13.76	10.32	8.41	0.82
Co	18	28.89	7.75	1.2	7.06	85.82	187	37.88	10.16	3.6	0.83	117.84
Cr	476	425	40	27	128	2103	67	40	31	57	31	3972
Cs	2.71	1.287	1.404	0.507	0.386	0.096	0.122	0.626	0.919	0.126	0.457	0.381
Cu	1.4	1.9	57.7	14.6	33.3	50.2	1817.7	66.3	2	3	15.5	16.3
Dy	1.914	0.934	1.526	1.021	0.254	0.692	0.934	0.903	1.125	0.578	1.007	0.488
Er	0.993	0.564	0.988	0.634	0.157	0.406	0.578	0.461	0.588	0.318	0.647	0.32
Eu	0.569	0.3516	1.242	0.802	0.1657	0.1187	0.4263	0.474	0.2448	0.2217	0.9034	0.0633
Ga	14.49	14.27	7.93	6	2.89	3.62	14.51	9.92	7.46	3.95	4.26	3.34
Gd	2.299	1.003	1.161	0.901	0.226	0.491	1.059	1.146	1.236	0.694	0.906	0.345
Hf	2.8	2.62	0.74	0.43	0.5	0.38	2.44	2.05	1.95	0.95	0.43	0.26
Ho	0.3704	0.1859	0.324	0.2051	0.0569	0.1301	0.1852	0.1695	0.2102	0.1145	0.2122	0.1148
In	0.0073	0.0231	0.3038	0.3052	0.0295	0.0142	0.409	0.021	0.0111	0.003	0.0534	0.0166
La	13.15	6.46	3.74	3.48	0.81	0.6	8	12.36	6.67	5.14	4	0.33
Li	87.4	36.3	3.2	1.7	3.2	8.1	44.3	18.6	57.9	19.2	2.5	13.1
Lu	0.1383	0.0881	0.1898	0.1186	0.0251	0.0635	0.0893	0.0706	0.0819	0.0454	0.1148	0.0499
Mo	0.78	1.09	6.79	3.15	8.19	0.49	2.78	3.86	0.93	3.64	3.07	0.21
Nb	3.817	3.347	1.25	0.615	0.695	0.357	2.933	2.545	2	1.243	0.695	0.252
Nd	13.1	6.54	4.62	3.77	0.78	1.18	6.72	9.97	6.88	4.23	4.32	0.7
Ni	189.6	159.4	25.6	2.1	31.5	1525.9	3805	125.4	29.1	23	3.7	2472.3
Pb	0.7	0.8	59.6	89.6	16.5	4	15.8	41.5	0.7	0.7	160.5	0.3
Pr	3.361	1.62	1.086	0.943	0.206	0.227	1.831	2.71	1.711	1.112	1.073	0.13
Rb	59.28	30.31	14.53	9.2	10.54	0.23	2.17	38.33	15.57	1.02	9.96	0.45
Sb	0.27	0.16	3.48	1.83	3.87	0.04	0.98	2.56	0.05	0.11	2.21	0.26
Sc	13	4.9	7.3	4.1	2.5	13.4	5.1	5.3	4.4	2.2	5.4	12
Sm	2.497	1.195	1.106	0.897	0.195	0.379	1.236	1.636	1.425	0.786	0.973	0.232
Sn	0.38	0.67	7.19	5.07	2.08	0.33	2.18	1.18	1.36	0.37	2.07	0.16
Sr	24.9	74.8	14.3	7.5	2.6	158.7	26	10.7	7.2	32.3	13.3	33.6
Ta	0.297	0.272	0.103	0.051	0.047	0.021	0.226	0.22	0.178	0.133	0.051	0.015
Tb	0.3332	0.1505	0.2164	0.1508	0.0409	0.0931	0.1477	0.1583	0.1793	0.1018	0.1538	0.0635
Th	2.159	1.832	0.842	0.646	0.461	0.099	1.545	1.688	1.424	1.321	0.793	0.073
Ti	2968	2690	495	297	199	991	2070	1178	1263	387	314	779
Tl	0.263	0.239	2.285	1.671	1.2	0.043	0.283	0.44	0.111	0.009	1.112	0.045
Tm	0.1418	0.0855	0.1518	0.0969	0.0222	0.06	0.088	0.0635	0.0858	0.0434	0.101	0.0493
U	0.598	0.532	0.337	0.264	0.151	0.024	0.419	0.515	0.394	0.373	0.272	0.014
V	87.1	78.2	19.7	13.6	9.2		40.5	24.4	25.3	8.3	16.8	
W	1.21	0.5	0.65	0.4	0.49	0.05	0.22	0.86	0.24	0.06	0.73	0.05
Y	10.52	5.18	8.44	5.75	1.49	3.72	5.46	4.79	6.13	3.28	5.68	2.69
Yb	0.926	0.569	1.113	0.713	0.155	0.404	0.592	0.411	0.539	0.28	0.711	0.349
Zn	28	25	227	21	62	60	305	40	52	6	13	63
Zr	113	103	27	17	21	13	100	80	76	38	15	9

	16SH16	16SH17	16SH19	16SH21	16SH22	16SH23	16SH25	16SH25 SP	16SH26	16SH27	16SH29	16SH32
Al ₂ O ₃ (wt.%)	8.55	6.28	7.33	14.21	15.29	10.76	15.25	15.3	13.7	16.72	15.4	3.43
BaO	0.004	0.02	0.14	0.02	0.02	0.01	0.04	0.04	0.01	0.06	0.02	0.01
CaO	3.837	0.067	7.496	5.125	7.559	1.715	4.426	4.401	1.355	0.156	1.681	0.058
Cr ₂ O ₃	0.55	0.002	0.75	0.12	0.09	0.02	0.06	0.06	0.19	0.03	0.05	0.05
Fe ₂ O ₃	9.05	2.76	15.38	6.83	7.96	2.85	8.93	8.92	12.4	8.65	3.12	1.7
K ₂ O	0.03	1.29	0.22	0.14	0.5	0.15	0.78	0.77	0.14	3.51	0.57	0.79
LOI	6.21	2.23	11.74	2.27	4.5	2.83	4.41	4.47	6.81	5.33	3.3	8.95
MgO	17.67	2.08	11.03	4.24	7.76	2.71	7.2	7.22	12.99	5.69	5.06	0.48
MnO	0.197	0.014	0.487	0.129	0.192	0.059	0.162	0.16	0.176	0.114	0.046	0.008
Na ₂ O	0.21	0.07	0.06	4.69	1.9	3.99	2.46	2.44	1.3	0.09	4.68	0.1
P ₂ O ₅	0.023	0.03	0.026	0.07	0.075	0.063	0.098	0.097	0.056	0.05	0.107	0.017
SiO ₂	52.54	84.29	43.89	60.43	52.36	73.38	54.34	54.43	49.47	58.02	64.95	83.46
TiO ₂	0.38	0.2	0.34	0.79	0.89	0.27	0.72	0.73	0.78	0.66	0.56	0.12
Total	99.25	99.32	98.89	99.07	99.09	98.79	98.89	99.03	99.37	99.08	99.55	99.17
Al (ppm)	44981	33789	39680	67185	81771	49922	81566	79131	69590	51424	71716	17771
Ba	19	176	1155	129	190	75	338	329	29	432	161	98
Be	1	1	1	1	1	1	1	1	1	1	1	1
Ca	26070	514	49173	34799	53181	12090	31164	30285	8999	701	11841	443
Cd	1	1	1	1	1	1	1	1	1	1	1	1
Co	124	6	75	58	45	12	34	34	96	39	12	3
Cr	1300	36	1300	778	569	111	389	384	1201	200	344	315
Cu	15	6	21	94	102	6	82	84	154	149	10	38
Fe	59800	19215	95000	44106	53649	19411	60235	59273	80590	53412	21095	11428
K	162	10632	1745	1065	4094	1136	6419	6210	1021	27536	4639	6300
Li	55	24	13	13	33	22	48	48	72	30	37	3
Mg	99839	12475	63608	21441	44998	12574	41938	40954	72367	16863	25476	2716
Mn	1468	115	3574	930	1455	447	1212	1192	1277	767	332	73
Mo	1	1	1	1	1	1	1	1	1	1	1	5
Na	1121	500	500	31000	13430	27651	17314	16720	8707	500	31000	500
Ni	2742	34	1294	270	90	43	120	120	454	96	43	20
P	100	129	105	298	330	286	439	429	226	212	473	67
Pb	15	15	15	15	15	15	15	15	15	15	15	40
S	764	130	615	3548	1034	130	2191	2263	621	5608	130	1191
Sc	29	4	25	34	46	5	28	28	43	17	8	8
Sr	6	5	54	162	140	163	294	282	83	4	178	3
Ti	2180	1145	1943	4569	5378	1615	4284	4224	4455	3837	3348	681
V	160	31	154	252	303	46	196	195	279	161	107	39
W	6	6	6	6	6	6	6	6	6	6	6	6
Y	8	5	16	16	20	11	16	15	13	5	5	6
Zn	152	34	77	87	90	24	46	45	70	45	10	58
Ba	16	183.7	1233.8	146.7	206.2	95.6	355	356.8	31.2	335.2	222	106.7
Be	0.28	0.53	0.45	0.32	0.47	0.39	0.59	0.57	0.28	0.39	0.68	0.19
Bi	0.47	0.47	0.47	0.47	0.47	0.47	0.47	0.47	0.47	0.47	0.47	0.76

	16SH16	16SH17	16SH19	16SH21	16SH22	16SH23	16SH25	16SH25 SP	16SH26	16SH27	16SH29	16SH32
Cd	0.081	0.013	0.09	0.137	0.073	0.052	0.066	0.053	0.043	0.038	0.021	0.093
Ce	2.7	13.44	4.4	8.7	8.48	26.47	18.92	19.49	7.03	2.67	23.17	5.25
Co	138.25	7.37	87.46	68.38	52.7	13.66	39.63	40.3	111.21	46.39	13.08	4.03
Cr	3641	36	4500	870	623	118	417	419	1314	213	369	347
Cs	0.279	0.625	3.26	0.212	0.945	0.224	0.81	0.808	0.687	1.471	0.785	0.434
Cu	10.9	1.7	13.6	93.1	100.2	2	79	82.7	154.9	153.9	3.9	44.5
Dy	1.395	0.907	2.548	3.006	3.694	1.94	2.847	2.771	2.299	0.728	1.615	0.992
Er	0.869	0.48	1.673	1.857	2.291	1.078	1.633	1.604	1.405	0.491	0.902	0.742
Eu	0.2272	0.3791	0.4366	0.6472	0.7684	0.5836	0.8977	0.8969	0.4874	0.1235	0.543	0.2425
Ga	8.95	9.06	8.48	12.88	17.38	8.7	17.94	17.83	15.65	16.93	14.89	14.11
Gd	1.201	1.142	1.923	2.597	3.061	2.095	2.758	2.751	2	0.557	1.923	0.644
Hf	0.7	1.57	0.66	1.49	1.7	2.71	2.37	2.33	1.33	1.58	2.82	0.67
Ho	0.2954	0.1788	0.5552	0.6326	0.7832	0.3762	0.5802	0.573	0.4738	0.1638	0.3188	0.2265
In	0.0338	0.0104	0.0298	0.0592	0.0691	0.0031	0.0522	0.0531	0.0575	0.0215	0.0081	0.2936
La	1.09	7.01	1.97	3.73	3.44	12.07	8.62	8.93	2.82	0.98	10.57	2.27
Li	51.4	26	11.3	13.7	33.6	22.6	48.9	49.9	73.4	26.8	36.2	2.9
Lu	0.1267	0.0611	0.2467	0.2514	0.3341	0.1489	0.2319	0.2311	0.2022	0.0819	0.1193	0.1312
Mo	0.39	1.1	0.25	0.69	0.37	0.78	1.1	1.04	0.37	0.84	1.2	7.15
Nb	0.704	2.242	0.569	2.083	2.087	3.211	3.018	3.032	1.476	2.105	3.663	1.258
Nd	2.33	6.37	3.71	6.66	6.77	12.13	10.36	10.24	5.1	1.42	11.19	2.39
Ni	3018	35.9	1443.5	303	98.6	46.9	129.5	130.3	503.1	104.3	46.1	22.7
Pb	0.6	0.4	0.3	1.5	0.6	1.2	1.1	1.2	0.4	2.6	1.1	46.7
Pr	0.458	1.66	0.712	1.333	1.36	3.145	2.475	2.451	1.031	0.33	2.786	0.628
Rb	0.28	28.86	8.3	4.05	15.23	3.1	19.56	19.22	1.82	77.29	13.08	34.29
Sb	0.73	0.1	0.06	0.08	0.2	0.04	0.27	0.3	0.13	0.35	0.04	1.29
Sc	22.6	4.5	28	41.8	50.9	8.3	30.6	31.2	39	15	15.8	9.4
Sm	0.805	1.253	1.33	2.038	2.235	2.331	2.542	2.496	1.574	0.433	2.132	0.614
Sn	0.33	0.4	0.27	1.46	0.75	0.19	0.36	0.34	0.43	0.8	0.29	14
Sr	6.7	5.2	55.5	171.2	142.7	165.9	290.6	286.6	83.5	4.5	178.7	3.2
Ta	0.045	0.165	0.041	0.117	0.137	0.312	0.225	0.221	0.092	0.158	0.278	0.095
Tb	0.2046	0.1579	0.362	0.4432	0.5479	0.3185	0.4362	0.4352	0.348	0.1088	0.2714	0.1286
Th	0.16	1.182	0.14	0.334	0.326	2.373	1.342	1.344	0.18	0.338	1.918	1.093
Ti	2180	1150	2046	4806	5487	1618	4309	4413	4605	3942	3279	722
Tl	0.061	0.159	0.268	0.092	0.078	0.019	0.123	0.126	0.026	0.579	0.081	0.439
Tm	0.1332	0.0675	0.2453	0.2646	0.3364	0.1529	0.2334	0.2277	0.1971	0.0774	0.122	0.1176
U	0.04	0.452	0.047	0.143	0.081	0.686	0.36	0.351	0.066	0.245	0.462	0.433
V		30.1		262	311.7	44.8	196.8	200.9	290.3	164	105.6	43.3
W	0.05	0.25	0.05	0.24	0.15	0.2	0.25	0.25	0.22	0.64	0.36	0.1
Y	7.41	5.16	15.63	16.4	21.08	11.09	15.59	15.32	11.45	3.9	9.19	5.5
Yb	0.872	0.44	1.656	1.686	2.241	0.943	1.537	1.552	1.387	0.526	0.792	0.856
Zn	156	34	78	89	90	23	44	43	70	43	8	59
Zr	24	65	22	50	60	108	89	89	45	58	107	28

	16SH34	16SH35	16SH36	16SH37	BT-15-SH-049	BT-15-SH-052	BT-15-SH-054	BT-15-SH-055	BT-15-SH-056	BT-15-SH-059
Al ₂ O ₃ (wt.%)	6.85	14.49	15.61	10.97	11.48	11.17	13.79	12.29	14.23	12.67
BaO	0.004	0.01	0.02	0.004	0.08	0.03	0.05	0.04	0.02	0.01
CaO	6.595	6.526	4.613	5.013	7.92	6.71	8.73	7.58	7.96	5.83
Cr ₂ O ₃	0.27	0.01	0.01	0.08	0.17	0.11	0.01	0.08	0.01	0.05
Fe ₂ O ₃	12.81	9.08	10.7	17.41	9.22	14.75	10.66	7.36	10.38	10.41
K ₂ O	0.02	0.07	0.77	0.02	0.63	0.43	0.54	0.68	0.53	0.11
LOI	6.89	7.21	6.24	6.81	6.18	8.61	5.62	9.51	5.06	7.69
MgO	21.26	4.74	5.05	11.4	8.8	6.98	6.88	8.62	6.85	8.31
MnO	0.229	0.231	0.335	0.348	0.29	0.48	0.28	0.13	0.26	0.26
Na ₂ O	0.14	4.6	3.78	0.14	1.59	0.89	2.2	2.88	2.07	2.71
P ₂ O ₅	0.039	0.068	0.075	0.045	0.05	0.04	0.06	0.67	0.07	0.06
SiO ₂	44.33	50.71	50.27	46.27	53.39	49.83	50.27	48.8	51.29	50.86
TiO ₂	0.47	0.85	0.92	0.73	0.68	0.66	0.8	0.71	0.83	0.71
Total	99.91	98.58	98.4	99.25	100.46	100.69	99.88	99.34	99.56	99.66
Al (ppm)	37425	75521	68981	58863	58349	55804	68983	63315	71638	64014
Ba	11	39	141	19	689	274	445	397	208	59
Be	1	1	1	1	1	1	1	2	1	1
Ca	46678	45217	31944	35130	56322	48333	61791	55135	57159	41705
Cd	1	1	1	1	1	1	1	1	1	1
Co	74	56	57	61	55	64	41	29	44	42
Cr	1300	84	97	571	1096	724	87	503	81	309
Cu	23	125	90	35	87	97	122	34	129	105
Fe	87901	60681	70971	95000	60793	95000	70191	50340	69262	69002
K	121	496	6241	70	5334	3426	4525	5831	4403	941
Li	16	24	26	34	58	64	44	37	39	40
Mg	124589	27044	23715	66483	51653	41036	40073	51653	40237	48639
Mn	1756	1710	2438	2647	2104	3633	2063	1043	1931	1907
Mo	1	1	1	1	1	1	1	1	1	1
Na	1128	31000	25873	892	11216	5993	14712	19580	13877	18156
Ni	468	230	75	144	169	178	70	255	74	82
P	175	293	319	195	207	180	269	2962	308	244
Pb	15	15	15	15	15	15	16	28	15	15
S	130	3308	7456	130	130	130	130	147	387	554
Sc	27	36	36	47	43	38	35	17	36	37
Sr	8	106	90	9	158	79	214	376	175	142
Ti	2820	5019	5439	4366	4067	3869	4683	4299	4914	4163
V	170	250	293	291	263	240	253	135	261	244
W	6	6	6	6	6	6	6	6	6	6
Y	10	15	17	17	12	16	15	27	16	13
Zn	103	101	191	572	73	92	78	89	94	119
Ba	9.1	42.4	206.5	18.7	741.9	287.1	508.6	414.8	217.9	64.8
Be	0.28	0.35	0.45	0.52	0.31	0.35	0.35	2.43	0.34	0.44
Bi	0.47	0.47	0.47	0.47	0.47	0.47	0.47	0.47	0.47	0.47

	16SH34	16SH35	16SH36	16SH37	BT-15-SH-049	BT-15-SH-052	BT-15-SH-054	BT-15-SH-055	BT-15-SH-056	BT-15-SH-059
Cd	0.089	0.091	0.206	1.162	0.101	0.085	0.114	0.131	0.136	0.192
Ce	6.09	8.07	9.4	4.52	5.14	6.99	7.89	179.37	7.86	6.89
Co	82.56	66.41	66.82	67.19	63.8	75.44	50.22	34.94	53.6	50.8
Cr	1858	86	104	578	1205	810	97	543	90	343
Cs	0.205	0.115	0.479	0.15	0.546	0.562	0.702	0.625	0.611	0.606
Cu	20.6	124.3	86.1	26.4	83.7	97.9	119.2	30.4	127.7	104.5
Dy	1.749	2.988	3.417	3.101	2.392	2.933	3.081	6.411	3.228	2.685
Er	0.997	1.713	1.943	1.972	1.449	1.852	1.894	2.441	1.97	1.64
Eu	0.4635	0.8938	0.5684	0.5177	0.6962	0.7716	0.7677	4.2214	0.736	0.6876
Ga	8.59	15.49	16.93	17.03	13.48	12.24	14.98	15.87	15.8	13.64
Gd	1.631	2.624	2.976	2.333	2.039	2.504	2.62	11.972	2.79	2.285
Hf	0.89	1.56	1.69	1.34	1.21	1.2	1.52	6.09	1.54	1.33
Ho	0.3498	0.5943	0.6778	0.6641	0.495	0.6283	0.642	1.0087	0.6614	0.5394
In	0.0397	0.0663	0.0715	0.1086	0.0498	0.0558	0.0583	0.0477	0.0604	0.0579
La	2.57	2.97	3.68	1.67	1.97	3.01	3.03	80.04	3.19	2.52
Li	12.8	23.8	25.6	33.4	57.3	63.8	41.9	34.8	35.2	38.8
Lu	0.121	0.2255	0.2527	0.3137	0.1865	0.2757	0.2533	0.2677	0.2739	0.2206
Mo	0.12	0.37	0.4	0.25	0.46	0.67	0.36	0.25	0.37	0.34
Nb	1.067	1.941	1.966	1.414	1.411	1.391	1.761	7.616	1.892	1.582
Nd	4.42	6.44	7.15	4.13	4.42	5.47	6.47	95.9	6.48	5.33
Ni	500.7	256.8	83.2	150.7	193	204.8	82.1	282.8	84.4	95.8
Pb	0.4	1.2	1.3	2.1	0.8	1.2	1	11.1	0.8	1.7
Pr	0.878	1.264	1.419	0.774	0.845	1.079	1.217	23.154	1.259	1.039
Rb	0.53	1.03	27.33	0.49	16.28	9.97	13.14	11.56	12.82	3.03
Sb	0.2	0.16	0.13	0.68	0.19	0.07	0.15	0.2	0.47	0.17
Sc	24.3	40.4	44.5	48.9	48.7	42.8	38.7	18.8	39.9	41.1
Sm	1.3	2.041	2.288	1.607	1.515	1.837	2.028	17.394	2.067	1.731
Sn	0.48	0.87	1.66	2.27	0.36	0.51	0.69	1.33	0.63	0.61
Sr	10.3	105.9	95.1	10.7	161.9	82.9	217.1	378.8	173.5	143.3
Ta	0.066	0.118	0.125	0.093	0.084	0.089	0.111	0.365	0.117	0.098
Tb	0.2696	0.4403	0.5196	0.4291	0.3554	0.4283	0.4555	1.3111	0.4627	0.3936
Th	0.194	0.301	0.361	0.238	0.212	0.221	0.276	8.87	0.32	0.233
Ti	2848	5164	5544	4350	4200	4087	4838	4413	5024	4322
Tl	0.011	0.04	0.496	0.008	0.175	0.12	0.151	0.166	0.117	0.041
Tm	0.1385	0.2304	0.278	0.2986	0.2034	0.2716	0.2668	0.3099	0.279	0.2355
U	0.061	0.084	0.089	0.066	0.063	0.061	0.079	2.06	0.091	0.073
V		253.6	299.7	285.7	257.6	240.9	261.7	128.4	267.3	249.9
W	0.05	0.2	0.33	0.35	0.12	0.09	0.1	0.4	0.1	0.1
Y	9.4	15.71	18	16.98	13.12	17.76	17.24	29.4	17.78	14.83
Yb	0.855	1.532	1.753	2.042	1.307	1.83	1.754	1.865	1.775	1.504
Zn	111	105	211	563	78	103	86	94	101	127
Zr	31	56	60	46	44	43	53	260	57	47

	BT-15-SH-061	BT-15-SH-063	BT-15-SH-065	BT-15-SH-067	BT-15-SH-068	BT-15-SH-069	BT-15-SH-070	BT-15-SH-073
Al ₂ O ₃ (wt.%)	14.19	14.79	14.8	14.41	16.29	15.7	12.66	16.77
BaO	0.02	0.004	0.02	0.02	0.09	0.05	0.03	0.04
CaO	3.61	5.99	7.17	7.84	1.46	1.16	5.00	4.76
Cr ₂ O ₃	0.08	0.01	0.01	0.04	0.07	0.06	0.07	0.06
Fe ₂ O ₃	10.92	9.14	10.33	10.04	3.54	4.07	10.84	8.21
K ₂ O	0.82	0.11	0.44	0.33	2.86	1.33	0.54	0.87
LOI	6.45	7.47	5.45	4.48	3.51	2.81	7.52	5.39
MgO	8.48	5.28	6.45	7.93	2.22	2.33	10.57	8.25
MnO	0.25	0.24	0.22	0.21	0.09	0.09	0.20	0.19
Na ₂ O	1.72	4.41	1.78	1.84	2.81	4.55	1.78	2.52
P ₂ O ₅	0.08	0.07	0.07	0.07	0.12	0.12	0.06	0.06
SiO ₂	52.25	51.38	51.96	52.44	67.21	67.42	49.94	52.09
TiO ₂	0.89	0.85	0.86	0.84	0.5	0.49	0.75	0.74
Total	99.74	99.74	99.57	100.47	100.77	100.16	99.95	99.95
Al (ppm)	64514	71292	77158	72127	78790	73801	60443	84479
Ba	183	46	162	149	781	413	246	346
Be	1	1	1	1	1	1	1	1
Ca	25388	41889	53108	55231	10358	8257	34555	34052
Cd	1	1	1	1	1	1	1	1
Co	50	56	42	44	10	15	53	42
Cr	468	80	72	232	421	331	449	352
Cu	119	140	130	116	15	30	160	111
Fe	71258	59821	71133	65758	23026	26739	69210	54409
K	6806	892	3863	2767	23054	10921	4791	7426
Li	54	26	36	33	20	22	76	71
Mg	43291	29368	39475	45732	12778	12217	56366	48414
Mn	1776	1753	1700	1485	623	589	1500	1427
Mo	1	1	1	1	1	1	1	1
Na	11639	27870	12579	12629	17576	28729	12361	16783
Ni	110	150	81	85	31	53	108	142
P	324	290	313	295	513	499	253	285
Pb	15	15	15	21	18	16	21	17
S	276	668	130	130	130	130	402	241
Sc	36	34	39	39	8	7	38	36
Sr	121	110	152	131	88	150	179	232
Ti	5239	4991	5272	4866	2925	2912	4491	4447
V	284	253	285	271	66	64	252	238
W	6	6	6	6	6	6	6	6
Y	12	14	15	13	10	9	13	15
Zn	110	98	100	91	43	45	85	100
Ba	202	50.3	166.8	156.9	860.5	444.7	265.1	356.8
Be	0.65	0.36	0.56	0.61	0.76	0.91	0.63	0.3
Bi	0.47	0.47	0.47	0.47	0.47	0.47	0.47	0.47

	BT-15-SH-061	BT-15-SH-063	BT-15-SH-065	BT-15-SH-067	BT-15-SH-068	BT-15-SH-069	BT-15-SH-070	BT-15-SH-073
Cd	0.113	0.113	0.113	0.15	0.032	0.054	0.181	0.176
Ce	7.74	7.74	7.87	8.56	30.67	24.09	9.34	9.2
Co	61.34	67.17	49.94	54.52	12.41	18.71	62.45	49.31
Cr	529	89	81	263	480	377	499	388
Cs	0.948	0.148	0.609	0.608	1.481	0.725	0.862	1.43
Cu	119.3	139.4	126.1	117.7	12.8	29.7	160.2	109
Dy	2.58	2.793	2.849	2.768	2.111	1.873	2.538	2.767
Er	1.559	1.643	1.718	1.593	1.097	1.004	1.557	1.727
Eu	0.9135	0.7449	0.8009	0.7784	0.738	0.6563	0.6501	0.6486
Ga	16.34	16.21	17.05	16.07	19.25	16.54	14.43	16
Gd	2.325	2.606	2.573	2.463	2.361	2.166	2.279	2.455
Hf	1.84	1.61	1.61	1.69	3.53	3.31	1.41	1.54
Ho	0.5156	0.5678	0.5672	0.5533	0.3856	0.3538	0.5295	0.5608
In	0.0668	0.0692	0.0662	0.0641	0.0226	0.0214	0.0566	0.0571
La	3.08	3.22	3.03	3.32	14.81	10.84	3.85	3.8
Li	55.7	25.5	34.3	31.4	20.4	22.6	73.7	69.7
Lu	0.2036	0.2273	0.2181	0.2148	0.1452	0.1234	0.2253	0.2477
Mo	0.49	0.47	0.4	0.59	0.49	0.69	0.43	0.45
Nb	2.191	1.953	2.036	1.963	4.511	4.42	1.807	2.016
Nd	6.17	6.46	6.42	6.66	14.03	12.04	6.05	6.46
Ni	127.1	176	92.4	99.7	37.5	63	120.7	163.1
Pb	2.5	0.9	1.5	3.1	1.8	3.3	7.2	1.6
Pr	1.211	1.257	1.257	1.325	3.651	2.961	1.273	1.338
Rb	24.91	2.2	11.88	8.85	78.99	29.18	15.07	22.71
Sb	0.11	0.11	0.26	0.51	0.11	0.16	0.71	0.13
Sc	41.4	38.5	42.4	44.7	9.8	8.7	42.6	38.9
Sm	1.908	2.025	2.074	1.98	2.713	2.435	1.827	1.902
Sn	0.87	0.86	0.61	0.62	0.66	0.54	0.62	0.59
Sr	124.1	110.6	160.3	140.9	88.4	156.2	183.8	238
Ta	0.138	0.119	0.119	0.121	0.35	0.329	0.109	0.128
Tb	0.3916	0.4394	0.4229	0.4191	0.3488	0.3161	0.3899	0.418
Th	0.374	0.291	0.306	0.365	2.672	2.406	0.359	0.422
Ti	5520	5174	5401	5100	3063	3043	4589	4489
Tl	0.212	0.051	0.13	0.098	0.394	0.2	0.14	0.114
Tm	0.2132	0.2312	0.2326	0.232	0.1478	0.1396	0.2342	0.243
U	0.107	0.081	0.091	0.1	0.686	0.699	0.101	0.119
V	293.8	260.8	292.8	284.5	63.7	61.5	254.8	235.2
W	0.12	0.19	0.1	0.07	0.35	0.51	0.24	0.2
Y	13.38	15.16	15.62	14.74	11.52	10.39	14.08	15.9
Yb	1.438	1.509	1.493	1.449	0.942	0.867	1.481	1.664
Zn	121	107	106	101	47	49	91	106
Zr	67	58	60	61	142	134	50	54

	BT-15-SH-074	BT-15-SH-075	BT-15-SH-076	BT-15-SH-077	BT-15-SH-077 SP	DW-15-SH-081	DW-15-SH-086	DW-15-SH-087
Al ₂ O ₃ (wt.%)	14.03	15.6	12	14.1	13.98	11.69	10.43	12.6
BaO	0.02	0.02	0.004	0.03	0.02	0.01	0.004	0.004
CaO	7.33	10.16	5.46	8.20	8.32	7.27	12.05	9.30
Cr ₂ O ₃	0.19	0.08	0.44	0.01	0.01	0.06	0.15	0.14
Fe ₂ O ₃	9.21	7	10.16	13.77	13.54	9.02	9.69	9.98
K ₂ O	0.4	0.51	0.03	0.69	0.67	0.69	0.04	0.1
LOI	8.79	7.22	7.4	3.15	3.11	13.69	12.57	5.73
MgO	6.52	6.23	7.26	7.19	7.15	7.05	7.07	9.58
MnO	0.27	0.21	0.30	0.23	0.22	0.17	0.25	0.26
Na ₂ O	2.74	2.12	2.08	2.52	2.56	1.36	1.89	1.74
P ₂ O ₅	0.06	0.07	0.06	0.06	0.06	0.05	0.04	0.05
SiO ₂	49.75	49.91	53.67	49.6	49.55	48.12	44.96	50.17
TiO ₂	0.62	0.84	0.68	0.81	0.82	0.66	0.58	0.71
Total	99.92	99.97	99.56	100.33	100	99.85	99.73	100.37
Al (ppm)	71338	76589	60577	72423	70230	58175	55182	64271
Ba	203	202	28	228	221	97	26	53
Be	1	1	1	1	1	1	1	1
Ca	53041	65120	38943	59661	58862	51151	82006	60746
Cd	1	1	1	1	1	1	1	1
Co	58	42	127	43	42	44	66	62
Cr	1196	517	1300	77	75	402	965	882
Cu	97	76	87	72	72	103	97	111
Fe	61871	45471	67246	89212	89815	59058	67064	66012
K	3412	4241	257	5890	5609	5776	297	839
Li	31	30	33	39	38	50	43	51
Mg	38405	35637	42588	41608	41842	40622	43233	56520
Mn	2014	1562	2286	1704	1708	1261	1961	1994
Mo	1	1	1	1	1	1	1	1
Na	18474	14003	13909	17108	17085	9460	13655	11964
Ni	381	131	1089	66	65	92	469	305
P	246	309	257	243	251	218	194	230
Pb	20	19	17	15	15	15	15	16
S	1352	1795	2899	130	130	1657	1951	442
Sc	39	42	39	39	38	36	35	39
Sr	87	146	75	190	180	77	72	82
Ti	3759	4957	4056	4957	4817	3885	3584	4237
V	248	276	245	281	278	235	221	248
W	6	6	6	6	6	6	6	6
Y	13	19	16	14	14	13	13	12
Zn	99	64	132	54	53	60	76	63
Ba	217.2	221.3	31.5	248.6	238.1	103.8	27.8	57.4
Be	0.19	0.4	0.3	0.27	0.31	0.46	0.32	0.47
Bi	0.47	0.47	0.47	0.47	0.47	0.47	0.47	0.47

	BT-15-SH-074	BT-15-SH-075	BT-15-SH-076	BT-15-SH-077	BT-15-SH-077 SP	DW-15-SH-081	DW-15-SH-086	DW-15-SH-087
Cd	0.082	0.048	0.159	0.055	0.062	0.077	0.082	0.064
Ce	7.37	8.09	7.84	6.13	6.23	6.3	5.23	5.77
Co	65.93	51.71	146.77	50.84	51.06	51.56	74.74	73.78
Cr	1297	580	3128	84	85	441	1036	977
Cs	0.482	0.795	0.13	0.838	0.838	0.45	0.698	0.361
Cu	92.5	74	84	67.8	68.5	102.1	90.6	105.8
Dy	2.49	3.528	3.056	2.807	2.853	2.582	2.489	2.502
Er	1.615	2.265	1.959	1.76	1.754	1.589	1.515	1.501
Eu	0.5313	0.75	0.638	0.7379	0.7335	0.6094	0.5508	0.6966
Ga	14.81	15.66	12.96	16.06	15.64	13.18	11.15	13.65
Gd	2.183	2.9	2.522	2.317	2.343	2.199	2.067	2.302
Hf	1.27	1.72	1.34	1.32	1.34	1.17	1.05	1.25
Ho	0.5253	0.747	0.6525	0.5781	0.5837	0.5196	0.5144	0.5084
In	0.0542	0.0603	0.0623	0.0583	0.0582	0.0448	0.0451	0.0566
La	3.41	3.5	3.07	2.26	2.26	2.38	1.92	2.2
Li	28.1	27.7	30.9	35.9	36.4	49.8	37.7	49.4
Lu	0.2216	0.3223	0.293	0.249	0.2481	0.2176	0.207	0.2044
Mo	0.34	0.27	0.57	0.29	0.26	0.21	0.26	0.25
Nb	1.335	1.973	1.618	1.543	1.511	1.312	1.111	1.374
Nd	5.6	6.55	5.96	5.11	5.16	4.79	4.34	4.82
Ni	421.9	154	1225.8	74.5	73.1	106.4	514.5	344.2
Pb	0.8	0.7	1	0.5	0.4	1	0.8	5.8
Pr	1.129	1.317	1.175	0.954	0.979	0.962	0.812	0.949
Rb	9	14.22	0.63	15.66	14.99	16.58	1.23	2.12
Sb	0.08	0.09	0.11	0.1	0.09	0.85	0.86	1.16
Sc	41.8	47.1	41.8	41.6	41.7	40.4	37	42.5
Sm	1.657	2.192	1.885	1.737	1.725	1.619	1.482	1.675
Sn	0.55	0.66	0.64	0.36	0.34	0.44	0.43	5.42
Sr	90.5	150.8	76.2	191.1	185.9	79.9	74.6	86.5
Ta	0.081	0.13	0.103	0.096	0.092	0.077	0.068	0.087
Tb	0.3783	0.509	0.4509	0.404	0.4146	0.3874	0.353	0.3741
Th	0.334	0.31	0.301	0.2	0.212	0.205	0.176	0.199
Ti	3792	5157	4112	5012	4931	4007	3528	4335
Tl	0.109	0.072	0.053	0.071	0.065	0.131	0.021	0.034
Tm	0.2281	0.324	0.2949	0.2504	0.2492	0.2223	0.2137	0.2175
U	0.105	0.087	0.105	0.06	0.057	0.067	0.041	0.058
V	234.5	283.5		283.8	284.2	237.7	208.7	245.6
W	0.07	0.15	0.53	0.05	0.05	0.65	0.08	0.22
Y	14.29	20.74	17.44	15.74	15.82	14.3	13.82	13.93
Yb	1.515	2.163	1.93	1.604	1.665	1.46	1.435	1.404
Zn	103	69	140	59	59	66	79	70
Zr	43	61	46	45	46	42	37	43

	DW-15-SH-090	FW-15-SH-001	FW-15-SH-002	FW-15-SH-003	FW-15-SH-004	FW-15-SH-005	FW-15-SH-006	FW-15-SH-009
Al ₂ O ₃ (wt.%)	11.2	13.58	12.84	11.16	2.68	6.32	12.59	11.29
BaO	0.004	0.004	0.02	0.004	0.004	0.01	0.01	0.02
CaO	12.08	3.81	7.13	4.93	0.38	6.36	4.49	16.31
Cr ₂ O ₃	0.16	0.12	0.06	0.09	0.02	0.75	0.2	0.23
Fe ₂ O ₃	9.97	9.4	8.46	12.35	1.43	12.04	9.65	9.02
K ₂ O	0.02	0.22	0.82	0.17	0.02	0.35	0.23	0.01
LOI	13.46	9.93	12.48	11.6	1.44	16.58	8.97	8.64
MgO	7.17	9.99	5.3	11.16	0.19	11.59	8.72	8.62
MnO	0.26	0.26	0.20	0.20	0.02	0.32	0.21	0.39
Na ₂ O	1.42	1.66	3.51	1.17	0.66	0.18	2.19	0.63
P ₂ O ₅	0.05	0.05	0.27	0.04	0.01	0.02	0.07	0.24
SiO ₂	43.86	50.17	47.1	46.13	93.81	43.29	49.68	43.27
TiO ₂	0.63	0.74	0.75	0.62	0.05	0.33	0.64	0.69
Total	100.29	99.92	98.94	99.61	100.69	98.14	97.64	99.36
Al (ppm)	57380	62733	64194	56619	13533	31448	61444	58142
Ba	15	59	151	39	7	61	66	207
Be	1	1	1	1	1	1	1	1
Ca	79071	27118	50696	35006	2661	45206	32000	100000
Cd	1	1	1	1	1	14	1	1
Co	73	57	28	52	9	147	73	43
Cr	1048	713	351	561	89	1300	1250	1300
Cu	106	96	105	85	36	74	91	62
Fe	67129	61924	56462	82148	9673	79466	63562	61183
K	231	1804	6843	1417	180	2973	1961	169
Li	78	68	31	46	1	42	62	46
Mg	42352	52959	30749	65389	975	66891	49490	51134
Mn	2011	1857	1471	1469	50	2421	1555	2984
Mo	1	1	1	1	6	1	1	1
Na	9950	11099	22817	8117	4837	1439	14567	4715
Ni	401	216	64	161	45	1167	675	263
P	202	234	1146	186	35	104	291	1044
Pb	15	15	15	15	15	16	18	16
S	684	3135	5616	3594	6209	8164	14220	2946
Sc	37	37	25	35	2	22	33	21
Sr	56	126	289	127	14	289	160	85
Ti	3769	4433	4420	3690	232	1925	3778	4067
V	233	265	192	226	10	141	216	185
W	6	6	6	6	6	6	6	6
Y	12	13	14	10	2	8	12	14
Zn	79	123	76	149	356	174	143	111
Ba	16.1	62.6	158.3	41.4	6.6	66.8	71.6	217.7
Be	0.32	0.62	1.22	0.49	0.14	0.58	0.55	0.71
Bi	0.47	0.47	0.47	0.47	0.47	0.47	0.47	0.47

	DW-15-SH-090	FW-15-SH-001	FW-15-SH-002	FW-15-SH-003	FW-15-SH-004	FW-15-SH-005	FW-15-SH-006	FW-15-SH-009
Cd	0.058	0.075	0.112	0.196	0.731	0.063	0.101	0.224
Ce	4.78	7.66	36.33	4.21	5.27	3.17	11.16	32.31
Co	85.92	65.95	34.52	60.81	9.11	168.77	84.21	51.45
Cr	1166	793	397	607	96	4500	1378	1651
Cs	0.162	0.618	0.642	0.48	0.042	0.547	0.435	0.188
Cu	103.4	93.8	105.8	83.9	37.1	75.2	89	60.4
Dy	2.262	2.655	2.959	1.933	0.39	1.391	2.263	2.721
Er	1.569	1.669	1.62	1.296	0.221	0.862	1.372	1.501
Eu	0.3752	0.6697	1.1441	0.4409	0.1311	0.4155	0.7975	1.177
Ga	12.87	15.65	16.63	12.75	1.74	12	14.99	13.49
Gd	1.839	2.186	3.887	1.693	0.436	1.158	2.196	3.486
Hf	1.11	1.25	1.91	1.01	0.3	0.57	1.4	1.89
Ho	0.5043	0.5519	0.562	0.4109	0.0754	0.2846	0.474	0.5175
In	0.0453	0.061	0.0475	0.0484	0.0699	0.0431	0.0549	0.0658
La	1.74	3.4	16.1	1.48	2.18	1.29	4.66	14.72
Li	76.3	67.3	28.9	44.9	1.2	44.5	64.3	40.5
Lu	0.2155	0.2377	0.2191	0.1782	0.0325	0.1216	0.1863	0.211
Mo	0.21	0.43	0.68	0.19	5.74	0.73	0.74	0.86
Nb	1.185	1.412	3.156	1.155	0.547	0.689	1.629	2.763
Nd	3.88	5.31	22.25	3.53	2.58	2.62	7.14	19.77
Ni	457.5	243	75.7	178.7	50.3	1311.1	750.2	296.2
Pb	0.9	3.8	3.3	1.7	2.1	3.8	4.3	9.2
Pr	0.771	1.108	5.094	0.714	0.617	0.51	1.558	4.645
Rb	0.66	5.14	21.68	4.85	0.45	13.15	5.73	0.55
Sb	1.24	0.79	2.26	1.24	0.99	16.8	1.38	3.52
Sc	40.6	43.3	27.8	39.4	2.2	25.6	37.1	24.7
Sm	1.346	1.68	4.59	1.196	0.494	0.88	1.834	4.072
Sn	0.42	2.37	0.45	0.43	0.22	0.72	1.29	1.41
Sr	57.5	128.8	310.3	127.8	14	302.7	167	89.1
Ta	0.075	0.088	0.162	0.067	0.034	0.035	0.098	0.149
Tb	0.3353	0.3828	0.5257	0.3002	0.0652	0.1988	0.3493	0.4874
Th	0.173	0.202	1.599	0.181	0.463	0.118	0.428	1.523
Ti	3884	4470	4554	3759	223	2031	3899	4189
Tl	0.015	0.056	0.142	0.068	0.013	0.11	0.072	0.03
Tm	0.219	0.2409	0.2207	0.1917	0.0321	0.1214	0.1977	0.2115
U	0.104	0.063	0.423	0.045	0.166	0.047	0.187	0.39
V	228.6	261.9	195.9	224.5	6		190.5	
W	0.8	0.73	5.5	0.56	0.15	3.42	0.7	2.3
Y	13.26	14.44	15.96	11.19	2.02	8.45	12.89	15.12
Yb	1.499	1.579	1.457	1.191	0.204	0.82	1.287	1.403
Zn	85	129	84	153	354	184	147	116
Zr	38	43	75	35	12	22	51	71

	FW-15-SH-009 SP	FW-15-SH-013	FW-15-SH-017	FW-15-SH-021	LM-15-SH-023	LM-15-SH-024	LM-15-SH-028	LM-15-SH-032
Al ₂ O ₃ (wt.%)	11.06	13.07	13.1	11.42	12.2	8.96	8.03	12.32
BaO	0.02	0.01	0.02	0.01	0.09	0.07	0.03	0.05
CaO	16.45	5.37	5.10	4.46	0.81	0.547	0.09	1.26
Cr ₂ O ₃	0.23	0.15	0.12	0.09	0.01	0.01	0.002	0.06
Fe ₂ O ₃	9.04	9.1	8.8	11.79	2.03	5.62	3.59	2.85
K ₂ O	0.02	0.5	0.45	0.19	3.98	3.12	1.4	2.52
LOI	8.65	11.5	12.64	9.54	3.32	2.49	2.52	4.11
MgO	8.61	8.05	8.36	10.02	4.07	2.75	2.87	4.3
MnO	0.39	0.24	0.17	0.24	0.05	0.057	0.03	0.06
Na ₂ O	0.63	1.57	3.48	1.29	0.93	0.61	0.02	1.82
P ₂ O ₅	0.25	0.05	0.05	0.04	0.10	0.066	0.04	0.10
SiO ₂	43.4	48.4	44.95	48.6	72.74	75.36	81.94	70.36
TiO ₂	0.69	0.71	0.72	0.64	0.45	0.24	0.25	0.41
Total	99.43	98.71	97.96	98.32	100.79	99.89	100.81	100.21
Al (ppm)	53144	65625	66201	55872	49963	46694	39498	42934
Ba	184	98	116	39	620	585	237	261
Be	1	1	1	1	1	1	1	1
Ca	100000	38529	36867	31135	5634	4041	572	8508
Cd	1	1	1	1	1	1	1	1
Co	40	58	55	50	3	10	7	9
Cr	1300	899	781	539	29	48	20	360
Cu	56	128	96	72	6	6	6	6
Fe	57308	60322	58981	76588	13218	40010	23698	17644
K	116	4131	3774	1557	31758	25048	11498	20261
Li	42	62	39	57	31	28	41	33
Mg	47721	47249	49380	56954	19052	16730	16653	16267
Mn	2777	1798	1256	1743	287	431	128	340
Mo	1	1	1	1	1	1	1	2
Na	4441	10668	23061	8825	6393	3992	500	11702
Ni	246	253	170	163	62	29	19	116
P	974	227	236	193	420	283	185	415
Pb	15	15	18	15	15	15	15	15
S	2817	5450	9029	10671	130	130	130	130
Sc	20	41	41	34	3	3	4	2
Sr	79	166	236	92	30	18	7	56
Ti	3788	4225	4337	3703	2615	1466	1476	2402
V	172	258	262	229	52	30	36	61
W	6	6	6	6	6	6	6	6
Y	13	15	11	12	3	3	5	3
Zn	102	126	87	468	13	23	22	20
Ba	211.3	105.6	123.8	42.1	691	618.4	253.5	283
Be	0.7	0.8	0.6	0.48	0.69	0.46	0.6	0.57
Bi	0.47	0.47	0.47	0.47	0.47	0.47	0.47	0.47

	FW-15-SH-009 SP	FW-15-SH-013	FW-15-SH-017	FW-15-SH-021	LM-15-SH-023	LM-15-SH-024	LM-15-SH-028	LM-15-SH-032
Cd	0.226	0.123	0.066	0.889	0.041	0.02	0.029	0.048
Ce	31.78	7.79	7.78	4.88	4.16	24.29	16.03	14.21
Co	51.8	68.96	64.36	58.23	4.49	12.33	9.16	12.15
Cr	1654	1019	852	591	31	42	22	405
Cs	0.186	0.649	0.447	0.488	1.642	0.378	0.661	1.91
Cu	59.6	129.1	93	69.2	1.4	1.6	1.4	4.1
Dy	2.72	2.837	2.314	2.318	0.425	0.854	1.01	0.722
Er	1.481	1.751	1.418	1.404	0.282	0.421	0.581	0.432
Eu	1.1791	0.6932	0.5463	0.4678	0.1865	0.4354	0.3532	0.3449
Ga	13.34	16.06	15.73	12.54	9.42	12.58	10.53	12.68
Gd	3.541	2.516	2.059	1.978	0.431	1.167	1.194	0.942
Hf	1.87	1.24	1.31	1.08	2.24	1.88	1.8	2.51
Ho	0.5313	0.5875	0.4735	0.4836	0.0907	0.1518	0.1915	0.1451
In	0.0678	0.0724	0.0511	0.1283	0.0024	0.0139	0.0137	0.0169
La	14.81	3.63	3.14	1.85	2.05	12.52	7.95	6.88
Li	40.5	66.2	39.5	59.1	33.6	30.3	40.8	34
Lu	0.2141	0.2474	0.1926	0.2073	0.0456	0.0511	0.0853	0.0605
Mo	0.8	0.39	0.38	0.3	0.44	1.75	0.55	1.71
Nb	2.8	1.431	1.432	1.228	3.279	2.188	2.491	3.546
Nd	19.64	5.86	5.54	4.09	2.01	9.69	7.24	6.84
Ni	297.8	295.1	192.8	187.4	71.6	26.7	24	135.4
Pb	9.2	1.8	2.6	2.8	0.8	0.5	1	1.4
Pr	4.561	1.205	1.133	0.778	0.528	2.638	1.906	1.684
Rb	0.5	13.43	12.3	5.34	62.16	34.25	26.8	56.55
Sb	3.73	0.54	1.35	1.03	0.14	0.08	0.13	0.18
Sc	24.5	45.8	44.6	38.2	4.4	4	5.1	3.3
Sm	4.207	1.832	1.602	1.401	0.429	1.548	1.36	1.177
Sn	1.47	1.83	1.52	0.8	0.29	0.72	0.35	0.38
Sr	90.2	176.9	244.1	95.4	29.4	18.7	7.2	58.1
Ta	0.148	0.085	0.089	0.072	0.231	0.193	0.184	0.265
Tb	0.4718	0.4123	0.3403	0.344	0.0619	0.1478	0.166	0.1219
Th	1.549	0.233	0.21	0.173	0.961	1.647	1.273	1.755
Ti	4157	4495	4439	3826	2699	1416	1493	2483
Tl	0.03	0.12	0.132	0.066	0.379	0.395	0.121	0.322
Tm	0.2145	0.2523	0.2013	0.2127	0.0412	0.0548	0.0823	0.0589
U	0.395	0.082	0.07	0.052	0.363	0.497	0.372	0.535
V		251.7	253.8	221.7	55.4	31.9	37.1	53.2
W	2.21	1.39	1.64	0.55	0.72	0.24	0.34	0.71
Y	15.12	16.71	12.28	13.31	2.86	3.96	5.76	4.06
Yb	1.388	1.594	1.329	1.361	0.301	0.346	0.537	0.424
Zn	115	135	92	482	15	21	23	22
Zr	72	44	46	38	90	74	74	103

	LM-15-SH-033	LM-15-SH-034	LM-15-SH-035	LM-15-SH-037	LM-15-SH-039	LM-15-SH-040	LM-15-SH-041	LM-15-SH-042
Al ₂ O ₃ (wt.%)	2.98	2.34	13.9	8.32	3.63	2.63	4.19	6.45
BaO	0.004	0.004	0.02	0.004	0.004	0.004	0.004	0.004
CaO	2.93	2.273	2.11	3.04	2.71	0.698	12.20	4.34
Cr ₂ O ₃	0.6	0.31	0.12	0.86	0.34	0.49	0.33	0.51
Fe ₂ O ₃	9.77	10.16	12.15	9.63	10.56	10.54	19.93	21.64
K ₂ O	0.01	0.01	0.27	0.02	0.01	0.02	0.61	0.63
LOI	10.67	8.94	7.33	6.86	8.45	8.3	15.27	10.29
MgO	27.62	27.19	16.93	15.51	25.2	27.46	10.5	13.33
MnO	0.13	0.107	0.21	0.25	0.10	0.077	0.95	0.62
Na ₂ O	0.02	0.04	1.62	0.07	0.02	0.05	0.02	0.02
P ₂ O ₅	0.01	0.012	0.09	0.03	0.01	0.012	0.02	0.03
SiO ₂	44.39	47.92	44.58	54.58	48.58	48.89	35.07	41.56
TiO ₂	0.13	0.12	0.74	0.38	0.17	0.11	0.2	0.33
Total	99.22	99.42	100.08	99.56	99.75	99.27	99.29	99.74
Al (ppm)	14838	12560	64013	37693	17570	13603	21210	33221
Ba	5	5	192	19	4	14	44	47
Be	1	1	1	1	1	1	1	1
Ca	20876	16424	14238	21297	19317	4957	77282	30405
Cd	1	1	1	1	1	1	1	1
Co	106	115	77	163	121	120	136	218
Cr	1300	1300	759	1300	1300	1300	1300	1300
Cu	14	51	34	57	38	17	33	40
Fe	65949	72300	80134	63834	70595	72697	95000	95000
K	78	95	2239	169	109	80	5157	5259
Li	15	15	59	36	26	13	10	20
Mg	163137	164549	87265	86349	145790	161489	61415	78057
Mn	928	815	1525	1848	742	573	7152	4669
Mo	1	1	1	1	1	1	1	1
Na	500	500	11208	798	500	500	500	500
Ni	2168	2675	1269	1910	2617	2627	2170	2504
P	51	50	403	135	71	47	89	129
Pb	15	15	15	15	15	15	15	15
S	804	833	130	130	710	936	2114	488
Sc	9	12	27	21	12	11	14	22
Sr	32	33	66	7	34	6	113	42
Ti	760	745	4416	2225	1031	648	1144	1922
V	61	55	242	174	77	54	86	140
W	6	6	6	6	6	6	6	6
Y	2	2	11	8	3	1	8	8
Zn	64	71	148	173	55	62	96	68
Ba	6	4	204.4	22.9	4.3	12.6	47.5	53.6
Be	0.28	0.11	0.57	0.65	0.21	0.15	0.38	0.51
Bi	0.47	0.47	0.47	0.47	0.47	0.47	0.47	0.47

	LM-15-SH-033	LM-15-SH-034	LM-15-SH-035	LM-15-SH-037	LM-15-SH-039	LM-15-SH-040	LM-15-SH-041	LM-15-SH-042
Cd	0.031	0.029	0.119	0.272	0.033	0.031	0.187	0.07
Ce	0.69	0.61	7.46	3.26	1.04	0.72	3.43	3.48
Co	119.42	118.64	88.9	185.06	135.27	130.18	158.33	187
Cr	4091	2088	828	4500	2332	3016	2339	3915
Cs	0.322	0.472	0.735	0.214	0.715	0.443	11.512	9.871
Cu	13	50.9	30.6	56.9	36.5	16.7	32.2	39.4
Dy	0.348	0.442	2.069	1.6	0.456	0.33	1.283	1.516
Er	0.239	0.314	1.299	0.965	0.333	0.22	0.946	0.998
Eu	0.0438	0.0374	0.457	0.2578	0.0559	0.0393	0.3065	0.1991
Ga	3.43	2.79	21.54	9.4	4.45	3.01	5.02	7.38
Gd	0.255	0.317	1.931	1.225	0.349	0.243	1.047	1.204
Hf	0.26	0.29	1.8	0.68	0.34	0.25	0.44	0.64
Ho	0.075	0.0948	0.4261	0.3296	0.1073	0.0727	0.2786	0.3321
In	0.0147	0.0171	0.0209	0.0484	0.0169	0.0131	0.0201	0.0265
La	0.28	0.19	3.14	1.25	0.42	0.36	2.67	2.27
Li	14.8	15	61.1	38.5	26.8	14.4	6.2	20
Lu	0.04	0.0523	0.1802	0.1596	0.0546	0.034	0.1542	0.161
Mo	0.1	0.15	0.22	0.24	0.08	0.1	0.28	0.22
Nb	0.25	0.244	2.143	0.69	0.319	0.196	0.353	0.609
Nd	0.6	0.47	5.17	2.46	0.83	0.5	2.73	2.9
Ni	2434.9	2680.9	1427.6	2144.3	2891.5	2759.6	2478.9	2901.5
Pb	1	0.3	1.4	0.6	0.3	0.3	4.8	0.8
Pr	0.105	0.096	1.096	0.513	0.149	0.098	0.598	0.606
Rb	0.42	0.64	5.29	0.84	1.34	0.9	23.69	23.42
Sb	0.25	0.26	0.11	0.09	0.1	0.16	0.23	0.08
Sc	11.2	14.1	30.3	24.4	14.2	12.7	17.4	26.4
Sm	0.183	0.196	1.466	0.871	0.254	0.166	0.711	0.866
Sn	0.18	0.22	0.38	0.37	0.16	0.24	0.18	0.18
Sr	33.5	35.3	69.5	7.8	36.1	7.4	119.1	44.3
Ta	0.012	0.017	0.146	0.038	0.016	0.013	0.022	0.036
Tb	0.05	0.0595	0.3167	0.2244	0.0666	0.046	0.1815	0.2134
Th	0.059	0.063	0.404	0.165	0.079	0.054	0.118	0.15
Ti	783	722	4494	2308	1083	649	1224	2092
Tl	0.041	0.028	0.054	0.029	0.05	0.028	0.386	0.397
Tm	0.0379	0.0457	0.1822	0.1446	0.052	0.0347	0.1391	0.1429
U	0.018	0.02	0.183	0.067	0.026	0.017	0.046	0.057
V			229.3		18.3		31.1	
W	0.05	0.05	0.1	0.1	0.05	0.05	0.05	0.05
Y	2.06	2.37	11.89	8.52	2.63	1.77	8.67	9.27
Yb	0.243	0.306	1.196	0.968	0.323	0.239	0.92	1.006
Zn	69	60	152	179	60	55	105	76
Zr	9	10	65	25	12	9	16	23

	LM-15-SH-043	LM-15-SH-044	LM-15-SH-046	LM-15-SH-046 SP	LM-15-SH-047	LM-15-SH-048	LM-15-SH-080	LM-15-SH-080
Al ₂ O ₃ (wt.%)	6.24	12.94	4.26	4.24	7.22	10.85	12.35	11.8
BaO	0.004	0.02	0.004	0.004	0.004	0.004	0.02	0.02
CaO	1.211	0.52	1.41	1.34	13.41	0.466	4.86	5.39
Cr ₂ O ₃	0.46	0.01	0.38	0.38	0.38	0.1	0.09	0.08
Fe ₂ O ₃	8.93	4.25	9.28	9.31	10.07	8.81	5.99	5.67
K ₂ O	0.01	0.54	0.01	0.01	0.01	0.03	0.31	0.29
LOI	5.82	1.85	6.61	6.44	15.19	6.77	3.99	4.01
MgO	14.58	1.99	26.14	26.39	14.8	12.73	10.6	10.05
MnO	0.117	0.12	0.12	0.12	0.31	0.129	0.18	0.176
Na ₂ O	0.08	4.8	0.02	0.02	0.03	0.06	4.22	4.34
P ₂ O ₅	0.024	0.09	0.01	0.02	0.03	0.064	0.06	0.062
SiO ₂	60.66	72.44	51.94	52.16	38.07	59.12	57.19	57.26
TiO ₂	0.27	0.31	0.2	0.2	0.34	0.45	0.72	0.68
Total	98.4	99.89	100.34	100.59	99.84	99.59	100.6	99.81
Al (ppm)	33090	62727	18747	14390	37761	55345	61029	62638
Ba	4	138	5	3	7	15	169	152
Be	1	1	1	1	1	1	1	1
Ca	8690	3619	10037	9174	88866	3251	34492	39004
Cd	1	1	1	1	1	1	1	1
Co	193	11	89	86	92	34	32	30
Cr	1300	45	1300	1300	1300	666	547	517
Cu	64	47	11	10	9	7	11	9
Fe	62800	27421	63502	60161	68338	59785	39405	40556
K	70	4413	70	70	74	170	2643	2338
Li	23	22	10	9	24	74	41	37
Mg	87155	11385	153552	144655	88330	73755	60870	61454
Mn	870	809	928	893	2348	927	1329	1360
Mo	1	2	1	1	1	1	1	1
Na	500	30058	500	533	555	500	27374	30716
Ni	2439	123	1702	1634	1324	253	382	323
P	100	409	76	73	121	273	267	275
Pb	15	16	15	15	15	15	19	15
S	8738	2358	130	130	130	130	130	130
Sc	20	4	10	5	24	21	36	36
Sr	7	83	8	7	68	4	152	164
Ti	1652	1798	1189	1113	2028	2661	4290	4056
V	114	36	85	82	144	130	238	229
W	6	6	6	6	6	6	6	6
Y	4	7	4	3	8	8	12	12
Zn	64	87	60	58	47	138	84	88
Ba	2.9	146.7	5	4.4	6.8	15.8	184.1	166.5
Be	0.32	0.61	0.13	0.17	0.35	0.33	0.46	0.54
Bi	0.47	0.47	0.47	0.47	0.47	0.47	0.47	0.47

	LM-15-SH-043	LM-15-SH-044	LM-15-SH-046	LM-15-SH-046 SP	LM-15-SH-047	LM-15-SH-048	LM-15-SH-080	LM-15-SH-080
Cd	0.023	0.212	0.101	0.048	0.066	0.094	0.046	0.04
Ce	1.69	24.93	1.25	1.28	3.25	9.47	7.12	7.16
Co	187	13.73	99.41	98.41	103.62	38.9	38.66	34.28
Cr	3012	52	2791	2741	2729	691	615	532
Cs	0.335	0.199	0.128	0.134	0.257	0.47	0.31	0.355
Cu	62.4	47.6	9.2	9.1	6.5	3.5	7.4	6.5
Dy	0.821	1.416	0.773	0.735	1.367	1.631	2.498	2.528
Er	0.536	0.786	0.444	0.452	0.919	1.059	1.498	1.544
Eu	0.0924	0.603	0.1358	0.1337	0.3029	0.2492	0.5078	0.4817
Ga	6.74	11.36	4.73	4.73	7.93	14.32	9.34	8.71
Gd	0.608	1.606	0.613	0.58	1.101	1.428	2.102	2.166
Hf	0.55	3.01	0.41	0.49	0.64	1.81	1.61	1.46
Ho	0.1791	0.2753	0.1596	0.1514	0.2888	0.3436	0.5144	0.5206
In	0.0242	0.0394	0.0185	0.0183	0.0295	0.0199	0.0405	0.0467
La	0.67	12.97	0.35	0.37	1.54	3.96	2.88	2.83
Li	29.8	23.9	8	7.7	19.2	75.2	40.7	39.4
Lu	0.0925	0.1191	0.0653	0.063	0.1269	0.1551	0.219	0.2368
Mo	0.35	0.96	0.08	0.08	0.24	0.86	0.25	0.6
Nb	0.492	3.355	0.357	0.363	0.625	2.023	1.901	1.644
Nd	1.27	10.9	1.06	1.23	2.57	5.32	5.36	5.54
Ni	2556.3	140.2	1877.2	1848.2	1468.6	266.7	440.9	335.3
Pb	0.9	2.3	0.7	0.2	0.4	0.4	0.5	0.3
Pr	0.283	2.872	0.216	0.204	0.481	1.234	1.079	1.076
Rb	0.32	11.92	0.35	0.28	0.28	0.88	6.28	5.43
Sb	0.31	0.11	0.07	0.07	0.07	0.06	0.3	0.31
Sc	24	5	14.3	8.1	26.3	23.5	40.4	40.4
Sm	0.427	1.9	0.436	0.422	0.784	1.29	1.662	1.737
Sn	0.33	0.55	0.16	0.16	0.28	0.48	0.57	0.64
Sr	7.3	87.5	8.7	8.4	70.8	4.4	161	169.4
Ta	0.032	0.262	0.023	0.022	0.04	0.151	0.118	0.108
Tb	0.105	0.2306	0.1121	0.1055	0.2008	0.2403	0.3693	0.3703
Th	0.116	2.216	0.065	0.084	0.149	0.944	0.438	0.44
Ti	1629	1889	1186	1175	2014	2657	4403	3945
Tl	0.048	0.124	0.008	0.006	0.016	0.006	0.04	0.036
Tm	0.0859	0.1149	0.0641	0.0623	0.13	0.1548	0.2136	0.2291
U	0.036	0.597	0.024	0.029	0.029	0.262	0.107	0.094
V		35.4				145.4	239.6	242.2
W	0.05	0.82	0.05	0.05	0.08	0.46	0.08	0.06
Y	4.55	7.89	3.95	3.62	8.55	8.84	13.62	13.42
Yb	0.602	0.758	0.405	0.428	0.85	1.068	1.41	1.558
Zn	56	89	65	65	52	123	92	77
Zr	20	121	14	18	22	69	59	52

	TL-16-SH-010	TL-16-SH-011	TL-16-SH-015	TL-16-SH-018	TL-16-SH-022	TL-16-SH-024	TL-16-SH-029	TL-16-SH-037	TL-16-SH-044
Al ₂ O ₃ (wt.%)	13	15.6	16.23	16.44	17.21	12.46	14.13	10.4	16.59
BaO	0.004	0.05	0.16	0.09	0.12	0.02	0.1	0.01	0.05
CaO	1.954	6.213	0.829	4.723	4.291	3.938	4.272	12.605	10.06
Cr ₂ O ₃	0.12	0.01	0.01	0.02	0.002	0.002	0.02	0.13	0.09
Fe ₂ O ₃	12.16	10.38	6.72	4.72	4.43	5.71	5.49	9.29	9.06
K ₂ O	0.12	1.46	3.88	2.35	2.16	0.39	2.76	0.07	1.81
LOI	8.87	5.99	3.73	2.72	1.96	1.51	4.51	3.33	11.01
MgO	15.62	3.79	1.41	1.91	1.81	2.96	3.09	11.82	5.09
MnO	0.166	0.198	0.066	0.089	0.088	0.074	0.111	0.177	0.466
Na ₂ O	0.39	2.84	2.53	4.43	5.38	4.81	3.19	2.36	2.54
P ₂ O ₅	0.052	0.633	0.387	0.202	0.234	0.015	0.251	0.021	0.075
SiO ₂	47.06	50.97	62.9	61.6	61.92	67.01	61.49	49.44	42.06
TiO ₂	0.63	1.05	0.7	0.5	0.48	0.84	0.54	0.35	0.92
Total	100.11	99.18	99.56	99.79	100.07	99.71	99.95	100	99.83
Al (ppm)	70590	83361	79863	87696	85263	64079	70018	53524	87335
Ba	48	399	1340	818	984	123	830	29	438
Be	1	1	2	1	1	1	1	1	1
Ca	13942	44675	5715	34182	28403	27282	28771	73990	62009
Cd	1	1	1	1	1	1	1	1	1
Co	63	27	19	14	9	13	17	52	54
Cr	784	47	78	112	21	34	116	858	608
Cu	121	119	60	27	21	14	19	110	113
Fe	86655	73377	45423	33440	29136	38907	36208	62950	63652
K	937	11911	29643	19562	16881	3029	21474	446	14517
Li	79	22	13	16	15	8	24	22	71
Mg	94595	23372	7986	11627	10378	17081	17591	68264	30541
Mn	1324	1493	471	692	648	538	807	1286	3535
Mo	1	1	3	2	3	4	2	1	1
Na	2829	20036	16378	30567	31000	31000	20699	16659	17908
Ni	249	32	31	39	11	8	44	177	307
P	231	2749	1636	888	1002	62	1065	90	326
Pb	15	24	23	15	17	15	15	15	15
S	130	388	13079	219	130	442	698	265	327
Sc	38	18	10	9	6	21	13	40	44
Sr	39	1037	417	929	1162	188	635	90	136
Ti	3756	6508	4188	3071	2785	5040	3115	2047	5645
V	254	219	130	86	75	83	125	174	308
W	6	6	6	6	6	6	6	6	6
Y	11	27	17	11	13	16	13	7	14
Zn	91	136	74	82	83	25	75	54	104
Ba	41.2	405.2	1449.7	847.6	1076	134.9	892.4	31.3	466.6
Be	0.24	1.87	2.36	1.19	1.46	0.56	1.39	0.16	0.39
Bi	0.47	0.47	0.47	0.47	0.47	0.47	0.47	0.47	0.47

	TL-16-SH-010	TL-16-SH-011	TL-16-SH-015	TL-16-SH-018	TL-16-SH-022	TL-16-SH-024	TL-16-SH-029	TL-16-SH-037	TL-16-SH-044
Cd	0.104	0.126	0.084	0.094	0.081	0.032	0.077	0.068	0.116
Ce	4.47	172.86	116.21	63.14	99.15	4.02	84.86	3.16	7.53
Co	69.09	34.92	23.69	15.16	10.07	17.42	19.56	58.67	60.28
Cr	791	45	82	120	26	35	127	913	614
Cs	0.647	2.395	13.894	2.106	0.784	0.336	2.693	0.232	1.294
Cu	117.1	113.4	62.6	25	19.3	8.6	17.4	109	108.6
Dy	1.799	6.248	3.859	2.065	2.491	2.59	2.783	1.49	2.651
Er	1.149	2.759	1.765	0.982	1.278	1.891	1.362	0.926	1.686
Eu	0.3961	4.2658	2.4741	1.3214	1.7319	1.4361	1.7818	0.3148	0.9262
Ga	15.28	24.09	21.55	21.07	22.04	16.74	18.49	9.49	17.24
Gd	1.444	10.369	6.258	3.247	4.067	2.014	4.488	1.256	2.292
Hf	1.16	5.31	4.42	3.48	4.32	4.85	3.38	0.58	1.64
Ho	0.3846	1.0609	0.6861	0.3671	0.4621	0.5846	0.5002	0.3184	0.5827
In	0.0418	0.0704	0.0445	0.0321	0.0303	0.0416	0.033	0.0332	0.0702
La	1.73	76.61	52.9	29.63	48.89	1.47	40.15	1.23	3
Li	61.7	25.8	15.2	15	14.8	8.5	23	22.5	71.6
Lu	0.1778	0.3291	0.2313	0.1329	0.1916	0.3185	0.1817	0.1269	0.2494
Mo	0.84	0.45	3.04	1.78	2.93	6.01	1.57	0.33	0.44
Nb	1.156	8.567	7.374	6.432	8.873	4.421	4.82	0.576	2.03
Nd	3.53	91.83	57.14	31.21	45.19	3.91	40.4	2.5	5.42
Ni	269	33.8	33.4	41.4	11.4	9	49.4	192.6	316.4
Pb	0.5	22.1	17.4	11.1	16.5	0.6	9.9	0.3	0.5
Pr	0.695	22.524	14.48	7.913	11.962	0.658	10.406	0.512	1.079
Rb	2.93	38.82	115.43	60.85	55.76	7.96	88.77	1.14	58.17
Sb	0.26	0.29	7.91	0.32	0.13	0.07	0.53	0.12	0.05
Sc	41.2	20.8	11.9	9.6	6	23.7	14.1	46.4	47.9
Sm	1.089	15.939	9.63	5.078	6.722	1.366	6.808	0.919	1.723
Sn	0.49	1.32	1.09	0.84	0.98	1.07	0.83	0.24	0.64
Sr	38.9	1085.9	449.9	888.5	1163.5	197	646.3	97.6	143.4
Ta	0.073	0.4	0.364	0.337	0.4	0.403	0.271	0.036	0.131
Tb	0.2615	1.1976	0.7382	0.3962	0.4876	0.3754	0.5498	0.2194	0.4024
Th	0.197	8.884	7.037	4.124	6.412	1.115	5.836	0.116	0.281
Ti	3715	6392	4283	2955	2779	5037	3157	2090	5480
Tl	0.019	0.225	1.047	0.279	0.344	0.055	0.527	0.017	0.271
Tm	0.173	0.3716	0.2504	0.1328	0.1857	0.293	0.1878	0.1293	0.2395
U	0.058	2.117	1.953	1.292	1.926	0.159	1.453	0.031	0.081
V	239	227.7	141.9	82.1	71.7	88	124.9	198.5	320.5
W	0.66	1.94	5.35	0.49	0.56	0.18	0.36	0.1	0.46
Y	10.41	29.77	19.26	10.29	13.32	17.34	13.77	8.42	14.9
Yb	1.179	2.259	1.72	0.86	1.224	2.021	1.226	0.832	1.635
Zn	78	123	68	72	73	22	68	47	90
Zr	40	223	186	138	186	177	141	19	56

	TL-16-SH-046	TL-16-SH-047	TL-16-SH-048	TL-16-SH-048 SP	TL-16-SH-049	TL-16-SH-052	TL-16-SH-057	TL-16-SH-057
Al ₂ O ₃ (wt.%)	4.16	15.86	3.06	3.04	11.37	5.76	2.38	2.58
BaO	0.004	0.01	0.004	0.004	0.004	0.004	0.004	0.004
CaO	3.239	4.346	1.088	1.074	6.333	3.058	0.767	0.936
Cr ₂ O ₃	0.52	0.49	0.52	0.5	0.002	0.75	0.85	0.8
Fe ₂ O ₃	10.89	7.79	12.6	12.55	20.55	10.5	12.14	11.47
K ₂ O	0.05	0.11	0.02	0.02	0.31	0.04	0.02	0.01
LOI	9.95	4.97	12.2	12.19	3.15	10.25	11.96	12.51
MgO	30.52	5.14	32.76	33.01	4.08	26.3	34.53	34.39
MnO	0.162	0.111	0.146	0.147	0.298	0.159	0.162	0.161
Na ₂ O	0.06	5.69	0.02	0.02	2.9	0.06	0.02	0.02
P ₂ O ₅	0.019	0.083	0.014	0.015	0.106	0.026	0.007	0.007
SiO ₂	39.73	53.2	36.73	36.91	48.73	42.5	36.4	36.3
TiO ₂	0.23	0.89	0.16	0.16	1.84	0.31	0.13	0.14
Total	99.53	98.7	99.29	99.62	99.69	99.69	99.32	99.29
Al (ppm)	22207	84714	16592	16397	58920	30770	13260	13594
Ba	13	56	15	14	33	8	8	8
Be	1	1	1	1	1	1	1	1
Ca	22828	31613	7829	7882	44509	22048	5570	6612
Cd	1	1	1	1	1	1	1	1
Co	108	129	124	126	52	107	132	125
Cr	1300	1300	1300	1300	16	1300	1300	1300
Cu	23	120	13	14	27	48	6	6
Fe	77867	55637	89862	90904	95000	74845	86452	79446
K	329	859	121	108	2276	236	87	70
Li	28	31	30	29	12	46	9	9
Mg	185978	31315	200104	202146	24180	159093	210183	203197
Mn	1243	851	1132	1135	2228	1225	1286	1201
Mo	1	1	1	1	1	1	1	1
Na	500	31000	500	500	20385	500	500	500
Ni	1795	1092	1391	1415	19	1497	1488	1464
P	85	372	64	63	444	119	30	31
Pb	15	15	15	15	15	15	15	15
S	400	1037	535	503	130	450	130	130
Sc	16	49	14	14	40	18	10	8
Sr	6	129	4	4	64	15	2	2
Ti	1436	5595	1009	1010	11048	1895	830	852
V	92	302	74	74	472	121	67	61
W	6	6	6	6	6	6	6	6
Y	5	19	4	3	25	6	3	3
Zn	60	137	56	52	111	81	76	79
Ba	11.5	58.4	13.2	12.8	35.7	5.3	4	5.7
Be	0.11	0.26	0.08	0.06	0.55	0.13	0.1	0.09
Bi	0.47	0.47	0.47	0.47	0.47	0.47	0.47	0.47

	TL-16-SH-046	TL-16-SH-047	TL-16-SH-048	TL-16-SH-048 SP	TL-16-SH-049	TL-16-SH-052	TL-16-SH-057	TL-16-SH-057
Cd	0.022	0.103	0.018	0.019	0.035	0.051	0.017	0.024
Ce	2.02	9.01	1.51	1.49	10.67	2.08	0.92	0.99
Co	114.56	142.07	132.6	132.68	66.75	112.85	139.04	133.97
Cr	3326	3348	3474	3440	13	4500	4500	4500
Cs	2.171	0.68	0.505	0.478	1.912	1.298	0.136	0.129
Cu	21.3	117.7	12	12.4	14.3	48.3	4	3
Dy	0.938	3.746	0.639	0.636	4.987	1.196	0.422	0.514
Er	0.556	2.23	0.407	0.413	3.091	0.779	0.281	0.333
Eu	0.2645	0.7902	0.1337	0.1439	1.0577	0.1233	0.0798	0.1086
Ga	4.79	14.74	3.7	3.6	18.5	6.59	3.23	3.35
Gd	0.735	3.225	0.53	0.561	4.202	0.925	0.366	0.442
Hf	0.4	1.69	0.27	0.27	2.26	0.54	0.23	0.27
Ho	0.1932	0.787	0.1443	0.1425	1.0395	0.2596	0.0909	0.1086
In	0.0203	0.0586	0.0161	0.0144	0.0881	0.025	0.0119	0.0121
La	0.74	3.35	0.82	0.81	3.92	0.78	0.39	0.43
Li	30.2	35.8	33.3	30.8	14	52.6	8.7	10.3
Lu	0.0842	0.3063	0.0545	0.0603	0.418	0.1246	0.0444	0.0503
Mo	0.17	0.54	0.1	0.12	0.48	0.12	0.26	0.09
Nb	0.438	2.08	0.288	0.284	2.879	0.676	0.224	0.316
Nd	1.58	7.02	1.18	1.15	9.18	1.75	0.8	0.84
Ni	1834.4	1142.2	1423.6	1426.2	20.1	1514	1546.8	1494.7
Pb	0.5	0.6	0.6	0.6	0.3	0.2	0.3	0.4
Pr	0.295	1.375	0.231	0.217	1.724	0.313	0.141	0.156
Rb	3.29	2.41	1.04	0.96	7.51	2.63	0.69	0.62
Sb	0.06	0.04	0.91	0.88	0.07	0.05	0.04	0.04
Sc	17.9	53.4	15.9	15.1	46.3	21	10.9	10.1
Sm	0.572	2.351	0.381	0.379	3.096	0.582	0.247	0.307
Sn	0.21	0.68	0.17	0.2	0.48	0.22	0.17	0.16
Sr	7.5	135.2	5.8	5.3	71.2	17.4	3.4	3.2
Ta	0.027	0.139	0.016	0.018	0.179	0.044	0.014	0.019
Tb	0.1295	0.5562	0.0947	0.0945	0.7445	0.1698	0.0602	0.0766
Th	0.07	0.306	0.048	0.042	0.363	0.096	0.038	0.034
Ti	1412	5513	992	987	11208	1845	818	861
Tl	0.056	0.111	0.033	0.033	0.02	0.065	0.005	0.004
Tm	0.0792	0.3194	0.0593	0.0606	0.4386	0.1156	0.0395	0.0492
U	0.019	0.074	0.017	0.015	0.103	0.027	0.018	0.011
V					370			
W	0.09	0.09	0.47	0.48	0.05	0.07	0.05	0.05
Y	5.2	20.58	3.68	3.61	28.01	6.9	2.54	2.96
Yb	0.551	2.01	0.399	0.383	2.811	0.816	0.285	0.334
Zn	50	121	46	43	98	69	63	67
Zr	14	60	10	9	79	19	8	9

	TL-16-SH-060	TL-16-SH-061	TL-16-SH-062	TL-16-SH-066	TL-16-SH-069	TL-16-SH-071	TL-16-SH-074	TL-16-SH-075	TL-16-SH-076
Al ₂ O ₃ (wt.%)	3.71	14.48	13.93	13.28	13.17	1.37	12.1	13.47	13.59
BaO	0.004	0.02	0.03	0.01	0.09	0.004	0.04	0.004	0.01
CaO	1.592	10.286	7.919	9.909	5.215	1.817	6.698	9.538	9.349
Cr ₂ O ₃	0.36	0.05	0.03	0.002	0.06	0.78	0.13	0.01	0.01
Fe ₂ O ₃	9.02	10.52	12.29	13.09	11.12	10.2	11.1	12.51	14.19
K ₂ O	0.04	0.8	2.19	0.27	1.82	0.02	2.04	0.08	0.36
LOI	11.06	2.85	2.66	3.06	3.31	14.94	4.78	6.68	4.14
MgO	34.24	8.12	7.14	6.48	10.04	35.17	12.19	7.38	7.17
MnO	0.142	0.169	0.192	0.209	0.157	0.123	0.202	0.179	0.233
Na ₂ O	0.02	2.09	2.71	2.29	3.21	0.02	1.78	2.38	1.6
P ₂ O ₅	0.014	0.08	0.128	0.051	0.055	0.008	0.044	0.073	0.063
SiO ₂	39.81	49.74	49.67	50.73	51.14	35.13	48.12	46.91	48.45
TiO ₂	0.16	0.78	1.08	0.72	0.59	0.07	0.53	0.85	0.87
Total	100.18	99.98	99.99	100.1	99.96	99.61	99.74	100.07	100.04
Al (ppm)	19320	76658	69682	68839	68449	7501	63175	70436	71481
Ba	8	162	271	72	725	5	308	27	104
Be	1	1	1	1	1	1	1	1	1
Ca	11128	63472	53808	59796	36524	13212	46677	59498	56896
Cd	1	1	1	1	1	1	1	1	1
Co	100	34	34	46	44	114	53	47	48
Cr	1300	321	205	21	414	1300	826	48	48
Cu	17	75	115	45	7	6	88	19	54
Fe	61991	73657	82493	90098	76793	73265	76762	85718	95000
K	307	6556	17211	2101	14570	70	16471	607	2822
Li	19	25	13	25	33	1	51	41	37
Mg	199647	48652	40786	38273	58954	214568	72071	43719	42605
Mn	1059	1274	1367	1572	1165	954	1499	1363	1736
Mo	1	1	1	1	1	1	1	1	1
Na	500	15141	17976	16173	22114	500	12443	16723	11460
Ni	2196	86	62	55	119	2081	201	66	56
P	61	343	535	218	237	33	186	319	267
Pb	15	15	15	15	15	15	15	15	15
S	245	247	1733	130	130	202	130	378	336
Sc	13	36	35	38	35	7	36	33	38
Sr	5	235	121	154	169	4	101	44	127
Ti	961	4816	6416	4332	3567	425	3173	5031	5252
V	69	214	250	246	223	42	214	258	280
W	6	6	6	6	6	6	6	6	6
Y	4	19	27	16	13	1	11	18	17
Zn	59	67	91	69	68	55	71	49	75
Ba	7.6	175.8	304.9	80.2	784	1.7	343.8	27.8	115.9
Be	0.11	0.33	0.5	0.3	0.31	0.05	0.28	0.4	0.28
Bi	0.47	0.47	0.47	0.47	0.47	0.47	0.47	0.47	0.47

	TL-16-SH-060	TL-16-SH-061	TL-16-SH-062	TL-16-SH-066	TL-16-SH-069	TL-16-SH-071	TL-16-SH-074	TL-16-SH-075	TL-16-SH-076
Cd	0.016	0.069	0.088	0.038	0.035	0.021	0.064	0.037	0.04
Ce	1.54	9.61	14.6	6.37	6.81	0.66	5.32	8.32	6.96
Co	106.57	41.19	42.99	53.21	49.81	118.41	62.14	53.62	55.72
Cr	2464	333	216	18	423	4500	891	56	45
Cs	3.098	0.869	0.721	0.533	0.402	0.017	0.721	0.56	0.817
Cu	15.4	70.5	109.7	39.8	2.6	2.8	86.1	17.4	48.7
Dy	0.693	3.671	5.339	3.006	2.356	0.249	2.147	3.178	3.237
Er	0.462	2.346	3.423	1.884	1.525	0.154	1.398	1.905	2.027
Eu	0.1422	0.7866	1.1185	0.6611	0.4476	0.1049	0.5049	0.7264	0.6857
Ga	4.05	16	15.44	15.65	12.35	1.86	13.7	17.87	16.55
Gd	0.588	3.037	4.509	2.534	1.975	0.225	1.716	2.696	2.733
Hf	0.31	1.65	2.54	1.3	1.23	0.14	0.98	1.57	1.38
Ho	0.1523	0.7995	1.1548	0.6473	0.5006	0.0496	0.4635	0.6692	0.6873
In	0.0139	0.0592	0.0751	0.0519	0.0456	0.0085	0.0437	0.0522	0.0587
La	0.6	3.61	5.54	2.29	2.56	0.28	2.2	3.12	2.43
Li	24.9	29.5	15.2	25.6	35.9	0.7	64.8	42.3	41.1
Lu	0.0689	0.3437	0.5082	0.2638	0.2185	0.0252	0.2002	0.2609	0.2747
Mo	0.12	0.4	0.33	0.62	0.21	0.18	0.3	0.74	0.43
Nb	0.296	2.512	4.058	1.484	1.401	0.111	0.97	1.968	1.717
Nd	1.17	7.54	11.25	5.1	4.92	0.5	3.89	6.62	6.03
Ni	2259.6	90.3	64.7	58.3	123.3	2100.2	217	72.8	59.4
Pb	0.3	0.5	1.2	0.3	1	1.4	0.6	0.5	0.3
Pr	0.22	1.44	2.241	0.982	1.007	0.088	0.789	1.326	1.13
Rb	3.7	25.15	53.83	4.47	24.4	0.25	31.52	1.55	6
Sb	0.04	0.36	0.13	0.15	0.06	0.31	0.59	0.16	0.24
Sc	16.1	41.2	41.5	42.2	39.7	8.1	41.9	39.9	43.4
Sm	0.385	2.253	3.533	1.835	1.489	0.171	1.255	1.999	2.086
Sn	0.2	0.52	0.67	0.43	0.53	0.16	0.36	1.01	0.43
Sr	5.9	248.3	125.8	163.6	176.1	5	109.5	45.1	137.5
Ta	0.018	0.161	0.259	0.095	0.096	0.007	0.064	0.126	0.103
Tb	0.0984	0.5344	0.7845	0.4466	0.3379	0.0393	0.3063	0.4559	0.4718
Th	0.093	0.315	0.497	0.213	0.396	0.02	0.287	0.352	0.209
Ti	991	4811	6604	4288	3567	419	3296	5272	5268
Tl	0.025	0.1	0.184	0.023	0.108	0.016	0.334	0.009	0.038
Tm	0.0646	0.3422	0.5047	0.2797	0.2241	0.0245	0.2004	0.2834	0.2921
U	0.024	0.08	0.129	0.056	0.106	0.012	0.081	0.098	0.059
V		227.3	269.6	250.4	236		240.3	261	295.2
W	0.19	0.13	0.1	0.23	0.62	0.6	0.31	0.6	0.09
Y	4.06	21.57	30.85	17.21	13.99	1.47	13	18.51	18.54
Yb	0.453	2.239	3.322	1.78	1.428	0.169	1.344	1.818	1.829
Zn	51	59	83	59	58	46	64	43	63
Zr	11	59	93	44	44	6	34	55	47

	TL-16-SH-077	TL-16-SH-078	TL-16-SH-079	TL-16-SH-081	TL-16-SH-081	TL-16-SH-085	TL-16-SH-090	TL-16-SH-092	TL-16-SH-093
Al ₂ O ₃ (wt.%)	18.13	17.71	17.22	2.8	2.77	11.49	15.07	14.6	11.21
BaO	0.12	0.11	0.07	0.004	0.004	0.004	0.06	0.03	0.03
CaO	5.93	6.299	3.732	6.237	7.346	15.424	1.912	8.42	8.826
Cr ₂ O ₃	0.01	0.01	0.02	1.11	1.06	0.2	0.02	0.01	0.1
Fe ₂ O ₃	9.2	10.18	7.33	11.81	10.73	10.75	5.93	10.69	8.81
K ₂ O	2.53	1.87	2.96	0.03	0.03	0.02	2.17	0.89	0.45
LOI	4.21	4.11	3.66	10.79	10.59	7.63	3.92	2.87	5.16
MgO	3.33	4.9	4.39	28.55	28.07	7.54	2.14	6.9	8.17
MnO	0.145	0.176	0.102	0.166	0.17	0.247	0.096	0.223	0.221
Na ₂ O	3.03	2.9	4.21	0.05	0.07	0.16	2.49	2.5	1.97
P ₂ O ₅	0.543	0.456	0.32	0.012	0.014	0.051	0.235	0.067	0.054
SiO ₂	51.3	50.24	54.48	38.17	38.95	45.39	65.02	52.11	54.2
TiO ₂	0.94	0.9	0.76	0.14	0.15	0.66	0.6	0.82	0.64
Total	99.41	99.86	99.28	99.87	99.95	99.57	99.68	100.14	99.83
Al (ppm)	93145	90809	88874	15250	14176	59660	77011	73541	57716
Ba	973	909	603	15	17	16	505	209	210
Be	2	2	2	1	1	1	1	1	1
Ca	41678	43516	26234	44376	49892	100000	13337	56577	60734
Cd	1	1	1	1	1	1	1	1	1
Co	22	30	20	123	116	64	19	48	54
Cr	47	82	174	1300	1300	1300	163	94	678
Cu	92	97	86	10	11	96	40	174	107
Fe	63829	69046	51198	82735	72213	75755	41007	71707	60221
K	20360	14837	23454	172	188	97	17134	7044	3572
Li	24	30	21	18	17	22	21	24	25
Mg	19719	28380	26265	170074	160596	45124	12606	39406	47735
Mn	1078	1287	761	1319	1227	1876	703	1604	1630
Mo	1	1	1	1	1	1	1	1	1
Na	20655	19596	28424	517	500	918	16653	16763	13609
Ni	26	41	71	2253	2092	413	71	75	190
P	2336	1937	1389	54	63	218	997	291	228
Pb	24	21	18	15	15	15	15	15	15
S	130	130	163	177	130	2209	178	404	130
Sc	16	21	14	12	11	34	13	36	36
Sr	1356	1186	630	40	42	28	261	213	198
Ti	5791	5429	4585	831	865	3982	3588	4863	3806
V	204	214	117	75	66	217	106	252	225
W	6	6	6	6	6	6	6	6	6
Y	23	23	16	3	3	15	11	13	11
Zn	133	127	91	72	80	95	83	99	86
Ba	1101.1	1000.7	671.2	11.3	15.9	16.4	564	236.5	227.6
Be	2.41	2.36	2.5	0.09	0.05	0.26	1.06	0.38	0.3
Bi	0.47	0.47	0.47	0.47	0.47	0.47	0.47	0.47	0.47

	TL-16-SH-077	TL-16-SH-078	TL-16-SH-079	TL-16-SH-081	TL-16-SH-081	TL-16-SH-085	TL-16-SH-090	TL-16-SH-092	TL-16-SH-093
Cd	0.102	0.081	0.053	0.025	0.05	0.088	0.062	0.093	0.145
Ce	146.01	137.33	155.3	0.93	1.23	5.81	55.35	8.14	5.29
Co	27.64	36.63	24.23	133.19	128.04	71.25	23.13	55.51	60.38
Cr	46	86	176	4500	4500	1424	171	93	702
Cs	4.233	2.766	1.93	2.022	1.89	0.269	2.015	1.005	0.93
Cu	89	94.1	83.7	6.8	9.9	91.3	39.3	171.4	104.2
Dy	5.179	5.131	3.699	0.525	0.558	2.789	2.523	2.773	2.274
Er	2.384	2.439	1.62	0.299	0.338	1.822	1.311	1.596	1.419
Eu	3.4587	3.2236	2.2536	0.1114	0.1269	0.5613	0.9899	0.7246	0.4937
Ga	25.92	23.04	21.54	3.69	3.5	12.23	18.97	16.62	12.36
Gd	8.691	8.227	6.801	0.421	0.454	2.285	3.541	2.506	1.967
Hf	5	4.66	7.43	0.22	0.24	1.26	3.3	1.54	1.13
Ho	0.8999	0.9023	0.6413	0.1029	0.114	0.5997	0.4681	0.5711	0.4827
In	0.0638	0.0655	0.0387	0.0128	0.0142	0.0496	0.0359	0.0611	0.0606
La	65.74	61.88	69.71	0.38	0.46	2.23	25.21	3.18	2
Li	24.2	31	20.9	16.1	17	21.5	23.5	24.8	26
Lu	0.2928	0.3275	0.201	0.0438	0.05	0.2629	0.1884	0.2118	0.1944
Mo	0.66	0.33	0.51	0.47	0.14	0.36	0.68	0.63	0.51
Nb	11.271	8.052	12.328	0.222	0.284	1.553	4.323	1.811	1.365
Nd	75.91	69.58	68.73	0.93	0.97	4.73	27.7	6.16	4.46
Ni	27.3	43.8	72.8	2374.2	2217.6	416.8	75.1	78	201.7
Pb	18.9	12.3	13	0.4	0.5	0.9	10.3	1	0.5
Pr	18.545	17.453	18.324	0.16	0.196	0.889	6.797	1.22	0.854
Rb	58.57	42.31	125.01	1.65	1.78	0.54	58.42	25.2	13.61
Sb	1.32	1.16	0.63	0.04	0.04	0.39	0.15	0.11	0.16
Sc	18.1	23.4	15.7	13.9	13.1	38.6	14.8	41.7	41.1
Sm	13.088	11.979	10.818	0.288	0.373	1.599	4.904	1.923	1.441
Sn	1.44	1.3	1.46	0.35	0.28	0.57	0.93	0.78	0.58
Sr	1418.9	1212.9	644.9	38.8	47.2	26.9	270.8	226.7	207.1
Ta	0.426	0.399	0.754	0.008	0.015	0.095	0.341	0.118	0.084
Tb	0.9846	0.957	0.7572	0.0755	0.0807	0.4035	0.437	0.4192	0.3457
Th	7.98	7.096	21.462	0.035	0.053	0.225	4.161	0.319	0.211
Ti	5837	5531	4717	841	904	4043	3725	5002	3928
Tl	0.251	0.182	0.727	0.01	0.01	0.026	0.41	0.237	0.115
Tm	0.3262	0.3428	0.2137	0.0456	0.054	0.2586	0.1913	0.2288	0.199
U	2.653	1.281	5.428	0.011	0.017	0.059	1.082	0.091	0.062
V	215.6	229.1	126.7			246.4	114.2	270.5	250.5
W	1.22	0.46	1.27	0.1	0.06	0.14	0.57	0.08	0.11
Y	25.71	25.93	17.19	2.87	3.09	16.31	12.88	14.73	12.75
Yb	2.05	2.119	1.374	0.306	0.35	1.72	1.255	1.473	1.298
Zn	118	113	81	61	70	82	76	86	76
Zr	282	254	312	8	9	44	134	55	39

	TL-16-SH-093 SP	TL-16-SH-094	TL-16-SH-095	TL-16-SH-098	TL-16-SH-099	TI-16-SH-103	TL-16-SH-104	TL-16-SH-104 SP
Al ₂ O ₃ (wt.%)	11.19	13	2.57	15.56	4.92	2.9	3.57	3.27
BaO	0.03	0.1	0.004	0.05	0.004	0.004	0.004	0.004
CaO	8.884	5.037	4.989	4.203	19.959	0.075	0.061	0.048
Cr ₂ O ₃	0.1	0.03	0.97	0.02	0.38	0.89	3.75	3.75
Fe ₂ O ₃	8.85	7.16	10.41	9.01	10.23	11.04	9.55	9.47
K ₂ O	0.45	2.64	0.03	0.97	0.04	0.02	0.02	0.02
LOI	5.05	5.34	12.51	5.49	15.18	12.68	12.82	12.82
MgO	8.19	2.4	30.07	5.24	14.29	35.33	34.97	34.63
MnO	0.224	0.157	0.142	0.212	0.313	0.135	0.152	0.151
Na ₂ O	1.96	3.18	0.05	3.31	0.42	0.02	0.02	0.02
P ₂ O ₅	0.052	0.132	0.012	0.091	0.028	0.014	0.016	0.017
SiO ₂	54.28	60.09	37.88	55.73	33.85	36.02	34.63	34.3
TiO ₂	0.64	0.44	0.14	0.81	0.27	0.15	0.16	0.16
Total	99.9	99.71	99.77	100.7	99.88	99.24	99.66	98.64
Al (ppm)	60450	66882	14096	81042	27456	16040	19501	15930
Ba	216	865	17	410	7	6	15	12
Be	1	1	1	1	1	1	1	1
Ca	64425	35471	35778	29603	100000	555	338	311
Cd	1	1	1	1	1	1	1	1
Co	54	10	117	29	88	108	123	116
Cr	691	206	1300	153	1300	1300	1300	1300
Cu	106	22	7	29	36	6	7	26
Fe	63531	49814	73616	62049	73957	78139	66872	61499
K	3701	20920	225	7959	227	134	82	72
Li	26	23	16	58	10	4	3	3
Mg	50604	14178	180731	31097	87746	214443	212417	194421
Mn	1716	1177	1137	1642	2540	1086	1227	1106
Mo	1	1	1	1	1	1	2	1
Na	14309	21408	560	22506	3295	500	500	500
Ni	195	46	2197	52	917	1930	1946	1841
P	234	588	53	383	119	61	71	68
Pb	15	15	15	15	15	15	15	15
S	130	615	216	230	149	174	316	189
Sc	37	9	12	31	19	13	11	10
Sr	196	101	26	139	104	2	2	2
Ti	3974	2664	843	4860	1699	900	954	851
V	236	67	74	225	116	72	109	96
W	6	6	6	6	6	6	6	6
Y	12	9	3	17	7	4	3	3
Zn	88	44	71	83	69	54	100	93
Ba	226.2	935.4	13.4	415.2	5.9	1.7	3.5	2.9
Be	0.37	0.77	0.14	0.52	0.16	0.34	0.08	0.72
Bi	0.47	0.47	0.47	0.47	0.47	0.47	0.47	0.47

	TL-16-SH-093 SP	TL-16-SH-094	TL-16-SH-095	TL-16-SH-098	TL-16-SH-099	TI-16-SH-103	TL-16-SH-104	TL-16-SH-104 SP
Cd	0.119	0.035	0.026	0.049	0.018	0.015	0.044	0.023
Ce	5.51	28.2	1	13.75	2.35	1.61	1.16	1.2
Co	58.94	12.03	125.99	34.5	98.68	113.32	122.04	120.41
Cr	675	200	4500	178	2665	4500	4500	4500
Cs	0.909	0.309	2.061	0.717	0.207	0.034	0.029	0.024
Cu	106.3	19.8	7.1	24.9	34	4.2	6.6	21.2
Dy	2.276	1.775	0.503	3.036	1.09	0.615	0.543	0.52
Er	1.408	0.923	0.329	1.803	0.663	0.331	0.348	0.355
Eu	0.5009	0.8974	0.1219	0.8614	0.2299	0.1792	0.0869	0.0874
Ga	12.35	14.33	3.55	17.42	6.07	3.32	4.76	4.34
Gd	2.017	2.18	0.437	2.77	0.891	0.549	0.423	0.509
Hf	1.14	2.77	0.23	2.04	0.5	0.24	0.24	0.22
Ho	0.4878	0.3476	0.107	0.6179	0.2251	0.1218	0.1114	0.106
In	0.0563	0.0168	0.0125	0.0376	0.0213	0.0125	0.0151	0.0125
La	1.97	12.83	0.39	5.96	0.94	0.78	0.42	0.46
Li	24	23.3	15.6	60.7	6.4	4.4	2.6	2.3
Lu	0.1961	0.1294	0.0481	0.2586	0.0998	0.0485	0.0471	0.0455
Mo	0.58	0.8	0.15	1.47	0.48	0.31	0.32	0.21
Nb	1.41	3.965	0.238	2.696	0.542	0.264	0.265	0.241
Nd	4.4	13.59	0.85	8.62	1.88	1.3	0.91	0.98
Ni	197.1	46.5	2322.8	60.3	995.9	1977	1959.4	1912.1
Pb	0.6	1	0.18	0.8	0.18	0.3	0.3	0.3
Pr	0.843	3.52	0.155	1.908	0.373	0.23	0.177	0.18
Rb	13.74	33.53	2.4	19.76	0.38	0.68	0.53	0.48
Sb	0.15	0.04	0.04	0.04	0.04	0.07	0.04	0.04
Sc	39.4	10	14.6	36.4	22.3	12.8	10.9	10.7
Sm	1.46	2.567	0.288	2.348	0.634	0.406	0.329	0.324
Sn	0.61	0.4	0.25	0.47	0.26	0.2	0.18	0.78
Sr	205.3	101.3	26.5	137.8	102.9	1.9	2.3	2.3
Ta	0.08	0.307	0.01	0.191	0.029	0.011	0.01	0.012
Tb	0.339	0.2987	0.0757	0.4638	0.15	0.0895	0.0845	0.0789
Th	0.204	2.452	0.039	0.986	0.074	0.031	0.054	0.053
Ti	3854	2637	869	5157	1738	855	900	848
Tl	0.119	0.199	0.02	0.103	0.006	0.005	0.003	0.003
Tm	0.2043	0.1345	0.047	0.2539	0.0968	0.0495	0.0495	0.0464
U	0.056	0.68	0.011	0.266	0.019	0.019	0.019	0.014
V	246.4	70.4		229				
W	0.11	0.12	0.05	0.16	0.05	0.15	0.06	0.07
Y	12.88	9.57	2.88	17.05	6.15	3.63	3.05	3.01
Yb	1.352	0.845	0.315	1.748	0.626	0.318	0.32	0.308
Zn	91	35	60	77	60	45	87	83
Zr	39	110	8	77	17	9	8	8

	TL-16-SH-105	TL-16-SH-106	TL-16-SH-107	TL-16-SH-109	TL-16-SH-111A	TL-16-SH-112	TL-16-SH-114	TL-16-SH-116A
Al ₂ O ₃ (wt.%)	3.05	15.64	3.79	4.03	2.7	2.43	5.88	7.49
BaO	0.004	0.04	0.004	0.004	0.004	0.004	0.01	0.004
CaO	0.082	5.067	3.025	3.59	0.696	0.043	21.884	8.322
Cr ₂ O ₃	0.32	0.11	0.96	0.41	0.58	0.83	0.91	0.54
Fe ₂ O ₃	9.05	9.93	11.93	12.61	11.11	11.32	13.46	10.18
K ₂ O	0.02	1.54	0.04	0.03	0.01	0.02	0.02	0.02
LOI	13.53	3.19	8.62	7.97	12.57	12.78	17.46	6.08
MgO	35.1	7.99	32.15	31.09	34.41	35.23	11.06	22.12
MnO	0.135	0.151	0.151	0.175	0.153	0.16	0.557	0.213
Na ₂ O	0.02	4.37	0.03	0.02	0.02	0.02	0.05	0.05
P ₂ O ₅	0.017	0.065	0.017	0.019	0.017	0.01	0.027	0.026
SiO ₂	37.43	51.65	38.76	39.16	36.45	35.83	28.12	44.47
TiO ₂	0.14	0.71	0.19	0.21	0.14	0.11	0.27	0.34
Total	98.85	100.47	99.66	99.32	98.82	98.73	99.7	99.85
Al (ppm)	16586	81991	19987	21423	12764	13436	33903	41511
Ba	7	340	11	16	4	5	64	12
Be	1	1	1	1	1	1	1	1
Ca	599	35471	20704	25079	4588	344	100000	59577
Cd	1	1	1	1	1	1	1	1
Co	103	62	120	122	126	122	109	68
Cr	1300	718	1300	1300	1300	1300	1300	1300
Cu	7	116	22	26	21	66	10	6
Fe	63028	68792	81314	87187	72601	81008	95000	72422
K	104	12653	274	190	70	77	125	131
Li	10	33	9	10	4	3	22	39
Mg	209409	47630	187169	183397	174931	213988	69664	134450
Mn	1051	1159	1158	1360	1143	1279	4693	1705
Mo	1	1	1	1	1	1	1	1
Na	500	29993	500	500	500	500	500	588
Ni	2309	182	1373	1206	1745	1879	1130	260
P	72	273	72	80	72	41	115	114
Pb	15	15	15	15	15	15	15	15
S	176	130	359	255	374	248	130	130
Sc	11	40	13	14	9	9	24	32
Sr	2	107	6	6	2	2	47	3
Ti	815	4272	1121	1223	813	654	1693	2031
V	61	277	91	90	56	60	137	170
W	6	6	6	6	6	6	6	6
Y	3	17	4	4	2	2	11	8
Zn	51	113	69	79	68	79	109	75
Ba	5.9	357.3	8.2	14.6	1.4	1.4	59.8	10.7
Be	0.15	0.71	0.68	0.39	0.67	0.37	1	0.9
Bi	0.47	0.47	0.47	0.47	0.47	0.47	0.47	0.47

	TL-16-SH-105	TL-16-SH-106	TL-16-SH-107	TL-16-SH-109	TL-16-SH-111A	TL-16-SH-112	TL-16-SH-114	TL-16-SH-116A
Cd	0.047	0.067	0.04	0.029	0.029	0.035	0.046	0.051
Ce	1.76	9.95	1.41	1.59	1.48	0.98	3.55	3.32
Co	110.62	68.32	124.93	128.43	129.09	124.79	107.93	69.17
Cr	2104	773	4500	2783	3732	4500	4500	3614
Cs	0.305	0.404	0.678	1.203	0.056	0.025	0.112	0.398
Cu	5.1	110.1	18.5	23	17.6	59.1	7.3	1.4
Dy	0.545	3.179	0.69	0.785	0.407	0.334	1.465	1.283
Er	0.34	2.076	0.406	0.457	0.268	0.223	0.94	0.793
Eu	0.1248	0.6509	0.1473	0.1816	0.0714	0.1	0.2494	0.2029
Ga	3.16	15.86	4.39	4.7	3.34	3.13	8.01	7.19
Gd	0.439	2.524	0.521	0.651	0.379	0.276	1.284	0.959
Hf	0.28	1.4	0.3	0.37	0.26	0.17	0.5	0.58
Ho	0.1175	0.6846	0.1386	0.1608	0.0874	0.0693	0.3147	0.2798
In	0.0139	0.0596	0.0152	0.0203	0.0146	0.0097	0.0265	0.0277
La	0.79	4.41	0.54	0.57	0.56	0.5	1.59	1.36
Li	9.6	34.3	8.4	9.9	3.9	3.1	15	34.5
Lu	0.0548	0.3072	0.0621	0.0716	0.0384	0.0326	0.1346	0.1245
Mo	0.2	0.42	0.17	0.19	0.15	0.13	0.2	0.17
Nb	0.243	1.593	0.343	0.363	0.302	0.176	0.485	0.564
Nd	1.13	6.1	1.19	1.38	1.02	0.77	2.68	2.33
Ni	2430.5	193.2	1417.1	1242.6	1763.3	1892.5	1087.9	260.2
Pb	0.4	1	0.4	0.5	0.3	0.4	0.4	0.3
Pr	0.236	1.403	0.222	0.235	0.207	0.147	0.538	0.468
Rb	1.74	17.63	1.98	1.89	0.25	0.43	0.29	0.68
Sb	0.32	0.51	0.04	0.04	0.2	0.08	0.23	0.6
Sc	11.6	42.7	13.9	15.2	9.6	9.3	22	32
Sm	0.307	1.917	0.412	0.46	0.296	0.245	0.847	0.747
Sn	0.19	0.69	0.25	0.23	0.23	0.16	0.33	0.3
Sr	1.9	102.2	7.9	7.7	1.6	2.2	47	4.5
Ta	0.012	0.104	0.019	0.02	0.016	0.009	0.029	0.032
Tb	0.0819	0.4457	0.0914	0.1107	0.0634	0.0499	0.2177	0.1843
Th	0.071	0.454	0.064	0.049	0.032	0.036	0.11	0.139
Ti	793	4283	1075	1223	817	623	1521	1956
Tl	0.007	0.092	0.167	0.022	0.009	0.006	0.013	0.031
Tm	0.0511	0.307	0.058	0.071	0.0382	0.0333	0.1383	0.1179
U	0.019	0.119	0.016	0.018	0.015	0.017	0.031	0.044
V		277.3		85.6				
W	2.01	0.69	0.1	0.05	0.27	0.11	0.86	0.75
Y	3.34	16.34	3.67	4.21	2.38	2.12	10.44	7.44
Yb	0.355	2.025	0.381	0.459	0.266	0.23	0.884	0.813
Zn	46	101	59	66	58	67	90	63
Zr	10	49	11	12	9	6	17	20

	TL-16-SH-116B	TL-16-SH-118	TL-16-SH-120	TL-16-SH-124
Al ₂ O ₃ (wt.%)	5.87	3.61	3.29	14.11
BaO	0.004	0.004	0.004	0.02
CaO	14.037	2.822	1.165	9.208
Cr ₂ O ₃	0.44	0.43	1.76	0.1
Fe ₂ O ₃	8.69	12.51	9.87	7.83
K ₂ O	0.02	0.04	0.04	0.37
LOI	3.65	9.49	10.53	3.92
MgO	19.91	30.02	33.62	8.5
MnO	0.215	0.16	0.111	0.156
Na ₂ O	0.1	0.09	0.02	1.03
P ₂ O ₅	0.03	0.017	0.016	0.052
SiO ₂	47.24	39.74	38.18	54.03
TiO ₂	0.36	0.19	0.15	0.64
Total	100.56	99.11	98.74	99.97
Al (ppm)	30981	18975	17518	77847
Ba	4	17	11	208
Be	1	1	1	1
Ca	88268	19410	8240	62005
Cd	1	1	1	1
Co	47	128	111	66
Cr	1300	1300	1300	678
Cu	6	16	14	110
Fe	59149	85937	69251	56552
K	97	243	291	3195
Li	33	14	13	46
Mg	114961	175059	201238	53167
Mn	1636	1234	865	1234
Mo	1	1	1	1
Na	951	952	500	7743
Ni	164	1108	2004	278
P	127	75	70	234
Pb	15	15	15	15
S	130	548	390	1159
Sc	48	13	11	40
Sr	9	11	3	82
Ti	2137	1112	880	3991
V	203	80	86	268
W	6	6	6	6
Y	10	4	3	12
Zn	60	59	64	105
Ba	3.7	16	4.4	201.9
Be	0.37	0.53	1.03	0.67
Bi	0.47	0.47	0.47	0.47

	TL-16-SH-116B	TL-16-SH-118	TL-16-SH-120	TL-16-SH-124
Cd	0.056	0.02	0.024	0.108
Ce	3.34	1.45	1.56	5.91
Co	49.8	135.09	115.91	69.25
Cr	3004	2879	4500	700
Cs	0.247	1.403	2.623	0.445
Cu	2.1	10.7	10.4	99.5
Dy	1.637	0.689	0.559	2.18
Er	1.115	0.427	0.361	1.305
Eu	0.2469	0.1707	0.1186	0.5907
Ga	6.26	3.94	4.17	14.85
Gd	1.357	0.577	0.426	1.833
Hf	0.65	0.31	0.29	1.23
Ho	0.3642	0.1426	0.1233	0.4599
In	0.0359	0.0174	0.0151	0.0596
La	1.28	0.5	0.62	2.54
Li	27.9	12.6	12	43.3
Lu	0.1458	0.0564	0.0553	0.2021
Mo	0.21	0.1	0.11	0.96
Nb	0.622	0.341	0.272	1.377
Nd	2.5	1.29	0.97	4.13
Ni	171.8	1149.3	2036.6	281.3
Pb	0.3	0.7	0.3	1
Pr	0.528	0.248	0.208	0.889
Rb	0.32	2.39	2.95	10.43
Sb	1.06	0.66	0.3	0.1
Sc	49.2	13.7	11.1	41.4
Sm	0.95	0.379	0.372	1.386
Sn	0.43	0.38	0.3	0.62
Sr	8.8	12.2	6.1	77.8
Ta	0.038	0.019	0.014	0.088
Tb	0.2539	0.1014	0.0767	0.3234
Th	0.174	0.051	0.077	0.373
Ti	2177	1095	822	3969
Tl	0.017	0.105	0.053	0.212
Tm	0.1607	0.0615	0.0485	0.1943
U	0.043	0.013	0.017	0.105
V	202.3	84.6		265.6
W	0.74	0.3	0.05	0.33
Y	9.96	3.97	3.24	12.11
Yb	1.042	0.395	0.374	1.302
Zn	53	51	55	90
Zr	23	11	10	43